

**Some pages of this thesis may have been removed for copyright restrictions.**

If you have discovered material in Aston Research Explorer which is unlawful e.g. breaches copyright, (either yours or that of a third party) or any other law, including but not limited to those relating to patent, trademark, confidentiality, data protection, obscenity, defamation, libel, then please read our [Takedown policy](#) and contact the service immediately (openaccess@aston.ac.uk)

AN INVESTIGATION INTO PROTEIN MODIFICATION BY  
SHORT-CHAIN LIPID OXIDATION PRODUCTS:

Development of mass spectrometry-based approaches for  
their detection and assessment of the effect on cellular  
proteins structure and activity

BEBIANA DA COSTA SOUSA

Doctor of Philosophy

ASTON UNIVERSITY

September 2019

© Bebiana da Costa Sousa, 2019

Bebiana da Costa Sousa asserts her moral right to be identified as the author of this thesis

This copy of the thesis has been supplied on condition that anyone who consults it is understood to recognise that its copyright belongs to its author and that no quotation from the thesis and no information derived from it may be published without appropriate permission or acknowledgement.

# Aston University

## **An investigation into protein modification by short-chain lipid peroxidation products: development of mass spectrometry-based approaches for their detection and assessment of the effect on cellular proteins structure and activity**

Bebiana da Costa Sousa

Doctor of Philosophy in Life and Health Sciences

2019

## **Thesis Summary**

The oxidative modification of lipids containing polyunsaturated fatty acids results in a wide diversity of reactive products, including short-chain aldehydes, which can covalently modify proteins, a process called lipoxidation, and affect their function. The detection of lipoxidation adducts is extremely challenging due to their low abundance, so there is a need for new detection methods. Using the model proteins lysozyme and human serum albumin, five reporter ions for acrolein modification, eight for 4-hydroxyhexenal and one for 2-chlorohexadecanal were found by LC-MS/MS-based label-free method. Subsequently, a targeted multiple reaction monitoring method was developed as a potential tool for the identification and characterization of these modifications of human serum albumin in biological samples. Comparison between three different chromatographic methods for the separation of intact proteins unmodified or modified by short-chain aldehydes demonstrated that anion exchange chromatography was the best method for protein isoform separation while reverse phase chromatography was the best for the separation of lipoxidized proteins.

To understand the cellular effects of lipoxidation by small aldehydes, two cellular proteins were studied. The Cys328-mediated effect of short-chain aldehydes on vimentin organization was evaluated by confocal microscopy, which showed that aldehydes caused vimentin aggregation around the nucleus, and Cys328 was important in both assembly of the filament network and as a target for lipoxidation. The effect of short-chain aldehydes on the glycolytic enzyme pyruvate kinase was also studied, and this protein was found to be highly susceptible to modification; under pathophysiological concentrations acrolein, malondialdehyde and 4-hydroxyhexenal were able to inhibit its activity in a time- and dose-dependent manner. Similar inhibition was observed in breast cancer cells, altering cellular metabolism and suggesting that these aldehydes may contribute to mechanisms of tumorigenesis. Overall, this work has improved the analytical tools for detecting protein lipoxidation, as well as understanding of its functional effects.

Keywords: oxidative stress, pyruvate kinase, metabolism, vimentin

## ACKNOWLEDGMENTS

I would like to start by thanking my supervisors Prof. Corinne M. Spickett and Prof. Andrew R. Pitt for providing me with this opportunity to do a PhD in the Oxidative Stress group as part of the MASSTRPLAN project. Thank you for all the knowledge, skills, guidance and advice provided through out these three and a half years which helped me grow into a more self-confident researcher in the field on -omics.

Thank you to all of the MASSTRPLAN team. From students, to PIs and collaborators, it was a pleasure to share all of the experiences that this project had to offer with you.

To Angela Criscuolo and Ken Cook, thank you for the teaching on chromatography, and support provided while I was on secondment. Thank you for the opportunity to work in a world leading company such as Thermo. It was a pleasure to work with someone so smart, passionate and friendly as Angela, which resulted in the data on chapter 4 and a paper publication which is being prepared. Thank you to Dr. Dolores Pérez-Sala for allowing me to join her microscopy team at CIB for a month; thank you for all the teaching and support and for the data collected that made into chapter 6 of this thesis. Sofia Duarte and Andreia Mónico, thank you for all the help around the lab and for making me feel so welcome in Madrid, it would not have been possible without you. To Dr. Mark Jeeves and Dr. Raquel Saborano at the University of Birmingham, thank you for the NMR data collection and analysis for the metabolome analysis reported in the chapter 5 of this thesis.

At Aston University, thank you Catarina Afonso as we started this adventure together, our little Portuguese mafia, and I could not have asked for a better partner. I would also like to acknowledge all of the students that worked with me during these three years and contributed for the success of this thesis: thank you Eleanor Bhurru for the help developing the targeted mass spectrometry methods in chapter 2 and thank you Jed Ashman, Tanzim Ahmed and Will Dann for performing enzymatic activity and cell viability assays that contributed for the chapter 5 of this thesis and our joint paper. To Romina Medeiros, thank you so much for the friendship and incentive, keeping me sane during your short but lovely stay in our team. To all the other PhD students who shared this journey with me, thank you for the stories shared around the lunch table, those were at the same time the most smart and dumb discussions I have ever had. In special, to Savannah Gibson to whom a thank you is not enough for being one of my best friends. Thank you for always being present, for listening and helping, and most importantly for all the coffee and strawbs provided during the writing up of this thesis, it was much appreciated. I would also like to thank Debbie Toomeoks for being what I can only describe as my English mom. Thank you for taking care of me when I needed the most, including moving twice, for all the coffees and sweets shared and all the trips around Europe that I will never forget.

Last but not least I would like to thank my friends, some close others abroad, you all made this journey possible and a little bit easier. In special to Raquel Saborano, ten years ago we met on our first day at university as undergrads and I could not have asked for a better friend to go through my PhD journey with. Thank you for all the conversations, all the coffee shop visits, the mandatory cinema on Sundays and in general for being such a great friend. Looking forward for the next adventure with you, one where we are no longer students! Thank you to Madalena Sobral, who even from far was always present when I most needed a friend during these last few years. To all my family, in particular to my parents Carlos Sousa and Natalia Costa and brothers Tiago Sousa and Renato Sousa, thank you! You know I do all of this for you, always have and always will. You are my support; my reason and I love you all.

# List of contents

<b><u>LIST OF ABBREVIATIONS.....</u></b>	<b><u>10</u></b>
<b><u>LIST OF FIGURES.....</u></b>	<b><u>14</u></b>
<b><u>LIST OF TABLES.....</u></b>	<b><u>25</u></b>
<b><u>CHAPTER 1. INTRODUCTION.....</u></b>	<b><u>26</u></b>
1.1. LIPIDS AND LIPID PEROXIDATION PRODUCTS.....	27
1.1.1. LIPIDS .....	27
1.1.2. OVERVIEW ON OXIDANTS AND OXIDATIVE STRESS.....	30
1.1.3. LIPID PEROXIDATION: MECHANISMS AND PRODUCTS .....	31
1.1.4. FATTY ACID FREE-RADICAL OXIDATION PRODUCTS.....	33
1.2. ALDEHYDES AS SHORT CHAIN LIPID PEROXIDATION PRODUCTS .....	36
1.2.1. ALKANALS .....	37
1.2.2. ALKENALS .....	38
1.2.3. SUBSTITUTED ALDEHYDES .....	40
1.2.4. CHLOROALDEHYDES.....	45
1.3. POST-TRANSLATIONAL PROTEIN MODIFICATION BY ALDEHYDES .....	47
1.3.1. MECHANISM OF ADDUCTION.....	47
1.3.2. ALDEHYDE-PROTEIN ADDUCTION: STRUCTURE AND EVIDENCE .....	48
1.3.3. REVERSIBILITY AND DETOXIFICATION OF ALDEHYDE-PROTEIN ADDUCTS .....	52
1.4. DETECTION METHODS FOR ALDEHYDIC OXIDATION PRODUCTS.....	53
1.4.1. ANALYSIS OF FREE ALDEHYDES AND THEIR METABOLITES .....	53
1.4.2. ANALYSIS OF ALDEHYDES AS ADDUCTS WITH MACROMOLECULES .....	54
1.4.3. ANTIBODY-BASED METHODS .....	54
1.4.4. PROTEIN ANALYSIS BY MASS SPECTROMETRY .....	55
1.4.4.1. SAMPLE PREPARATION .....	55
1.4.4.2. ENRICHMENT AND LABELLING APPROACHES .....	56
1.4.4.3. SEPARATION.....	58
1.4.4.4. INTACT PROTEIN AND TOP-DOWN PROTEOMICS.....	58
1.4.4.5. BOTTOM-UP PROTEOMICS.....	59
1.4.4.6. UNTARGETED OR SHOTGUN MASS SPECTROMETRY APPROACH.....	60
1.4.4.7. TARGETED AND SEMI-TARGETED APPROACHES .....	61
1.4.5. QUANTIFICATION OF ALDEHYDES IN HUMAN PLASMA OR SERUM .....	63

1.4.6. METABOLOMICS BY NUCLEAR MAGNETIC RESONANCE (NMR) .....	63
1.5. AIMS AND HYPOTHESIS OF THE WORK PRESENTED IN THIS THESIS .....	65

**CHAPTER 2. A MASS SPECTROMETRY APPROACH FOR THE IDENTIFICATION AND LOCALIZATION OF SMALL ALDEHYDE MODIFICATIONS OF PROTEINS.....66**

2.1. INTRODUCTION .....	67
2.2. MATERIAL AND METHODS .....	70
2.2.1. CHEMICALS.....	70
2.2.2. TREATMENT OF LYSOZYME OR HUMAN SERUM ALBUMIN WITH ALDEHYDES IN VITRO ...	70
2.2.3. DIRECT INFUSION MS ANALYSIS OF MODIFIED LYSOZYME .....	70
2.2.4. PLASMA COLLECTION AND ALDEHYDE TREATMENT .....	70
2.2.5. PROTEIN IN-GEL DIGESTION .....	71
2.2.6. LIQUID CHROMATOGRAPHY-TANDEM MASS SPECTROMETRY (LC-MS/MS) ANALYSIS	71
2.2.7. MULTIPLE REACTION MONITORING (MRM) .....	72
2.2.8. DATABASE SEARCHES .....	73
2.3. RESULTS .....	74
2.3.1. LYSOZYME AS A MODEL SYSTEM TO STUDY LIPID-PROTEIN ADDUCTS.....	74
2.3.2. HUMAN SERUM ALBUMIN LIPOXIDATION ANALYSIS BY LC-MS/MS .....	82
2.3.2.1. ACROLEIN.....	82
2.3.2.2. 4-HYDROXY-2-HEXENAL.....	86
2.3.3. DEVELOPING AN MRM APPROACH AS A POTENTIAL DIAGNOSTIC TOOL FOR ACROLEIN-HSA MODIFICATIONS .....	89
2.3.4. TESTING THE DEVELOPED MRM APPROACH FOR ACROLEIN-HSA MODIFICATIONS ON POOLED HUMAN PLASMA .....	94
2.4. DISCUSSION .....	98

**CHAPTER 3. SYNTHESIS OF 2-CHLOROHEXADECANAL AND ITS ADDUCTION TO PROTEINS .....103**

3.1. Introduction .....	104
3.2. Material and Methods.....	107
3.2.1. Multi-step synthesis of hexadecanal from hexadecanol .....	107
3.2.1.1. Synthesis of hexadecanal (Corey-Suggs oxidation).....	107
3.2.1.2. Synthesis of dimethylacetal hexadecanal (protection) .....	107
3.2.1.3. Synthesis of 2-chloro-methylacetal hexadecanal (chlorination).....	107
3.2.1.4. Acid hydrolysis of 2-chloro-methylacetal hexadecanal (deprotection) .....	108

3.2.2.	Direct conversion of alcohol into chloroaldehyde .....	108
3.2.2.1.	First attempt .....	108
3.2.2.2.	Second attempt .....	108
3.2.3.	<sup>1</sup> H NMR analysis .....	109
3.2.4.	GC-FID analysis .....	109
3.2.5.	Treatment of model proteins with 2-chlorohexadecanal <i>in vitro</i> .....	109
3.2.6.	Liquid Chromatography-Mass Spectrometry (LC-MS) Analysis .....	109
3.2.7.	Database Search.....	109
3.3.	Results .....	111
3.3.1.	Multi-step reaction synthesis of 2-chlorohexadecanal.....	111
3.3.2.	Direct conversion of hexadecanol to hexadecanal and 2-chloro-hexadecanal ...	118
3.3.2.1.	First Attempt at Direct Synthesis of 2-chloro-hexadecanal.....	118
3.3.2.2.	Second Attempt at Direct Synthesis of 2-chloro-hexadecanal.....	121
3.3.3.	Lipoxidation of lysozyme by 2-chloro-hexadecanal.....	123
3.3.4.	Lipoxidation of human serum albumin by 2-chloro-hexadecanal.....	126
3.4.	Discussion.....	128

**CHAPTER 4. CHROMATOGRAPHY METHODS FOR SEPARATION OF PROTEINS  
MODIFIED BY SHORT-CHAIN ALDEHYDES.....132**

4.1.	Introduction .....	133
4.2.	Material and Methods.....	137
4.2.1.	Materials.....	137
4.2.2.	Treatment of proteins with aldehydes <i>in vitro</i> .....	137
4.2.3.	Ion Exchange Chromatography (IEC).....	137
4.2.4.	Reverse Phase Chromatography .....	137
4.2.5.	Mass Spectrometry for intact protein analysis .....	138
4.2.6.	Mass Spectrometry for peptide analysis .....	138
4.2.7.	In-gel digestion .....	139
4.2.8.	SMART Digestion.....	139
4.2.9.	Data processing .....	139
4.3.	Results .....	140
4.3.1.	Protein separation by ion exchange chromatography .....	140
4.3.2.	Intact protein separation by reverse phase chromatography.....	146
4.3.3.	Comparison between protein digestion methods .....	149
4.4.	Discussion.....	155



**CHAPTER 5. SHORT-CHAIN LIPID PEROXIDATION PRODUCTS FORM COVALENT ADDUCTS WITH PYRUVATE KINASE AND INHIBIT ITS ACTIVITY IN VITRO AND IN BREAST CANCER CELLS .....158**

5.1. Introduction .....159

5.2. Material and Methods .....162

5.2.1. Synthesis of 4-hydroxy-2(E)-hexenal.....162

5.2.2. Treatment of pyruvate kinase with aldehydes in vitro.....162

5.2.3. Cell culture and aldehyde treatment .....162

5.2.4. XTT cell viability assay .....162

5.2.5. Cell harvesting, lysis and protein concentration assessment .....163

5.2.6. Pyruvate kinase activity assays .....163

5.2.7. Protein in-solution digestion.....163

5.2.8. Cellular extract in-gel digestion.....164

5.2.9. Liquid Chromatography-Tandem Mass Spectrometry (LC-MS/MS) Analysis .....164

5.2.10. Database Searches.....164

5.2.11. Protein structure visualization using PyMOL.....165

5.2.12. Glycolysis Stress Test with Seahorse XF Extracellular Flux Analyzer.....165

5.2.13. NMR sample preparation.....165

5.2.14. NMR acquisition and analysis.....166

5.2.15. Statistical analysis .....166

5.3. Results .....167

5.3.1. Identification and mapping of lipoxidation on pyruvate kinase.....167

5.3.2. Inhibition of pyruvate kinase activity following treatment *in vitro* .....174

5.3.3. The effect of longer treatment times on activity and lipoxidation of pyruvate kinase .....177

5.3.4. Comparison of aldehyde effects on MCF-7 cell pyruvate kinase activity and cell viability .....186

5.3.5. Acrolein effect on the MCF-7 cells metabolism .....189

5.4. Discussion.....195

**CHAPTER 6. EFFECT OF REACTIVE SHORT-CHAIN ALDEHYDES ON INTERMEDIATE FILAMENTS NETWORK ORGANIZATION .....202**

6.1. Introduction .....203

6.2. Material and Methods .....206

6.2.1. Cell culture and aldehyde treatment .....206

6.2.2. Fluorescence microscopy and cell imaging .....	206
6.2.3. Statistical analysis .....	207
6.3. Results .....	208
6.3.1. Effect of short-chain aldehydes on vimentin network by confocal microscopy ...	208
6.3.2. Mutation of Cys328 confers protection from lipoxidation on the vimentin network .....	211
6.3.3. Monitoring the effect of ACR and MDA treatment by time-lapse microscopy .....	214
6.4. Discussion.....	216
<b><u>CHAPTER 7. CONCLUSION.....</u></b>	<b><u>218</u></b>
7.1. General discussion .....	219
7.2. Summary and perspectives.....	223
<b><u>CHAPTER 8. LIST OF REFERENCES.....</u></b>	<b><u>224</u></b>
<b><u>CHAPTER 9. APPENDIX.....</u></b>	<b><u>252</u></b>
9.1 List of aldehyde modifications .....	253
9.2 List of publications .....	257

## List of abbreviations

AA	arachidonic acid
ACR	acrolein
AEC	anion exchange chromatography
AFs	actin filaments
ALA	$\alpha$ -linolenic acid
ALS	amyotrophic lateral sclerosis
AP-1	activator protein 1
ARE	antioxidant response element
ARP	aldehyde reactive probe
ATP	adenosine triphosphate
BBB	blood brain barrier
BHZ	biotin hydrazide
BMVEC	brain microvascular endothelial cells
BNZ	benzaldehyde
CDK	cyclin-dependent kinase
CEC	cation exchange chromatography
CEP	2-carboxyethyl pyrrole
CID	collision-induced dissociation
CIHDA	2-chlorohexadecanal
CML	carboxymethyllysine
COX	cyclooxygenases
CRT	crotonaldehyde
DHA	docosahexaenoic acid
DNA	deoxyribonucleic acid
DNPH	2,4,-dinitrophenylhydrazine
DTT	dithiothreitol
E2F	E2F transcription factor family
ECD	electron capture dissociation
eEF2	elongation factor 2
EGFR	epidermal growth factor receptor
EMP-lysine	<i>N</i> -(5-ethyl-2-methylpyridinium) lysine
eNOS	endothelial nitric oxide
EP	ethylpyrrole
EPA	eicosapentaenoic acid
ESI	electrospray ionization

FALDH	fatty aldehyde dehydrogenase
FDP-lysine	<i>N</i> -(3-formyl-3,4-dehydropiperidino)-lysine
GAPDH	glyceraldehyde-3-phosphate dehydrogenase
GC	gas chromatography
GFAP	glial fibrillary acidic protein
GFP	green fluorescent protein
GO	glyoxal
GSH	glutathione
HDA	hexadecanal
HDDA	4-hydroxydodecadienoic acid
HDDE	4-hydroxydodeca-2,6-dienal
HHA	4-hydroxyhexenoic acid
HHE	4-hydroxy-2-hexenal
HHP-lysine	<i>N</i> -3-[(hept-1-enyl)-4-hexylpyridinium] lysine
HNA	4-hydroxynonenoic acid
HNE	4-hydroxy-2-nonenal
HODE	hydroxyoctadecadienoic acid
HpETE	hydroxyeicoatetraenoic acid
HPLC	high-performance liquid chromatography
HPODE	hydroperoxyoctadecadienoic acid
HSA	human serum albumin
HXL	hexanal
IEC	ion exchange chromatography
IP	isoelectric point
IFs	intermediate filaments
JNK	c-Jun N-terminal kinases
LA	linoleic acid
LC-MS	liquid chromatography mass spectrometry
LDL	low-density lipoprotein
LOX	lipoxygenases
LPO	lipid peroxidation
LPS	lipopolysaccharide
MALDI	matrix-assisted laser desorption/ionization
MAPs	microtubules-associated proteins
MAPK	mitogen-activated protein kinase
MDA	malondialdehyde

MP-lysine	<i>N</i> -(2-methylpyridinium) lysine
MPO	myeloperoxidase
MRM	multiple reaction monitoring
MS	mass spectrometry
MTs	microtubules
NFs	neurofilaments
NFκB	nuclear factor kappa B
NLS	neutral loss scanning
NMR	nuclear magnetic resonance
NPS	nonporous silica
Nrf2	nuclear erythroid-2 related factor 2
OHE	4-oxo-2-hexenal
ONE	4-oxo-2-nonenal
OxPL	oxidized phospholipids
PA	palmitic acid
PC	phosphatidylcholine
PE	phosphatidylethanolamine
PEP	phosphoenolpyruvate
PERK	protein kinase RNA-like endoplasmatic reticulum kinase
PFBO	pentafluorobenzyl oxime
PFK	phosphofructokinase
PG	phosphatidylglycerol
PI	phosphatidylinositol
PIS	precursor ion scanning
PKC	protein kinase C
PKM1	pyruvate kinase isoform 1
PKM2	pyruvate kinase isoform 2
PL	phospholipid
POVPC	1-O-palmitoyl-2-O-(5-oxovaleryl)-sn-glycero-3-phosphocholine
PPAR	peroxisome proliferator-activated receptor gamma
PROS	partially reduced oxygen species
PS	phosphatidylserine
PTM	post translational modification
PTP1B	protein-tyrosine phosphatase 1B
pTSA	p-toluene sulfonic acid
PUFAs	polyunsaturated fatty acids

RCIS	reactive chloride species
RCS	reactive carbonyl species
Rf	retention factor
RFP	red fluorescent protein
RNS	reactive nitrogen species
ROS	reactive oxygen species
RPLC	reverse-phase chromatography
SDS-PAGE	polyacrylamide gel electrophoresis
SEC	size exclusion chromatography
SIFT-MS	selected ion flow tube mass spectrometry
SOD	superoxide dismutase
SRM	single reaction monitoring
TBARS	thiobarbituric acid reactive substances
TCA	tricarboxylic acid
TCCA	trichloroisocyanuric acid
TEMPO	2,2,6,6-tetramethylpiperidine 1-oxyl
TFA	trifluoroacetic acid
TLC	thin-layer chromatography
TMOF	trimethyl orthoformate
TMSC	trimethyl silyl chloride
TOF	time of flight
Trx	thioredoxin
UPC3	mitochondrial uncoupling protein 3
UV	ultraviolet
WT	wild-type

## List of figures

<b>FIGURE 1.1. LIPID CATEGORIES ACCORDING TO THE LIPID MAPS LIPID-CLASSIFICATION SYSTEM.....</b>	<b>27</b>
<b>FIGURE 1.2. STRUCTURE OF THREE <math>\Omega</math>3 AND TWO <math>\Omega</math>6 UNSATURATED FATTY ACIDS. EXAMPLE OF <math>\Omega</math>3 FATTY ACIDS ARE LINOLENIC ACID (ALA), EICOSAPENTAENOIC ACID (EPA) AND DOCOSAHEXAENOIC ACID (DHA), AND OF <math>\Omega</math>6 FATTY ACIDS ARE LINOLEIC ACID (LA) AND ARACHIDONIC ACID (AA). .....</b>	<b>28</b>
<b>FIGURE 1.3. STRUCTURE OF GLYCEROPHOSPHOLIPIDS. R<sup>1</sup> AND R<sup>2</sup> REPRESENT FATTY ACYL CHAINS ESTERIFIED TO THE GLYCEROL. X CORRESPOND TO THE DIFFERENT POLAR HEADS.....</b>	<b>29</b>
<b>FIGURE 1.4. STRUCTURE OF GLYCEROPHOSPHOLIPIDS HOLDING AN ETHER BOND INSTEAD OF AN ESTER BOND. A-PLASMOLOGENS WITH A VINYL ETHER BOND; B- ETHER LIPID (PLATELET-ACTIVATING FACTOR (PAF)).....</b>	<b>29</b>
<b>FIGURE 1.5. MECHANISMS OF GENERATION OF REACTIVE OXYGEN SPECIES. ....</b>	<b>31</b>
<b>FIGURE 1.6. LIPID PEROXIDATION MECHANISM. HYDROGEN-ATOM ABSTRACTION BY ALKOXYL RADICAL; OXYGEN ADDITION TO CARBON RADICAL; PEROXYL RADICAL REARRANGEMENT.....</b>	<b>32</b>
<b>FIGURE 1.7. SCHEMATIC EXPLANATION OF LONG AND SHORT CHAIN LIPID PEROXIDATION PRODUCTS. ....</b>	<b>33</b>
<b>FIGURE 1.8. FORMATION OF HYDROPEROXIDES FROM LINOLEIC ACID. FOLLOWING HYDROGEN ABSTRACTION, OXYGEN ADDS TO ALL THREE REACTIVE CARBON POSITIONS (C9, C11 AND C13). OTHER OXIDATIVE SPECIES CAN RESULT FROM THE REARRANGEMENT, FURTHER OXIDATION OR BREAKDOWN OF THESE HYDROPEROXIDES, INCLUDING HNE. ADAPTED FROM [23]. ....</b>	<b>34</b>
<b>FIGURE 1.9. MAJOR PATHWAYS OF FREE RADICAL OXIDATION OF ARACHIDONIC ACID. THE PRIMARY OXIDATION PRODUCTS ARE HYDROPEROXIDES. ONLY 11-HPETE SHOWN HERE AS EXAMPLE FOR SIMPLICITY, HOWEVER THERE ARE SIX HYDROPEROXYL RADICALS GENERATED FROM FREE RADICAL OXIDATION OF ARACHIDONIC ACID. SECONDARY OXIDATION PRODUCTS ARE GENERATED BY FURTHER OXIDATION, DECOMPOSITION OR REDUCTION OF THE HYDROPEROXIDES. ADAPTED FROM [23]. ....</b>	<b>35</b>
<b>FIGURE 1.10. SCHEMATIC REPRESENTATION OF THE FORMATION OF HHE AND HOHA FROM DHA. HYDROLYSIS OF DHA GENERATES HOHA WHICH IN TURN PRODUCES CEP-PROTEIN ADDUCT. OXIDATIVE CLEAVAGE OF DHA ALSO FORMS HHE WHICH GENERATES A SIMILAR PROTEIN MODIFICATION, EP-PROTEIN ADDUCT. ADAPTED FROM [59].....</b>	<b>36</b>
<b>FIGURE 1.11. MECHANISMS OF CARBON-CARBON BOND CLEAVAGE. (I) REDUCTION OF HYDROPEROXIDE TO AN ALKOXYL RADICAL IN THE PRESENCE OF A TRANSITION METAL FOLLOWED BY <math>\beta</math>-SCISSON; (II) HOCK REARRANGEMENT OF A HYDROPEROXIDE AND MIGRATION OF A C-C TO A C-O BOND AND CLEAVAGE; (III) CYCLIZATION TO FORM A DIOXETANE AND SUBSEQUENT CLEAVAGE. ADAPTED FROM [63]. ....</b>	<b>37</b>
<b>FIGURE 1.12. STRUCTURE OF THE THREE MOST COMMON ALKANALS TO OCCUR AS LIPID PEROXIDATION PRODUCTS. ....</b>	<b>38</b>
<b>FIGURE 1.13. STRUCTURE OF THE MOST COMMON ALKENALS TO OCCUR AS LIPID PEROXIDATION PRODUCTS. ....</b>	<b>39</b>
<b>FIGURE 1.14. STRUCTURE OF THE MOST COMMON HYDROXYALKENALS TO OCCUR AS LIPID PEROXIDATION PRODUCTS. ....</b>	<b>41</b>
<b>FIGURE 1.15. SCHEMATIC SUMMARY OF SIGNALING PROTEINS KNOWN TO BE MODIFIED BY HNE. ....</b>	<b>42</b>
<b>FIGURE 1.16. STRUCTURE OF THE MOST COMMON OXOALKENALS TO OCCUR AS LIPID PEROXIDATION PRODUCTS. ....</b>	<b>43</b>

<b>FIGURE 1.17. STRUCTURE OF TWO BIS-ALDEHYDES KNOWN TO OCCUR AS PRODUCTS OF LIPID PEROXIDATION.</b> .....	44
<b>FIGURE 1.18. PLASMALOGENS ARE TARGETS OF HOCL AT THE ALKENE CHAIN, AT THE AMINE POLAR HEAD (HIGHLIGHTED IN BLUE) AND AT THE VINYL ETHER BOND (HIGHLIGHTED IN RED). THE LATTER IS THE RESPONSIBLE FOR THE PRODUCTION OF A-CHLORO-ALDEHYDES.</b> .....	46
<b>FIGURE 1.19. MECHANISM OF ADDUCTION OF SHORT-CHAIN ALDEHYDES TO PROTEINS. (A) SCHIFF'S BASE FORMATION MECHANISM. THE EXAMPLE INCLUDES BUTANAL AS THE ELECTROPHILE AND THE AMINO ACID LYSINE AS THE NUCLEOPHILE. THIS REACTION IS A CONDENSATION AND THEREFORE LOSES WATER. (B) MICHAEL ADDITION MECHANISM. THE EXAMPLE IS ACROLEIN AS THE ELECTROPHILE AND CYSTEINE AS THE NUCLEOPHILE.</b> .....	48
<b>FIGURE 1.20. PRODUCTS FORMED BY REACTION OF ACROLEIN WITH AMINO ACID SIDE CHAINS. WHERE REACTIONS OCCURRED BY MICHAEL ADDITION, ONLY LYSINE ADDUCTS ARE SHOWN BUT AS INDICATED IN THE FIGURE, THESE CAN ALSO HAPPEN ON A CYSTINE, HISTIDINE OR ARGININE RESIDUE.</b> .....	49
<b>FIGURE 1.21. PRODUCTS FORMED BY REACTION OF 4-HYDROXY-NONENAL WITH AMINO ACID SIDE CHAINS.</b> .....	50
<b>FIGURE 1.22. PRODUCTS FORMED BY REACTION OF GLYOXAL OR MALONDIALDEHYDE WITH AMINO ACID SIDE CHAINS.</b> .....	51
<b>FIGURE 1.23. DIAGRAM ILLUSTRATING THE REVERSIBILITY OF PROTEIN MODIFICATION BY REACTIVE CARBONYL SPECIES AND THE DETOXIFICATION OF THESE BY THIOL-CONTAINING COMPOUNDS SUCH AS GLUTATHIONE.</b> .....	52
<b>FIGURE 1.24. SCHEMATIC REPRESENTATION OF VARIOUS TYPES OF TANDEM MASS SPECTROMETRY EXPERIMENTS. (A) PRODUCT ION SCANNING GENERATES FRAGMENT ION SPECTRA FOR THE IDENTIFICATION OF THE AMINO ACID SEQUENCE OF SPECIFIC PEPTIDES. THE FIRST ANALYZER (MS1) SELECTS ONE PRECURSOR ION AT A TIME, THEN THE SELECTED ION UNDERGOES CID IN THE COLLISION CELL, AND THE FRAGMENTS ARE ANALYZED BY THE SECOND ANALYZER (MS2). THIS PROCESS IS REPEATED FOR DIFFERENT PRECURSORS. (B) PRECURSOR ION SCANNING SETS THE SECOND ANALYZER (MS2) TO TRANSMIT ONLY ONE SPECIFIC FRAGMENT. MS1 IS SCANNED TO DETECT ALL THE PRECURSOR IONS THAT GENERATE THIS FRAGMENT. (C) NEUTRAL LOSS SCANNING SCANS BOTH ANALYZERS TO DETECT THE MASS DIFFERENCE OF IONS PASSING THROUGH MS1 AND MS2, SUCH DIFFERENCE CORRESPONDS TO A NEUTRAL FRAGMENT LOST IN THE COLLISION CELL. (D) MRM INVOLVES A SERIES OF ONE PRECURSOR ION AND ONE SPECIFIC FRAGMENT FOR THAT PRECURSOR BEING SELECTED BY MS1 AND MS2, RESPECTIVELY. THE INSTRUMENT CYCLES THROUGH A SERIES OF TRANSITIONS (PRECURSOR-FRAGMENT PAIR) WHICH IS PARTICULARLY USEFUL TO DETECT SPECIFIC ANALYTES IN COMPLEX SAMPLES. ADAPTED FROM [244].</b> .....	59
<b>FIGURE 1.25. ROEPSTORFF AND FOHLMAN NOMENCLATURE SYSTEM FOR PROTONATED PEPTIDE FRAGMENTATION.</b> .....	61
<b>FIGURE 2.1. REDUCTION OF INTACT LYSOZYME BY DTT TREATMENT. THE LEFT HAND PANELS CORRESPOND TO UNPROCESSED (RAW) MS DATA SHOWING THE CHARGE STATE ENVELOPE FOR THE PROTEIN, AND THE RIGHT HAND PANELS SHOW DECONVOLUTED DATA GIVING THE MASS OF THE INTACT LYSOZYME. LYSOZYME WAS TREATED FOR 30 MINS AT ROOM TEMPERATURE WITH VARYING CONCENTRATIONS OF</b>	



DTT: (A) CONTROL TREATMENT IN THE ABSENCE OF DTT; (B) 10 mM DTT TREATMENT; (C) 100 mM DTT TREATMENT; (D) 200 mM DTT TREATMENT.....	75
<b>FIGURE 2.2. DECONVOLUTED ESI-MS SPECTRA OF LYSOZYME OBTAINED AFTER REACTION WITH ACROLEIN AT 4MM.</b> TREATMENT FOR 1 H SHOWING NO ADDUCTS BEING FORMED (A). TREATMENT FOR 2 H (B), 4 H (C) OR 6 H (D) SHOWING THE FORMATION OF SEVERAL ACROLEIN MICHAEL ADDUCTS, EACH ADDING 58 DA (N=3).....	76
<b>FIGURE 2.3. DECONVOLUTED ESI-MS SPECTRA OF LYSOZYME.</b> SPECTRA OBTAINED AFTER REACTION WITH ACROLEIN FOR 2 HOURS AT 8 MM (A) AND 14 MM (B), AND FOR 4 HOURS AT 8 MM (C) AND 14 MM (D). (N=3).....	77
<b>FIGURE 2.4. SDS-PAGE (DENATURING GEL ELECTROPHORESIS) RESULTS FOR LYSOZYME.</b> UNTREATED AND TREATED LYSOZYME WITH 4 MM, 8 MM OR 14 MM ACROLEIN FOR 2 HOURS. GEL STAINED WITH COOMASSIE BLUE STAINING. THE HIGHLIGHTED SECTIONS BOXED IN WHITE WERE CUT FOR FURTHER ANALYSIS: (1) 15-20 kDA; (2) 25-30 kDA; (3) 40-45 kDA.....	78
<b>FIGURE 2.5. MS/MS SPECTRA OF LYSOZYME TRYPTIC PEPTIDE.</b> CELAAAMK MODIFIED ON A CYSTEINE RESIDUE BY ACROLEIN (58 DA). (A) THE Y AND B IONS INDICATED BY THE ARROWS CONFIRM THE PEPTIDE SEQUENCE AND THE MODIFICATION ON THE CYSTEINE RESIDUE. (B) X-AXIS ADJUSTED TO 50-150 DA FOR IMMONIUM IONS IDENTIFICATION: LEUCINE (L) AT M/Z 72 DA AND 86 DA, LYSINE (K) AT M/Z 84 DA AND 129 DA, GLUTAMIC ACID (E) AT M/Z 102 DA, METHIONINE (M) AT M/Z 104 DA AND ACROLEIN-MODIFIED CYSTEINE (C) AT M/Z 134 DA. THE BASE STRUCTURE OF AN IMMONIUM ION IS SHOWN NEXT TO THE SPECTRUM.....	80
<b>FIGURE 2.6. PROPOSED STRUCTURES OF THE DIAGNOSTIC IONS FOUND FOR THE REDUCED ACROLEIN MODIFICATIONS ON LYSINE AND CYSTEINE.</b> ....	82
<b>FIGURE 2.7. SDS-PAGE (DENATURING GEL ELECTROPHORESIS) RESULTS FOR HUMAN SERUM ALBUMIN.</b> UNTREATED AND TREATED HSA WITH ACROLEIN AT 4 MM, 8 MM OR 14 MM FOR 2 HOURS. GEL STAINED WITH COOMASSIE BLUE STAINING. THE HIGHLIGHTED SECTION BOXED IN WHITE WAS CUT OUT FOR FURTHER ANALYSIS.....	83
<b>FIGURE 2.8. MS/MS SPECTRA OF HUMAN SERUM ALBUMIN TRYPTIC PEPTIDE.</b> KQTALVELVK MODIFIED ON A LYSINE RESIDUE BY ACROLEIN (58 DA). THE Y AND B IONS INDICATED BY THE ARROWS CONFIRM THE PEPTIDE SEQUENCE AND THE MODIFICATION ON THE CYSTEINE RESIDUE. IMMONIUM IONS FOR ACROLEIN-MODIFIED LYSINE FOUND AT M/Z 142 DA. ....	84
<b>FIGURE 2.9. PROPOSED STRUCTURES OF THE DIAGNOSTIC IONS FOUND FOR THE REDUCED ACROLEIN MODIFICATIONS ON LYSINE, CYSTEINE AND HISTIDINE.</b> ....	85
<b>FIGURE 2.10. SDS-PAGE (DENATURING GEL ELECTROPHORESIS) RESULTS FOR HUMAN SERUM ALBUMIN.</b> UNTREATED AND TREATED HSA WITH HHE AT 8 MM OR 16 MM FOR 2 HOURS. GEL STAINED WITH COOMASSIE BLUE STAINING. THE HIGHLIGHTED SECTION BOXED IN WHITE WAS CUT OUT FOR FURTHER ANALYSIS. ARROWS IDENTIFY POSSIBLE PROTEIN CROSSLINKING. ....	86
<b>FIGURE 2.11. PROPOSED STRUCTURES OF THE DIAGNOSTIC IONS FOUND FOR 4-HYDROXY-HEXENAL (HHE) MODIFICATIONS ON LYSINE (A), HISTIDINE (H) AND ARGININE (R).</b> ....	88
<b>FIGURE 2.12. MULTIPLE REACTION MONITORING (MRM) FOR THE IDENTIFICATION OF THREE HUMAN SERUM ALBUMIN PEPTIDES MODIFIED BY ACROLEIN.</b> UNTREATED AND TREATED HSA WITH ACR AT 8 MM FOR	

2 HOURS. KLAASQAALG MODIFIED ON LYSINE RESIDUE (A), RHPDYSVLLLLR MODIFIED ON HISTIDINE RESIDUE (B) AND KVPQVSTPTLVEVSR MODIFIED ON THE LYSINE (C). .....	91
<b>FIGURE 2.13. MS/MS SIGNAL INTENSITIES PRODUCED BY THREE HUMAN SERUM ALBUMIN PEPTIDES TREATED WITH DIFFERENT CONCENTRATIONS OF ACROLEIN (0 mM, 4 mM, 8 mM AND 14 mM).</b> TWO TRANSITIONS FOR PEPTIDE-SPECIFIC PRODUCT IONS (GREEN AND BLUE) AND ONE TRANSITION FOR RESIDUE AND MODIFICATION-SPECIFIC REPORT ION (YELLOW). KLAASQAALG MODIFIED ON LYSINE RESIDUE (A), RHPDYSVLLLLR MODIFIED ON HISTIDINE RESIDUE (B) AND KVPQVSTPTLVEVSR MODIFIED ON THE LYSINE (C). (N=1). .....	93
<b>FIGURE 2.14. MULTIPLE REACTION MONITORING (MRM) FOR THE IDENTIFICATION OF THREE HUMAN SERUM ALBUMIN PEPTIDES MODIFIED BY ACROLEIN IN HUMAN PLASMA.</b> UNTREATED AND TREATED HUMAN PLASMA WITH ACR AT 8 mM FOR 2 HOURS. KLAASQAALG MODIFIED ON LYSINE RESIDUE (A), RHPDYSVLLLLR MODIFIED ON HISTIDINE RESIDUE (B) AND KVPQVSTPTLVEVSR MODIFIED ON THE LYSINE RESIDUE (C). .....	95
<b>FIGURE 2.15. MS/MS SIGNAL INTENSITIES PRODUCED BY THREE HUMAN SERUM ALBUMIN PEPTIDES IDENTIFIED IN HUMAN PLASMA AFTER TREATMENT WITH DIFFERENT CONCENTRATIONS OF ACROLEIN (0 mM, 4 mM, 8 mM AND 14 mM).</b> TWO TRANSITIONS FOR PEPTIDE-SPECIFIC PRODUCT IONS (GREEN AND BLUE) AND ONE TRANSITION FOR RESIDUE AND MODIFICATION-SPECIFIC REPORT ION (YELLOW). KLAASQAALG MODIFIED ON LYSINE RESIDUE (A), RHPDYSVLLLLR MODIFIED ON HISTIDINE RESIDUE (B) AND KVPQVSTPTLVEVSR MODIFIED ON THE LYSINE (C). (N=1). .....	97
<b>FIGURE 3.1. COREY-SUGGS OXIDATION OF HEXADECANOL TO HEXADECANAL USING PYRIDINIUM CHLOROCHROMATE AS CATALYST.</b> .....	111
<b>FIGURE 3.2. <sup>1</sup>H NMR SPECTRUM OF THE STARTING MATERIAL HEXADECANOL (A) AND THE PRODUCT OF ITS OXIDATION, HEXADECANAL (B).</b> A- <sup>1</sup> H NMR: 3.63 PPM (2H, T, CH <sub>2</sub> ); 1.56 PPM (2H, M, CH <sub>2</sub> ); 1.28 PPM (26H, M, CH <sub>2</sub> ); 0.88 PPM (3H, T, CH <sub>3</sub> ). B- <sup>1</sup> H NMR: 9.77 PPM (1H, T, C(=O)H); 2.40 PPM (2H, M, CH <sub>2</sub> ); 1.63 PPM (2H, M, CH <sub>2</sub> ); 1.28 PPM (24H, M, CH <sub>2</sub> ); 0.88 PPM (3H, T, CH <sub>3</sub> ). INTERNAL REFERENCE (TMS) AT 0.0 PPM. ....	112
<b>FIGURE 3.3. INTRODUCTION OF A PROTECTIVE GROUP TO HEXADECANAL BY TRIMETHYL ORTHOFORMATE (TMOF) IN METHANOL AND USING P-TOLUENESULFONIC ACID (PTSA) AS CATALYST, RESULTING IN HEXADECANAL DIMETHYL ACETAL.</b> .....	113
<b>FIGURE 3.4. <sup>1</sup>H NMR SPECTRUM OF HEXADECANAL DIMETHYL ACETAL, PRODUCT OF THE REACTION OF HEXADECANAL WITH TMOF IN THE PRESENCE OF PTSA.</b> <sup>1</sup> H NMR: 4.36 PPM (1H, T, (OR')CH(OR'')); 3.31 PPM (6H, s, OCH <sub>3</sub> ); 2.30 PPM (2H, TD, CH <sub>2</sub> ); 1.59 PPM (2H, TT, CH <sub>2</sub> ); 1.26 PPM (24H, M, CH <sub>2</sub> ); 0.88 PPM (3H, T, CH <sub>3</sub> ). INTERNAL REFERENCE (TMS) AT 0.0 PPM. ....	113
<b>FIGURE 3.5. CHLORINATION REACTION OF HEXADECANAL DIMETHYL ACETAL TO A 2-CHLORO-ALDEHYDE DIMETHYL ACETAL, USING MANGANESE CHLORIDE (MnCl<sub>2</sub>) AND MANGANESE OXIDE (MnO<sub>2</sub>), IN A MIXTURE OF ACETONITRILE AND METHANOL, AND TRIMETHYLSILYL CHLORIDE (TMSC) AS CATALYST.</b> .....	114
<b>FIGURE 3.6. <sup>1</sup>H NMR SPECTRUM OF 2-CHLOROHEXADECANAL DIMETHYL ACETAL, THE PRODUCT OF THE CHLORINATING OF HEXADECANAL DIMETHYL ACETAL.</b> <sup>1</sup> H NMR: A- 3.61 PPM (6H, s, OCH <sub>3</sub> ); B- 5.23 PPM (1H, D, (OR')CH(OR'')); C- 3.82 PPM (1H, M, CHCL); D- 1.55 PPM (2H, M, CH <sub>2</sub> ); E- 1.20 PPM	

(24H, M, CH <sub>2</sub> ); F- 0.82 PPM (3H, T, CH <sub>3</sub> ); A- 3.38 PPM (6H, S, OCH <sub>3</sub> ); B- 4.25 PPM (1H, T, (OR')CH(OR'')); C- 2.25 PPM (2H, M, CH <sub>2</sub> ). INTERNAL REFERENCE (TMS) AT 0.0 PPM. ....	114
<b>FIGURE 3.7. ACID HYDROLYSIS OF 2-CHLOROHEXADECANAL DIMETHYL ACETAL WITH TFA TO OBTAIN 2-CHLOROHEXADECANAL. THE LAST STEP OF THE MULTI-STEP SYNTHESIS. ....</b>	<b>115</b>
<b>FIGURE 3.8. <sup>1</sup>H NMR SPECTRUM OF 2-CHLOROHEXADECANAL, THE PRODUCT OF TFA ACID HYDROLYSIS REACTION. <sup>1</sup>H NMR: A- 9.28 PPM (1H, D, C(=O)H); B- 4.89 PPM (1H, M, CHCL); C- 1.45 PPM (2H, M, CH<sub>2</sub>); D- 1.06 PPM (24H, M, CH<sub>2</sub>); E- 0.68 PPM (3H, T, CH<sub>3</sub>). 1- 3.49 PPM (6H, S, CH<sub>3</sub>); 2- 5.10 PPM (1H, D, OCH); 3- 3.96 PPM (1H, M, CHCL). I- 3.36 PPM (6H, S, CH<sub>3</sub>); II- 3.77 PPM (1H, T, OCH); III- 2.19 PPM (2H, M, CH<sub>2</sub>). INTERNAL REFERENCE (TMS) AT 0.0 PPM. ....</b>	<b>116</b>
<b>FIGURE 3.9. GC-FID SPECTRA OF 2-CHLOROHEXADECANAL AS A PRODUCT OF ACID HYDROLYSIS, THE LAST STEP OF A MULTI-STEP REACTION. GC DATA ACQUIRED WITH AN ISOTHERMAL ANALYSIS AT 260 °C FOR 2 MINUTES. A – HEXADECANOL (1.06 MIN, 99.9%); B – HEXADECANAL (0.99 MIN, 37.9%; 1.02 MIN, 58.5%); C – PRODUCT OF THE ACID HYDROLYSIS (0.95 MIN, 7.4%; 1.05 MIN, 1.8 %, 1.12 MIN, 60.7 %; 1.19 MIN, 30%). ....</b>	<b>117</b>
<b>FIGURE 3.10. FIRST ATTEMPT AT THE DIRECT CONVERSION OF HEXADECANOL TO A-CHLOROHEXADECANAL AND HEXADECANAL. ....</b>	<b>118</b>
<b>FIGURE 3.11. <sup>1</sup>H NMR SPECTRUM OF 2-CHLOROHEXADECANAL, THE PRODUCT OF DIRECT CONVERSION FROM HEXADECANOL (1<sup>ST</sup> APPROACH). <sup>1</sup>H NMR: A- 9.5 PPM (1H, D, C(=O)H); B- 4.2 PPM (1H, M, CHCL); C- 1.8 PPM (2H, M, CH<sub>2</sub>); D- 1.3 PPM (24H, M, CH<sub>2</sub>); E- 0.9 PPM (3H, T, CH<sub>3</sub>). A- 9.7 PPM (1H, T, C(=O)H); B- 2.4 PPM (2H, M, CH<sub>2</sub>); C- 1.6 PPM (2H, M, CH<sub>2</sub>). INTERNAL REFERENCE (TMS) AT 0.0 PPM. ....</b>	<b>119</b>
<b>FIGURE 3.12. GC-FID SPECTRA OF 2-CHLOROHEXADECANAL AS A PRODUCT OF DIRECT CONVERSION FROM HEXADECANOL. GC DATA ACQUIRED WITH A GRADIENT STARTING FROM 150 °C TO 300 °C AT A RATE OF 25 °C/MIN, TOTAL RUN TIME OF 14.5 MINUTES. A – HEXADECANOL (6.3 MIN, 99.7 %); B – HEXADECANAL (5.9 MIN, 93.9 %); C – PRODUCT OF THE DIRECT CONVERSION (5.9 MIN, 8%; 6.3 MIN, 9.5 %; 6.7 MIN, 59.1 %; 6.9 MIN, 23.4 %). ....</b>	<b>120</b>
<b>FIGURE 3.13. SECOND ATTEMPT AT THE DIRECT CONVERSION OF HEXADECANOL TO A-CHLOROHEXADECANAL AND HEXADECANAL. ....</b>	<b>121</b>
<b>FIGURE 3.14. <sup>1</sup>H NMR SPECTRUM OF 2-CHLOROHEXADECANAL, THE PRODUCT OF DIRECT CONVERSION FROM HEXADECANOL (2<sup>ND</sup> APPROACH). <sup>1</sup>H NMR: A- 9.5 PPM (1H, D, C(=O)H); B- 4.2 PPM (1H, M, CHCL); C- 1.8 PPM (2H, M, CH<sub>2</sub>); D- 1.3 PPM (24H, M, CH<sub>2</sub>); E- 0.9 PPM (3H, T, CH<sub>3</sub>). A- 9.7 PPM (1H, T, C(=O)H); B- 2.4 PPM (2H, M, CH<sub>2</sub>); C- 1.6 PPM (2H, M, CH<sub>2</sub>). INTERNAL REFERENCE (TMS) AT 0.0 PPM. ....</b>	<b>122</b>
<b>FIGURE 3.15. GC-FID SPECTRA OF 2-CHLOROHEXADECANAL AS A PRODUCT OF DIRECT CONVERSION FROM HEXADECANOL. GC DATA ACQUIRED WITH A GRADIENT STARTING FROM 150 °C TO 300 °C AT A RATE OF 25 °C/MIN, TOTAL RUN TIME OF 14.5 MINUTES. THREE PEAKS WERE IDENTIFIED: HEXADECANAL AT 5.9 MIN, 5.7%; HEXADECANOL AT 6.3 MIN, 1.7%, 2-CHLOROHEXADECANAL AT 6.7 MIN, 60.9%. OTHER THREE PEAKS AT AROUND 6.9 MIN WITH A TOTAL OF 12.3% WERE IDENTIFIED AS UNKNOWN IMPURITIES. ....</b>	<b>122</b>

<b>FIGURE 3.16. SDS-PAGE (DENATURING GEL ELECTROPHORESIS) RESULTS FOR LYSOZYME UNTREATED AND TREATED WITH 8 MM OR 16 MM 2-CHLORO-HEXADECANAL (2-CLHDA) FOR 2, 4 OR 24 HOURS. GEL STAINED WITH COOMASSIE BLUE STAINING. THE HIGHLIGHTED SECTIONS BOXED IN WHITE WERE CUT FOR FURTHER ANALYSIS.....</b>	<b>123</b>
<b>FIGURE 3.17. MS/MS SPECTRA OF LYSOZYME TRYPTIC PEPTIDE. CELAAAMKR MODIFIED ON A LYSINE RESIDUE BY 2-CHLOROHEXADECANAL BY SCHIFF BASE FORMATION WITH LOSS OF HCL FOLLOWED BY NABH<sub>4</sub> REDUCTION (+ 222 DA). THE Y AND B IONS INDICATED BY THE ARROWS CONFIRM THE PEPTIDE SEQUENCE AND THE MODIFICATION ON THE CYSTEINE RESIDUE. IMMONIUM IONS FOR HEXADECANAL-MODIFIED LYSINE FOUND AT M/Z 323 DA. ....</b>	<b>125</b>
<b>FIGURE 3.18. PROPOSED STRUCTURE FOR THE REPORTER ION OBSERVED AT M/Z 323 DA. A) STRUCTURE OF THE LYSINE RESIDUE IMMONIUM ION (M/Z 101.1 DA). B) STRUCTURE OF THE 2-CLHDA-LYSINE REPORTER ION (M/Z 323 DA).....</b>	<b>125</b>
<b>FIGURE 3.19. SDS-PAGE (DENATURING GEL ELECTROPHORESIS) RESULTS FOR HUMAN SERUM ALBUMIN UNTREATED AND TREATED WITH 8 MM OR 16 MM 2-CHLORO-HEXADECANAL FOR 2, 4 OR 24 HOURS. GEL STAINED WITH COOMASSIE BLUE STAINING. THE HIGHLIGHTED SECTIONS BOXED IN WHITE WERE CUT FOR FURTHER ANALYSIS.....</b>	<b>126</b>
<b>FIGURE 3.20. STRUCTURE OF UNREDUCED AND REDUCED HEXADECANAL AND 2-CHLOROHEXADECANAL ADDUCTS. (A) 2-CHLOROHEXADECANAL ADDUCTS WITH AMINES BY SCHIFF BASE FORMATION FOLLOWED BY IMINE REDUCTION BUT NOT THE CARBON CHAIN UNSATURATION; (B) 2-CHLOROHEXADECANAL ADDUCTS WITH THIOL (CYSTEINE RESIDUE) BY NUCLEOPHILIC ATTACK OF C-CL FOLLOWED BY REDUCTION OF THE REMAINING CARBONYL; (C) HEXADECANAL ADDUCT WITH AMINE BY SCHIFF BASE FORMATION FOLLOWED BY IMINE REDUCTION. ....</b>	<b>130</b>
<b>FIGURE 4.1. BASE PEAK CHROMATOGRAMS RESULTING FROM ANION EXCHANGE CHROMATOGRAPHY SEPARATION OF DIFFERENT PROTEIN ISOFORMS. RETENTION TIME 0.0 TO 10.0 MINUTES. PROTEIN USED WERE INSULIN, UBIQUITIN AND HUMAN SERUM ALBUMIN.....</b>	<b>140</b>
<b>FIGURE 4.2. BASE PEAK CHROMATOGRAMS FROM ANION EXCHANGE CHROMATOGRAPHY SEPARATION OF UNTREATED AND HHE OR HNE TREATED PROTEIN. A-INSULIN; B-UBIQUITIN; C-HUMAN SERUM ALBUMIN. RETENTION TIMES VARYING FROM 0.0 TO 14.0 MINUTES. UNTREATED SAMPLES DATA IN BLACK, HHE TREATMENT DATA IN RED AND HNE TREATMENT IN BLUE. EACH PEAK WAS ASSIGNED A NUMBER FOR LATER IDENTIFICATION.....</b>	<b>141</b>
<b>FIGURE 4.3. MS SPECTRA OF UNTREATED OR HHE/HNE-TREATED INTACT PROTEIN SEPARATED BY AEC. THE SPECTRA CORRESPOND TO THE PEAKS IN FIGURE 4.2 AND THESE ARE LABELLED WITH THE SAME NUMBER AS THE CORRESPONDING CHROMATOGRAPHIC PEAK. (A) INSULIN (z=4+), ISOFORM IN PEAKS 3 AND 4 FROM FIGURE 2 ARE SHOWN; (B) UBIQUITIN (z=6+), MS DATA FROM SINGLE PEAK IN CHROMATOGRAM.; (C) HSA, MS DATA FROM PEAK AT HIGHEST RELATIVE ABUNDANCE AND FOR ALDEHYDE-TREATED SAMPLES, THE SAME RETENTION TIME WAS SELECTED. UNTREATED SAMPLES DATA IN BLACK, HHE TREATMENT DATA IN RED AND HNE TREATMENT IN BLUE.....</b>	<b>142</b>
<b>FIGURE 4.4. BASE PEAK CHROMATOGRAMS RESULTING FROM CATION EXCHANGE CHROMATOGRAPHY SEPARATION OF DIFFERENT PROTEIN ISOFORMS. RETENTION TIME WAS 0.0 TO 10.0 MINUTES. PROTEIN USED WERE INSULIN, UBIQUITIN AND HUMAN SERUM ALBUMIN. ....</b>	<b>143</b>

<b>FIGURE 4.5. BASE PEAK CHROMATOGRAMS FROM CATION EXCHANGE CHROMATOGRAPHY SEPARATION OF UNTREATED AND HHE OR HNE TREATED PROTEIN. A-INSULIN; B-UBIQUITIN. RETENTION TIMES VARIED FROM 1.0 TO 9.0 MINUTES. UNTREATED SAMPLES DATA IN BLACK, HHE TREATMENT DATA IN RED AND HNE TREATMENT IN BLUE. EACH PEAK WAS ASSIGNED A NUMBER FOR LATER IDENTIFICATION. ....</b>	<b>144</b>
<b>FIGURE 4.6. MS SPECTRA OF UNTREATED OR HHE/HNE-TREATED INTACT PROTEIN SEPARATED BY CEC. THE SPECTRA CORRESPOND TO THE PEAKS IN FIGURE 4.5 AND THESE ARE LABELLED WITH THE SAME NUMBER AS THE CORRESPONDING CHROMATOGRAPHIC PEAK. (A) INSULIN (z=3+), MS DATA FOR SINGLE CHROMATOGRAM PEAK FOR UNTREATED AND HHE-TREATED AND FOR THE TWO PEAKS FOR HNE-TREATED; (B) UBIQUITIN (z=6+), MS DATA FROM THE SINGLE PEAK 1 FOR UNTREATED PROTEIN, PEAKS 1 AND 2 FOR HHE-TREATED PROTEIN AND PEAKS 1, 2, 3 AND 5 FOR HNE-TREATED PROTEIN. UNTREATED SAMPLES DATA IN BLACK, HHE TREATMENT DATA IN RED AND HNE TREATMENT IN BLUE. ....</b>	<b>145</b>
<b>FIGURE 4.7. BASE PEAK CHROMATOGRAMS FROM REVERSE PHASE CHROMATOGRAPHY SEPARATION OF UNTREATED AND HHE OR HNE TREATED PROTEIN. A-INSULIN; B-UBIQUITIN; C-HSA. RETENTION TIMES VARYING FROM 2.5 TO 5.5 MINUTES UNTREATED SAMPLES DATA IN BLACK, HHE TREATMENT DATA IN RED AND HNE TREATMENT IN BLUE. MORE THAN ONE PEAK WAS OBSERVED IN EACH CHROMATOGRAM; THEREFORE A NUMBER WAS ASSIGNED FOR LATER IDENTIFICATION. ....</b>	<b>147</b>
<b>FIGURE 4.8. MS SPECTRA OF UNTREATED OR HHE/HNE-TREATED INTACT PROTEIN SEPARATED BY REVERSE PHASE CHROMATOGRAPHY. THE SPECTRA CORRESPOND TO THE PEAKS IN FIGURE 4.7 AND THESE ARE LABELLED WITH THE SAME NUMBER AS THE CORRESPONDING CHROMATOGRAPHIC PEAK. A-INSULIN (z=4+), MS DATA SHOWN FOR PEAK 1 FOR UNTREATED, PEAKS 1 AND 3 FOR HHE-TREATED AND PEAKS 1, 3 AND 5 FOR HNE-TREATED; B-UBIQUITIN (z=6+), MS DATA SHOWN FOR PEAK 1 FOR UNTREATED, PEAKS 1 AND 2 FOR HHE-TREATED AND PEAKS 1, 2, 3 AND 5 FOR HNE-TREATED. UNTREATED SAMPLES DATA IN BLACK, HHE TREATMENT DATA IN RED AND HNE TREATMENT IN BLUE. ....</b>	<b>148</b>
<b>FIGURE 4.9. PERCENTAGE OF HSA MODIFIED PEPTIDES DETECTED AFTER SMART AND IN-GEL DIGESTION. ....</b>	<b>154</b>
<b>FIGURE 5.1. MS/MS SPECTRA OF MODIFIED PYRUVATE KINASE TRYPTIC PEPTIDES. LC-MS/MS WAS CARRIED OUT AS DESCRIBED IN THE EXPERIMENTAL SECTION, AND PEPTIDES IDENTIFIED BY MASCOT SEARCHES AS CONTAINING ADDUCTS WERE MANUALLY VALIDATED. (A) CLAAALIVLTESGR MODIFIED ON THE CYSTEINE RESIDUE BY ACROLEIN FORMING A MICHAEL ADDUCT; (B) MICHAEL ADDUCT OF HHE OF THE CYSTEINE RESIDUE OF CDENILWLDYK; (C) GDLGIEIPAЕКVFLAQK MODIFIED BY MDA AS A SCHIFF'S BASE ON LYSINE. THE Y AND B IONS INDICATED BY THE ARROWS CONFIRM THE PEPTIDE SEQUENCE AND THE MODIFICATION ON THE CYSTEINE OR LYSINE RESIDUES RESPECTIVELY. FIGURE FROM [422]. ....</b>	<b>168</b>
<b>FIGURE 5.2. MAPPING OF LIPOXIDATION ADDUCTS TO THE CRYSTAL STRUCTURE OF PYRUVATE KINASE. BACKBONE STRUCTURE WITH MODIFIED RESIDUES INDICATED IN SPACE-FILL FORM, SHOWING THE LOCATION OF ADDUCTS OF ACROLEIN (A), HHE (B) AND MDA (C). THE MODIFIED RESIDUES ARE COLOR-CODED WITH ORANGE INDICATING THOSE FOUND ONLY AT 380 μM, GREEN FOR THOSE FOUND</b>	

ADDITIONALLY AT 760  $\mu$ M AND BLUE FOR ONES FOUND ADDITIONALLY AT 5 MM. FIGURE FROM [422].  
.....171

**FIGURE 5.3. SPACE FILLING MODELS OF PYRUVATE KINASE SHOWING SURFACE HYDROPHOBICITY AND SITES OF ADDUCTION AT HIGH ALDEHYDE CONCENTRATIONS.** SURFACE VIEWS WITH INCREASING HYDROPHOBICITY SHOWN IN DARKER RED. THE LOCATION OF ADDUCTS OF ACROLEIN (A), HHE (B) AND MDA (C) ARE SHOWN COLOR-CODED WITH ORANGE INDICATING THOSE FOUND ONLY AT 380  $\mu$ M, GREEN FOR THOSE FOUND ADDITIONALLY AT 760  $\mu$ M AND BLUE FOR ONES FOUND ADDITIONALLY AT 5 MM. FIGURE FROM [422].  
.....173

**FIGURE 5.4. INVERSE RELATIONSHIP BETWEEN THE DOSE-DEPENDENT EFFECT OF ALDEHYDES ON THE ACTIVITY OF PYRUVATE KINASE IN VITRO AND THE PERCENTAGE OF MODIFIED PYRUVATE KINASE PEPTIDES IDENTIFIED.** PYRUVATE KINASE WAS TREATED WITH 38  $\mu$ M, 380  $\mu$ M, 760  $\mu$ M AND 5 MM FINAL CONCENTRATIONS OF ACROLEIN, 4-HYDROXY-HEXENAL OR MALONDIALDEHYDE FOR 10 MINUTES BEFORE THE ASSESSMENT OF ITS ACTIVITY BY SPECTROPHOTOMETRIC ASSAY OF NADH OXIDATION AT 340 NM (N=4; MEAN  $\pm$  SEM; \* P<0.1 \*\* P<0.01 \*\*\* P<0.001 \*\*\*\* P<0.0001). PEPTIDE MODIFICATION WAS DETERMINED FROM THE TOTAL NUMBER OF MODIFIED PEPTIDES AS A % OF THE TOTAL MODIFIABLE PEPTIDES IN THE SEQUENCE. FIGURE FROM [422].  
.....175

**FIGURE 5.5. DOSE-DEPENDENT EFFECT OF SHORT TREATMENTS WITH ACROLEIN, 4-HYDROXY-HEXENAL AND MALONDIALDEHYDE ON THE ACTIVITY OF IN-VITRO PYRUVATE KINASE.** PYRUVATE KINASE WAS TREATED WITH 2  $\mu$ M, 20  $\mu$ M, 100  $\mu$ M, 200  $\mu$ M, 500  $\mu$ M AND 1 MM OF EACH ALDEHYDE FOR 10 MINUTES BEFORE THE ASSESSMENT OF ITS ACTIVITY (N=3; MEAN  $\pm$  SEM; \* P<0.1 \*\* P<0.01 \*\*\* P<0.001 \*\*\*\* P<0.0001). FIGURE FROM [422].  
.....176

**FIGURE 5.6. EFFECT OF LONGER TREATMENTS WITH ACROLEIN, 4-HYDROXY-HEXENAL AND MALONDIALDEHYDE ON THE ACTIVITY OF PYRUVATE KINASE IN VITRO.** PYRUVATE KINASE WAS TREATED WITH 2  $\mu$ M, 10  $\mu$ M, 20  $\mu$ M AND 100  $\mu$ M OF EACH ALDEHYDE FOR 30 MINUTES, 1 HOUR, 2 HOURS OR 4 HOURS BEFORE THE ASSESSMENT OF ITS ACTIVITY (N=3; MEAN  $\pm$  SEM; \* P<0.1 \*\* P<0.01, \*\*\* P<0.001 AND \*\*\*\* P<0.0001). FIGURE FROM [422].  
.....178

**FIGURE 5.7. INVERSE RELATIONSHIP BETWEEN THE DOSE-DEPENDENT EFFECT OF ALDEHYDES ON THE ACTIVITY OF PYRUVATE KINASE IN VITRO AND THE PERCENTAGE OF MODIFIED PYRUVATE KINASE PEPTIDES IDENTIFIED.** PYRUVATE KINASE WAS TREATED WITH 2  $\mu$ M, 10  $\mu$ M, 20  $\mu$ M AND 100  $\mu$ M OF EACH ALDEHYDE FOR 2 HOURS OR 4 HOURS BEFORE THE ASSESSMENT OF ITS ACTIVITY (N=3; MEAN  $\pm$  SEM; \* P<0.1 \*\* P<0.01, \*\*\* P<0.001 AND \*\*\*\* P<0.0001). FIGURE FROM [422].  
.....183

**FIGURE 5.8. MAPPING OF LIPOXIDATION ADDUCTS FORMED AT LOW CONCENTRATIONS FOR 4 H TREATMENTS.** BACKBONE STRUCTURE WITH MODIFIED RESIDUES INDICATED IN SPACE-FILL FORM, SHOWING THE LOCATION OF ADDUCTS OF ACROLEIN AT 2 H (A); ACROLEIN AT 4 H (B) AND HHE AT BOTH TIME POINTS (C). THE MODIFIED RESIDUES ARE COLOR-CODED WITH YELLOW INDICATING THOSE FOUND ONLY AT 10  $\mu$ M, ORANGE FOR THOSE FOUND ADDITIONALLY AT 20  $\mu$ M, GREEN FOR THOSE FOUND ADDITIONALLY AT 100  $\mu$ M AND BLUE FOR ONES FOUND ADDITIONALLY AT 200  $\mu$ M. FIGURE FROM [422].  
.....184

**FIGURE 5.9. SPACE FILLING MODELS OF PYRUVATE KINASE SHOWING SURFACE HYDROPHOBICITY AND SITES OF ADDUCTION AT LOW TREATMENT CONCENTRATIONS.** SURFACE VIEWS WITH HYDROPHOBICITY

MAPPED IN RED AND SHOWING THE LOCATION OF ADDUCTS OF ACROLEIN (A), HHE (B) AND MDA (C). THE MODIFIED RESIDUES ARE COLOR-CODED WITH YELLOW INDICATING THOSE FOUND ONLY AT 10  $\mu$ M, ORANGE FOR THOSE FOUND ADDITIONALLY AT 20  $\mu$ M, GREEN FOR THOSE FOUND ADDITIONALLY AT 100  $\mu$ M AND BLUE FOR ONES FOUND ADDITIONALLY AT 200  $\mu$ M. FIGURE FROM [422]. ..... 185

**FIGURE 5.10. DOSE- AND TIME-DEPENDENCE OF ALDEHYDE TREATMENT ON THE ACTIVITY OF PYRUVATE KINASE AND VIABILITY OF ALDEHYDE-TREATED MCF-7 CELLS.** PYRUVATE KINASE ACTIVITY IS SHOWN ON THE LEFT FOR ACROLEIN (A), 4-HYDROXYL-2(E)-HEXENAL (C) AND MALONDIALDEHYDE (E), WHILE CELL VIABILITY IS SHOWN ON THE RIGHT: ACROLEIN (B), 4-HYDROXYL-2(E)-HEXENAL (D) AND MALONDIALDEHYDE (F). CELLS WERE TREATED WITH 2  $\mu$ M, 10  $\mu$ M, 20  $\mu$ M, 100  $\mu$ M AND 200  $\mu$ M OF EACH ALDEHYDE FOR 2 HOURS OR 24 HOURS BEFORE PROTEINS WERE EXTRACTED AND 10  $\mu$ G OF EXTRACT WERE USED FOR PYRUVATE KINASE ACTIVITY TO BE ASSESSED. CELL VIABILITY ASSAYS WERE PERFORMED WITH N=3 FOR MDA AND HHE AND N=4 FOR ACR (MEAN  $\pm$  SEM; \* P<0.1 \*\* P<0.01, \*\*\* P<0.001 AND \*\*\*\* P<0.0001). \* COMPARISON BETWEEN TREATMENTS AND CONTROL FOR EACH INCUBATION TIME. # COMPARISON BETWEEN INCUBATION TIMES. FIGURE FROM [422] (THIS DATA WAS ACQUIRED BY THE CO-AUTHORS TANZIM AHMED AND WILL L DANN AND USED IN THIS THESIS WITH THEIR PERMISSION). ..... 187

**FIGURE 5.11. MS/MS SPECTRA OF DIFFERENT PYRUVATE KINASE TRYPTIC PEPTIDE FROM MCF-7 CELLULAR EXTRACTS.** CDENILWLDYK (A) AND AEGSDVANAVLDGADCIMLSGETAK (B) MODIFIED ON A CYSTEINE RESIDUE BY ACR. THE Y AND B IONS INDICATED BY THE ARROWS CONFIRM THE PEPTIDE SEQUENCE AND THE MODIFICATION ON THE CYSTEINE RESIDUE. FIGURE FROM [422]. 188

**FIGURE 5.12. EXTRACELLULAR ACIDIFICATION RATE (ECAR) PROFILE OF UNTREATED AND ACROLEIN-TREATED MCF-7.** CELLS WERE TREATED WITH 2, 10 OR 100 mM ACROLEIN PRIOR TO THE ASSAY. ADDITION OF GLUCOSE AT 15 MIN PROMOTED GLYCOLYSIS AND THE ACIDIFICATION INCREASE BY RELEASE OF PROTONS (H<sup>+</sup>) BY THE CELLS. OLIGOMYCIN INHIBITS ATP SYNTHASE, DRIVING GLYCOLYSIS TO ITS MAXIMUM RATE. LATER, A COMPETITIVE INHIBITOR OF GLUCOSE (2-DG) IS ADDED TO SHUT DOWN GLYCOLYSIS. .... 189

**FIGURE 5.13. REPRESENTATIVE <sup>1</sup>H NMR SPECTRUM OF THE METABOLOME OF MCF-7 CELLS.** SOME ASSIGNMENTS ARE INDICATED: THREE-LETTER CODES ARE USED FOR AMINO ACIDS, ADP - ADENOSINE DIPHOSPHATE, ATP - ADENOSINE TRIPHOSPHATE, BCAA - BRANCHED CHAIN AMINO ACIDS, NAD - NICOTINAMIDE ADENINE DINUCLEOTIDE, PCHO - PHOSPHOCHOLINE. .... 190

**FIGURE 5.14. <sup>1</sup>H NMR SPECTRA OF THE METABOLOME OF MCF-7 CELLS UNTREATED AND UPON TREATMENT WITH 2 mM, 10 mM AND 100 mM ACROLEIN FOR TWO HOURS.** ..... 192

**FIGURE 5.15. DOSE AND TIME-DEPENDENCE OF ACROLEIN TREATMENT ON THE METABOLISM OF MCF-7 CELLS.** CELLS WERE EXPOSED TO 2  $\mu$ M, 10  $\mu$ M AND 100  $\mu$ M OF ACROLEIN FOR 2 HOURS OR 24 HOURS FOLLOWED BY METABOLITES EXTRACTION AND ANALYSED BY <sup>1</sup>H NMR. (N=3; MEAN  $\pm$  SEM; \* P<0.1 \*\* P<0.01 \*\*\* P<0.001 \*\*\*\* P<0.0001). \* COMPARISON BETWEEN TREATMENTS AND CONTROL FOR EACH INCUBATION TIME. # COMPARISON BETWEEN INCUBATION TIMES. .... 193

**FIGURE 5.16. CELLULAR GLYCOLYSIS AND TCA CYCLE METABOLISM.** DIAGRAM REPRESENTING THE METABOLIC CHANGES DETECTED BY <sup>1</sup>H NMR AND SUMMARIZING THE CHANGES DISCUSSED ABOVE. GREEN ARROWS REPRESENT THE MOST ACTIVE REACTIONS ACCORDING TO THE OBSERVED CHANGES

IN THE LEVELS OF EACH METABOLITE. THESE POINT TO A CHANGE IN METABOLISM TO COMPENSATE THE LOSS OF PYRUVATE KINASE BY PROMOTING PYRUVATE FORMATION THROUGH AMINO ACIDS AND FUELLING THE TCA CYCLE METABOLISM VIA OTHER WAYS OTHER THAN GLYCOLYSIS. THE CHANNELLING OF GLYCOLYSIS INTERMEDIATES INTO THE PENTOSE PHOSPHATE PATHWAY WAS STUDIED AND IS PRESENTED IN GREY. ....200

**FIGURE 6.1. EFFECT OF ACROLEIN, 4-HYDROXYHEXENAL AND MALONDIALDEHYDE ON VIMENTIN ORGANIZATION IN CELLS.** SW13/CL.2 CELLS STABLY TRANSFECTED WITH RFP//VIMENTIN WT WERE TREATED WITH 10 mM ACR AND HHE AND 30 mM MDA FOR 1, 2 OR 24 HOURS AFTER WHICH CELLS WERE FIXES AND VIMENTIN NETWORK ANALYSED BY IMMUNOFLUORESCENCE. SCALE BARS, 20 MM. V9 ANTIBODY DETECTED VIMENTIN (GREEN) AND NUCLEI WERE COUNTERSTAINED WITH DAPI (BLUE). 208

**FIGURE 6.2. COMPARISON OF ACTIN AND VIMENTIN NETWORKS ORGANIZATION AFTER ACROLEIN, 4-HYDROXYHEXENAL AND MALONDIALDEHYDE TREATMENT.** SW13/CL.2 CELLS STABLY TRANSFECTED WITH RFP//VIMENTIN WT WERE TREATED WITH 10 mM ACR AND HHE AND 30 mM MDA FOR 1, 2 OR 24 HOURS, AFTER WHICH CELLS WERE FIXED AND THE VIMENTIN NETWORK ANALYSED BY IMMUNOFLUORESCENCE. SCALE BARS, 20 MM. V9 ANTIBODY (1:200) DETECTED VIMENTIN (GREEN) AND FILAMENTOUS ACTIN WAS STAINED WITH PHALLOIDIN-ALEXA568 (RED).....209

**FIGURE 6.3. RELATIVE QUANTIFICATION OF VIMENTIN CELL DISTRIBUTION.** VARIANCE IN VIMENTIN/ACTIN RATIO TO ASSESS THE EFFECT OF THE ALDEHYDE'S TREATMENT ON THE VIMENTIN NETWORK. (A) VIMENTIN/ACTIN RATIO EXPRESSED IN PERCENTAGE FOR CONTROL (NO TREATMENT), ACR AT 10 MM, MDA AT 30 MM AND HHE 10 MM; (B) VIMENTIN/ACTIN RATIO NORMALIZED AS PERCENTAGE OF CONTROL, COMPARISON BETWEEN TIME POINTS. (N=9; MEAN ± SEM; \* P<0.1 \*\* P<0.01, \*\*\* P<0.001 AND \*\*\*\* P<0.0001) \* COMPARISON OF CONDITIONS WITH CONTROL; # COMPARISON BETWEEN CONDITIONS. ....210

**FIGURE 6.4. EFFECT OF ACROLEIN, 4-HYDROXYHEXENAL AND MALONDIALDEHYDE ON VIMENTIN ORGANIZATION IN CELLS.** SW13/CL.2 CELLS STABLY TRANSFECTED WITH RFP//VIMENTIN CYS328SER (C328S) WERE TREATED WITH 10 MM ACR AND HHE AND 30 MM MDA FOR 1, 2 OR 24 HOURS AFTER WHICH CELLS WERE FIXED AND VIMENTIN NETWORK ANALYSED BY IMMUNOFLUORESCENCE. SCALE BARS, 20 MM. V9 ANTIBODY (1:200) DETECTED VIMENTIN (GREEN) AND NUCLEI WERE COUNTERSTAINED WITH DAPI (BLUE). ....211

**FIGURE 6.5. COMPARISON OF ACTIN AND VIMENTIN NETWORKS ORGANIZATION AFTER ACROLEIN, 4-HYDROXYHEXENAL AND MALONDIALDEHYDE TREATMENT.** SW13/CL.2 CELLS STABLY TRANSFECTED WITH RFP//VIMENTIN CYS328SER (C328S) WERE TREATED WITH 10 MM ACR AND HHE AND 30 MM MDA FOR 1, 2 OR 24 HOURS, AFTER WHICH CELLS WERE FIXED AND VIMENTIN NETWORK ANALYSED BY IMMUNOFLUORESCENCE. SCALE BARS, 20 MM. V9 ANTIBODY DETECTED VIMENTIN (GREEN) AND FILAMENTOUS ACTIN WAS STAINED WITH PHALLOIDIN-ALEXA568 (RED). ....212

**FIGURE 6.6. RELATIVE QUANTIFICATION OF VIMENTIN CELL DISTRIBUTION.** VARIANCE IN VIMENTIN/ACTIN RATIO TO ASSESS THE EFFECT OF THE ALDEHYDE'S TREATMENT ON THE VIMENTIN NETWORK. (A) VIMENTIN/ACTIN RATIO EXPRESSED IN PERCENTAGE FOR UNTREATED AND TREATED C238S MUTANT CELLS; (B) VIMENTIN/ACTIN RATIO EXPRESSED IN PERCENTAGE FOR UNTREATED AND TREATED SW13 CELL LINE, WHICH IS THE SAME AS SHOWN IN FIGURE 3A FOR COMPARISON. (N=3; MEAN ± SEM; \*



P<0.1 \*\* P<0.01, \*\*\* P<0.001 AND \*\*\*\* P<0.0001) \* COMPARISON OF CONDITIONS WITH CONTROL; # COMPARISON BETWEEN CONDITIONS.....213

**FIGURE 6.7. TIME-LAPSE MICROSCOPY MONITORING OF CELLS TREATED WITH 10 mM ACROLEIN.**

MICROGRAPHS WERE TAKEN EVERY 30 MINUTES FOR THE FIRST 4 HOURS AND THEN EVERY HOUR OVERNIGHT. HERE ARE SHOWN THE PICTURES TAKEN 1, 2, 4, 6, 8, 10 AND 12 HOURS AFTER THE TREATMENT. TWO DIFFERENT POSITIONS OF THE DISH, A AND B, FOLLOWED THE EFFECT OF THE SAME TREATMENT A DIFFERENT GROUP OF CELLS. MICROGRAPHS CONSIST OF GREEN FLUORESCENCE (VIMENTIN) AND DIFFERENTIAL INTERFERENCE CONTRAST (DIC) IMAGES OVERLAPPED.....214

**FIGURE 6.8. TIME-LAPSE MICROSCOPY MONITORING OF CELLS TREATED WITH 30 mM MALONDIALDEHYDE.**

MICROGRAPHS WERE TAKEN EVERY 30 MINUTES FOR THE FIRST 4 HOURS AND THEN EVERY HOUR OVERNIGHT. THE IMAGES TAKEN 1, 2, 4, 7, 10, 13 AND 16 HOURS AFTER THE TREATMENT ARE SHOWN. MICROGRAPHS CONSIST OF GREEN FLUORESCENCE (VIMENTIN) AND DIFFERENTIAL INTERFERENCE CONTRAST (DIC) IMAGES OVERLAP.....215

## List of tables

<b>TABLE 2.1. MODIFICATION OF LYSOZYME BY ACROLEIN.</b> .....	79
<b>TABLE 2.2. MODIFICATIONS OF HUMAN SERUM ALBUMIN BY ACROLEIN.</b> .....	84
<b>TABLE 2.3. MODIFICATIONS OF HUMAN SERUM ALBUMIN BY 4-HYDROXYL-HEXENAL (HHE).</b> .....	87
<b>TABLE 2.4. MRM TRANSITIONS FOR HUMAN SERUM ALBUMIN PEPTIDES UNMODIFIED OR MODIFIED BY ACROLEIN.</b> .....	89
<b>.TABLE 3.1. MODIFICATION OF LYSOZYME BY HEXADECANAL AND 2-CHLORO-HEXADECANAL</b> .....	124
<b>TABLE 3.2. MODIFICATION OF HUMAN SERUM ALBUMIN BY HEXADECANAL AND 2-CHLORO-HEXADECANAL.</b> .....	127
<b>TABLE 4.1. SEQUENCE COVERAGE OF INSULIN, UBIQUITIN AND HUMAN SERUM ALBUMIN. PROTEINS WERE DIGESTED BY IN-GEL OR SMART TRYPSIN DIGESTION, AND PEPTIDE MS ANALYSIS PERFORMED USING BIOPHARMA FINDER.</b> .....	150
<b>TABLE 4.2. MODIFICATION OF UBIQUITIN BY HHE OR HNE. PEPTIDES OBTAINED BY IN-GEL (G) OR SMART (S) TRYPSIN DIGESTION AND MS DATA WAS ANALYSED BY BIOPHARMA FINDER.</b> .....	151
<b>TABLE 4.3. MODIFICATION OF HUMAN SERUM ALBUMIN BY HHE OR HNE. PEPTIDES OBTAINED BY IN-GEL (G) OR SMART (S) TRYPSIN DIGESTION AND MS DATA WAS ANALYSED BY BIOPHARMA FINDER. ...</b>	151
<b>TABLE 5.1. PYRUVATE KINASE RESIDUES MODIFIED AFTER 10 MIN TREATMENT AT HIGH ALDEHYDE CONCENTRATIONS <i>IN VITRO</i>.</b> .....	169
<b>TABLE 5.2. PYRUVATE KINASE RESIDUES MODIFIED AFTER 4 HOURS TREATMENT WITH LOW CONCENTRATIONS OF ALDEHYDES.</b> .....	180
<b>TABLE 5.3. PYRUVATE KINASE RESIDUES MODIFIED AFTER 2 HOURS TREATMENT WITH LOW CONCENTRATIONS OF ALDEHYDES.</b> .....	182
<b>TABLE 5.4. PYRUVATE KINASE RESIDUES MODIFIED AFTER TREATMENT OF MCF-7 CELLS WITH ACROLEIN</b> .....	188
<b>TABLE 9.1. ALDEHYDE MODIFICATIONS SEARCHED ON MASCOT. SPECIFICITY SITE, MONOISOTOPIC AND AVERAGE MASS, COMPOSITION AND PROPOSED STRUCTURE FOR ACR, HHE, HNE, MDA AND 2-CLHDA ADDUCTS.</b> .....	253

## **Chapter 1. Introduction**

## 1.1. Lipids and lipid peroxidation products

### 1.1.1. Lipids

Lipids are a group of biomolecules that embraces a diversity of molecules with different structural features and different functions. Lipids are described as amphipathic small molecules that may originate entirely or in part by carbanion based condensation of thioesters (in the biosynthesis of fatty acyls, glycerolipids, glycerophospholipids, sphingolipids, saccharolipids, and polyketides) or by carbocation-based condensations of isoprene units (for prenyl and sterol lipids). These eight lipid categories are further subdivided on the basis of chemical structures (**Figure 1.1**) [1].

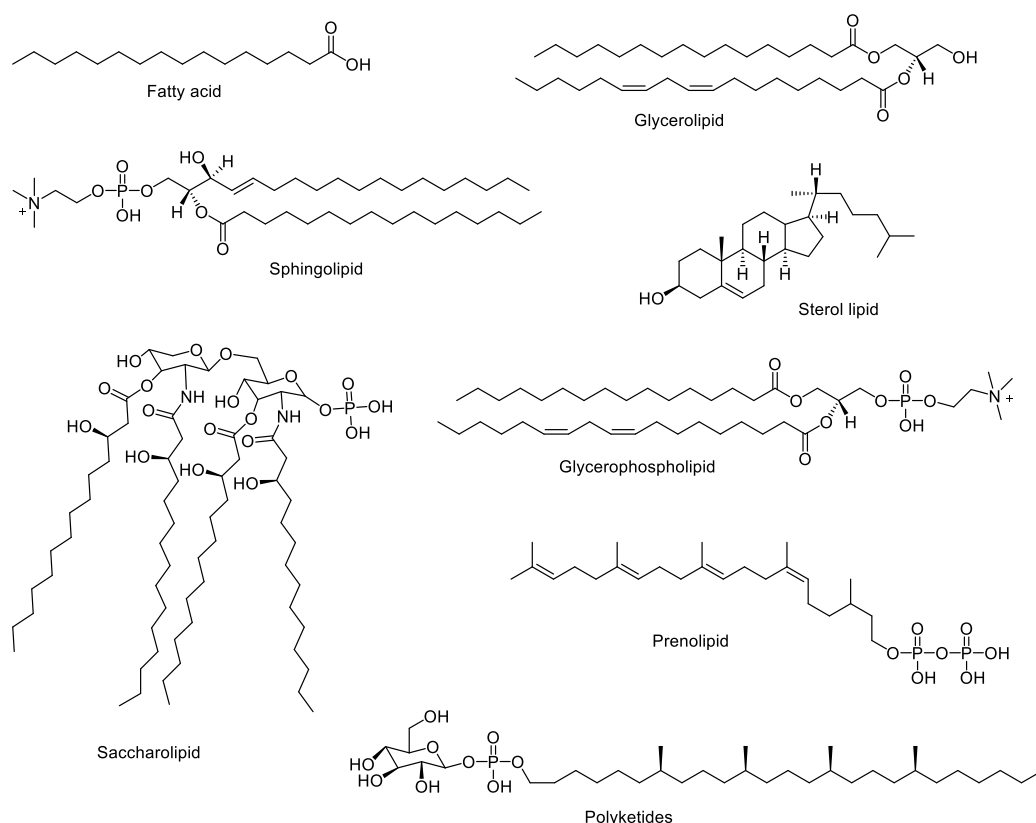


**Figure 1.1. Lipid categories according to the LIPID MAPS lipid-classification system.**

Fatty acids are carboxylic acids with aliphatic chains between 4 and 28 carbons long, which can be either saturated or unsaturated. Saturated fatty acids have no double bonds and therefore are less susceptible to oxidative damage. Palmitic acid (16:0) is one of the most common saturated fatty acid in cells and in fatty foods.

Unsaturated fatty acids have up to 5 double bonds and are susceptible to oxidation. Polyunsaturated fatty acids can be divided into two groups:  $\omega$ 3 and  $\omega$ 6 according to the position of their double bonds (the number of carbons from the  $\text{CH}_3$  end) [2]. The carboxylic acid ( $\text{COOH}$ ) is considered the beginning of the chain while the methyl ( $\text{CH}_3$ ) is the end of the chain. The  $\omega$ 3 fatty acids have a double bond at the third carbon atom from the end of the carbon chain [3]. The  $\omega$ 3 essential fatty acids for humans are  $\alpha$ -linolenic acid (ALA,

18:3), eicosapentaenoic acid (EPA, 20:5), and docosahexaenoic acid (DHA, 22:6) (**Figure 1.2**) [4]. Humans get these fatty acids through the diet from fish and plant sources. Linolenic acid is the dietary precursor of longer  $\omega$ 3 polyunsaturated fatty acids (PUFA) as EPA and DHA [5]. Some studies relate the ingestion of  $\omega$ 3 fatty acids with beneficial effect to health including mediating inflammation [6]. The oxidation of EPA produces E-resolvins, and oxidation of DHA leads to several other beneficial lipid mediators such as D-resolvins, protectins and maresins. All of these lipid mediators are known for their pro-resolution role in inflammation [7].

$\omega$ 6 Fatty acids have a double bond at the sixth carbon atom from the methyl end. These are known for their pro- and anti-inflammatory roles. During inflammation,  $\omega$ 6 fatty acids are converted to eicosanoids that bind to receptors and initiate reactions promoting cell repair [8]. As for  $\omega$ 3, some of the  $\omega$ 6 fatty acids are also classified as essential since humans cannot synthesize them. Linoleic acid (LA, 18:2) is an essential fatty acid and it is precursor for other  $\omega$ 6 fatty acids including the arachidonic acid (AA, 20:4) (**Figure 1.2**). This fatty acid is involved in a variety of inflammatory processes since it is the precursor of pro-inflammatory molecules. Via the enzymatic action of COX1/2 and 5-lipoxygenase, AA it gives rise to prostaglandins and leukotrienes respectively [9].

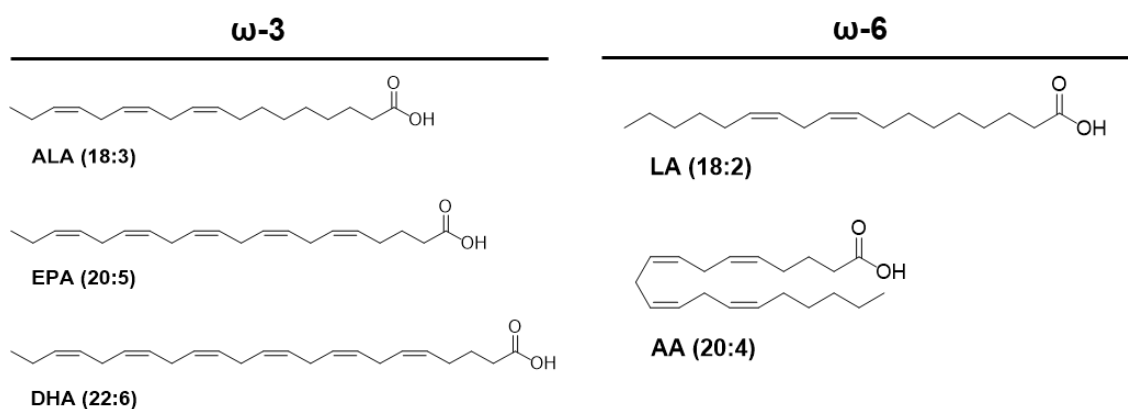


**Figure 1.2. Structure of three  $\omega$ 3 and two  $\omega$ 6 unsaturated fatty acids.** Example of  $\omega$ 3 fatty acids are linolenic acid (ALA), eicosapentaenoic acid (EPA) and docosahexaenoic acid (DHA), and of  $\omega$ 6 fatty acids are linoleic acid (LA) and arachidonic acid (AA).

Fatty acids can be found as free molecules but mostly they are found esterified to a glycerol appearing as, for example, phospholipids. Phospholipids (PL), are the major component of a cell membrane due to their characteristic amphipathicity [10] and are responsible for maintaining membrane stability and integrity [11]. This lipid category includes glycerophospholipids and sphingolipids. Glycerophospholipids, commonly referred to as phospholipids, come from phosphatidic acid and have an ester linkage at the *sn*-2 and

*sn*-1 positions to two fatty acids as well as a polar head linked to glycerol third carbon by a phosphodiester bond [12]. Depending on the polar head, phospholipids can be divided into six categories. These are phosphatidic acids (PA), phosphatidylcholines (PC), phosphatidylethanolamines (PE), phosphatidylserines (PS), phosphatidylglycerols (PG) and phosphatidylinositol (PI) (**Figure 1.3**).

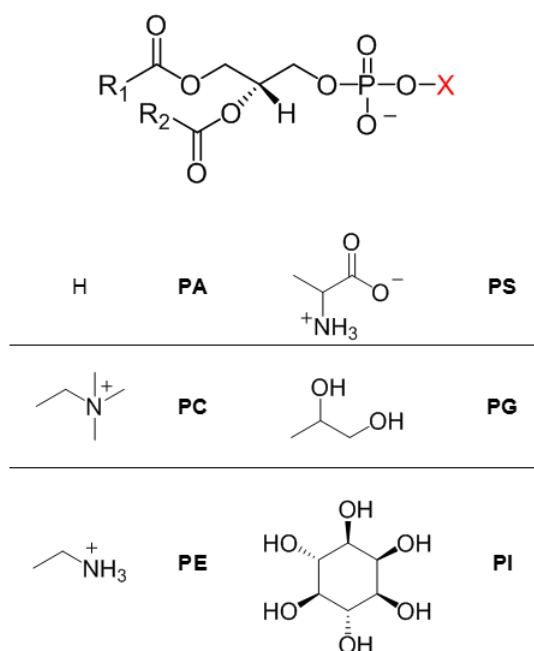


**Figure 1.3. Structure of glycerophospholipids.** R<sup>1</sup> and R<sup>2</sup> represent fatty acyl chains esterified to the glycerol. X correspond to the different polar heads.

Sometimes, instead of an ester bond, the fatty acids are linked to glycerol by a vinyl ether bond; plasmalogens are the phospholipids characterized by the presence of an ester linkage at the *sn*-2 position but a vinyl ether linkage at the *sn*-1 position (**Figure 1.4**). These molecules are resistant to the action of phospholipases since they only recognize and cleave ester bonds.

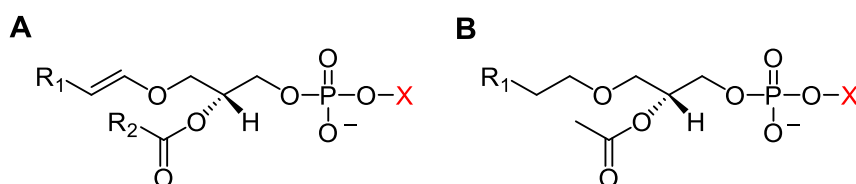


**Figure 1.4. Structure of glycerophospholipids holding an ether bond instead of an ester bond.** A-plasmalogens with a vinyl ether bond; B- ether lipid (Platelet-activating factor (PAF)).

Several studies have reported the importance of a specific lipid environment for the correct functioning of membrane proteins [12]. Although some proteins depend on being surrounded by a specific lipid shell, some multimeric proteins specifically bind individual

lipids that are important for the structure of these protein complexes [13]. Recent studies suggest that lipids can also act as protein co-factors modulating their activity [14]. Under several pathophysiological conditions, an imbalance occurs between oxidative and anti-oxidative species and lipids containing polyunsaturated chains are susceptible to oxidative damage caused by these species generated during oxidative stress.

### 1.1.2. Overview on oxidants and oxidative stress

Oxidative stress results from a redox imbalance and consequent increase in oxidative species such as partially reduced oxygen and nitrogen species (PROS and RNS). In normal conditions, these species have important roles in signaling, detoxification of xenobiotics and phagocytosis. However, in pathophysiological conditions an excess of these oxygen and nitrogen species can cause cellular damage and oxidative modifications of biomolecules such as lipids, proteins and DNA [15, 16]. Reactive oxygen species can be free radicals such as superoxide ( $O_2^{\cdot-}$ ) and the hydroxyl radical ( $\cdot OH$ ), which are the most unstable and reactive oxygen species and can cause significant damages. They can also be non-radical, such as hydrogen peroxide ( $H_2O_2$ ), which is a selective oxidant that can form other, more reactive oxidant species [17]. One place where ROS can be generated is in mitochondria during oxidative phosphorylation. During this process, electrons can accumulate and be transferred to oxygen molecules resulting in the production of ( $O_2^{\cdot-}$ ) [18]. This radical is polar and does not diffuse through cell membranes, so is generally less damaging than another ROS. However, it can generate  $H_2O_2$  by spontaneous dismutation or enzymatically by superoxide dismutase (SOD).  $H_2O_2$  is relatively non-polar and soluble so it does diffuse into the membrane and can cause damage outside the site of formation making it more toxic. Additionally,  $O_2^{\cdot-}$  can generate the hydroxyl radical ( $\cdot OH$ ), peroxynitrite ( $ONOO^{\cdot}$ ) and singlet oxygen ( $^1O_2$ ) [19, 20]. In the presence of a transition metal, such as iron,  $H_2O_2$  can give rise to the hydroxyl radical by the Fenton reaction, with oxidation of  $Fe^{2+}$  to  $Fe^{3+}$  [21].  $\cdot OH$  is the most reactive oxygen species of all those found in biological systems, since there are no enzymes capable of detoxifying this radical. There are two further mechanisms to generate  $\cdot OH$ . These are the decomposition of water that generates  $\cdot OH$  and  $\cdot H$  and the reaction of  $O_2^{\cdot-}$  with  $H_2O_2$  in the presence of transition metal such as iron ( $Fe^{2+}$ ) and copper ( $Cu^{2+}$ ), Haber-Weiss reaction. However, *in vivo*, it is mostly generated by the Fenton reaction [22]. **Figure 1.5** shows the different mechanisms involved in the generation of reactive oxygen species.

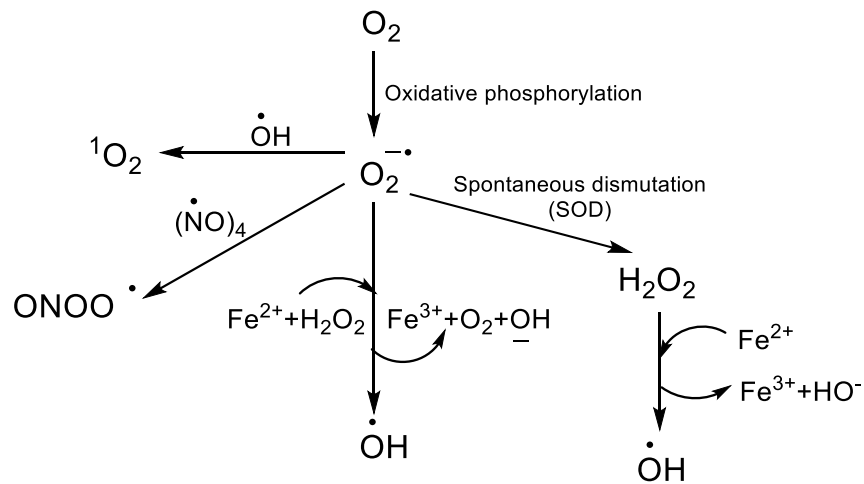


**Figure 1.5. Mechanisms of generation of reactive oxygen species.**

Free radicals can cause damage to important biomolecules, namely proteins, lipids, and DNA, changing their structure and thus being responsible for loss of function or even resulting in the formation of new deleterious species. Lipids are one of the major targets of oxidation in biological systems [23]. The development and progression of several diseases including age-related illnesses such as Alzheimer's disease, Parkinson's disease, multiple sclerosis, cardiovascular diseases, atherosclerosis, diabetes, liver and lung diseases have been associated with lipid peroxidation (LPO) [24-26]. Therefore, efforts have been made to understand the mechanism of lipid peroxidation and prevent its deleterious effects.

### 1.1.3. Lipid peroxidation: mechanisms and products

As previously mentioned, lipids are primary targets of the attack by PROS. Lipid peroxidation leads to the formation of a variety of oxidized products, produced by modification of polyunsaturated fatty acyl chains (PUFAs) [23]. While the enzymatic oxidation is regulated by receptors and intracellular signaling, the nonenzymatic oxidation results in new products with new bioactivities being formed, some of which may be deleterious to cells and tissues. In enzymatic lipid peroxidation, the oxidized products are generated by enzymes including lipoxygenases (LOX) and cyclooxygenases (COX), found in all mammalian species. In this case the lipid oxidation products often have a role in immunity and homeostasis. These biologically active oxidized phospholipids can initiate and modulate many cellular events [27]. For example, oxidized phospholipids (OxPL) can modulate the fate of an inflammatory response by intervening in the processes by removing apoptotic cells [28]. Nowadays, the importance of oxidized lipids as key players in the onset of cardiovascular diseases is well recognized and oxidized lipids, especially non-enzymatic



lipid peroxidation products, are considered as possible biomarkers for cardiovascular disease [29].

On the other hand, non-enzymatic lipid peroxidation is a chain reaction by which lipids are modified by free radicals such as  $O_2^{\cdot -}$  (superoxide radical),  $OH^{\cdot}$  (hydroxyl radical),  $HO_2^{\cdot}$  (perhydroxyl radical) and  $RO^{\cdot}$  (alkoxy radicals) at carbon-carbon double bonds. Lipids can also be modified by non-radical forms of oxygen such as  $H_2O_2$  (hydrogen peroxide) and  $^1O_2$  (singlet oxygen) as well as by hypochlorous acid (HOCl), product of the neutrophil enzyme myeloperoxidase. **Figure 1.6** gives an example of the attack of  $OH^{\cdot}$  on a phosphatidylcholine, one of the main constituents of cell membranes. This process can be divided into two phases: first an hydrogen is abstracted from a carbon by the oxygen-based radical and then an oxygen is inserted in the lipidic chain resulting in a lipid peroxy radical or hydroperoxide [20].

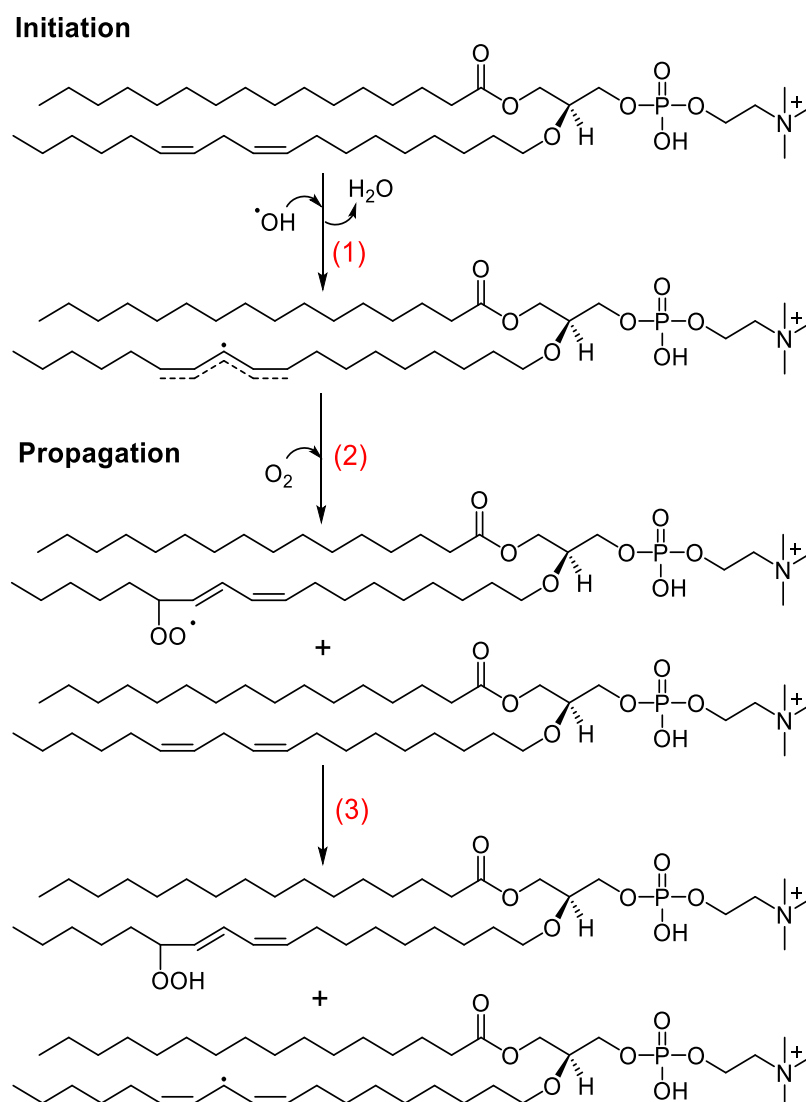


**Figure 1.6. Lipid peroxidation mechanism.** Hydrogen-atom abstraction by alkoxy radical; oxygen addition to carbon radical; peroxy radical rearrangement.

Lipid peroxidation starts with the attack of a free radical to generate a C-centred radical (L<sup>•</sup>) (1), which then reacts with molecular oxygen to generate a lipidic peroxy radical (LOO<sup>•</sup>) (2), which rearranges as shown above and the peroxy radical is capable of propagating the chain reaction (3) [30]. It is also able to react internally to generate cyclic endo peroxidases as well as allowing other cleavage reaction that generate lipid peroxidation breakdown products which can also promote further oxidation [31]. To break the chain reaction, a reaction needs to occur between two radicals, or an antioxidant molecule intervenes [32].

#### 1.1.4. Fatty acid free-radical oxidation products

During lipid oxidation, new oxidised products are generated with different numbers of oxygen molecules bound to the acyl chain, therefore increasing the lipid molecular weight. These products are the so-called long chain oxidation products. However, the alkoxy radicals can undergo  $\beta$ -cleavage generating short-chain oxidation products that can be either aldehydes or carboxylic acids (**Figure 1.7**) [33].

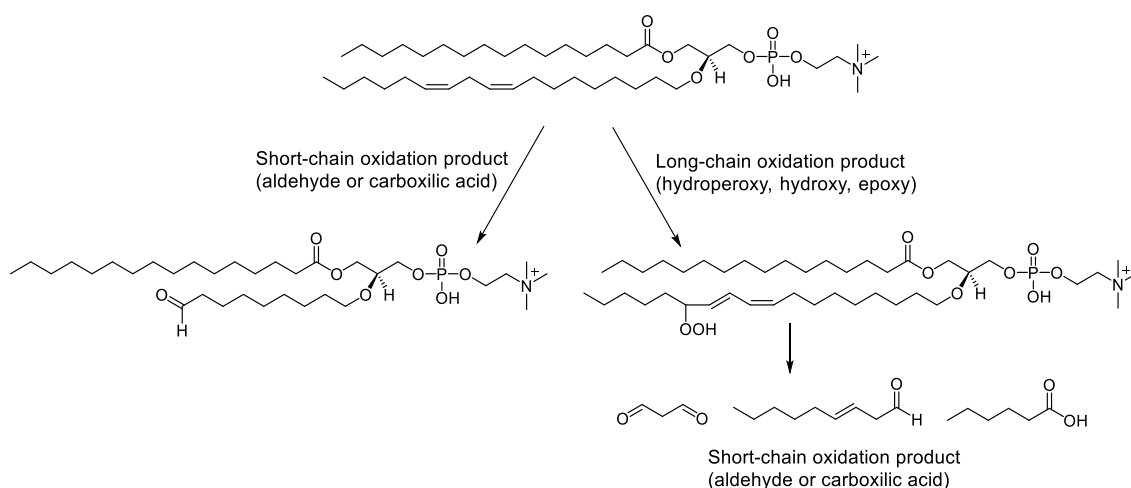


**Figure 1.7. Schematic explanation of long and short chain lipid peroxidation products.**

Polyunsaturated fatty acids, either free or esterified, are particularly prone to undergo peroxidation, with linoleic and arachidonic acids as common examples of fatty acids that are oxidizable. The oxidation of these results in a great diversity of products that are structurally different from the non-modified lipid presenting a new shape, polarity and consequently biological activity. The oxidation of linoleic acid results in the formation of 9-, 11- and 13-hydroperoxides due to the locations of the carbon radical (**Figure 1.8**). The 11-HPODE is only formed in the presence of good H-donor such as alpha-tocopherol since the loss of oxygen at C11 is much faster than any other position [34]. Therefore, 9-HPODE and 13-HPODE are the most common hydroperoxides resulting from linoleic acid peroxidation [35]. The main carbon chain of the fatty acid is preserved during the formation of the

hydroperoxides, the primary products, however prolonged peroxidation causes rearrangement or degradation and secondary oxidation products can be formed.

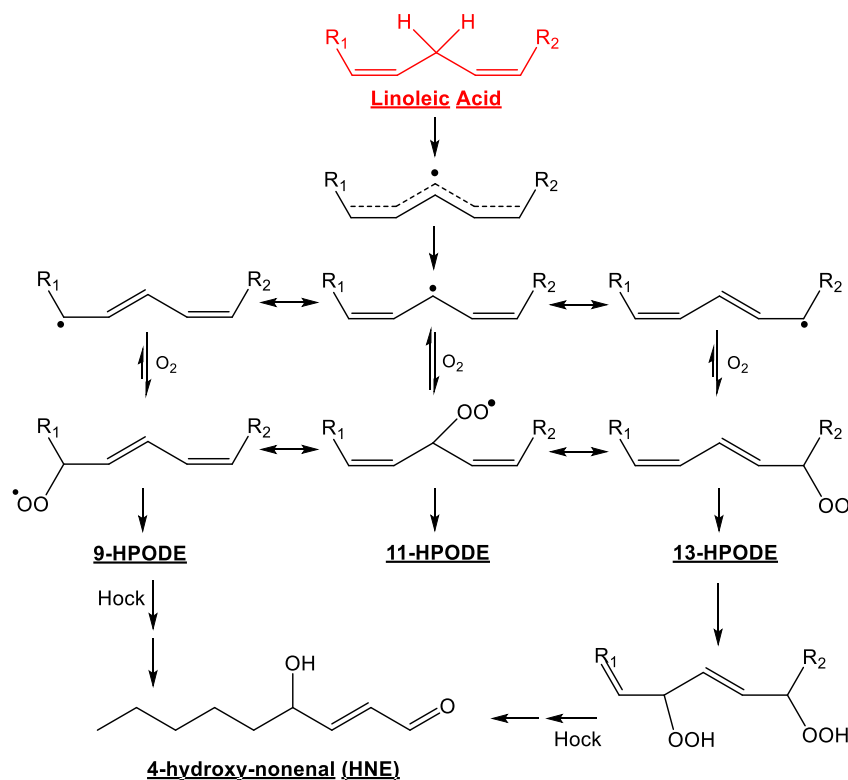


**Figure 1.8. Formation of hydroperoxides from linoleic acid.** Following hydrogen abstraction, oxygen adds to all three reactive carbon positions (C9, C11 and C13). Other oxidative species can result from the rearrangement, further oxidation or breakdown of these hydroperoxides, including HNE. Adapted from [23].

Linoleic acid is the most abundant fatty acid in LDL and atherosclerotic plaques [36]. Oxidized linoleic acid products have been found in LDL and plasma of atherosclerotic patients [36] and the degree of oxidation was dependent on its severity [37]. These species are signaling molecules which recruit monocytes/neutrophils to atherosclerosis lesions [38]. For example, 9-hydroxyoctadecadienoic acid (9-HODE) is pro-inflammatory and it has been reported in atherosclerosis [38], cardiac diseases such as infarction and coronary heart disease (CHD) [39], and it is known to induce PPAR $\gamma$ -regulated apoptosis in monocytes, which LA itself cannot replicate the same effect [40]. Understanding the mechanisms behind the HODEs signaling may contribute to novel therapeutic approaches to these diseases.

The arachidonic acid is another commonly oxidized  $\omega$ -6 fatty acid. As mentioned above, AA is responsible for inflammatory processes by being the precursor of prostaglandins and leukotrienes. While these are products of enzymatic lipid oxidation, free radical autooxidation of AA can also occur and several oxidized products can be formed (**Figure 1.9**).

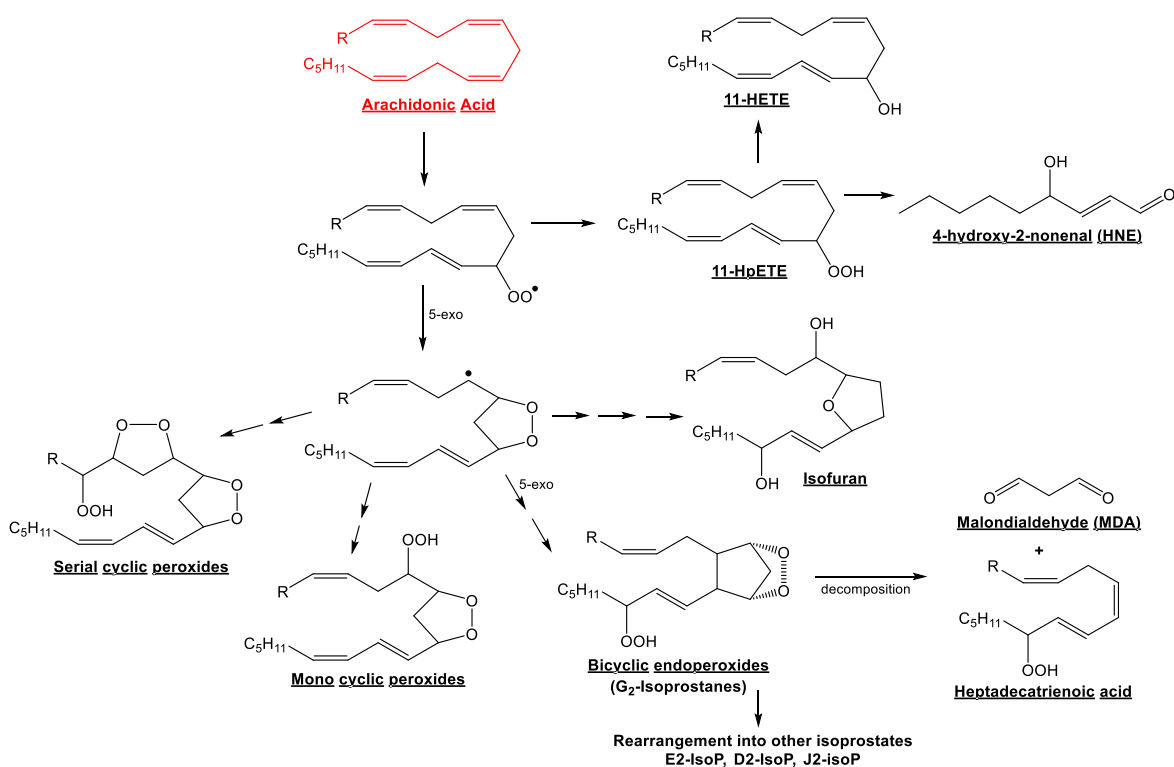


**Figure 1.9. Major pathways of free radical oxidation of arachidonic acid.** The primary oxidation products are hydroperoxides. Only 11-HpETE shown here as example for simplicity, however there are six hydroperoxyl radicals generated from free radical oxidation of arachidonic acid. Secondary oxidation products are generated by further oxidation, decomposition or reduction of the hydroperoxides. Adapted from [23].

In comparison with LA, AA is more susceptible to oxidation due to a higher number of bisallylic positions and six major hydroperoxyeicosatetraenoates (HPETEs) can be formed, as well as their reduced analogues, the hydroxyeicosatetraenoates (HETEs). In **Figure 1.9**, only one of the six hydroperoxides is shown (11-HPETE) and its multiple reaction pathways which occur by cyclization [41, 42]. Arachidonic acid is substrate for prostaglandin generation by cyclooxygenase and lipoxygenase enzymes. Isoprostanes are prostaglandin-like compounds generated from non-enzymatic free radical oxidation of arachidonic acid, and can be used as reliable markers for lipid peroxidation and oxidative stress in biological systems [43-45] due to their stability, specificity to lipid peroxidation and detection in free form or esterified in all biological fluids [46]. High levels of isoprostanes have been detected in urine from smokers [47], obese [48], diabetic [49], hypercholesterolemic [50] and Alzheimer's disease patients [51].

Linoleic and arachidonic acid are both  $\omega$ -6 fatty acids, however oxidation of  $\omega$ -3 fatty acids, such as EPA and DHA, is also biologically important since these fatty acids have been associated with protective roles against inflammation. In fact, studies have shown that consumption of these lower the risk of cardiovascular diseases [52-54]. Nevertheless,

oxidation of  $\omega$ -3 fatty acids generates a wide range of products and some of these have recently been reported as reactive against other biomolecules, therefore questioning the beneficial properties of  $\omega$ -3 PUFAs [55, 56]. For example, DHA is an important source of PUFAs in tissues and has six double bonds making it highly susceptible to oxidation [57, 58]. The wide range of oxidation products of these fatty acids include 4-hydroxy-hexenal (HHE) and 4-hydroxy-7-oxo-5-heptenoic acid (HOHA), both shown to be deleterious to proteins by generation of the adducts ethylpyrrole (EP) and 2-carboxyethylpyrrole (CEP), respectively [59] (**Figure 1.10**). The chemistry and analysis of the aldehydes formed by the oxidation of either  $\omega$ -3 or  $\omega$ -6 fatty acids are discussed in the next section of this introduction.

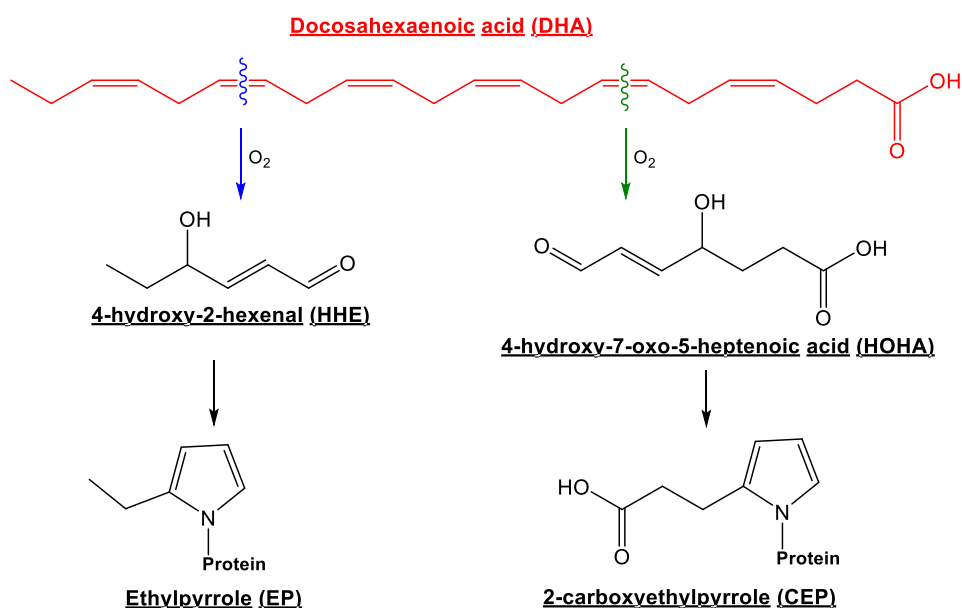


**Figure 1.10. Schematic representation of the formation of HHE and HOHA from DHA.** Hydrolysis of DHA generates HOHA which in turn produces CEP-protein adduct. Oxidative cleavage of DHA also forms HHE which generates a similar protein modification, EP-protein adduct. Adapted from [59].

## 1.2. Aldehydes as short chain lipid peroxidation products

Aldehydes are an example of PUFAs short-chain oxidation products [20, 23, 60]. As mentioned in the previous section, these can be generated by the decomposition of PUFAs through enzymatic or non-enzymatic mechanisms. Linoleic and arachidonic acids, both  $\omega$ -6-polyunsaturated fatty acyl chains, are good sources of aldehydes by cleavage of a C-C bond. The mechanisms by which a carbon-carbon bond can be cleaved are broadly classified into (i) reduction of hydroperoxide to an alkoxyl radical in the presence of a transition metal followed by  $\beta$ -scission; (ii) Hock rearrangement of a hydroperoxide and migration of a C-C to a C-O bond and cleavage; (iii) cyclization to form a dioxetane and subsequent cleavage (**Figure 1.11**). Similarly,  $\omega$ -3-polyunsaturated fatty acyl chains, for

example docosahexaenoic acid, can also undergo fragmentation and give rise to many reactive aldehydes. The insertion of additional oxygen molecules can give rise to some variants of these mechanisms. If three O<sub>2</sub> are added to the chain to form a hydroxyhydroperoxide, it can undergo β-scission or an epoxyhydroperoxide can undergo Hock cleavage [23, 61-63].

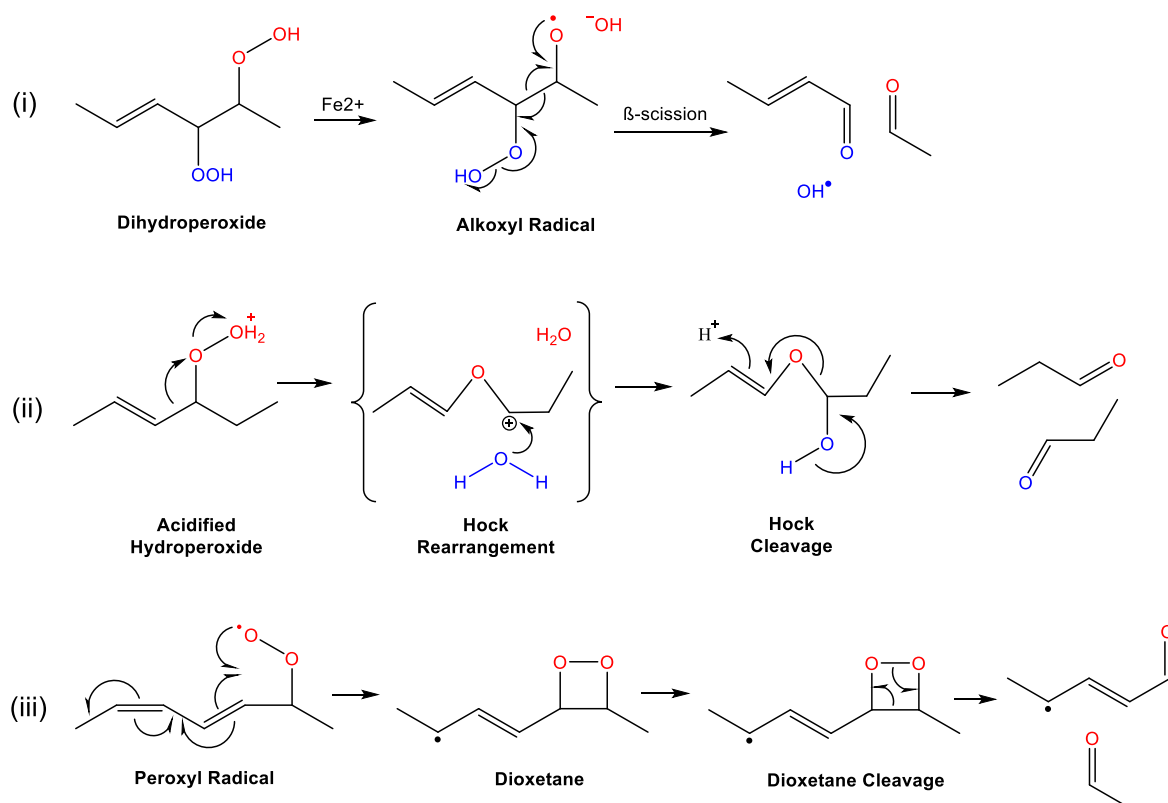


**Figure 1.11. Mechanisms of carbon-carbon bond cleavage.** (i) reduction of hydroperoxide to an alkoxy radical in the presence of a transition metal followed by β-scission; (ii) Hock rearrangement of a hydroperoxide and migration of a C-C to a C-O bond and cleavage; (iii) cyclization to form a dioxetane and subsequent cleavage. Adapted from [63].

These aldehydes have a carbonyl group or an α, β-unsaturated carbonyl, and may have other substitutions such as chlorination or hydroxylation, depending on the nature of the oxidant. Aldehydes can be classified on the basis of their chemical structure into alkanals, alkenals and γ-substituted-alkenals. This system of classification also focuses on their different reactivity towards biomolecules.

### 1.2.1. Alkanals

Alkanals are saturated carbon chains containing an aldehyde group. These are the simplest and least polar aldehydes. Several alkanals, varying in chain length from three to nine carbons, have been identified as lipid peroxidation products from linoleic and

arachidonic acid, both  $\omega$ -6 fatty acids. Identification of these was performed by comparison of their retention time to aldehyde standards on a high-performance liquid chromatography. Butyraldehyde (butanal), hexenal and nonanal have been reported as the major alkanal generated by lipid peroxidation [64] (**Figure 1.12**).

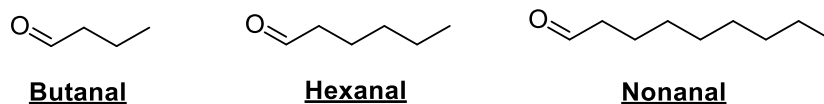


**Figure 1.12. Structure of the three most common alkanals to occur as lipid peroxidation products.**

Hexanal was shown to be the most abundant aldehyde of all of the identified, even compared with 4-hydroxy-2-nonenal (HNE), a well-known aldehyde discussed later in this introduction in the substituted aldehydes section [64]. Still, there is a lack of studies on the biological reactions and effects of these aldehydes, which may be due to their lower reactivity and toxicity compared with other aldehydes. Their functional group, a single carbonyl group, only allows them to react with amine groups by Schiff base formation, for example with amino acids such as lysine. Even though alkanals have low reactivity, some studies have reported their role in disease. Hexanal, heptanal and nonanal were found in bronchoalveolar lavage fluid of animals after exposure to ozone [65]. The ozonation process in human samples was also studied and shown to produce aldehydes as lipid ozonation products in human lungs. Mostly hexanal and nonanal were identified, but the increase in these aldehydes was unrelated to airway inflammation [66]. Additionally, a study on oesophageal and gastric adenocarcinoma identified an increase in aldehydes such as butanal, pentanal, hexanal, heptanal, octanal and nonanal in cancer patients exhaled breath by selected ion flow tube mass spectrometry (SIFT-MS) [67]. POVPC, a phosphatidylcholine with a five carbon chain alkanal esterified at the sn-2 position, has been detected in atherosclerotic plaque by LC-MS/MS and can form adducts with ApoB100 on LDL [68, 69].

### 1.2.2. Alkenals

Alkenals are aldehydes with a double bond in the carbon chain. Due to the structure of the PUFAs from which these are derived, alkenals from lipid peroxidation are often  $\alpha,\beta$ -unsaturated (double bond between carbons 2 and 3). Previous studies have listed some of these as products of  $\omega$ -6 fatty acids peroxidation [24, 64]. Many unsaturated aldehydes with chain length from 3 to 9 carbon have been identified, with propenal (acrolein), 2-heptenal, 2-octenal and 2-nonenal appearing in relatively higher amounts than the others [64] (**Figure 1.13**).

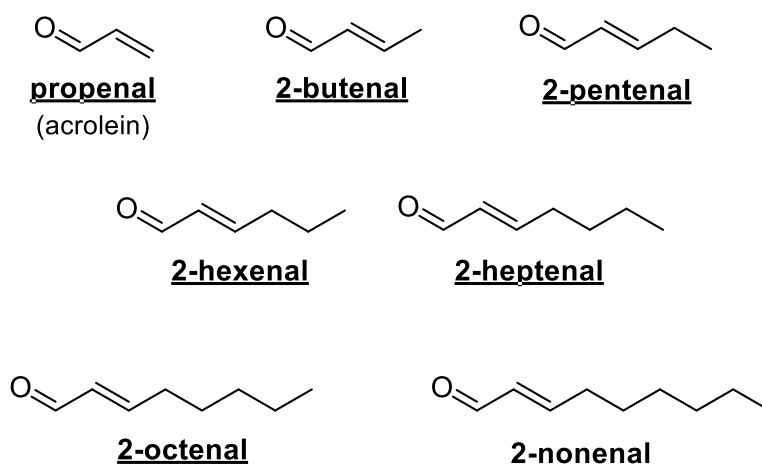


**Figure 1.13. Structure of the most common alkenals to occur as lipid peroxidation products.**

The shortest alkenal identified as an oxidation product is propenal, also known by the common name acrolein. With only three carbons, it is by far the strongest electrophile and therefore the most reactive, especially with thiol groups on proteins [70, 71]. Acrolein can be formed by combustion of organic matter, in tobacco smoke and from food processing [72, 73]. It can also be produced endogenously by the oxidation of non-lipids such as methionine, threonine, spermine, spermidine and glycerol [71]. In addition, there is evidence of lipid peroxidation of fatty acids as a source of acrolein *in vivo* [60, 71, 74], however the mechanisms still remain unclear. Previous reports proposed a mechanism for the formation of acrolein from the centre of the arachidonic aliphatic chain after it undergoes two  $\beta$ -cleavages [60], even though this has been debated recently [60]. Supporting the hypothesis of acrolein being a lipid peroxidation product is a study where acrolein was detected by ELISA from arachidonic acid autoxidation samples [74]. Acrolein is known to be involved in pathophysiological processes. For example, acrolein is capable of modifying the p50 subunit of NF- $\kappa$ B disrupting the regulation of gene expression. NF- $\kappa$ B is responsible for the expression of genes which regulate the antioxidant defence, apoptosis, and inflammatory and immunological responses, therefore its modification by acrolein may cause immunosuppression [75]. Some other signalling pathways have also been shown to be modified by acrolein, including nuclear erythroid-2 related factor 2 (Nrf2), ARE-dependent genes and PTP1B, which lead to increased oxidative stress and cellular damage. Exposure to acrolein can also cause membrane damage, increased membrane permeability and lead to functional defects or cell death [76, 77]. Acrolein accumulation creates an additional oxidative stress, increasing membrane permeability with time and eventually results in cell lysis [78]. It also impairs the mitochondrial respiratory function, increasing oxidative stress and stimulating PROS production and decreasing concentration of antioxidants such as GSH [79-82]. Tobacco smoke is a source of acrolein, which constitutes 50 to 60% of the total vapor phase electrophiles with a concentration in smoke ranged from 3 to 220



$\mu\text{g}/\text{cigarette}$  [83]. Therefore, the mouth and respiratory tract are commonly exposed to acrolein and the estimated concentrations of it in the airway can be as high as  $80\ \mu\text{M}$  [84], which is increased in smokers in comparison with healthy subjects. Inhaled acrolein has been linked to lung injury [85] and cardiovascular diseases [86, 87]. A recent study reported that acrolein can harm the vocal fold epithelial barrier integrity and may lead to inflammation by the invasion of xenobiotics [88]. The popularity of e-cigarettes continues to grow as these have been sold as a safer alternative to tobacco. However, recent studies have detected the presence of acrolein in aerosols from e-cigarettes [89, 90]. The formation of aldehydes from vaping has been associated with the decomposition of propylene glycol and glycerol present in the e-liquid. Nevertheless, their quantity may also vary according to the power output or the composition of flavouring compounds [91]. Besides, these were reported to be 4 to 6-fold lower than for tobacco [92] but long-term follow up studies are needed to confirm the effect of e-cigarettes in health.

Crotonaldehyde (2-butenal) is a simple  $\alpha,\beta$ -unsaturated aldehyde similar to acrolein. Although it is much less toxic, it can still modify proteins and DNA *in vivo* [93]. Crotonaldehyde reacts with deoxy guanosine to form adducts with DNA which were shown to be involved in tumour formation. This modification was shown to generate unique epitopes that may trigger autoantibodies in cancer patients [94]. 2-Butenal, and the five carbon analogue 2-pentenal, come from the oxidative breakdown of  $\omega$ -3 unsaturated fatty acids. In contrast, 2-heptenal, 2-octenal and 2-nonenal come from the breakdown oxidation of  $\omega$ -6 unsaturated fatty acids. These longer alkenals are less reactive towards proteins than acrolein or crotonaldehyde perhaps due to their insolubility in water, which would favour the nucleophilic attack. However, immunoreactivity assays and liquid chromatography coupled to mass spectrometry (LC-MS) were used to detect protein modification by 2-nonenal, found preferentially on lysine residues [95]. 2-nonenal has a characteristically unpleasant greasy and grassy odour and is a major contributor to the unpleasant cardboard flavour in aged beer. Analysis of body odour components also showed 2-nonenal to be present in increasing amounts in the body odours of older people [96]. 2-nonenal is generally less reactive than other 2-alkenals and therefore has received less attention. Nevertheless, there is evidence of inhibition of enzymes such as platelet membrane-bound phosphotyrosine phosphatase [97] and liver microsomal glucose-6-phosphatase [98] by this aldehyde.

### 1.2.3. Substituted aldehydes

Lipid peroxidation can also form more complex aldehydes from the breakdown oxidation of unsaturated fatty acids. These species not only contain a carbonyl group (CHO) and an

$\alpha,\beta$ -unsaturation (C=C) but also contain an additional functional group at the C4 position, including hydroperoxyl (-OOH), epoxy, hydroxyl (4-hydroxyalkenals) or keto (4-oxoalkenals). Due to their highly reactivity and toxicity to biomolecules,  $\alpha,\beta$ -substituted-alkenals have received the most attention in terms of their biological effects. The C3 position is especially susceptible to nucleophilic attack, allowing the formation of adducts with thiols and amines. Their bi-reactive nature is particularly important because it enables these compounds to crosslink proteins, which may contribute to the pathophysiology of diseases related to lipid peroxidation, such as Alzheimer's disease [99, 100]. The 4-hydroxy-alkenals are a well-known type of lipid oxidation products and include 4-hydroxy-2-hexenal (HHE), 4-hydroxy-2-nonenal (HNE) and 4-hydroxydodeca-2,6-dienal (HDDE) (**Figure 1.14**).

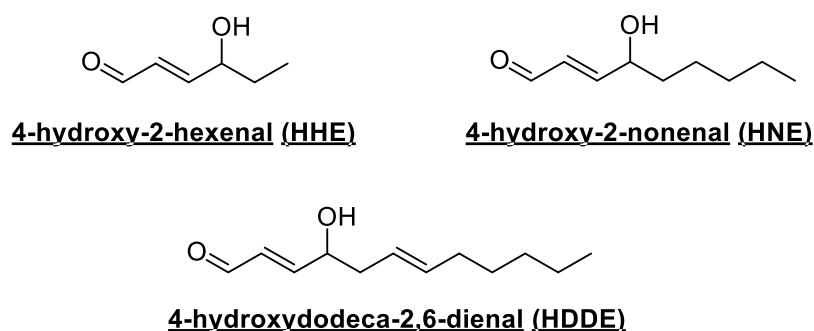


**Figure 1.14. Structure of the most common hydroxyalkenals to occur as lipid peroxidation products.**

HHE is a product of  $\omega$ -3 PUFAs oxidation while HNE is a product of  $\omega$ -6 PUFAs oxidation, via 15-hydroxyeicoatetraenoic acid (15-HpETE) or 13-hydroperoxylinoleic acid [101]. HDDE is a product of 12-HpETE, which is generated enzymatically by 12-lipoxygenase [101]. HNE can also be an enzymatic product of  $\omega$ -6 PUFAs by the action of 15-lipoxygenase (15-LOX) on arachidonate [102]. Several reviews have detailed the non-enzymatic processes of HNE generation by oxygen radical-dependent reactions [23, 62, 63]. HNE was discovered in the 1960s [70] and nowadays is considered a useful biomarker of lipid peroxidation [100]. HNE is highly reactive, which translates into a higher number of studies regarding its biological effects. HNE is known to be involved in the pathophysiology of Alzheimer's disease, cancer, cardiovascular diseases, diabetes, liver disease and Parkinson's disease. It has been suggested as a signalling molecule. MAPK, JNK, p58, PKC  $\beta$  and  $\delta$ , and Nrf2 are some of the signalling pathways found to be modulated by HNE [103], and a detailed review of the signalling pathways modulated by HNE has also been published previously [104]. **Figure 1.15** summarises the key signalling pathways that can be modulated by HNE. These signalling processes probably involve HNE reaction with signalling proteins, altering their activity usually by its inhibition [103]. The severity of the

effect of HNE on these mechanisms is dependent on HNE concentrations, with higher levels of HNE leading to more deleterious outcomes, including cell death [105].

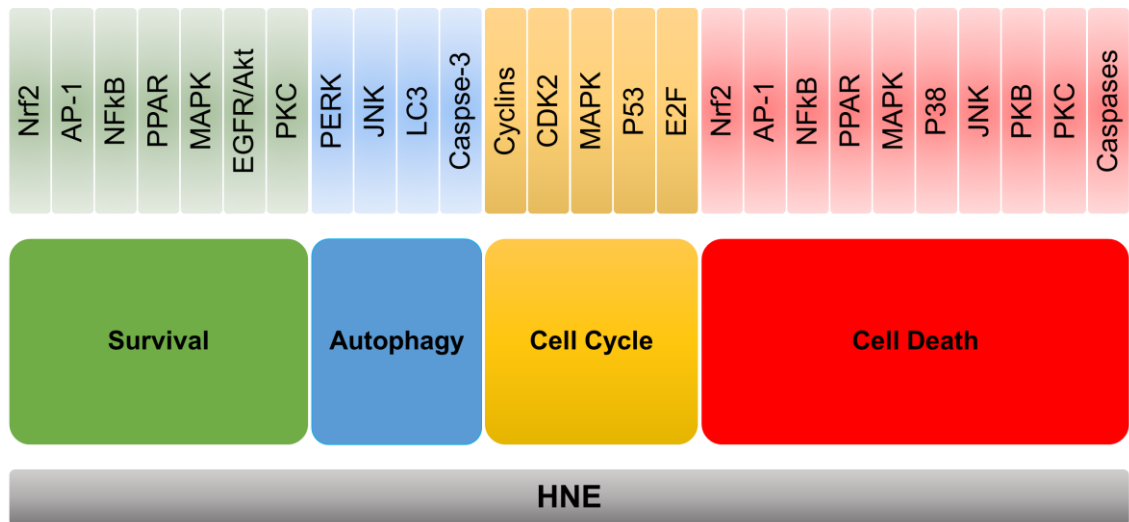


**Figure 1.15. Schematic summary of signaling proteins known to be modified by HNE.**

It has been demonstrated that Nrf2 binds to UPC3 (mitochondrial uncoupling protein 3) promoter in response to HNE, resulting in an important mechanism of protection of the heart under oxidative stress conditions. The Nrf2 pathway was shown to increase uncoupling proteins (UCP3) expression promoting cell survival [106]. However, HNE can also modulate mechanisms that lead to harmful consequences. For example, the modification of Src by HNE has been shown to be related to important cellular dysfunction. Src is the first proto-oncogene involved in cellular proliferation and differentiation that is ubiquitously expressed non-receptor protein tyrosine kinase. It was reported that HNE can activate Src through three different mechanisms: i) EGFR is activated by HNE inducing activation of Src; ii) PTP1B is inhibited by HNE, increasing EGFR-induced Src activation; and iii) HNE directly activates Src by modification of a cysteine residue [107]. The modification of Src by HNE leads to a constitutive activation of Src promoting survival, angiogenesis and proliferation which under cancer conditions helps a tumour to grow, demonstrating the connection between increased levels of HNE and cancer progression. Another protein involved in tumorigenesis that was shown to be regulated by HNE is the peroxisome proliferator-activated receptor (PPAR). There is evidence that under high glucose, Nox activity is increased leading to an increase in ROS formation. This generates oxidative stress that induces lipid peroxidation and consequently HNE production. In turn, HNE activates PPAR $\alpha$  and PPAR $\beta/\delta$  augmenting Nox expression and activity [108]. Hyperglycaemia can also activate PPAR through a different mechanism. It is known that high glucose accelerates atherosclerosis. This disease is characterised by monocytes being transformed into macrophages which then progress to become lipid-laden foam cells [109]. The foam cells

release HNE that activates PPAR $\delta$  in endothelial cells leading to an increase in thioredoxin interacting protein (TXNIP) expression and consequent cellular senescence [110]. Some studies have reported specific amino acids that appear to be modified by HNE leading to dysfunction. His71 and Cys177 were identified as major sites for HNE modification in CDK2 on colorectal cancer cells. These specific modifications inhibit the kinase activity, contributing to cell cycle arrest [111]. TRA DNA-binding protein (TDP-43) can also be modified by HNE, and it was reported to be directly modified on cys173, cys175 and cys198. This results in its solubilisation and mislocalization from nucleus to cytoplasm, consistent with what had been previously observed in sporadic amyotrophic lateral sclerosis (ALS) [112]. These findings show the importance of knowing the specific amino acid residues modified on each protein and relating those modifications to a specific function of the protein that could be used for the diagnostics or prognostics of diseases.

The  $\omega$ -3 essential fatty acids produce a different range of lipid oxidation products. The HHE is formed by decomposition of oxidized docosahexaenoic acid (DHA) [113, 114]. Only few studies have been reported on HHE, still there is evidence of it causing severe peritonitis, retinal or liver damage when injected [115] and causing apoptosis via modulation of NF $\kappa$ B signalling pathways [114]. However, lower levels of HHE have been shown to have protective effects against oxidative stress-induced cytotoxicity in vascular endothelial cells by stimulating the expression of antioxidants through the activation of Nrf2 [116, 117]. HDDE has also been found in human plasma although at lower concentrations than HHE or HNE, suggesting this aldehyde is produced *in vivo* [115, 118]. Previous studies on reactivity of 4-hydroxyalkenals comparing the reactivity of HHE, HNE and HDDE with phosphatidylethanolamine showed that HDDE was the most reactive [101], possibly due to a longer aliphatic chain which increased hydrophobicity, and suggests higher reactivity towards polar molecules such as phospholipids [101].

The same oxidation and cleavage mechanisms that generate 4-hydroxy-alkenals can also generate 4-oxo-alkenals such as 4-oxo-2-nonenal (ONE) and 4-oxo-2-hexenal (OHE) [119-122] (**Figure 1.16**).

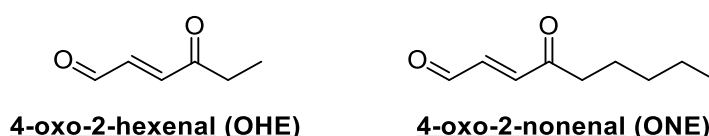


**Figure 1.16. Structure of the most common oxoalkenals to occur as lipid peroxidation products.**

Studies on ONE concluded that it is an even more reactive protein modification and cross-linking agent than HNE [123], depending on the mechanism of adduct formation. While the rate of Michael addition with cysteine and histidine residues is higher, the rate of

Schiff base formation is slower [123]. There is increasing biological interest in studying ONE as an oxidative stress marker, since it was demonstrated to covalently link to human serum albumin, the main protein found in human blood [124], and histones [125]. Attention on OHE has also increased as its mutagenic properties were demonstrated by the ability to form adducts with nucleosides [120, 126].

The hydroxy-alkenals and oxo-alkenals discussed above can be further oxidized to the more stable carboxylic acid form by the action of aldehyde dehydrogenases, generating species such as 4-hydroxyhexenoic acid (HHA), 4-hydroxynonenoic acid (HNA) and 4-hydroxydodecadienoic acid (HDDA). These products of the three aldehydes can be measured in human urine samples [118, 127]. Since HNE comes from  $\omega$ -6 fatty acids, HHE from  $\omega$ -3 fatty acids and HDDE is a lipoxygenase product, differential increases in their corresponding carboxylic acids in urine may be a marker of the type of mechanism of lipid peroxidation involved in a specific pathophysiological condition [127].

Bis-aldehydes are another significantly important short-chain oxidation product and, like 4-hydroxy-alkenals, are bifunctional and can also be a source of cross-linking between proteins, lipids and DNA [128]. The best known is malondialdehyde (MDA), commonly used marker of oxidative stress in clinical samples due to its reactivity and toxicity [129, 130], although it has been much criticized in this respect (**Figure 1.17**).

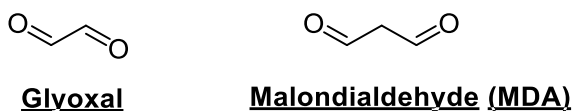


**Figure 1.17. Structure of two bis-aldehydes known to occur as products of lipid peroxidation.**

MDA is generated by the decomposition of oxidised arachidonic acid through enzymatic or non-enzymatic mechanisms. Enzymatically, MDA can be generated as a side product of the synthesis of thromboxane A<sub>2</sub>, by a well established mechanism [131]. The nonenzymatic generation of MDA is less well studied. During cyclization of peroxy radicals, a new free radical is formed which can cyclize again to form bicyclic endoperoxides and undergo cleavage to produce MDA [132]. The reactivity of MDA has been well-characterized previously [133]. MDA can be metabolized once formed, but it can also react with other biomolecules [129]. At physiological pH, MDA occurs in the enolate form with low reactivity, but when the pH drops, MDA reactivity increases. The main product of MDA reaction with DNA is pyrimido-[1,2- $\alpha$ ]-purin-10(3H)-one deoxyribose (M<sub>1</sub>D), which has been shown to induce mutations on mammalian cells [129]. Due to the bis-aldehyde property, MDA can react further, creating an interstrand crosslink in DNA leading to potent biological effects [134]. There is also evidence of MDA being responsible for DNA-histones crosslinking but the biological importance of this is still to be shown [128]. Proteins can also be modified by

MDA, especially on nucleophilic amino acid residues, such as lysine, histidine and arginine. There is evidence that MDA-modified lysines in apoB from oxidised low density lipoproteins (oxLDL) are involved in atherosclerosis inflammatory processes [135, 136]. Apart from direct modification of proteins, MDA can also interfere with protein synthesis by modification of eElongation factor 2 (eEF2), which catalyses the movement of the ribosome along the mRNA in protein synthesis. Hence, MDA is more than just a product of lipid peroxidation; it has its own toxicity towards biomolecules and needs to be considered as an important molecule to study when looking for pathophysiological explanations of diseases. Glyoxal is another bis-aldehyde, analogous to MDA but with a two carbon chain (**Figure 1.17**). There is limited evidence of this aldehyde being a lipid peroxidation product, and the more common source of glyoxal is the oxidation of glucose, especially in diabetes mellitus [60, 137]. Other less well known bis-aldehyde lipid peroxidation products are 2,4-decadienal, a product of oxidized fatty acids and trans-2-butene-1,4-dial, a product of further oxidation of the former [119]. However, it is still not clear if these aldehydes are actually lipid peroxidation breakdown products *in vivo*.

#### 1.2.4. Chloroaldehydes

Oxidizing compounds resulting from oxidative stress are most commonly derived from partially reduced oxygen species, as discussed previously in this report. These can react with other small molecules or ions such as halides generating, for example, reactive chloride species (RCIS) by reaction with the biologically abundant chloride ion. The production of hypochlorous acid (HOCl) is catalysed by the enzyme myeloperoxidase (MPO) [138]. MPO is present in human neutrophils, monocytes and some macrophages [139-141]. In inflammation, MPO is activated and produces mainly HOCl, a strong oxidizing and chlorinating agent, from the oxidation of Cl<sup>-</sup> using H<sub>2</sub>O<sub>2</sub> as a co-substrate [138]. HOCl reacts with unsaturated lipids at the double bond by an electrophilic addition of chloronium ion (Cl<sup>+</sup>) to form chlorohydrins or  $\alpha$ -chloro- $\beta$ -hydroxy derivatives [142]. Additionally, phospholipids with an amino group in the polar head can also be chlorinated. Plasmemyl phospholipids, containing a vinyl ether bond, are the most susceptible to attack by HOCl [143], and this reaction give rise to  $\alpha$ -chloroaldehydes (**Figure 1.18**).

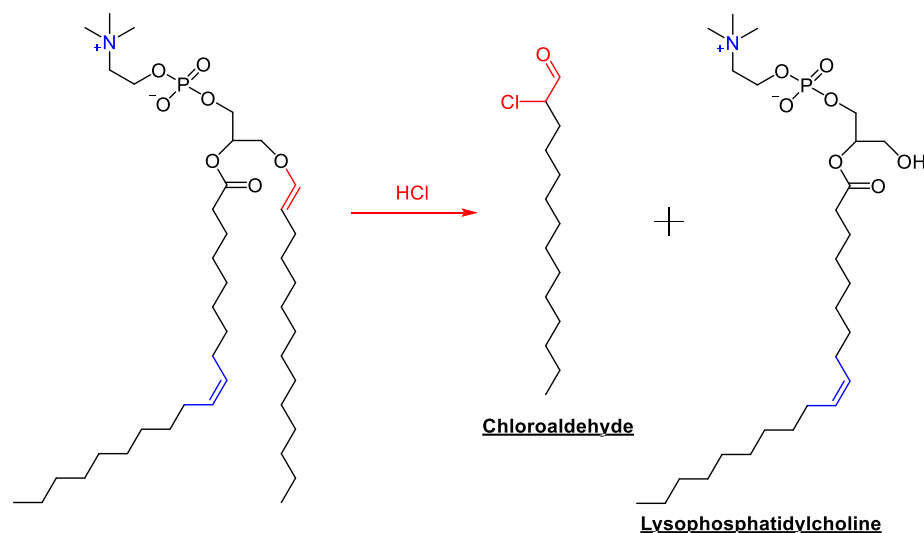


**Figure 1.18. Plasmalogens are targets of HOCl at the alkene chain, at the amine polar head (highlighted in blue) and at the vinyl ether bond (highlighted in red).** The latter is the responsible for the production of  $\alpha$ -chloro-aldehydes.

Although only a small amount of plasmalogens have been shown to be modified by chlorination, which is not enough to disrupt the membrane, alteration in plasmalogen content in specific membranes may have an effect on membrane protein function, making this modification worth studying [138]. As discussed before, plasmalogens are phospholipids with a vinyl ether-linked aliphatic chain at the *sn*-1 position. Hypochlorous acid attack leads to cleavage of the vinyl ether to yield an  $\alpha$ -chlorofatty aldehyde and a lysolipid [143]. The free  $\alpha$ -chloroaldehyde derived from the reaction of the vinyl ether with hypochlorous acid is the major halogenated lipid, and a precursor of other halogenated lipids [144]. An excess of HOCl can lead to a secondary oxidative modification of the lysolipid, leading to the complete degradation of the plasmalogen into a chlorohydrin derivative [145] or glycerophosphorylcholine with the release of the fatty acid at the *sn*-2 position [146].

Several studies have investigated the biological targets of  $\alpha$ -chloroaldehydes.  $\alpha$ -chlorohexadecanal and  $\alpha$ -chlorooctadecanal have both been detected as plasmalogen oxidation products in activated neutrophils [138] and have been found to be elevated significantly in atherosclerotic lesions in cardiovascular disease [147], and in mouse brain following systemic injection of endotoxin [148]. It was previously shown that 2-chlorohexadecanal bound to LDL is able to reduce nitric oxide production through inhibition of endothelial nitric oxide synthase (eNOS) activity, decreasing eNOS mRNA stability [149].

2-chlorohexadecanal is metabolized by oxidation to 2-chlorohexadecanoic acid or by reduction to 2-chlorohexadecanol [150]. These are also known to play biological roles, such as increase COX2 expression and prostacyclin production through increased NF $\kappa$ B

signaling in human coronary artery endothelial cells [151]. This study shown that  $\alpha$ -chloroaldehydes can be involved in pro-inflammatory pathways, therefore making it important to understand the mechanisms underlying such roles.  $\alpha$ -chloroaldehydes have also been shown to be involved in cell death pathways as the apoptosis of microvascular endothelial cells is related to  $\alpha$ -chloroaldehydes stimulating PROS production, caspase 3 activation, ATP depletion and decreasing cell-cell barrier function [152]. A potential mechanism by which  $\alpha$ -chloroaldehydes could cause these changes in cells is the adduction with amines in proteins and lipids. However, their reactivity is still not very well established compared to other lipid oxidation products. The reaction of  $\alpha$ -chloroaldehydes with proteins is discussed in the next section 1.3.

### **1.3. Post-translational protein modification by aldehydes**

Protein lipoxidation is described as the modification of proteins by lipid peroxidation products modifying the side chain of amino acids [153]. In fact, introduction of carbonyl groups into amino acids residues is a hallmark of oxidative damage to proteins. To note that direct oxidation proteins can also generate carbonyl groups, as this modification is not exclusive of lipoxidation. Lipoxidation occurs mainly on the nucleophilic residue cysteine, histidine, arginine and lysine [154]. This leads to the formation of a wide variety of adducts. Compounds containing aldehydes or ketones can react with amines (e.g. on lysine) to form Schiff base adducts by loss of water, whereas those containing an  $\alpha$ ,  $\beta$ -unsaturated moiety can also form Michael adducts by a nucleophilic addition reaction of the protein sidechain at the  $\beta$ -carbon. Bi-functional lipid oxidation products, such as dialdehydes or hydroxyalkenals, can react with proteins and still present free carbonyls, which can be exploited in some detection procedures or further react and give rise to intra or inter protein crosslinking.

#### **1.3.1. Mechanism of adduction**

Schiff bases, named after Hugo Schiff, are formed when a primary amine reacts with an aldehyde or a ketone [155]. A Schiff base is an analogue of an aldehyde where the carbonyl group (C=O) is exchanged by an imine (C=N). It can be synthesized from an amine and a carbonyl compound by nucleophilic addition forming a hemiaminals followed by dehydration to generate an imine (**Figure 1.19A**). In proteins, lysine residue side chain contains a  $\text{NH}_2$  that reversibly reacts with aldehydes giving rise to aldehyde-protein adducts. Alkanals only react with proteins by forming a Schiff base, since their only reactive group is the carbonyl. Originally defined by Arthur Michael, Michael addition is a nucleophilic addition of a nucleophile to an  $\alpha,\beta$ -unsaturated carbonyl [156]. The mechanism of this reaction is



displayed in **Figure 1.19B**. The nucleophile reacts with the electrophilic alkene in a conjugate addition reaction. Eventually, a proton is abstracted from the protonated base by the enolate to form the final adduct. In proteins, the thiol group of cysteines and the amine group of lysines can react reversibly with aldehydes, giving rise to aldehyde-protein adducts. Alkenal and  $\alpha,\beta$ -unsaturated aldehydes having a C-C double bond react with proteins by Michael addition.

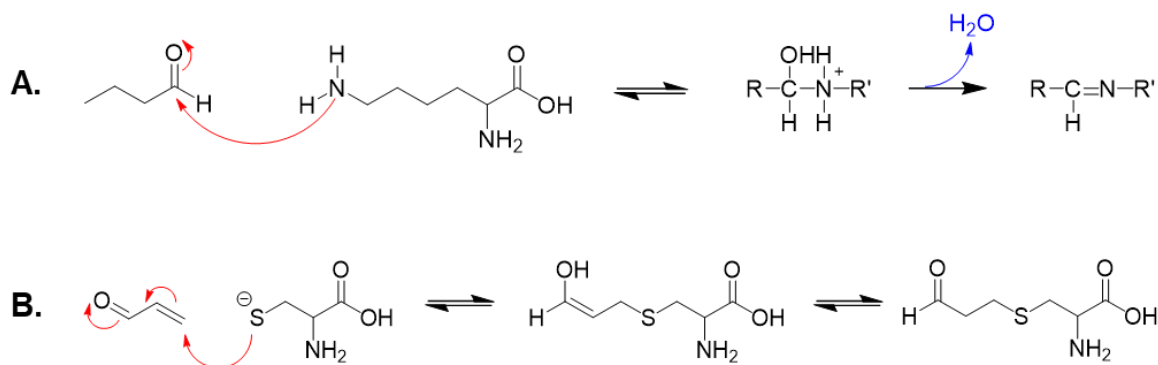


**Figure 1.19. Mechanism of addition of short-chain aldehydes to proteins.** (A) Schiff's base formation mechanism. The example includes butanal as the electrophile and the amino acid lysine as the nucleophile. This reaction is a condensation and therefore loses water. (B) Michael addition mechanism. The example is acrolein as the electrophile and cysteine as the nucleophile.

### 1.3.2. Aldehyde-protein adduction: Structure and Evidence

As adducts can rearrange, to provide evidence for their formation requires good understanding of the multiple structures that these can form. The reaction of amino acids with 2-alkenals have been most studied for acrolein (**Figure 1.20**).

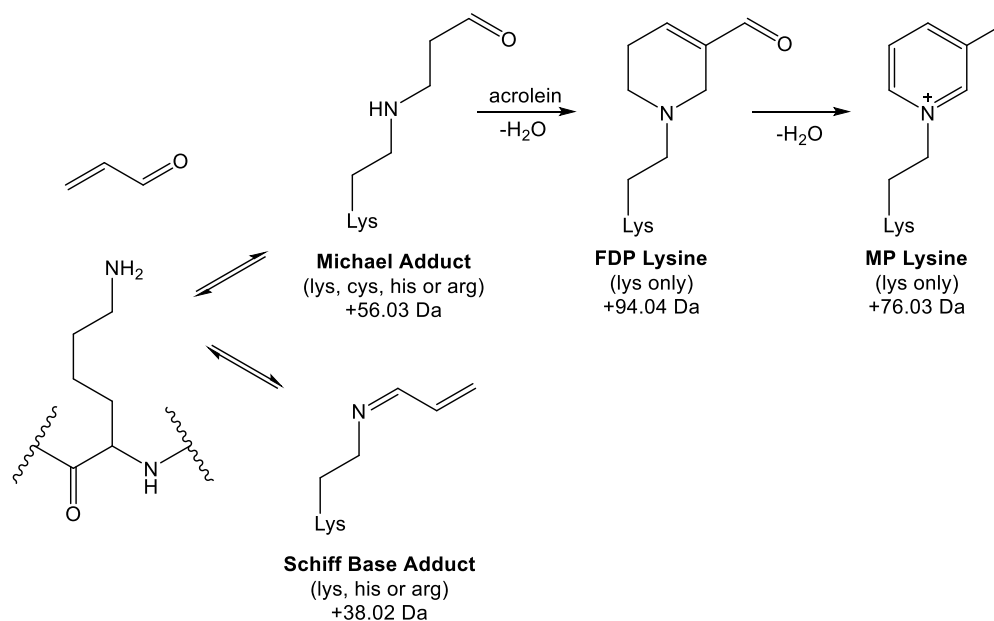


**Figure 1.20. Products formed by reaction of acrolein with amino acid side chains.** Where reactions occurred by Michael addition, only lysine adducts are shown but as indicated in the figure, these can also happen on a cysteine, histidine or arginine residue.

Acrolein has been shown to react with cysteine, lysine and histidine residues of proteins. It was previously shown that the primary product of acrolein reaction with proteins is a  $\beta$ -substituted propanal by Michael addition. However, more than one molecule of acrolein can react with the same amino acid residue. For example, two acrolein molecules can attach to one lysine side chain, forming the piperidine, *N*-(3-formyl-3,4-dehydropiperidino)-lysine (FDP-lysine) [74]. Crotonaldehyde, 2-pentenal and 2-hexenal can generate a similar product, suggesting that this type of adduct is common between alkenals reacting with proteins. Another type of condensation adducts that can be generated after lysine adducts with 2-alkenals are the pyridinium adducts, *N*-(2-methylpyridinium)lysine (MP-lysine) for acrolein and *N*-(5-ethyl-2-methylpyridinium)lysine (EMP-lysine) for crotonaldehyde [157, 158]. In the case of 2-nonenal, an analogous lysine-pyridinium adduct *N*-3-[(hept-1-enyl)-4-hexylpyridinium]lysine (HHP-lysine) is formed [95]. Similar adducts have been reported for 2-hexenal and 2-octenal [159, 160]. Protein amino acid residues can also react with more complex aldehydes such as 4-hydroxy-2-alkenals. The most studied of this aldehyde group is 4-hydroxy-2-nonenal (HNE) (**Figure 1.21**).

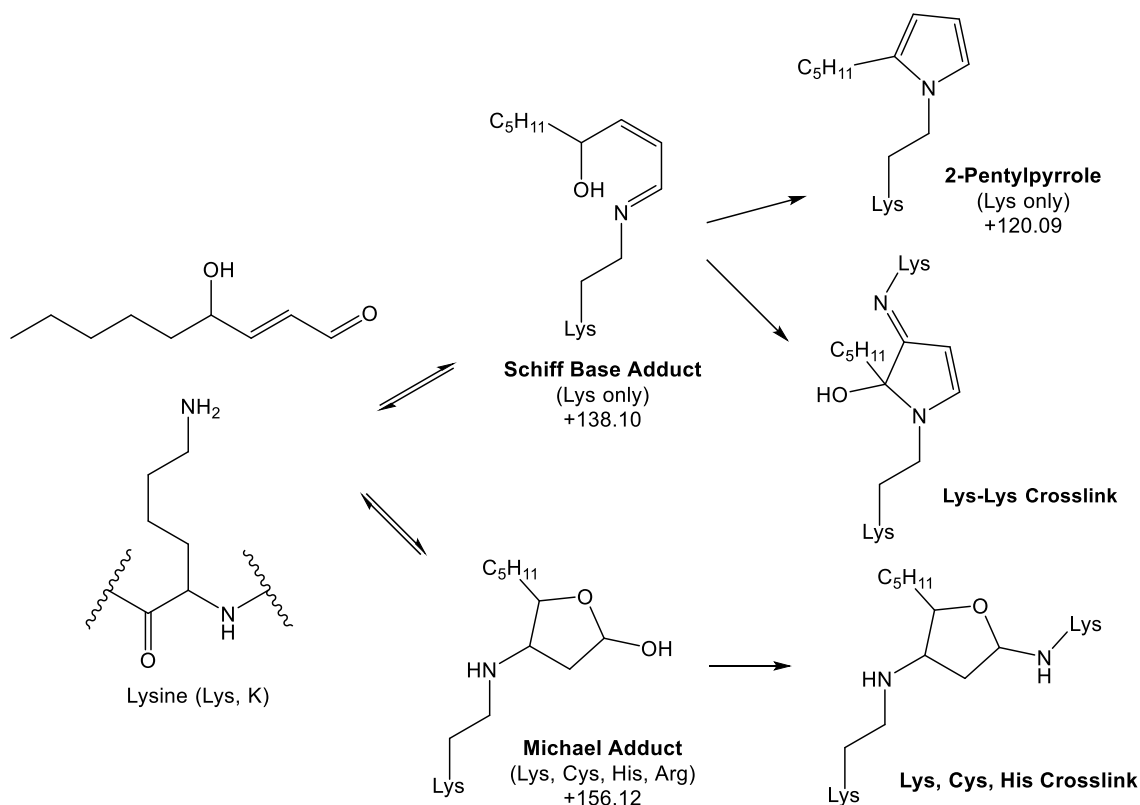
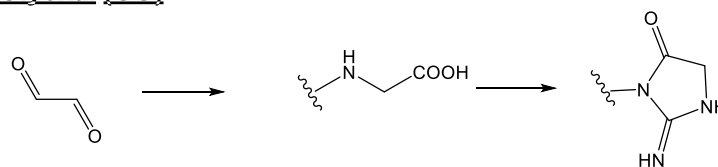


**Figure 1.21. Products formed by reaction of 4-hydroxy-nonenal with amino acid side chains.**

It is known that HNE as well as other 4-hydroxy-2-alkenals react with thiol groups on cysteines by Michael addition (a) [70, 161]. Moreover, HNE can also form Michael adducts with the imidazole group of histidine residues. In the first stage, the imidazole reacts with the unsaturation on 4-hydroxy-2-alkenals leaving the adduct with a free carbonyl group. This can afterwards undergo cyclization to form a cyclic hemiacetal [162] or crosslinking with other proteins or even inside the same protein [163]. For cyclization to occur, the hydroxyl at the aldehyde fourth carbon reacts with the carbonyl group to form the hemiacetal. Another amino acid residue that can be modified by HNE is lysine. Similar to the modification on histidine, HNE forms Michael adducts with lysine and generates a pyrrole adduct (b) [164]. The amino group of lysine reacts with the C3 of HNE by Michael addition. The free carbonyl group on the first carbon of HNE can further react with the same lysine residue forming a 1:2 HNE:amine. This can undergo oxidation and intermolecular cyclization to form the adduct 3-hydroxy-3-imino-1,2-dihydropyrrole-lysine (c).

Another common aldehyde addition product occurs from adducts from saturated aldehydes bearing two carbonyl groups such as glyoxal and malondialdehyde (**Figure 1.22**).

### Glyoxal (GO)



### Malondialdehyde (MDA)

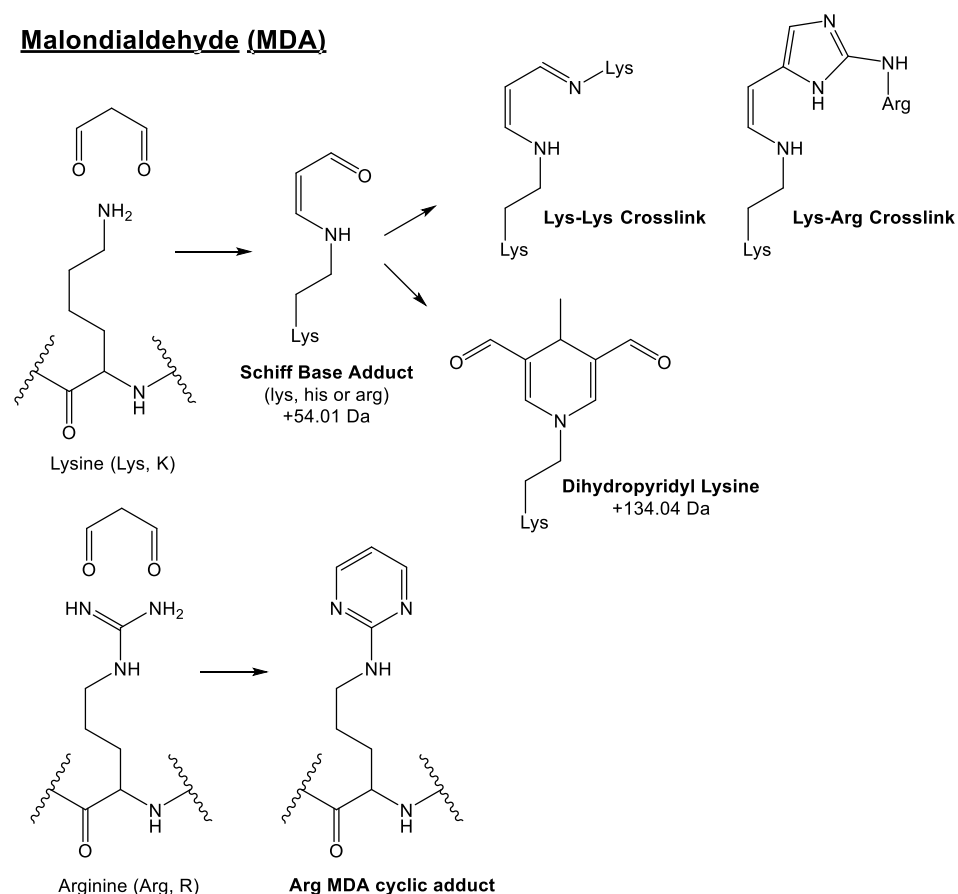


**Figure 1.22. Products formed by reaction of glyoxal or malondialdehyde with amino acid side chains.**

Glyoxal is responsible for the formation of carboxymethyllysine (CML) as well as lysine-lysine crosslinked dimers, resulting in intra or intermolecular crosslinking [165, 166]. A less common amino acid residue to form adducts is arginine. However, it was reported glyoxal reacts with arginine residues to form an imidazole [167]. Malondialdehyde (MDA) is known for specifically modifying lysine residues on proteins resulting in the Schiff base adduct *N*-(2-propenal)lysine [168]. As explained for the other aldehyde adducts, the MDA adduct has a carbonyl group free to react with another amino acid residue again by Schiff base formation. Again, this results in intra or intermolecular protein crosslinking [169]. ONE is another bis-aldehyde capable of reaction with nucleophilic amino acid residues such as lysine, histidine, cysteine and arginine [170]. The first group to react is the double bond via Michael addition resulting in a 4-oxononanal adducts. Due to the lower stability of this

product, further reactions occur to more stable adducts. From the reaction with lysine the adducts are dihydrofuran, dihydropyrrole and 4-ketoamide derivatives [171], from reaction with arginine the adduct is a substituted imidazole [172] and from reaction with cysteine and histidine the adducts are furan derivatives [173, 174].

### 1.3.3. Reversibility and detoxification of aldehyde-protein adducts

Protein carbonylation by reaction with aldehydes, by Michael addition and Schiff-base formation, are not completely stable and can be reversible [175, 176]. In the presence of lower levels of short-chain aldehydes, these can modify a protein but readily be followed by its “decarbonylation”. This reversible protein damage may reflect a reversible signaling mechanism [177-179].

Abundant proteins like human serum albumin can protect other proteins from modification by aldehydes by acting as carbonyl scavengers using their surface and easily accessible nucleophilic residues [180]. Antioxidants can also quench carbonyl species preventing the formation of protein-aldehyde adducts and promoting their excretion [181]. Glutathione (GSH) and other thiol-containing proteins, such as thioredoxin (Trx) are effective in decreasing protein carbonyls and may be regulating this decarbonylation process [177, 179]. Previous *in vitro* studies have shown Michael adducts to be reversible in the presence GSH [180] which thiol residue conjugates with aldehydes not only protecting other residues from its modification but also enabling it excreted [181, 182] (**Figure 1.23**). Even though dialdehyde such as glyoxal and malondialdehyde cannot react by Michael addition, it has been suggested that these can also be quenched by GSH as a cyclic adduct can be formed with the glutamate residue [183]. For  $\alpha,\beta$ -unsaturated aldehydes, such as HNE, carnosine is another highly selective scavenger as it reacts by both Michael addition and Schiff-base formation involving both functional groups of these aldehydes [175]. To characterize and detect these scavenger-aldehyde adducts in biological samples is critical since scavengers of carbonyl species are being suggested as good therapeutic target for inflammatory diseases [184].

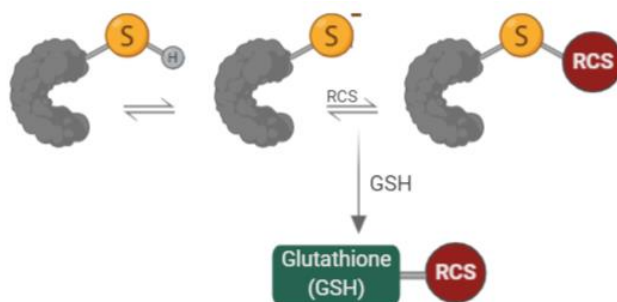


**Figure 1.23.** Diagram illustrating the reversibility of protein modification by reactive carbonyl species and the detoxification of these by thiol-containing compounds such as glutathione.

#### **1.4. Detection methods for aldehydic oxidation products**

To understand the biological significance of each lipid oxidation product, it is important to have reliable and sensitive methods to identify and quantify them. While some lipid oxidation products are stable, the aldehydes mentioned in the section above are highly reactive and therefore harder to detect. Aldehydes can be identified either in the free form or more likely as covalent adducts with proteins, DNA or aminophospholipids. Consequently, quantifying free aldehydes in complex clinical samples can represent a challenge and may not reflect the extent of their formation. However, the analysis of aldehydes as protein adducts also has its own challenges due to the number of possible products. To know the exact aldehydes formed, their targets and the masses of their modifications is usually required for the analysis.

##### **1.4.1. Analysis of free aldehydes and their metabolites**

Methods for the detection of free aldehydes and their quantification include spectrophotometric methods and gas or liquid chromatography coupled to mass spectrometry [185, 186]. The simplest approach is the direct spectrophotometric measurements; for example, HNE absorbs in the UV range at 220 nm [187]. However, a better approach would be to use aldehyde-reactive probes which allows their specific and sensitive detection and increase the stability of the aldehyde. The TBARS assay for malondialdehyde is extensively used due to its simplicity and low cost [188], but even when combined with other techniques such as HPLC, it has poor specificity among other limitations [129, 130]. 2,4-dinitrophenylhydrazine (DNPH), which gives a dinitrophenylhydrazone product with an absorbance at 380 nm [189], is often used to detect carbonyl groups on proteins by ELISA or western blotting.

A disadvantage of the use of probes is the lack of specificity and consequently chromatographic separation is required pre-column or post-column derivatization by reverse phase HPLC [190]. Gas chromatography can also be used but requires the sample to be volatile and it is usually coupled to mass spectrometry. Free HNE can be converted to pentafluorobenzyl oximes (PFBO) by reaction with pentafluorobenzyl hydroxylamine, followed by formation of trimethylsilyl ethers and the PFBO-TMS derivatives of HNE analysed by GC coupled to electron-capture negative-ion ionization (NICI) MS. This method was previously used to detect HNE in patients with thyroid dysfunction or migraines [191], and a similar method was also used to analyse MDA and HNE in human serum samples [186]. GC coupled to NICI-MS and PFBO derivatization were also used to detect  $\alpha$ -chloroaldehydes [192, 193]. In contrast, LC-MS requires minimal samples manipulation prior to analysis [186]. Several approaches have been used for the analysis of aldehydes by

LC-MS usually following DNPH derivatization to stabilize them [194]. For example, this approach allowed the detection of MDA, crotonaldehyde (CRT), benzaldehyde (BNZ), hexanal (HXL), HHE, HNE, 2,4-nonadienal and 2,4-decadienal in animal feed [195].

It is known that free aldehydes are metabolized and detoxified, therefore the analysis of their metabolites may help get a better representation of the aldehyde *in vivo*. HNE can be detoxified by conjugation to glutathione [196], as previously mentioned, and metabolized to 1,4-dihydranonane-mercapturic acid, which has been detected in urine [197]. 2,4-decadienal (DDE) can be oxidized to 2,4-decadienoic acid and cysteine-conjugated 2,4-decadien-1-ol, and both have been found in cell culture models and urine from mice by LC-MS [198]. The carboxylic acids of HHE, HNE and HDDE were detected by NICI-MS in human urine for aging and diabetes [118]. Similarly,  $\alpha$ -chloroaldehydes can be converted to the PFB ester form and analysed by GC coupled to NICI-MS [152] or can form adducts with GSH and be detected by LC-MS [199].

#### **1.4.2. Analysis of aldehydes as adducts with macromolecules**

The analysis of free aldehydes has several disadvantages as their high reactivity readily results in formation of adducts with a variety of biological molecules. Hence a large proportion of the aldehydes formed are likely to exist as adducts. Consequently, a full understanding of the roles of these aldehydes depend on analysis of the adducts formed through Schiff base reactions and Michael additions or rearrangement of these products, as described in 3.2. Although adducts with DNA bases are known to occur and are thought to contribute to the mutagenicity of acrolein and crotonaldehyde, most attention has focused on detecting the formation of adducts with proteins. The structures of a substantial number of protein adducts have been elucidated, and examples are shown in **Figure 24-26**. To this end, two main approaches exist: antibody-dependent techniques, and proteomic methods including protein identification and sequencing by mass spectrometry. These two approaches may also be combined.

#### **1.4.3. Antibody-based methods**

The development of antibodies against the adducts formed from MDA, HNE and others have increased in the past thirty years [200, 201]. These have been validated for ELISA, western blotting, immunocytochemistry and immunochemistry. The antibodies and antisera available for HNE have been previously reviewed [63]. A monoclonal antibody against acrolein adducts with proteins has also been developed [202, 203]. Another antibody against the same immunogen was shown to recognize acrolein-modified albumin with limited cross-reactivity with other albumin adducts [204]. A monoclonal antibody has been

raised against nonenal-modified keyhole limpet hemocyanin, and it was able to recognize the N $\epsilon$ -3-[(hept-1-enyl)-4-hexylpyridinium] lysine (HHP-lysine), a novel nonenal-lysine adduct [95]. Antibodies against aldehyde adducts with DNA bases have also been developed and have been developed and validated for FACS-based assay and ELISAs [205]. These antibodies have demonstrated the occurrence of adducts of aldehydes in tissues and, especially anti-HNE antibodies, have been applied to western blotting for lipoxidation identification [206]. Some antibodies such as anti-DNP have been broadly used for carbonyl-containing proteins [207], however carbonyls can arise from other modification than aldehydes, and even aldehydes only add a carbonyl group to the protein when reacted by Michael addition. Additionally, several of the antibodies available are polyclonal which decreases its specificity and increases cross-reactivity. Specificity is therefore the limitation of the antibody-based methods for aldehyde adducts detection. Antibody-based method have been recently reviewed by our group [31].

#### **1.4.4. Protein analysis by mass spectrometry**

Mass spectrometry (MS) is a powerful analytical technique for protein research. MS is used for identification, quantification and characterization of proteins [208]. The advance in instrumentation and the coupling with separation techniques such as liquid chromatography has moved the proteomics field forward and allowed analysis of hundreds of proteins in parallel to be a common experiment. Mass spectrometry (MS) measures the mass-to-charge ratio ( $m/z$ ) of ionized analytes. The main methods for ionization are electrospray ionization (ESI) and matrix-assisted laser desorption/ionization (MALDI). ESI generates ions from large and complex molecules in solution which makes MS a preferential ionization method to the analysis of molecules like proteins [209]. On the other hand, for MALDI the proteins are embedded within a matrix in a solid state and ions are generated by pulses of laser light [210]. The ions generated by ESI are more multiply-charged than MALDI, supporting the use of ESI over MALDI for large molecules analysis. Oxidative modifications of proteins alter their composition, and change their  $m/z$  ratio and potentially their ionization conditions [211]. Two different MS approaches can be applied to the analysis of proteins: top-down proteomics, which analyses intact proteins and their fragmentation within the mass spectrometer; and bottom-up proteomics, which analyses peptides from proteins digested with proteases prior to MS analysis.

##### **1.4.4.1. Sample preparation**

Bands or spots from western blotting or SDS-polyacrylamide gels stained with coomassie can be excised for protein analysis [212, 213]. Bottom-up approach requires the



proteins to be digested in-gel or in-solution, prior to MS analysis. Both protocols for protein digestion may cause artefacts to proteins such as oxidation of methionine and tryptophan or carboxymethylation of cysteine, which can interfere with interpretation of results [214]. The most commonly used protease is trypsin, which cleaves within the polypeptide chain on the carboxyl side of lysine or arginine residues, except when either is followed by proline, or an adjacent negatively charged residue that masks their positive charge [215, 216]. To increase the sequence coverage, alternative proteases can be used in combination with trypsin. Additionally, if the residues lysine and arginine are modified by lipoxidation as described above, the trypsin would miss these as cleavage sites, generating longer peptides that do not ionize as well and give low ion intensity, increasing the challenges with their detection [217]. Therefore, combination of different proteases could help overcome this limitation, including chymotrypsin (large hydrophobic), Asp-N (N-terminal to asp), Glu-C (N-terminal to Asp and Glu) and others [218]. New digestion methods, such as SMART digestion (Thermo), a kit for in-solution digestion designed for fast and highly reproducible digestion of proteins, may help to minimize sample handling. In this protocol, there is no need to perform additional steps of denaturation, reduction and alkylation, decreasing the causes of artefacts. Addition of surfactant can also improve sample digestion and therefore sequence coverage, such as ProteaseMax (Promega) [219] and Rapigest (Waters) [220], which are MS-compatible additives.

#### **1.4.4.2. Enrichment and labelling approaches**

Label-free MS analysis of post-translational modification of proteins is challenging due to the low stoichiometric levels of modified protein in the complex mixture, and thus it is difficult to identify them among other more abundant signals. This limitation can be overcome by enrichment tools that can be applied to bottom-up approaches, increasing its sensitivity and specificity [221].

The most commonly used enrichment technique for carbonyl formations is the biotin hydrazide label, which is then enriched by avidin capture. Chavez et al. introduced a biotin-tagged aldehyde reactive probe (ARP) that reacts with protein aldehydes forming a C=N bond on the carbonyl group resulting in a stable biotinylated oxime derivative followed by detection by western blotting or mass spectrometry [222]. This approach has been applied to enrich lipoxidation adducts of cardiac mitochondria, for which acrolein, HHE, HNE and ONE modifications among others were reported [223]. ARP-streptavidin for enrichment can either be used at the level of modified protein or modified peptides after proteolytic digestion [224]. The protein targets and modification sites identified in these enrichment studies can be useful to develop targeted assays. The same group also developed an alternative

method for relative quantification of site-specific carbonyl adducts, involving d0/d4-succinic anhydride labelling followed by enrichment using hydrazine-functionalized beads [225]. It was reported that HHE Michael adducts were the most abundant, but acrolein, HNE and ONE adducts to cystine, histidine and lysine were also reported. Comparison between carbonyl-labelling reagents indicated that 2,4-dinitrophenylhydrazine (DNPH), biotin hydrazide (BHZ) and O-(biotinylcarbazoylmethyl) hydroxylamine (ARP) were selective for aliphatic aldehydes and ketones and that better results are obtained from enrichment of peptides after digestion rather than labelling of the whole protein [226]. Therefore, biotin affinity with MS peptide analysis can provide information on a variety of protein modifications in clinical samples. However, this approach had limitations such as detection of carbonyls resulting from direct attack of free radicals on proteins instead of aldehydes from lipid peroxidation, and it would only enrich adducts generated by Michael addition bearing a carbonyl group and it will miss Schiff base adducts.

A novel approach to determine targets of small reactive aldehydes involves the chemical synthesis of an aldehyde analogue with an alkyne or azido termini, which allows their adducts to be selectively extracted from biological samples [227]. For example, alkynyl analogues of HNE can form adducts with protein that can be label with azido-biotin tags by Cu<sup>+</sup>-catalysed cycloaddition (Click chemistry). Using this technique it was found that heat shock proteins 70 and 90, and the 78-kDa glucose-regulated protein, were selectively adducted by HNE [228].

Yet, labelled methods also have disadvantages such as being expensive and an additional step in the analytical workflow. Additionally, most of the labelling probes rely on the detection of the carbonyl group which would not be present in the case of a Schiff-base formation resulting in non-detection of this type of modification on proteins. Other limitation of labels such as biotin is the low throughput and the difficulty in localising the modification by MS since the ionisation and peptide fragmentation can be compromised by the labelling [211]. Therefore, novel label-free methods with better sensitivity and specificity are needed to push the study of aldehydic protein modifications further.

#### **1.4.4.3. Separation**

Chromatography is a separation technique whereby molecules in a mixture applied onto a stationary phase are separated from each other by a mobile phase. Differences in adsorption, partition, affinity or molecular weight separate proteins/peptides in the mixture, since some remain longer in the stationary phase while others elute rapidly into the mobile phase [229]. Chromatographic methods coupled to mass spectrometry improve protein analysis by adding a separation step to reduce the diversity and complexity of proteins and peptides present in biological samples prior to MS analysis. The resolving power of the chromatography reduces the ion-suppression effect in MS and allows low abundance species such as post-translationally modified proteins and peptides to be detected [230].

Liquid chromatography coupled to mass spectrometry (LC-MS) is the most common analytical technique used in proteomics. LC has a broad selection of stationary and mobile phases that can be chosen and adapted to each study. The choice of appropriate LC method makes it possible to enrich low-abundance proteins presented in a complex sample. Reverse-phase, ion-exchange and size exclusion are the most commonly used liquid chromatography methods [231, 232] (detailed information on each method is available in the introduction of chapter 5). An advantage of LC is the ability to directly introduce the separated proteins or peptides into the mass spectrometer through electrospray ionization (ESI) for analysis [233]. The separation of peptides and proteins is key in both top-down and bottom-up MS approaches.

#### **1.4.4.4. Intact protein and top-down proteomics**

The analysis of intact protein by mass spectrometry is used to determine the mass of the protein, and changes in mass that can be indicative of post-translational modifications. Both ionization techniques mentioned above can be used, but ESI is more common as it is usually able to give better mass accuracies since it generates many different charges, giving rise to a higher number of peaks in the spectrum [234]. Nevertheless, multiple charging only works for a limited number of proteins in the mixture until the signals start to overlap and it becomes a challenge to deconvolute the data. This approach provides information on the total extent of modification on the whole protein and has been previously applied to detect several modifications on histones [235], glutathionylated haemoglobin [236], electrophilic modifications [237, 238] and characterization of monoclonal antibodies [239]. Top-down MS involves fragmentation of intact protein within the mass spectrometer and analysis of the fragment produced to determine the specific sites and nature of modification. Even though this approach has great potential for mapping lipoxidation modifications, it requires high-resolution instrumentation and is limited by their sensitivity [240]. The combination of

different techniques is useful to understand the extent and better characterize lipoxidation, since these can complement each other and provide more and better information on protein modification. For example, a top-down approach was used to investigate the formation of adducts between ubiquitin and several aldehydes including MDA and HNE and to assess an order of reactivity of these, while a bottom-up analysis of the tryptic peptides of the same samples allowed mapping of the modification sites [241].

#### 1.4.4.5. Bottom-up proteomics

In contrast to top-down, bottom-up approach involves the digestion of protein to peptides as described in 4.2.2.1. This approach is routinely performed by LC-MS and is advantageous in complex protein mixtures as it has the potential to identify low abundance proteins. The presence of post-translational modification requires confirmation by tandem MS to sequence the peptide and localize the specific site and nature of modification [211] and this can be performed by various types of tandem MS experiments including untargeted or semi-targeted/targeted approaches [242] (**Figure 1.24**). Untargeted techniques have commonly been applied to individual proteins due to the challenges of implementation in complex samples. However, to develop targeted and semi-targeted approaches, the selection of peptides to be fragmented has to be carried out by preliminary untargeted MS scan [243]. There have been significant efforts to develop new targeted and semi-targeted methods based on diagnostic ions for oxidative modification, but these require prior knowledge on the modified peptide and its fragmentation pattern.

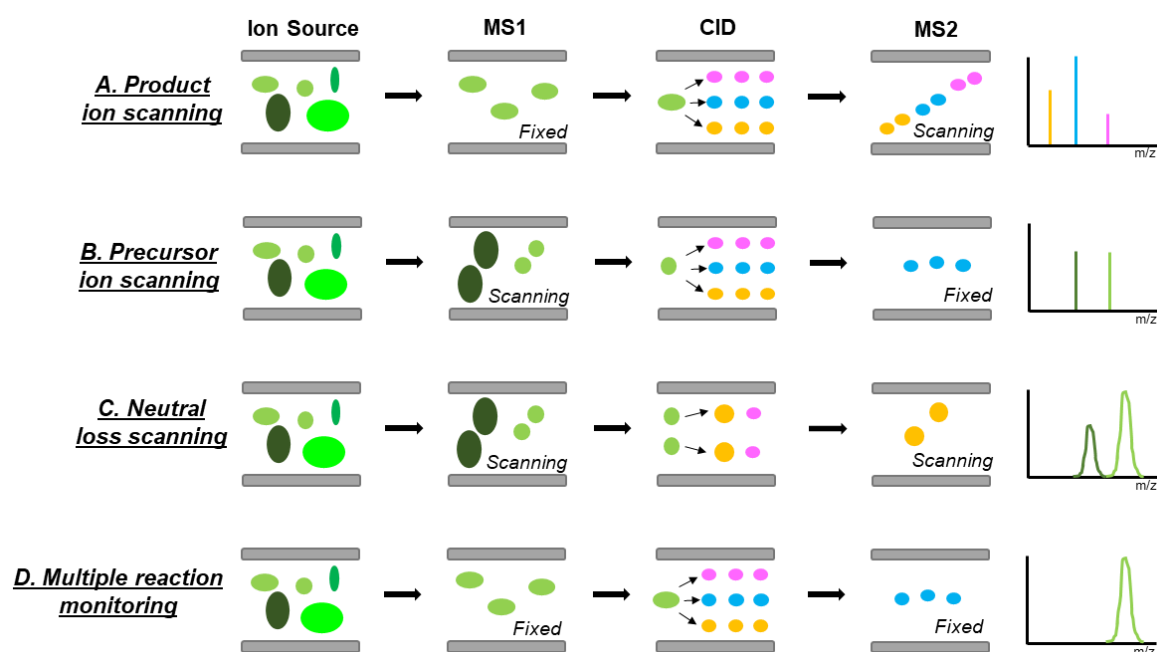


**Figure 1.24. Schematic representation of various types of tandem mass spectrometry experiments.** (A) Product ion scanning generates fragment ion spectra for the identification of the

amino acid sequence of specific peptides. The first analyzer (MS1) selects one precursor ion at a time, then the selected ion undergoes CID in the collision cell, and the fragments are analyzed by the second analyzer (MS2). This process is repeated for different precursors. (B) Precursor ion scanning sets the second analyzer (MS2) to transmit only one specific fragment. MS1 is scanned to detect all the precursor ions that generate this fragment. (C) Neutral loss scanning scans both analyzers to detect the mass difference of ions passing through MS1 and MS2, such difference corresponds to a neutral fragment lost in the collision cell. (D) MRM involves a series of one precursor ion and one specific fragment for that precursor being selected by MS1 and MS2, respectively. The instrument cycles through a series of transitions (precursor-fragment pair) which is particularly useful to detect specific analytes in complex samples. Adapted from [244].

#### 1.4.4.6. Untargeted or Shotgun Mass Spectrometry Approach

Untargeted approaches can also be referred to as shotgun or discovery approaches (**Figure 1.24A**). After digestion, the peptides are analysed by MS and the peptide mass fingerprint used to identify the proteins present by matching with theoretical masses of peptides in a database, since the large dataset generated would be too difficult to manually analyse [245]. The most common search engines and their advantages and disadvantages have been previously reviewed by our group [211]. These search engines have the option to include in the search the masses of specific post-translational modifications as variable modifications [246]. However, the number of modifications being search at once is limited due to the increase in false positive identifications [69, 243]. Even though these softwares are often able to detect the oxidative modifications, validation of the MS/MS data by *de novo* sequencing is essential to confirm the presence and location of the modification [247]. The fragmentation of peptide ions needs to be understood as this constitutes the basis for peptide identification and *de novo* sequencing validation [248]. The Roepstorff and Fohlman system [249] covers the cleavage of every single bond in a protonated peptide and the products are named A, B and C ions if the charge is retained on the N-terminal fragment or X, Y and Z if it is retained on the C-terminal fragment and the subscript numbers indicate the residues involved, counting from the relevant terminal (**Figure 1.25**). These nomenclature has been superseded by the Biemann system [250] which includes fragment ions generated by cleavage of side-chain groups. In this system the lettering is italicized lower case and the ion charge, and the hydrogens gained are implicit. More recently, another nomenclature system for peptide ion fragmentation was proposed to overcome some of the ambiguity in labelling fragment ions [251].

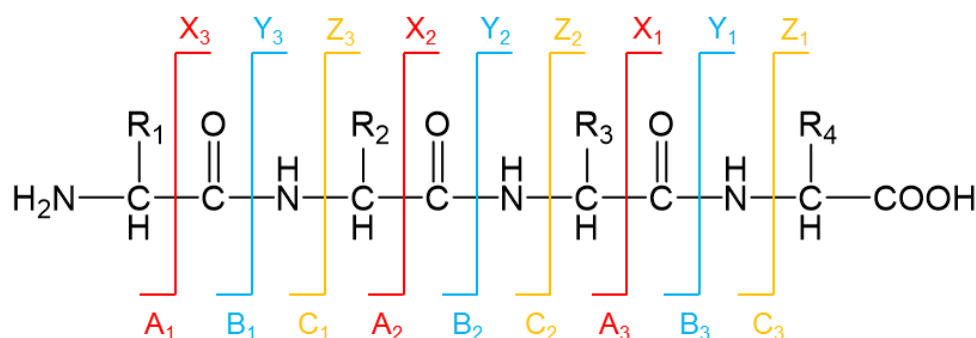


**Figure 1.25. Roepstorff and Fohlman nomenclature system for protonated peptide fragmentation.**

This approach allowed protein modification by HNE to be detected in Down syndrome cases in which 2D electrophoresis was carried out prior to MALDI-TOF peptide analysis and Mascot used for database search [252]. Using a similar approach, HNE modifications were found on complex I subunits in mitochondria from diabetic kidney, where two types of electrophoresis were used; the blue native polyacrylamide gel electrophoresis (BN-PAGE) and the denaturing SDS-PAGE, followed by protein digestion, separation by LC and peptide mapping by mass spectrometry [253]. Another study on ApoE by MALDI-TOF/TOF MS detected several acrolein adducts, for example the aldimine adduct with an increase in mass of 38 Da at Lys149 and Lys155, a propanal adduct with 56 Da at Lys135 and Lys138, MP-lysine adduct at Lys64, Lys67 and Lys254 and FDP-lysine at Lys68 [254]. Acrolein-modified ApoE has impaired binding to LDL receptor and heparin, possibly due to changes in folding proving the biological importance of lipoxidation. A label-free LC-MS/MS approach was used to investigate the sites of modification of chymotrypsin, cytochrome c,  $\beta$ -lactoglobulin and RNase A upon treatment with 2,4-dodecadienal [238]. A reporter ion at  $m/z$  286 was detected and deduced to correspond to the presence of a lysyl-pyridinium adduct. Such diagnostic ions can be used to develop semi-targeted (precursor ion scanning) or targeted (single or multiple reaction monitoring) mass spectrometry approaches for the detection of these modifications.

#### **1.4.4.7. Targeted and semi-targeted approaches**

Reporter ions are diagnostic for a specific analyte of interest, usually products from the fragmentations of the peptide. These are discovered by untargeted MS data analysis and have been used in the development of label-free methods [255]. While for semi-targeted methods the fragmentation product is the report ion, but the precursors are unknown, for targeted methods both precursor and fragment ions are fixed and used as reporters. Both methods increase the specificity for oxidative post-translational modifications, including

aldehyde adduction to proteins, and relative quantification can be achieved using relevant reporter ions.

Precursor ion scanning (PIS) (**Figure 1.24B**) and neutral loss scanning (NLS) (**Figure 1.24C**) are tandem MS routines which enables molecules to be identified by characteristic fragmentation ions. These are both examples of semi-targeted approaches. In PIs the second analyser is fixed to detect a specific fragment ion and the first analyser is scanning for precursor ions that generate this ion upon fragmentation. Immonium ions are internal fragments generated by the combination of a and y type cleavage and are reporter ions for each amino acid residue. The modified amino acid residue gives rise to a modified immonium ion, which has been the most commonly used reporter ion for protein modification [256, 257]. In neutral loss scanning, the diagnostic fragment it is not charged so its generation is detected by scanning in both analysers a mass offset corresponding to the mass of that fragment. For example, protein adducts of HNE can be monitored by neutral losses of 138 Da and 156 Da, for Schiff base and Michael adducts respectively [258, 259].

Targeted approaches include single reaction monitoring (SRM) and multiple reaction monitoring (MRM) (**Figure 1.24D**). For these, both precursor ion and product ion masses are fixed for analysis of an analyte of interest [260]. The peptides are filtered by the first quadrupole (Q1) based on the precursor ion  $m/z$ , followed by fragmentation of the peptides into product ions in a collision cell. The product ions are then filtered in Q3 based on the set product ion  $m/z$  value. The fragmentation from the  $m/z$  of the precursor to the  $m/z$  of the product ion is referred to as a transition and the success of an MRM experiment depends on the selection of the most appropriate transitions. Therefore, to develop an MRM routine, prior knowledge of the analytes is required. As this is not a discovery technique, its most common application is as a MS-based quantification tool [261, 262]. For example, HNE-modified HSA can now be quantified in plasma by a novel MRM routine that monitors two modified peptides each containing amino acid residues that were previously shown to be highly susceptible to HNE modification [263]. Another MRM method was developed to detect the presence of the enzyme CYP37A1 modified by isolevuglandin iso[4]LGE2 in human retinal samples, which was developed based on bottom-up MS data that identified three specific lysine residues for the adduction [264]. A similar approach was able to detect isoketallysine-lactam adducts in dendritic cells by stable isotope dilution MRM [265]. Methods for detection of isolevuglandins adducts *in vivo* is important since these cannot be detected as the free form in tissue due to high reactivity [266].

#### **1.4.5. Quantification of aldehydes in human plasma or serum**

The quantification of free aldehydes in serum may depend on their rate of production, breakdown, detoxification and adduction to macromolecules [267]. Additionally, adduct formation is a reversible reaction, unless reduction or cyclization happen, which may affect quantification. The concentration of free aldehydes has been measured in a number of diseases such as diabetes, rheumatoid arthritis and lung cancer. Different techniques result in different basal levels of aldehydes in health subjects, noting therefore a lack of consensus on these concentrations in plasma. HNE concentrations have been reported to be 80-960 nM while MDA varies from 0.36 to 15  $\mu$ M and ACR from 42 to 1260 nM in healthy subjects [31]. The quantification of these aldehydes has been previously reviewed [186] and it has been discussed that storage time can affect these concentrations by artefact formation [268]. Overall, a small increase in plasma aldehyde concentration is detected in case of disease, although larger increases have been reported in diabetics with an ACR and MDA concentrations of 6.35  $\mu$ M and 25.6  $\mu$ M, respectively [269]. Nevertheless, these concentrations should be interpreted carefully since aldehydes such as acrolein can have sources other than lipid peroxidation [71].

#### **1.4.6. Metabolomics by Nuclear Magnetic Resonance (NMR)**

During inflammatory diseases and cancer, cells change extensively their metabolism to meet the new metabolomic requirements [270]. Aldehydes can also cause alterations in metabolome by interaction with enzymes or metabolites themselves. Glycolytic enzymes are targets for reaction with lipid peroxidation aldehydic products. For example, HNE was reported to inactivate glyceraldehyde-3-phosphate dehydrogenase (GAPDH) by covalent binding primarily to amino acid residues on the surface of the enzyme in a time-dependent manner [271]. Similarly, acrolein cellular toxicity has been related to inactivation of GAPDH [272]. Other glycolytic enzymes such as pyruvate kinase and phosphofructokinase are also sensitive to cellular redox balance and to inactivation by aldehydes [273].

The proteomic studies reported above were performed by LC-MS/MS and reported specific sites of modification and mechanisms of inactivation. However, metabolomic studies can provide additional information on the mechanism of action. The study of the metabolomic state of a cell is important to understand the effect of protein modifications on metabolic pathways. Even though the most successful approaches for metabolomics are mass spectrometry and nuclear magnetic resonance (NMR) spectroscopy [274], NMR offers many advantages over MS. These include the quantification of metabolites in biological samples or cell extracts without complex sample preparation and the ability to analyse compounds that would be difficult to ionize for MS analysis. Using stable isotope



labels, NMR is also able to elucidate metabolic mechanisms by tracer-based metabolism approach, which allows changes in metabolites to be assigned to particular pathways [275]. The most important nuclei in biomolecular NMR studies are  $^1\text{H}$  (proton),  $^{13}\text{C}$ ,  $^{15}\text{N}$ , and  $^{31}\text{P}$ . Proton is the most sensitive and one-dimensional (1D)  $^1\text{H}$  NMR is the most widely used approach in metabolomics, but signal overlap might be a problem in metabolite identification. Two dimensional (2D) NMR, as well as the use of standards, can overcome ambiguous identification of metabolites in complex mixtures [276]. The combination of MS and NMR has been previously reviewed [277] and many improvements in metabolites characterization reported, both in their identification and quantitation. While MS quantifies isotopic labelling distribution, NMR gives the specific labelling position, information which is not always available from MS/MS data.

## **1.5. Aims and hypothesis of the work presented in this thesis**

Short-chain lipid peroxidation products such as aldehydes are highly reactive and able to modify proteins. Lipoxidation products occur in inflammatory pathologies, thus the importance of their study as potential diagnostic and prognostic markers of disease. Mass spectrometry based approaches are becoming increasingly important in lipidomic and proteomic research. However, there is still a need to improve the methods currently used, in particular the methods for detection of lipoxidation products. Subsequently, the biological implication of these products is still not completely understood. With this lack in knowledge in mind, the objectives of the thesis were as follows:

- Detection of reporter fragmentation ions by MS of proteins and peptides modified by aldehydic short-chain lipid peroxidation products (chapter 2);
- Development of targeted MS methods using reporter ions for the detection of lipoxidized proteins and peptides (chapter 2);
- Alternatives to 2-chlorohexadecanal synthesis and comparison of their reactivity with the reactivity of other aldehydes towards proteins and peptides (chapter 3);
- Test and comparison of chromatographic methods for native protein separation and lipoxidized proteins and peptides separation (chapter 4);
- Assessment of the effect of aldehyde adducts on the glycolytic enzyme pyruvate kinase activity and structure, determine the hotspots for modification by MS and analysis of the impact of the aldehydes in the cellular metabolism. The hypothesis was that the aldehydes were able to modify the enzymes altering its function and interfering with the normal cellular metabolism (chapter 5);
- Assessment of the cellular structural changes by confocal microscopy monitoring of the Cys328-mediated effect of small aldehydes on vimentin network and monitoring the ability of the cells to reorganize the network 24 hours after treatment (chapter 6).

**Chapter 2. A mass spectrometry approach for the  
identification and localization of small aldehyde  
modifications of proteins**

## 2.1. Introduction

Oxidative stress results from a redox imbalance and consequently a relative increase in oxidative species [17]. Free radicals cause damage to biomolecules including proteins, lipids and DNA, changing their structure and possibly their function. Lipids are a major target of oxidation in biological systems [23]. Polyunsaturated fatty acids (PUFAs), for example present in membrane phospholipids, are highly susceptible to oxidation due to the multiple unsaturation in the carbon chain [23]. Lipid peroxidation leads to the formation of a variety of oxidized products. Oxidized lipids are known to be key players in the development and progression of inflammatory and age-related diseases such as Alzheimer, Parkinson, multiple sclerosis, cardiovascular diseases, atherosclerosis, diabetes, liver and lung diseases [29, 278, 279]. Oxidised lipids can undergo fragmentation and give rise to short-chain oxidation products such as aldehydes [20, 23, 60]. Mechanism of formation and chemistry of these products are detailed in section 1.2.

Acrolein (ACR) and 4-hydroxy-hexenal (HHE) are two short aldehyde that are models of alkenals and substituted alkenals respectively. Acrolein, with only three carbons, is the shortest alkenal identified as lipid peroxidation products. It is also the most reactive specially with thiol groups from proteins [70, 71], and besides being a product of lipid peroxidation, it is also present in tobacco smoke and processed foods [72, 73]. It has been linked with inhibition of cell proliferation, enhancement of apoptosis, and disruption of gene expression necessary to regulate inflammation and antioxidant defense [75, 76, 80, 280]. HHE is one of the major lipid peroxidation products of  $\omega$ -3 PUFAs such as docosahexaenoic acid (DHA) [113] and it has been reported as the most prominent hydroxy-alkenal in human plasma [113, 114]. It has been linked with causing apoptosis via NF $\kappa$ B signalling pathways [114] and its reactivity has been compared with the reactivity of better known aldehydes such as HNE [101, 115]. However, lower levels of HHE have also been shown to protect against oxidative stress by stimulating the expression of antioxidants via Nrf2 activation [117].

Lipoxidation is the modification of proteins and peptides by reactive lipid oxidation products, including short-chain aldehydes [281]. Typical reactions of aldehydes with nucleophilic amino acid residues is detailed in section 1.3. Lipoxidation adducts have been found in several inflammatory diseases such as atherosclerosis [282] and Alzheimer's disease [283]. Human serum albumin has been identified as a major target of lipoxidation due to its abundance in plasma and nucleophilic residues such as Cys34, His146 and Lys199 [284]. This suggests that most of the reactive carbonyl species (RCS) such as aldehydes can be found as albumin adducts in plasma [285, 286]. A half-life in plasma of 3 weeks makes albumin and its lipoxidation adducts a good biomarker of systemic oxidative stress since these adducts would have been formed in the weeks prior to measurement

[287, 288]. Aldehyde-albumin adducts have been detected in disease such as chronic renal failure [289]; HNE adducts have been reported in type 2 diabetes mellitus [290], while acrolein adducts have been found in brain infarction [291] and ischaemia-reperfusion damage [286]. Therefore, new methods for the detection of these adducts in plasma are needed to improve the diagnosis and monitoring the extent of diseases.

The detection of free aldehydes is extremely challenging due to their short-life, high instability and high reactivity in plasma [285, 292]. Moreover, the detection of these as adducts in biological samples is as challenging due to their low abundance [281, 285]. Several techniques have been used, including antibodies, chemical probes and mass spectrometry, as described more extensively in section 1.4 [23, 31, 285]. Mass spectrometry can detect these adducts by the change in the mass-to-charge ratio ( $m/z$ ) of proteins and peptides and enables identification, characterization and localization of the modified amino acid [263, 293]. The fragmentation pattern of peptides depends on the excitation method used and low energy ionization, such as collision-induced dissociation (CID) and electron capture dissociation (ECD) [294], are the most commonly applied to proteins and peptides identification as these enable charge-induced cleavage of the peptide backbone and yield primarily b- and y-type fragment ions, as described in section 1.4.2., which allow for their *de novo* sequencing. However, in more complex samples the data output is much greater, making the identification of modifications difficult and time-consuming. To help overcome this, the information on the lower mass range of the fragmentation spectra can be used to identify reporter ions specific for each modification. This region contains immonium and related ions which are fragments of a single amino acid and their characteristic mass indicates which amino acids are present in a sequence. In case of a modification on a specific amino acid, its respective immonium and related ions are also found to be modified and can be used as report ions which are modification and amino acid specific [257]. These reporter ions can therefore be used to develop semi-targeted mass spectrometry approaches such as precursor ion scanning (PIS), neutral loss scanning (NLS) or multiple reaction monitoring (MRM), simplifying the analysis [31, 295-297].

Multiple reaction monitoring (MRM) is a targeted high-resolution MS/MS method that can be used to quantify selected protein-aldehyde modification in complex biological samples such as plasma. MRM involves “bottom-up” analysis of proteins that have been enzymatically digested, usually by trypsin, into peptides [211] using a triple quadrupole mass spectrometer. During MRM, the peptide masses are filtered in two stages based on defined  $m/z$  values. Initially, the peptides filtered by the first quadrupole (Q1) based on the set precursor ion  $m/z$  values. Q2 fragments the peptides as a collision cell into fragment ions (product ions), which are then subsequently filtered by Q3 based on the set product

ion  $m/z$  values. The fragmentation from the precursor to the product ion  $m/z$  values makes a transition and the selection of the most appropriate transitions determines the success of an MRM experiment. A fully validated MRM method is a powerful tool for protein quantification with higher selectivity than the alternative shotgun MS/MS approach [261]. For example, Cys34 and Lys199 were found to be the most reactive residues in HNE-modified human serum albumin and so a novel MRM approach was designed to quantify the levels of HNE-modified HSA in plasma using two modified peptides, each containing one of these most susceptible residues [263].

In this study, liquid chromatography coupled to tandem mass spectrometry was used to investigate protein modifications caused by acrolein and 4-hydroxy-hexenal, two short-chain aldehydes which have been less studied. Two proteins were used as models for the study of small aldehyde lipoxidation: lysozyme (14,306 Da), rich in lysine and cysteine residues, and human serum albumin (66,437 Da), the most abundant human plasma protein. The first aim was to generate adducts *in vitro* and characterize them by LC-MS/MS in order to localize the modified amino acid residues and possibly identify reporter ions for these modifications. The second aim was to develop a targeted MRM approach using these report ions to selectively identify and quantify albumin-aldehyde adducts. Firstly the method was tested with *in vitro* modified HSA and later validated for its suitability to identify albumin-aldehyde adducts in human plasma *in vitro* aldehyde-treated to determine whether the method is appropriate for use with biological samples.

## **2.2. Material and Methods**

### **2.2.1. Chemicals**

All reagents were purchased from Sigma-Aldrich Chemical Co. (Dorset, UK) unless otherwise indicated. All solvents were of LC-MS grade and ultrapure water (Type 1) was used for buffers and reactions. Formic acid and dithiothreitol (DTT) were purchased from ThermoFisher Scientific (Runcorn, UK).

### **2.2.2. Treatment of lysozyme or human serum albumin with aldehydes in vitro**

Lysozyme (1 mg/mL) was first reduced with 100 mM DTT. This step was omitted for HSA, which was used in its native form (1 mg/mL). Acrolein was added to the protein solution at 4, 8 or 14 mM and allowed to react for 2 hours at room temperature. HHE was added at 8 or 16 mM and allowed to react for 2 hours at 37 °C. To stabilize adducts, 50 mM NaBH<sub>4</sub> was added to the reaction and left for 1 hour at room temperature. For direct infusion mass spectrometry analysis, excess DTT was removed from the reduced lysozyme samples prior to the reaction with the aldehydes using Microcon Ultracel YM-10 centrifugal concentrators 10,000 MWCO (Millipore, Massachusetts, USA), according to the manufacturer's protocol.

### **2.2.3. Direct infusion MS analysis of modified lysozyme**

Modified lysozyme samples were dissolved in 50% acetonitrile, 0.5% formic acid in water and analysed by direct infusion into a 5600 TripleToF mass spectrometer (Sciex, Warrington, UK) using loop injection directly into a 2 µL/min flow rate of the same solvent and introduced into the source via a 20 µm i.d. steel capillary mounted on a standard nanospray source with a spray voltage of 2.4 kV, a source temperature of 150 °C, declustering potential of 100 and a curtain gas setting of 25. Data was summed for 3-5 minutes and deconvoluted using the Bio Tool Kit plugin and PeakView 2.2 software (Sciex, Warrington, UK) with a step size of 0.5 Da at high (30,000) resolution and Gaussian smoothed with a 3 point window.

### **2.2.4. Plasma collection and aldehyde treatment**

Ethical approval for the use of plasma from healthy volunteers was obtained from Aston University Ethics Committee (Project #954). Blood was collected by venepuncture from three healthy volunteers after overnight fasting and informed consent and collected into 50 mL tubes containing 0.1% EDTA. The blood was then centrifuged at 1,800 x g for 10 minutes at 5 °C. The supernatant was removed and centrifuged again at 15,000 x g for 10 minutes to obtain clear plasma. The plasma from all three volunteers was pooled (as these were all control samples and the number of individuals limited) and diluted to 1:4 with 25 mM ammonium

bicarbonate, followed by treatment of acrolein with the same conditions used to treat HSA described above. Treatment with HHE was performed at a ratio of 1:10, at 37 °C for 2 hours.

### **2.2.5. Protein in-gel digestion**

The reaction products from above were separated by 15% SDS-polyacrylamide gel electrophoresis followed by staining with Coomassie blue to visualize the bands prior to further processing. The separating gel (15 %) was prepared by adding 2.8 mL ddH<sub>2</sub>O, 3 mL of 40 % acrylamide/bis-acrylamide, 2 mL of 1.5 M Tris pH 8.8, 80 µL of 10 % SDS, 8 µL of TEMED and 80 µL of 10 % APS. The stacking gel (4 %) was prepared by adding 3.1 mL ddH<sub>2</sub>O, 0.5 mL of 40 % acrylamide/bis-acrylamide, 1.25 mL of 0.5 M Tris pH 6.8, 50 µL of 10 % SDS, 5 µL of TEMED and 50 µL of 10 % APS. The coomassie-stained bands present in the gel were excised and tryptic digestion was performed according to Verrastro et al., 2016 [298]. The gel pieces were washed with 500 µL of 100 mM NH<sub>4</sub>HCO<sub>3</sub> and then with 100 mM NH<sub>4</sub>HCO<sub>3</sub>/50% acetonitrile. 10 µL of 45 mM DTT in 150 µL NH<sub>4</sub>HCO<sub>3</sub> were added to the gel pieces and left incubating at 60 °C for 30 mins for reduction. Cysteine alkylation was performed by adding 10 µL of 100 mM iodoacetamide and left to react at room temperature for 30 min in the dark. The gel pieces were then washed in 100 mM NH<sub>4</sub>HCO<sub>3</sub>/50% acetonitrile and incubated in 50 µL of 100% acetonitrile for 10 min. The gel pieces were then dried completely using a vacuum centrifuge and resuspended in 25 µL of 0.1 µg/µL trypsin prepared in 25 mM ammonium bicarbonate. 25 µL of 25 mM ammonium bicarbonate was added to the trypsin digests and the digestions were incubated overnight at 37 °C. The gel pieces were pelleted by centrifugation and the supernatant was collected into a fresh tube. Further peptide extraction from the gel pieces was performed by adding 20 µL 5% formic acid and incubating at 37 °C for 20 mins, followed by addition of 40 µL acetonitrile and incubation for 20 mins at 37 °C. The gel pieces were pelleted by centrifugation, and the supernatant was removed and combined with the first supernatant. The peptide extracts were dried in a vacuum centrifuge for storage and resuspended in 30 µL H<sub>2</sub>O/acetonitrile (98:2, %) with 0.1% formic acid prior to MS analysis.

### **2.2.6. Liquid Chromatography-Tandem Mass Spectrometry (LC-MS/MS) Analysis**

Peptides were separated and analysed using an Ultimate 3000 system (Thermo Scientific, Hemel Hempstead, UK) coupled to a 5600 TripleTOF (ABSciex, Warrington, UK). The analysis was performed as previously described by Verrastro et al., 2016 [298]. Briefly, the peptide solution was loaded onto a C18 trap column (C18 PepMap™, 5 µm, 0.5 x 5mm, Thermo Scientific, Hemel Hempstead, UK) before separation on a nano-HPLC column (C18 PepMap™, 5 µm, 0.075 x 150mm, Thermo Scientific, Hemel Hempstead, UK) at 300 µL/min using a gradient elution running from 2% to 45% aqueous acetonitrile, 0.1% formic acid over



45 minutes. Ionization of the peptides was achieved with spray voltage set at 2.4 kV, a source temperature of 150 °C, declustering potential of 100V and a curtain gas setting of 25. Survey scans were collected in positive mode from 350 to 2000 Da using high-sensitivity TOF-MS mode. Information-dependent acquisition (IDA) was used to collect MS/MS data using the following criteria: the 10 most intense with +2 to +5 charge states and a minimum intensity of 200 cps were chosen for analysis, using dynamic exclusion for 12 s and standard rolling collision energy settings.

### 2.2.7. Multiple reaction monitoring (MRM)

The acrolein-treated HSA and plasma peptides were resuspended in 50% acetonitrile, 0.5% formic acid in water. Peptides were separated and analysed using an Ultimate 3000 system (Thermo Scientific, Hemel Hempstead, UK) coupled to a 5500 triple quadrupole (Sciex, Warrington, UK). The peptide solution was loaded onto a C18 column (C18 PepMap™ 100, 5 µm, 300 µm x 25 cm, Thermo Scientific, Hemel Hempstead, UK) column at 5 µL/min using a gradient elution running from 2% to 45% aqueous acetonitrile, 0.1% formic acid over 45 minutes. Ionization of the peptides was achieved with a spray voltage set at 5.5 kV, a source temperature of 150 °C, declustering potential of 70 V. MS/MS analysis was carried out in MRM scanning mode, using the chosen transitions to fix the precursor ion and product ion  $m/z$  values at the first and third quadrupole, respectively. The total scan time was 0.7 seconds, dwell time ranged between 20 and 70 depending on the transitions and collision energy was set at 35 V at the second quadrupole for all transitions except for the transitions using diagnostic ions, for which it was set as 41 V for  $m/z$  509.3 → 168.1 and 55 V for  $m/z$  566.3 → 159.1 and  $m/z$  600.4 → 142.1. Method parameters such as collision energy and dwell time required optimization to improve the sensitivity of the method. Collision energy was firstly calculated as  $CE = (slope) \times (m/z) + (intercept)$ , where slope and intercept were dependent on the peptide charge. This shows how this parameter depends on the mass and charge of the peptide and that some peptides fragment more easily than others [299]. The dwell time is the duration in which each  $m/z$  ion signal is collected. Increasing the dwell time improved sensitivity, however resulting in fewer points collected across each peak [300]. The dwell time for each transition also depended on the number of transitions being monitored in the method at once, as increasing the number of transitions would mean decreasing each dwell time to get the same total scan time. Practical dwell-time settings range between 10 ms for good sensitivity and 100 ms for excellent sensitivity [300].

### 2.2.8. Database Searches

The Mascot<sup>®</sup> probability based search engine (Matrix Science, London, version 2.4.0) was used to interrogate the SwissProt 2017-07 primary database. Mascot uses probability based scoring for protein identification using an adaptation of the MOWSE algorithm [301]. LC-MS .wiff files of each sample were searched for protein identification and oxidative post-translational modifications (oxPTMs). For protein identification, variable modifications of methionine oxidation and carbamidomethyl cysteine were used. For the analysis of the lipoxidation products, the initial searches additionally used a variable modification list including reduced and unreduced ACR (mass changes of 56.06 Da, 58.08 Da, 40.06 Da, 94.11 Da, 56.06 Da, 76.09 Da) or HHE (mass changes of 114.14 Da, 93.13 Da, 78.11 Da) adducts at cysteine, lysine and histidine residues. Other parameters for the searches were as follows: Enzyme: Trypsin; Peptide tolerance:  $\pm 0.6$  Da; MS/MS tolerance:  $\pm 0.6$  Da; Peptide charge state: +2, +3; Max Missed cleavages: 1; #13C: 0; Quantitation: None; Instrument: ESI-QUAD-TOF; Data format: Mascot Generic; Experimental mass values: Monoisotopic; Taxonomy: Chordata. All data identifying modifications were manually validated before inclusion.

## 2.3. Results

### 2.3.1. Lysozyme as a model system to study lipid-protein adducts

In the work reported in this section, the modifications of lysozyme by acrolein were evaluated as a model of lipid-protein adducts that may occur in inflammatory diseases. In order to increase the efficiency of the reaction between the protein and the aldehyde, the disulfide bonds on the lysozyme were reduced with dithiothreitol (DTT). Although lysozyme is known to have a single free cysteine residue, the reduction results in eight other cysteine residues available to react with the aldehyde from the reduction of 4 disulfide bonds. Therefore to increase the potential for reaction between the protein and the aldehyde, the disulfide bonds were first reduced with DTT and the results are shown in **Figure 2.1**. After deconvolution of the charge state envelope, the native lysozyme was observed at a mass of 14,306 Da (**Figure 2.1A**). The incubation of lysozyme with 10 and 100 mM DTT resulted in the reduction of one (at  $m/z$  14,308 Da) and three (at  $m/z$  14,312 Da) disulfide bonds, respectively (**Figure 2.1B** and **Figure 2.1C**). A DTT concentration of 200 mM was required to reduce the protein completely, with a mass after deconvolution of 14,314 Da (4 disulfide bonds reduced and a mass increase of 8 Da over the native form) (**Figure 2.1D**). The charge state envelope shifts to lower  $m/z$  range with increasing DTT treatment concentrations as the protein unfolds and becomes more highly charged. All subsequent reactions for adduct formation were conducted on lysozyme reduction with 100 mM DTT which typically reduced 2-3 disulfide bonds, as the higher concentration required for full reduction could interfere with the aldehyde treatments.

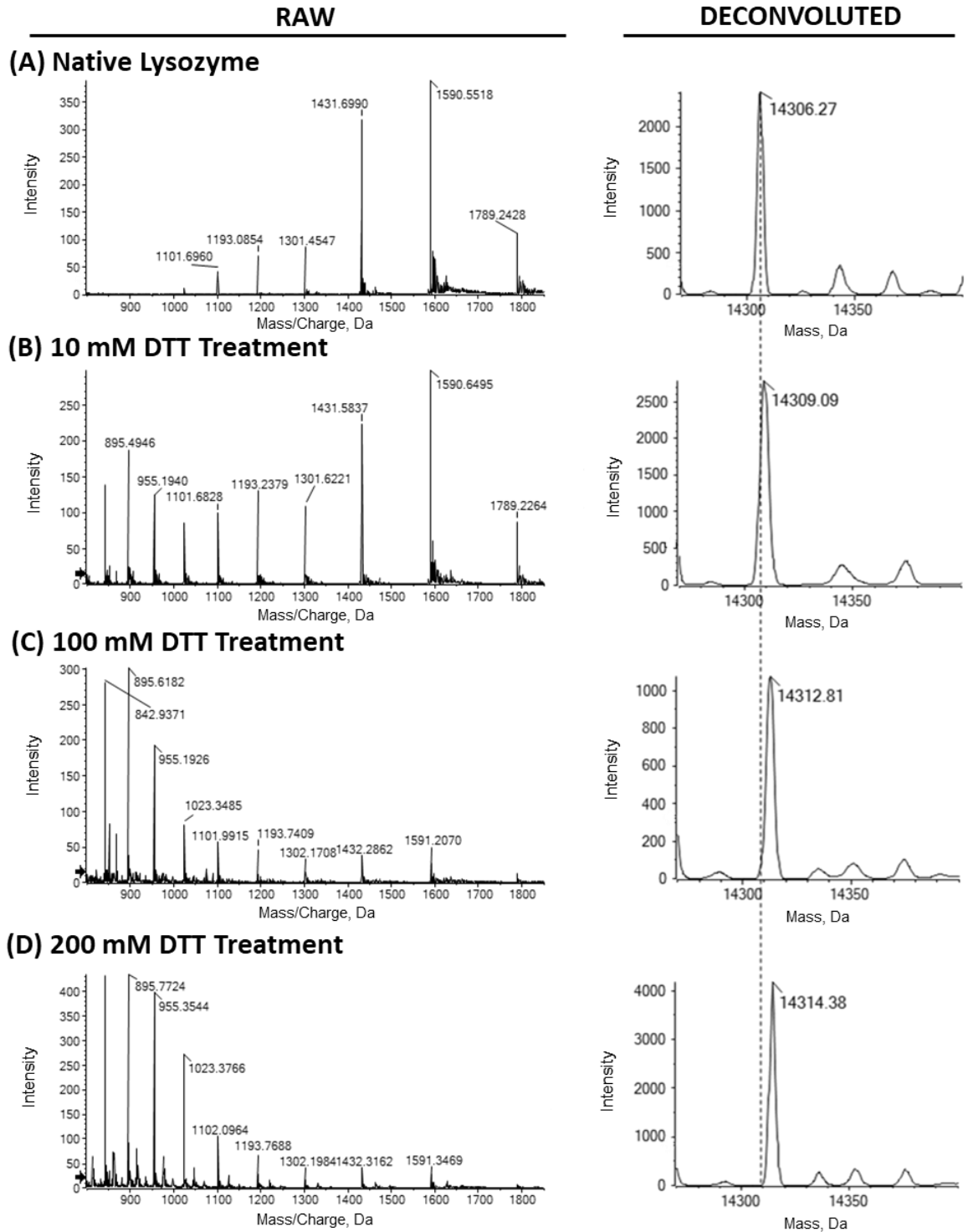


**Figure 2.1. Reduction of intact lysozyme by DTT treatment.** The left hand panels correspond to unprocessed (raw) MS data showing the charge state envelope for the protein, and the right hand panels show deconvoluted data giving the mass of the intact lysozyme. Lysozyme was treated for 30 mins at room temperature with varying concentrations of DTT: (A) control treatment in the absence of DTT; (B) 10 mM DTT treatment; (C) 100 mM DTT treatment; (D) 200 mM DTT treatment.

Peaks corresponding to reduced acrolein adducts of intact lysozyme were observed at mass increase of 58 Da, consistent with formation of a Michael adduct and subsequent stabilization by borohydride reduction. The optimal conditions for formation of acrolein-protein adducts were investigated. The DTT-reduced lysozyme was reacted with acrolein for different time lengths and at a range of different concentrations. First, the time-dependent effect was investigated with lysozyme incubated with 4 mM acrolein for 1 to 6 hours. The formation of acrolein adducts was then analysed by direct infusion mass spectrometry (**Figure 2.2**).

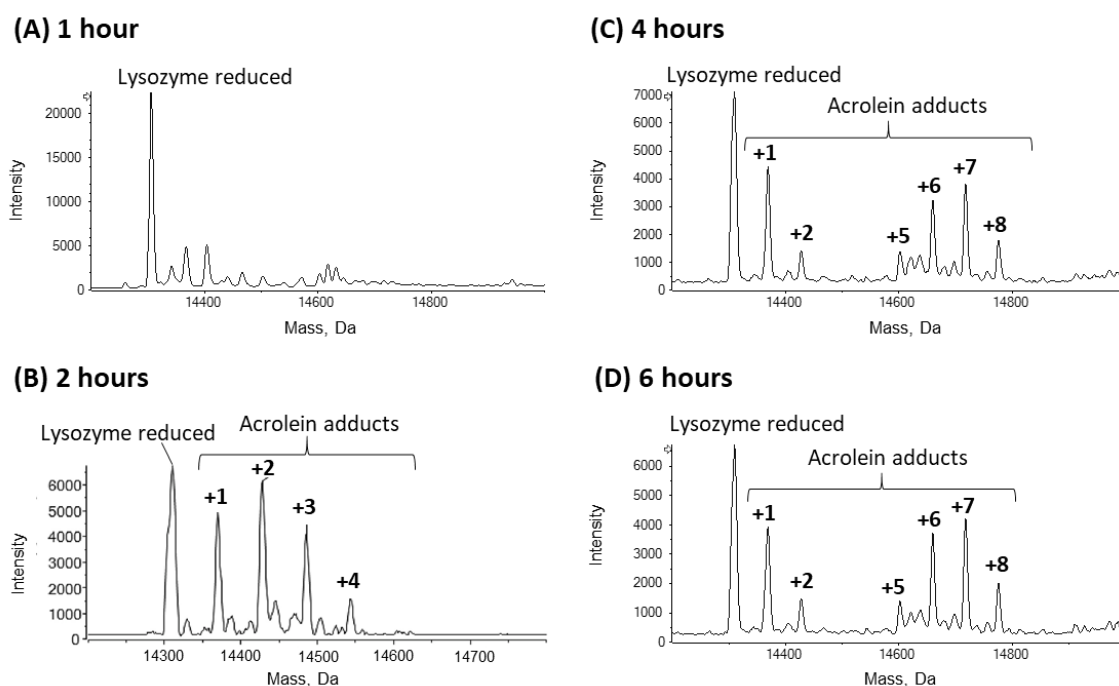


**Figure 2.2. Deconvoluted ESI-MS spectra of lysozyme obtained after reaction with acrolein at 4mM.** Treatment for 1 h showing no adducts being formed (A). Treatment for 2 h (B), 4 h (C) or 6 h (D) showing the formation of several acrolein Michael adducts, each adding 58 Da ( $n=3$ ).

Reduced native lysozyme was identified at  $m/z$  14,310 Da. The peak spacing between the acrolein adduct peaks was 58 Da, suggesting that lysozyme was modified by Michael addition of acrolein. **Figure 2.2** shows that after one hour reaction, no adducts were formed (A), while after two (B), four (C) and six (D) hours reaction some adducts appeared to be formed in a time-dependent manner. Reaction with acrolein at 4 mM for 2 h (**Figure 2.2B**) gave rise to a maximum of 4 adducts while reaction for longer than 2 h (**Figure 2.2C-D**) resulted in more extensive modification with up to 8 adducts being formed. Both 4 and 6 hour reactions resulted in the same number of modifications, so it seems that no more time is required beyond 4 h for 4 mM acrolein treatment. Therefore, the next step to evaluate the aldehyde concentration effect was performed at 2 and 4 hours, selected as the optimal time points.

To evaluate the concentration-dependent effect of acrolein-treatment, lysozyme was reacted with acrolein at 8 mM and 14 mM and left to react for 2 or 4 hours, as explained above. Any adducts were then stabilized by reaction with sodium borohydride for one hour and the deconvoluted MS spectra obtained for each condition are shown in **Figure 2.3**.

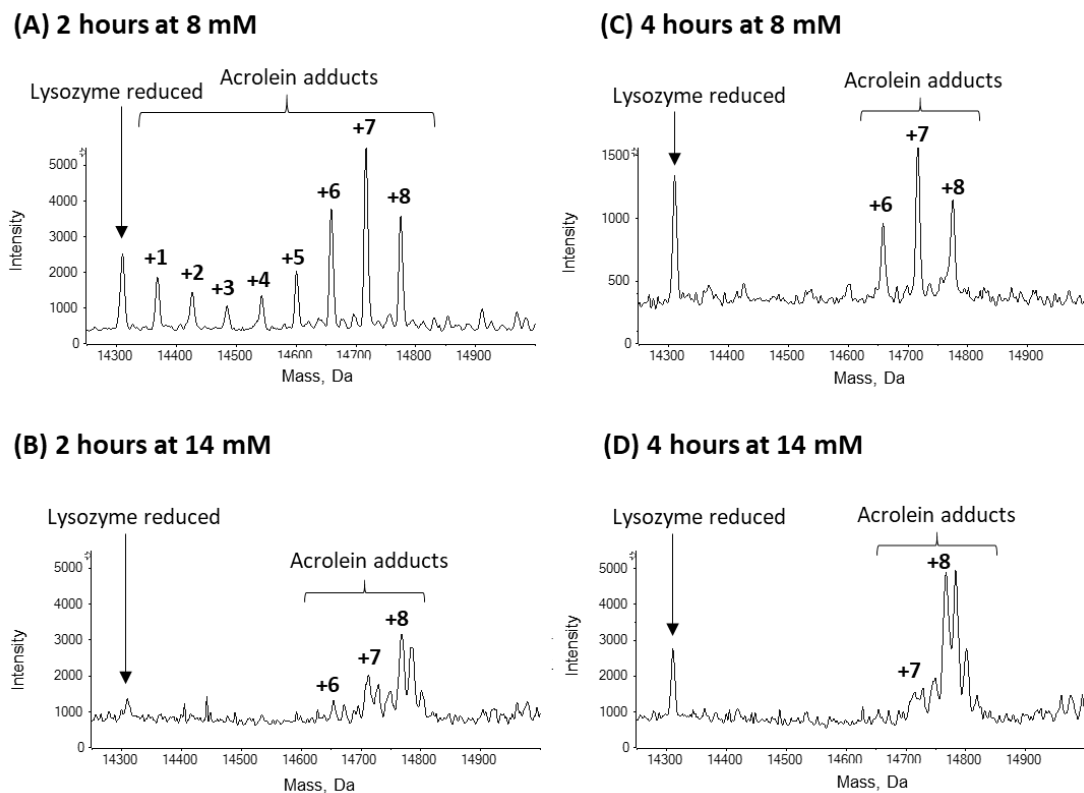


**Figure 2.3. Deconvoluted ESI-MS spectra of lysozyme.** Spectra obtained after reaction with acrolein for 2 hours at 8 mM (A) and 14 mM (B), and for 4 hours at 8 mM (C) and 14 mM (D). (n=3).

The aldehyde concentration increases resulted in an increase of the ratio modified/unmodified lysozyme, as the native lysozyme peak intensity decreased. Since the number of adducts did not increase, these might suggest that other complex modifications are happening that are not being analysed, including protein cross-linking. It is also possible to see that 8 mM acrolein for 2 h (**Figure 2.3A**) provides the best conditions for the formation of the different adducts while higher concentration or time length resulted in a more complete modification of the protein where only 6 to 8 adducts can be seen (**Figure 2.3B-D**). Leaving the protein and the aldehyde reacting for longer resulted in an extension of the reaction towards the modification increasing the number of adducts and the protein with lower modification is no longer present. From these optimization steps, 8 mM was chosen as the optimal aldehyde concentration and 2 hours as the optimal time of reaction for the formation of these aldehyde-protein adducts, and these were the conditions used in further experiments.

To determine the specific amino acid residues modified, a bottom-up proteomic approach was carried out by tryptic digestion of the modified protein and LC-MS/MS analysis of the peptides. Lysozyme was modified by acrolein (4, 8 and 14 mM) for 2 hours before separation by 15% SDS-PAGE (**Figure 2.4**).

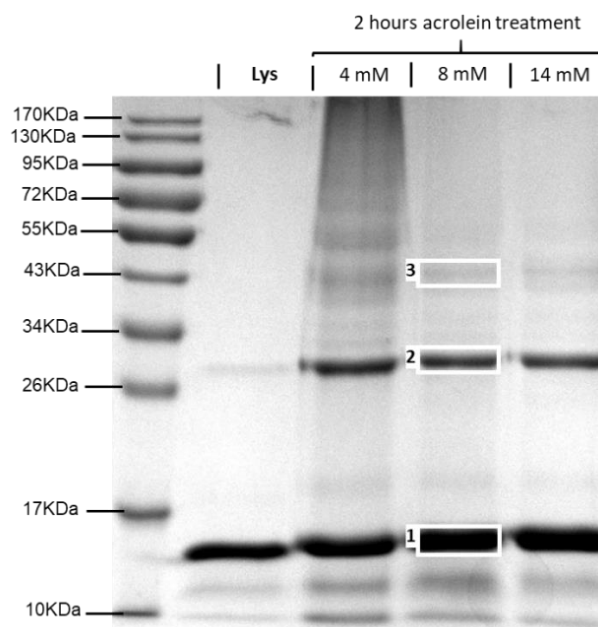


**Figure 2.4. SDS-PAGE (denaturing gel electrophoresis) results for lysozyme.** Untreated and treated lysozyme with 4 mM, 8 mM or 14 mM acrolein for 2 hours. Gel stained with Coomassie blue staining. The highlighted sections boxed in white were cut for further analysis: (1) 15-20 kDa; (2) 25-30 kDa; (3) 40-45 kDa.

The molecular weight of lysozyme is 14 kDa, which means untreated and acrolein treated lysozyme should appear in the highlighted section 1 in **Figure 2.4**, around the markers 15 to 20 kDa. There are two bands within this region but due to the difficulty to separate them, these were studied together. The second and third sections contain a band at approximately double or triple the molecular weight of lysozyme and could represent protein cross-linking. However, this could also represent protein agglomerates that were not disrupted by the SDS. To confirm the nature of the band in highlighted section 2, another gel was run with the band from the first gel cut and placed in the sample well of the second gel. It was possible to see that the bands appear around the 26 kDa marker in the second gel and no bands corresponding to the monomer molecular mass appeared, confirming the protein cross-linking hypothesis and that the proteins present in those bands were covalently linked rather than just being a protein agglomerate. Further analysis is required in order to determine if acrolein was responsible for the cross-link. Interestingly, the fourth lane in the gel displayed in **Figure 2.4** (2h, 14mM) shows bands in highlighted section 2 and 3 but the band at the lysozyme molecular weight seemed to disappear. This can be correlated with spectrum in Figure 2.3B, where native lysozyme peak disappeared and a

new range of peaks appeared that do not correspond to simple acrolein adducts, which may also be related to the protein cross-linking. Gel bands from **Figure 2.4** were excised from the gel, digested with trypsin and analysed by LC-MS/MS for characterization and localization of the acrolein modifications. Due to the difficulty in separating the two bands at 15-20 kDa, these were cut and analysed together. Trypsin cleaved lysozyme at lysine (K) and arginine (R) amino acid residues and the digested peptides were then separated by liquid chromatography and analysed by MSMS. Initially MASCOT software [246] was used to identify peptides modified with acrolein, and each potential modification was also confirmed by manual analysis of the MS/MS spectrum (**Figure 2.5**). This bottom-up approach allowed the identification of 5 peptides from lysozyme modified by acrolein, based on the peptide molecular weight, mass/charge ratio and charge of the peptide ion, ion score, and LC retention time. The majority of acrolein adducts occurred at cysteine residues, although some lysine adducts were also identified (**Table 2.1**).

**Table 2.1. Modification of lysozyme by acrolein.**

Modified Residues	Lysozyme modified peptides (a <sup>b</sup> )	Mass of modified peptide	m/z (charge)	Ion score	Rt (min)
Cys6	<b>C</b> <sub>6</sub> <sup>+56</sup> ELAAAMK <sub>13</sub>	891.42	446.5 (2+)	18	36.19
Cys6	<b>C</b> <sub>6</sub> <sup>+58</sup> ELAAAMK <sub>13</sub>	893.44	447.5 (2+)	79	27.57
Cys30	G <sub>22</sub> YSLGNWV <b>C</b> <sup>+58</sup> AAK <sub>33</sub>	1325.64	663.6 (2+)	80	38.35
Cys64	W <sub>62</sub> W <b>C</b> <sup>+58</sup> NDGR <sub>68</sub>	993.41	497.5 (2+)	35	32.31
Cys76	N <sub>74</sub> L <b>C</b> <sup>+56</sup> NIPCSALLSSDITASVNC <b>A</b> <sub>96</sub>	2506.19	836.4 (3+)	77	42.39
Cys76	N <sub>74</sub> L <b>C</b> <sup>+58</sup> NIPCSALLSSDITASVNC <b>A</b> <sub>96</sub>	2508.20	837.1 (3+)	50	43.84
Cys80, Lys96	N <sub>74</sub> LCNIP <b>C</b> <sup>+58</sup> SALLSSDITASVNC <b>A</b> <sub>96</sub> <sup>+58</sup>	2509.22	837.4 (3+)	92	44.29
Cys76, Cys80, Lys96	N <sub>74</sub> L <b>C</b> <sup>+58</sup> NIP <b>C</b> <sup>+58</sup> SALLSSDITASVNC <b>A</b> <sub>96</sub> <sup>+58</sup>	2510.24	838.1 (3+)	60	44.84
Cys115	<b>C</b> <sub>115</sub> <sup>+58</sup> KGTDVQAWIR <sub>125</sub>	1333.68	445.4 (3+)	17	31.19
Cys115	<b>C</b> <sub>115</sub> <sup>+56</sup> <b>K</b> <sup>+58</sup> GTDVQAWIR <sub>125</sub>	1389.71	464.1 (3+)	28	30.24
Lys116	<b>C</b> <sub>115</sub> <b>K</b> <sup>+58</sup> GTDVQAWIR <sub>125</sub>	1390.70	464.4 (3+)	30	31.08

a (subscript) – amino acid position in the mature protein for the start and end residues.

b (superscript) – mass difference corresponding to the modification on the affected residue (shown in red).



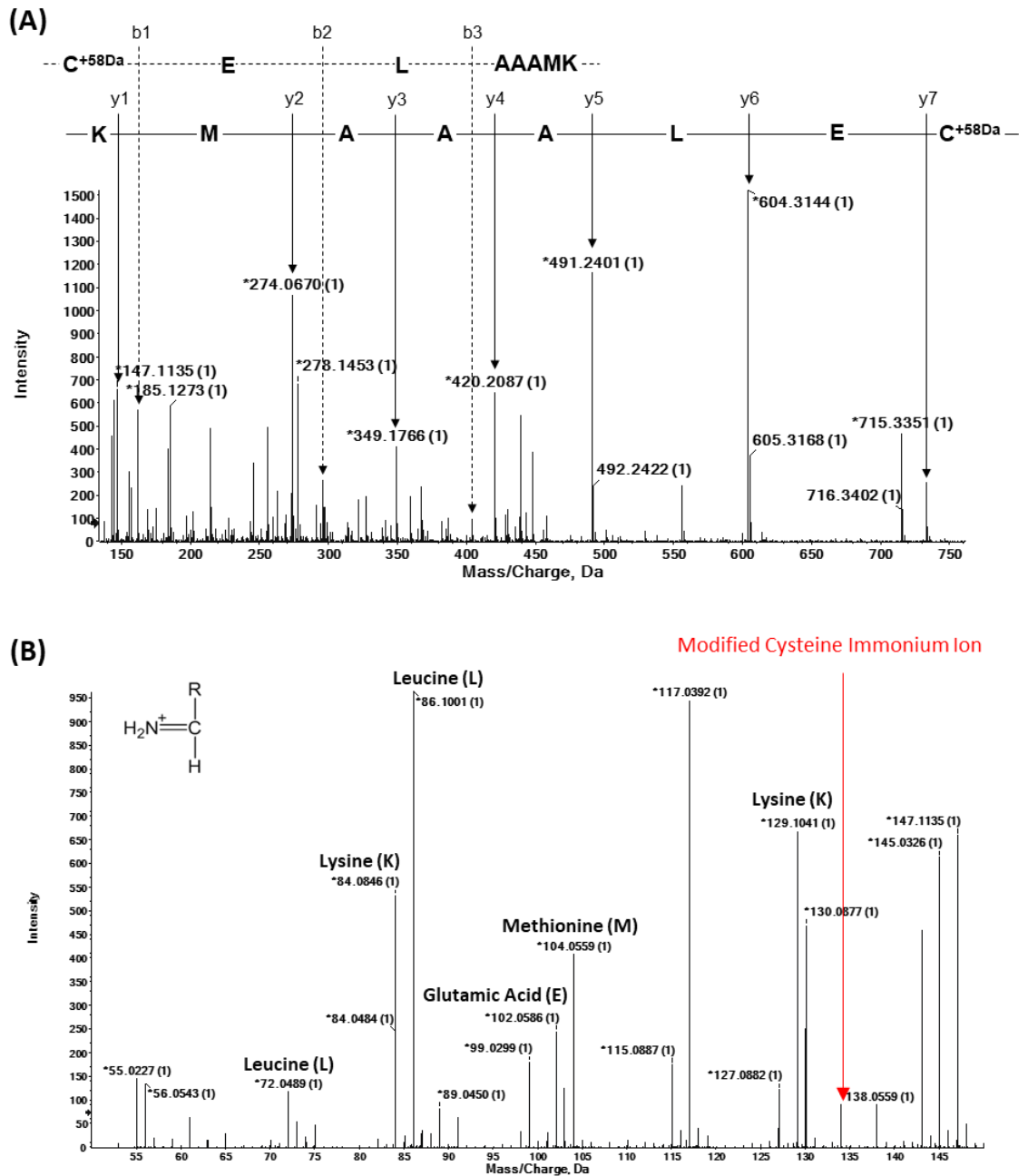


**Figure 2.5. MS/MS spectra of lysozyme tryptic peptide.** CELAAAMK modified on a cysteine residue by acrolein (58 Da). (A) The y and b ions indicated by the arrows confirm the peptide sequence and the modification on the cysteine residue. (B) x-axis adjusted to 50-150 Da for immonium ions identification: leucine (L) at m/z 72 Da and 86 Da, lysine (K) at m/z 84 Da and 129 Da, glutamic acid (E) at m/z 102 Da, methionine (M) at m/z 104 Da and acrolein-modified cysteine (C) at m/z 134 Da. The base structure of an immonium ion is shown next to the spectrum.

Peptide fragmentation is not often a clean process and the spectrum may show peaks from side chain cleavages (generating y- and b-ions) and internal fragments. This makes the analysis more complex and increases the difficulty of reading the peptide sequence. In the example shown in **Figure 2.5A** it was possible to sequence the peptide and confirm the modification identified previously by MASCOT database search. This bottom-up proteomic approach allowed us to identify 8 amino acid residues modified by acrolein: Cys6, Cys30, Cys64, Cys76, Cys80, Lys96, Cys155 and Lys116. This information corroborates the intact protein analysis where up to 8 acrolein molecules adducted per protein were identified (**Figure 2.3A**). One lysozyme peptide (NLCNIPCSALLSSDITASVNCAK) was found to contain 3 acrolein adducts, at Cys76, Cys80 and Lys96.

The immonium ion (breaking of two bonds in the peptide either side of the amino acid residue) of each amino acid residue can be seen in an MS/MS spectrum and these are helpful for their identification. In case of modification, the immonium ion is not seen in the spectrum due to the structure and mass change of the amino acid residue. Some amino acids, like tryptophan (W), proline (P) and histidine (H), give a strong immonium ion signal while others do not give much information. **Figure 2.5B** shows the same MS/MS spectrum with x-axis adjusted to 50-150 Da where the immonium ions can be identified. It was possible to identify the immonium ion for leucine (L) at  $m/z$  72 Da and  $m/z$  86 Da, for lysine (K) at  $m/z$  84 Da and  $m/z$  129 Da, for glutamic acid (E) at  $m/z$  102 Da and finally for methionine (M) at  $m/z$  104 Da, confirming the presence of these amino acid residues in the peptide and so corroborating the results from the analysis of b- and y-ions. Alanine (A) and cysteine (C) immonium ions do not give strong MS signals, hence they are not usually observed in the spectrum. Additionally, a peak at  $m/z$  134 Da was identified as cysteine immonium ion (76 Da) plus the acrolein modification (58 Da), which can be used as a diagnostic fragmentation product of acrolein-cysteine adducts. The same approach was applied to the other modified peptides and two diagnostic fragments were consistently observed at  $m/z$  134.06 Da and  $m/z$  117.04 Da for acrolein-cysteine adducts, while acrolein-lysine adducts gave diagnostic fragments at  $m/z$  142.12 and  $m/z$  159.15 (**Figure 2.6**). These fragment products are aldehyde- and amino acid residue-specific, which make them potential diagnostic ions to be used with targeted methods for the detection of these modifications in more complex mixtures such as biological samples.

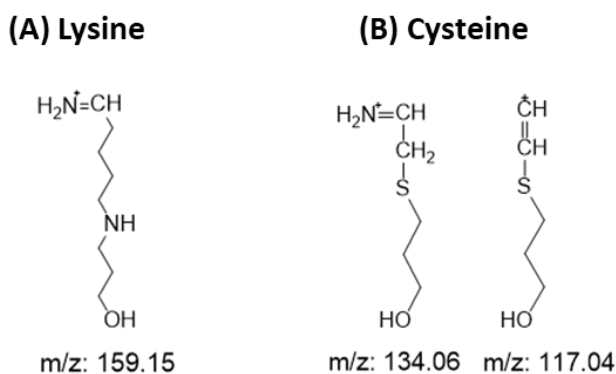


**Figure 2.6. Proposed structures of the diagnostic ions found for the reduced acrolein modifications on lysine and cysteine.**

### 2.3.2. Human serum albumin lipoxidation analysis by LC-MS/MS

As lysozyme had been used as a model system, once the protocols had been optimized the methodology developed was then tested on a biologically relevant protein, human serum albumin (HSA). This is most abundant protein in human blood, responsible for transportation of different molecules such as hormones and fatty acids and, therefore likely to be susceptible to adduct formation.

#### 2.3.2.1. Acrolein

As previously described, to increase the efficiency of the reaction between the lysozyme and the aldehyde, the disulfide bonds on the protein were reduced with dithiothreitol (DTT). However, in these experiments the analysis was performed on unreduced HSA, which should better represent the protein in the organism. HSA was reacted with acrolein at 4, 8 and 14 mM and for 2h, as these were the optimum conditions for the lysozyme experiments. Similarly, the reaction products were reduced by sodium borohydride to improve the adducts' stability.

The analysis of acrolein-HSA adducts by direct infusion mass spectrometry of the intact protein was not possible, probably due to the size of the protein. Hence to investigate the HSA modifications by acrolein, a bottom-up approach was applied, the same method as described for lysozyme. This allowed the identification of amino acid sequence and the acrolein modified amino acid residues. Acrolein-treated HSA as well as the native HSA were separated by 15% SDS-PAGE (**Figure 2.7**).

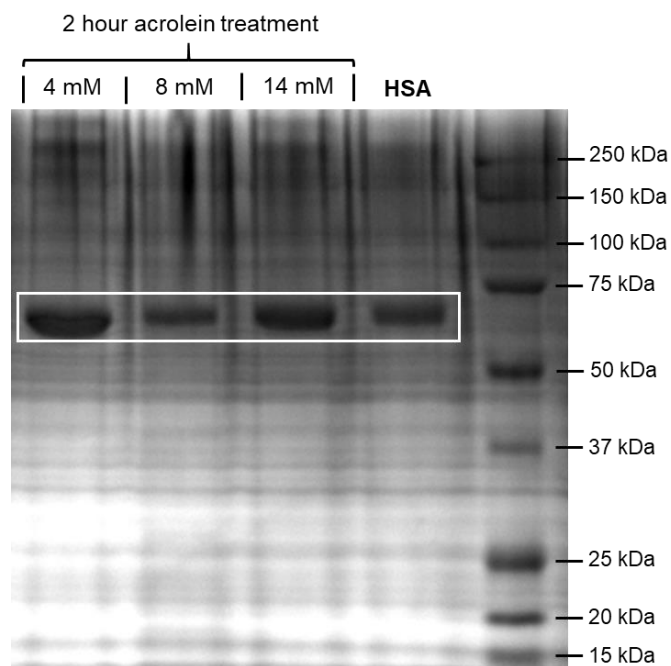


**Figure 2.7. SDS-PAGE (denaturing gel electrophoresis) results for human serum albumin.** Untreated and treated HSA with acrolein at 4 mM, 8 mM or 14 mM for 2 hours. Gel stained with Coomassie blue staining. The highlighted section boxed in white was cut out for further analysis.

The molecular weight of Human serum albumin is 66,437 Da, according to the amino acid sequence. The protein appears on the gel between the markers 50 kDa and 75kDa. The gel run was followed by in-gel trypsin digestion of the main bands. The resulting peptides were then separated by liquid chromatography and analysed by MS/MS. MASCOT analysis identified 11 acrolein modifications on lysine (K), histidine (H) and cysteine (C) in 11 different peptides (**Table 2.2**), based on peptide molecular weight, mass/charge ratio and charge of the peptide ion, ion score and LC retention time. These modifications were confirmed by manual analysis of the tandem mass spectrometry (MS/MS) data. *De novo* sequencing of each peptide confirmed the amino acid sequence as well as the location of the modification on specific amino acid residues. An example of this approach is given in **Figure 2.8** for the amino acid sequence KQTALVELVK identified as modified by a reduced acrolein adduct on a lysine residue.

**Table 2.2. Modifications of human serum albumin by acrolein.**

Modified Residues	HSA modified peptides (a <sup>b</sup> )	Observed mass of modified peptide	m/z (charge)	Ion score	Rt (min)
His67	S <sub>65</sub> L <sup>H<sup>+58</sup></sup> TLFGDK <sub>73</sub>	1074.57	359.2 (3+)	43	28.51
Lys137	K <sub>137</sub> <sup>+58</sup> YLVEIAR <sub>144</sub>	1112.62	557.3 (2+)	16	27.69
His146	R <sub>145</sub> H <sup>+58</sup> PYFYAPELLFFAK <sub>159</sub>	1956.03	653.0 (3+)	66	41.35
Lys262	A <sub>258</sub> DLAK <sup>+58</sup> YICENQDSISSK <sub>274</sub>	1998.96	667.3 (3+)	73	31.29
Lys276	Y <sub>263</sub> ICENQDSISSKLK <sub>276</sub> <sup>+58</sup>	1741.86	581.6 (3+)	109	26.71
His288	S <sub>287</sub> H <sup>+58</sup> CIAEVENDEMPADLPSLAADFVESK <sub>313</sub>	3031.38	1011.5 (3+)	61	42.41
His338	R <sub>337</sub> H <sup>+58</sup> PDYSVLLLLR <sub>348</sub>	1524.88	509.3 (3+)	83	34.59
Cys392	Q <sub>390</sub> NC <sup>+56</sup> ELFEQLGEYK <sub>402</sub>	1655.75	829.4 (2+)	42	41.14
Lys414	K <sub>414</sub> <sup>+58</sup> VPQVSTPTLVEVSR <sub>428</sub>	1696.97	566.3 (3+)	59	30.89
Lys525	K <sub>525</sub> <sup>+58</sup> QTALVELVK <sub>534</sub>	1185.73	396.3 (3+)	52	28.84
Lys574	K <sub>574</sub> <sup>+58</sup> LVAASQAALG <sub>584</sub>	1198.73	600.4 (2+)	62	33.67

a (subscript) – amino acid position in the mature protein for the start and end residues.

b (superscript) – mass difference corresponding to the modification on the affected residue (shown in red).

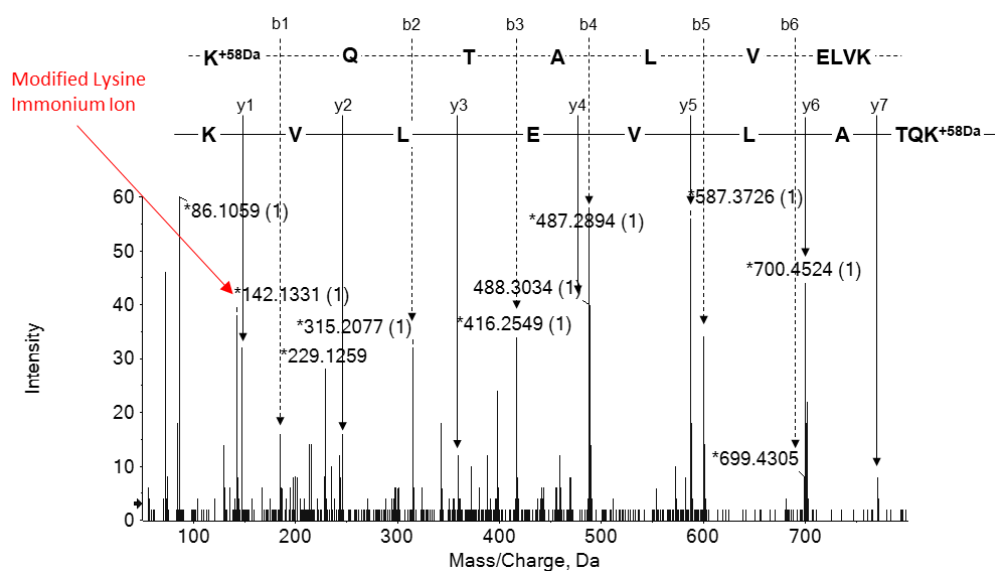


**Figure 2.8. MS/MS spectra of human serum albumin tryptic peptide.** KQTALVELVK modified on a lysine residue by acrolein (58 Da). The y and b ions indicated by the arrows confirm the peptide sequence and the modification on the cysteine residue. Immonium ions for acrolein-modified lysine found at m/z 142 Da.

It was possible to sequence the peptide and confirm the modification identified by database search. Mainly histidine and lysine residue were found to be modified and only one cysteine: His67, Lys137, His146, Lys262, Lys276, His288, His338, Cys392, Lys414, Lys525 and Lys574. This contrasts with lysozyme, where mainly cysteine residues were found to be modified; this difference may be due to the DTT reduction which generates cysteines in the free thiol form, instead of being in disulfide bonds, and therefore these are available to react with the acrolein. In its native state HSA has 17 disulfide bonds and only one free cysteine, which is not the cysteine that was found to be modified, suggesting that this cysteine was made available for reaction possibly by rearrangement of albumin after lysine modification and the only free cysteine residue is well buried and protected in the protein's structure. Figure 2.8 shows an example of an HSA peptide modified by acrolein on Lys525, where the peptide could be sequenced using the b and y fragment ions. The modified lysine immonium ion was also detected at  $m/z$  142.12, which is an additional diagnostic fragmentation product of acrolein-lysine adduct not observed in section 2.3.1. HSA peptide analysis provided information on acrolein-histidine modifications and a diagnostic fragmentation product was found at  $m/z$  168.11 Da. The structure of these two ions is in **Figure 2.9**, which is an update on all the diagnostic ions found for acrolein modifications.

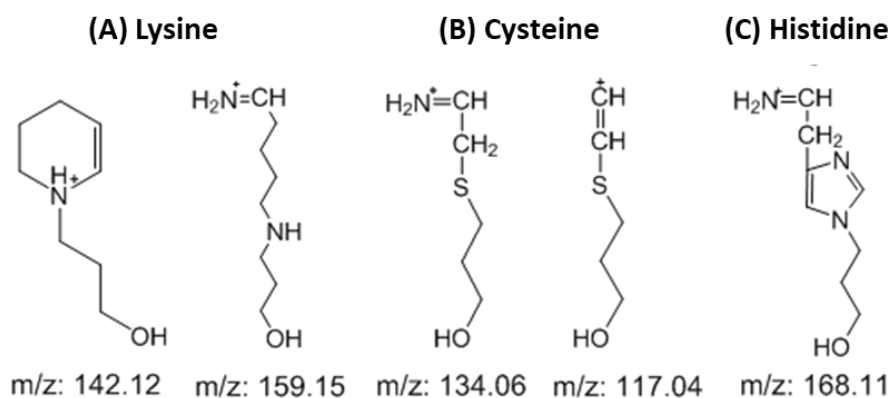


**Figure 2.9. Proposed structures of the diagnostic ions found for the reduced acrolein modifications on lysine, cysteine and histidine.**

These fragment products are aldehyde- and amino acid residue-specific, which makes them potential diagnostic ions to be used with targeted methods for the detection of these modifications in more complex mixtures such as biological samples. Section 2.3.3 describes the application of these diagnostic ions on MRM (multiple reaction monitoring) approaches.

### 2.3.2.2. 4-hydroxy-2-hexenal

The lipoxidation of human serum albumin by another short-chain aldehyde was also performed. 4-hydroxy-hexenal (HHE), the 6-carbon analogue of the well-studied HNE was used to treat HSA for 2 hours at 8 and 16 mM. The same mass spectrometry approach was used and the HHE-modified HSA, as well as the untreated protein, were separated by 15% SDS-PAGE. HSA ran in the gel between the markers for 55 kDa and 72 kDa according to its expected molecular weight of 66.4 kDa, and this region is highlighted in **Figure 2.10**.

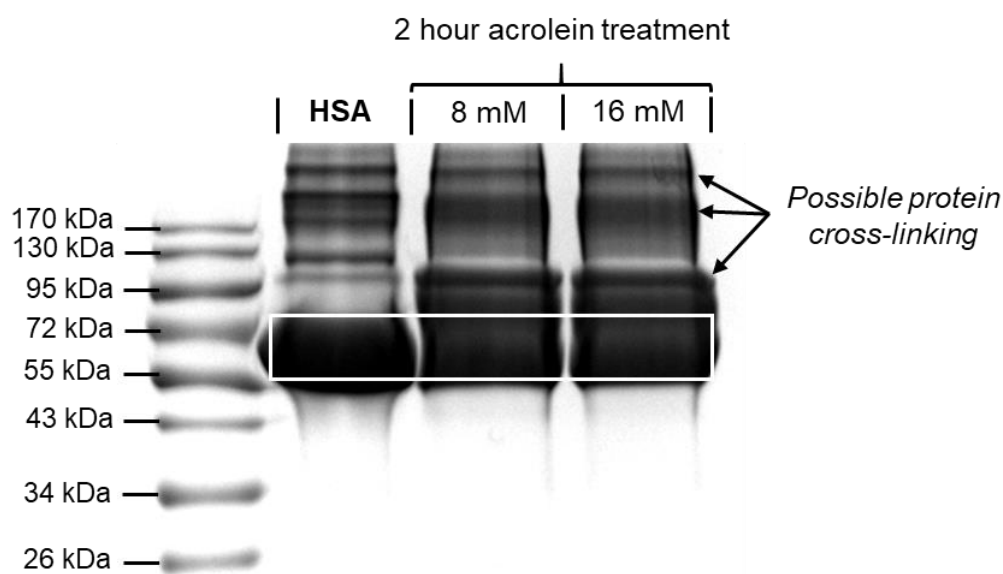


**Figure 2.10. SDS-PAGE (denaturing gel electrophoresis) results for human serum albumin.** Untreated and treated HSA with HHE at 8 mM or 16 mM for 2 hours. Gel stained with Coomassie blue staining. The highlighted section boxed in white was cut out for further analysis. Arrows identify possible protein crosslinking.

Following the same proteomic approach previously described, including in-gel tryptic digestion and analysis of the peptides by LC-MS/MS. MASCOT analysis identified 12 HHE modifications on lysine (K), histidine (H), cysteine (C) and arginine (R) residues distributed in 14 different peptides (**Table 2.3**), based on peptide molecular weight, mass/charge ratio and charge of the peptide ion, ion score and LC retention time.

**Table 2.3. Modifications of human serum albumin by 4-hydroxyl-hexenal (HHE).**

Modified Residues	HSA modified peptides (a <sup>b</sup> )	Observed mass of modified peptide	m/z (charge)	Ion score	Rt (min)
Cys75	<sup>74</sup> LC <sup>+96</sup> TVATLR <sub>81</sub>	971.55	486.76 (2+)	27	35.62
Cys124	<sup>115</sup> LVRPEVDVMC <sup>+114</sup> TAFHDNEETFLK <sub>136</sub>	2706.30	677.59 (4+)	29	31.91
Cys124	<sup>115</sup> LVRPEVDVMC <sup>+114</sup> TAFHDNEETFLKK <sub>137</sub>	2834.39	709.61 (4+)	32	29.62
Lys137	<sup>137</sup> K <sup>+78</sup> YLYEIAR <sub>144</sub>	1132.63	567.32 (2+)	15	29.21
Cys245	<sup>241</sup> VHTEC <sup>+114</sup> CHGDLLECADDR <sub>257</sub>	2085.86	522.46 (4+)	44	23.89
Cys245	<sup>241</sup> VHTEC <sup>+114</sup> CHGDLLEC*ADDRADLAK <sub>262</sub>	2584.14	647.04 (4+)	47	26.26
His247	<sup>241</sup> VHTECCH <sup>+114</sup> GDLLC*ADDRADLAK <sub>262</sub>	2584.14	647.04 (4+)	33	26.47
Cys265	<sup>263</sup> YIC <sup>+114</sup> ENQDSISSK <sub>274</sub>	1499.68	750.85 (2+)	29	22.82
Cys279	<sup>275</sup> LKEC* <sup>+114</sup> EKPLLEK <sub>286</sub>	1602.84	535.28 (3+)	40	20.46
His288	<sup>287</sup> SHC <sup>+114</sup> IAEVENDEMPADLPSLAADFVESK <sub>313</sub>	3030.38	758.61 (4+)	25	39.59
Cys360	<sup>360</sup> C <sup>+114</sup> CAAADPHEC*YAK <sub>372</sub>	1551.62	776.80 (2+)	45	22.83
Arg410	<sup>403</sup> FQNALLVR <sup>+96</sup> YTK <sub>413</sub>	1447.82	483.62 (3+)	22	32.98
His464	<sup>446</sup> MPC*AEDYLSVVLNQLCVLH <sup>+114</sup> EK <sub>466</sub>	2574.25	859.10 (3+)	40	46.30
Cys477	<sup>473</sup> VTKCC <sup>+114</sup> TESLVNR <sub>484</sub>	1465.73	489.59 (3+)	39	24.61
Cys477	<sup>476</sup> CC <sup>+114</sup> TESLVNR <sub>484</sub>	1137.52	569.75 (2+)	59	28.67

a (subscript) – amino acid position in the mature protein for the start and end residues.

b (superscript) – mass difference corresponding to the modification on the affected residue (shown in red).



These modifications were confirmed by manual analysis of the tandem mass spectrometry (MS/MS) data and *de novo* sequencing of each peptide confirmed the amino acid sequence, as well as the location of the modification. Mainly cysteine and histidine residues were found to be modified and only one lysine and one arginine: Cys75, Cys124, Lys137, Cys245, His247, Cys265, Cys279, His288, Cys360, Arg410, His464 and Cys477.

The HHE-modified immonium ions of these residues were also detected and as previously described, these were hypothesized to be reporter ions for these modifications. Diagnostic fragments were observed at  $m/z$  215.18 and 243.17 Da for HHE-lysine adducts generated by Michael addition, at  $m/z$  197.16, 180.14 and 179.15 for HHE-lysine adducts generated by Schiff base, at  $m/z$  224.14 Da for HHE-histidine adducts and at  $m/z$  226.16 Da for HHE-arginine adducts generated by Michael addition at  $m/z$  208.14 Da for HHE-arginine adducts generated by Schiff base. **Figure 2.11** shows the proposed structures for these aldehyde- and amino acid residue-specific reporter ions. These could be used to develop targeted label free mass spectrometry approaches such as MRM (multiple reaction monitoring).

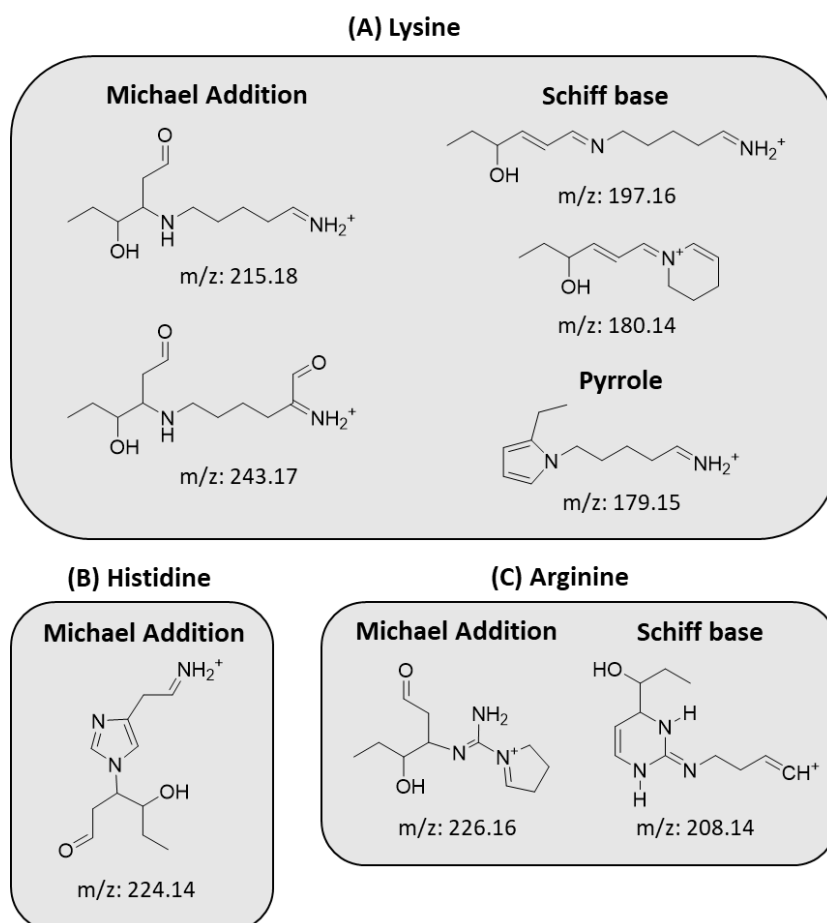


**Figure 2.11. Proposed structures of the diagnostic ions found for 4-hydroxy-hexenal (HHE) modifications on lysine (A), histidine (H) and arginine (R).**

### 2.3.3. Developing an MRM approach as a potential diagnostic tool for acrolein-HSA modifications

The detection and analysis of lipoxidation adducts in biological samples is challenging due to their low abundance. Even though mass spectrometry is a good technique to detect the mass shift caused by the adducts, the data output is much greater in complex samples. To overcome this issue, new targeted methods are needed to simplify the detection of adducts in biological samples such as human plasma. Therefore, a multiple reaction monitoring (MRM) approach was developed to detect acrolein modifications on human serum albumin (**Table 2.4**).

**Table 2.4.** MRM transitions for human serum albumin peptides unmodified or modified by acrolein.

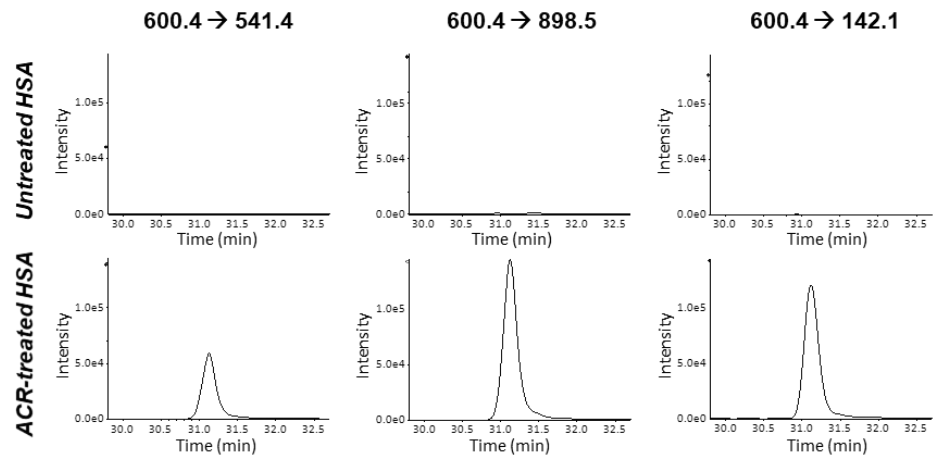
HSA peptides (a <sup>b</sup> )	Q1 m/z (charge)	Q3 m/z	Ion Series	CE	Dwell Time (ms)
<sup>337</sup> RHPDYSVLLLLR <sub>348</sub>	509.3 (3+)	564.3	B4	35.0	40
		885.4	B7	35.0	40
		<b>168.1</b>	<b>RI</b>	41.0	35
<sup>337</sup> RHPDYSVLLLLR <sub>348</sub>	489.9 (3+)	756.3	B6	35.0	60
		613.4	Y5	35.0	60
<sup>414</sup> KVPQVSTPTLVEVSR <sub>428</sub>	566.3 (3+)	511.3	B4	35.0	70
		798.5	B7	35.0	70
		<b>159.1</b>	<b>RI</b>	55.0	60
<sup>414</sup> KVPQVSTPTLVEVSR <sub>428</sub>	547.3 (3+)	589.3	Y5	35.0	10
		740.4	B7	35.0	25
<sup>574</sup> KLVAASQAALG <sub>584</sub>	600.4 (2+)	541.4	B5	35.0	20
		898.5	B9	35.0	20
		<b>142.1</b>	<b>RI</b>	55.0	25
<sup>574</sup> KLVAASQAALG <sub>584</sub>	507.3 (2+)	712.4	B8	35.0	25
		284.2	B3	35.0	10

Transitions were designed based on the MS/MS data on acrolein-treated HSA tryptic digests obtained in Section 3.2. The  $m/z$  of the modified peptides was set as the parent ion. Ions from the b or y fragmentation series were used as the product ions for each chosen peptide, generally selecting the ions with highest intensity. The reporter ions previously described in 3.2 were also selected for each modified peptide with respect to its modified residue. The collision energy (CE) and dwell time of each transition were optimized by trial and error.

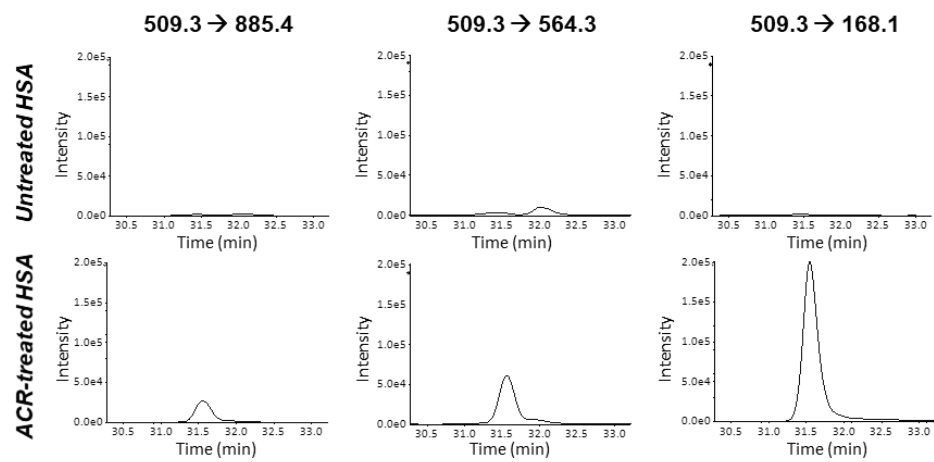
Three peptides were shown to be selective for the identification of acrolein adducts on HSA: **KLVAASQAALG** modified on the lysine residue (Lys574), **RHPDYSVLLLLR** modified on the histidine residue (His338) and **KVPQVSTPTLVEVSR** modified on the lysine residue (Lys414). For each, three transitions were selected for the modified and two transitions for the corresponding unmodified peptide. Specifically, the transitions using the reporter ions were of most interest as these are novel and have never been reported for identification of acrolein adducts. The reporter ions used were two lysine modifications specific ( $m/z$  142.1 and  $m/z$  159.1) and one histidine modification specific ( $m/z$  168.1). **Figure 2.12** shows the XICs for the three transitions selected for the modified peptide in untreated and *in vitro* acrolein-treated human serum albumin.

The first two transitions studied for each peptide were chosen here as peptide-specific ion transitions. These were only detected in the acrolein treated sample, not in the untreated control sample, except for the peptide in **Figure 2.12C** (**KVPQVSTPTLVEVSR**). Regarding the transitions including the reporter ions,  $m/z$  600.4 $\rightarrow$ 142.1 and  $m/z$  509.3 $\rightarrow$ 168 proved to be excellent at detecting lysine and histidine modified peptides, respectively. These generated high intensity signal peaks for the treated samples while not being detected in the untreated sample. Additionally, these ions eluted at the same retention time as the peptide-specific ions, supporting the hypothesis of these being selective of their acrolein-modified residue. However, the transition  $m/z$  566.3 $\rightarrow$ 159.1 gave a relatively low intensity and broad signal and was also detected in the untreated sample at even higher intensity.

**A) KLAASQAALG**



**B) RHPDYSVLLLLR**



**C) KVPQVSTPTLVEVSR**

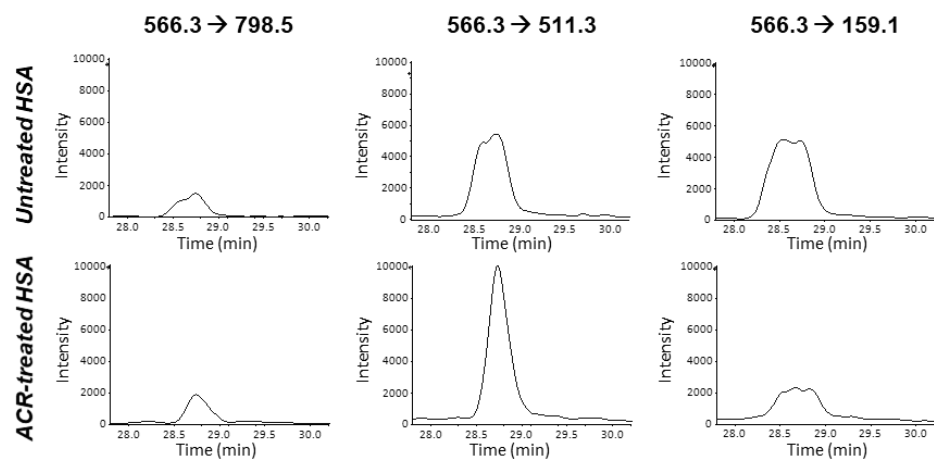
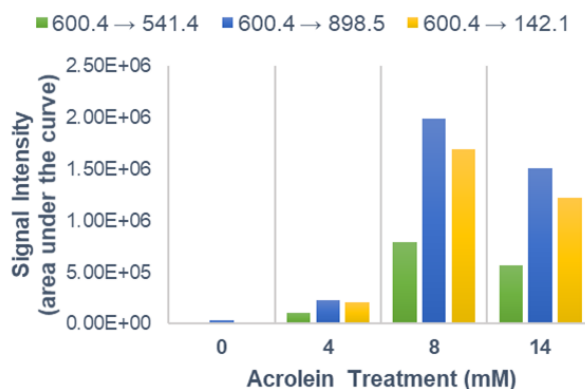


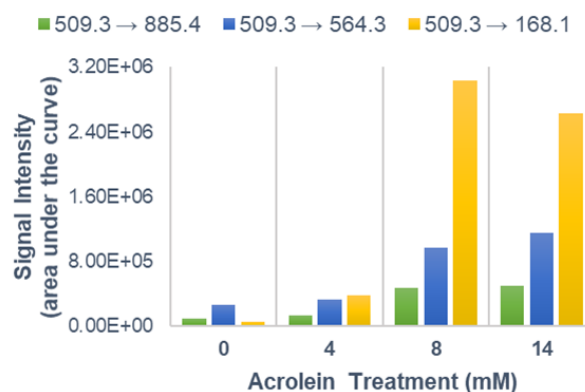
**Figure 2.12. Multiple reaction monitoring (MRM) for the identification of three human serum albumin peptides modified by acrolein.** Untreated and treated HSA with ACR at 8 mM for 2 hours. KLAASQAALG modified on lysine residue (A), RHPDYSVLLLLR modified on histidine residue (B) and KVQPQVSTPTLVEVSR modified on the lysine (C).

The same MRM method was used to study the effect of different acrolein concentration treatments in amount of modified-peptide detected. **Figure 2.13** shows a plot of the area under the curve as the signal intensity for the peaks detected of each of the modified-peptide transitions after acrolein treatment at 4, 8 and 14 mM. Transitions for KLVAASQAALG (**Figure 2.13A**) showed an interesting pattern not observed for the other peptides. The 4 mM treatment resulted in the lowest amount of modified peptide while 8 mM appeared to be producing the highest, instead of 14 mM as for the other two peptides, confirmed by the three transitions tested. Once more, treatment of HSA with 4 mM acrolein produced fewer RHPDYSVLLR modified peptides when compared to higher concentration treatments. Interestingly, these showed very similar intensities for this peptide and the transition 509.3 → 168.1 presented the highest signal intensity of all three transitions for this modified peptide (**Figure 2.13B**). The product ion  $m/z$  511.3 for KVPQVSTPTLVEVSR was detected at higher intensity than  $m/z$  789.5 for all the concentrations studied. For both transitions, 4 and 8 mM resulted in similar levels of modification and thus similar signal intensity. The highest concentration treatment at 14 mM resulted in higher levels of this modified peptide in comparison with the lower concentration treatments mainly detected by the ion  $m/z$  511.3. The reporter ion  $m/z$  159.1 was detected with the highest intensity at 4 and 14 mM while at 8 mM the amount detected was even lower than the control (**Figure 2.13C**).

### A. KLAASQAALG



### B. RHPDYSVLLLR



### C. KVPQVSTPTLVEVSR

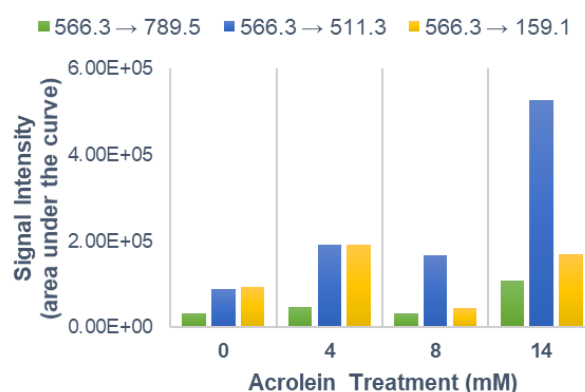


**Figure 2.13. MS/MS signal intensities produced by three human serum albumin peptides treated with different concentrations of acrolein (0 mM, 4 mM, 8 mM and 14 mM). Two transitions for peptide-specific product ions (green and blue) and one transition for residue and modification-specific report ion (yellow). KLAASQAALG modified on lysine residue (A), RHPDYSVLLLR modified on histidine residue (B) and KVPQVSTPTLVEVSR modified on the lysine (C). (n=1).**

#### 2.3.4. Testing the developed MRM approach for acrolein-HSA modifications on pooled human plasma

The next step was to test these transitions on an acrolein-treated human plasma pool with the goal of detecting acrolein-modified HSA within a complex mixture of proteins. Plasma pooled from healthy volunteers was diluted to 1:4 to give a human serum albumin concentration of roughly 10 mg/mL [302] and treated with acrolein as described for HSA previously. **Figure 2.14** shows the XICs for the MRM analysis of the untreated plasma and acrolein-treated plasma at 8 mM. The MRM method used was the same as described in **Table 2.4**.

All 14 transitions (for treated and untreated peptides) were successfully detected in plasma, although only the XICs for the transitions for the modified peptides are shown in **Figure 2.14**, for both treated and untreated plasma. These transitions eluted at the same retention time as observed for HSA supporting the hypothesis that these are selective for acrolein-albumin modifications. Here it is evident that the MRM method developed can be applied to complex biological samples of human plasma, without the need for much sample preparation as it was used as whole and no proteins were precipitated from the plasma.

Just as observed for HSA, all the three transitions tested for KLAASQAALG were detected in the acrolein-treated plasma while not being detected in the untreated plasma showing their power to detect this lysine modification not only in HSA but also in human plasma (**Figure 2.14A**). Once more, the diagnostic ion  $m/z$  142.1 proved to be a reporter ion for lysine modification even in a complex sample. In the XIC for RHPDYSVLLLLR, the peptide-specific transitions  $509.3 \rightarrow 885.4$  and  $509.3 \rightarrow 564.3$  gave rise to two peaks instead of one as observed for HSA (**Figure 2.14B**), suggesting that in plasma there are two precursors sharing the same mass and producing the same fragmentation product, varying only on retention time. When compared with the untreated plasma, this peptide showed a small increase in the signal intensity for the peptide-specific product ions while the reporter ion clearly shows an increase in intensity upon acrolein treatment. The transitions  $509.3 \rightarrow 168.1$ , using the report ion, was the best at detecting this histidine modification in the plasma. On the other hand, the peptide KVPQVSTPTLVEVSR showed that the reporter ion for lysine modification at  $m/z$  159.1 was detected in the treated and the untreated plasma samples at roughly the same intensity (**Figure 2.14C**). This pattern was also observed on the analysis of HSA, evidently showing that this ion is not selective for lysine modification on this particular peptide. Nevertheless, the transitions  $509.3 \rightarrow 168.1$  and  $600.4 \rightarrow 142.1$ , for RHPDYSVLLLLR modified on the histidine and KLVAAASQAALG modified on the lysine residues respectively, were detected at high intensities in the acrolein-treated plasma and at very low intensities in the untreated plasma, as described above. The detection of these in the control sample might be expected at low intensities

due to *in vivo* albumin-acrolein modifications that could already be present in the plasma at the time of collection.

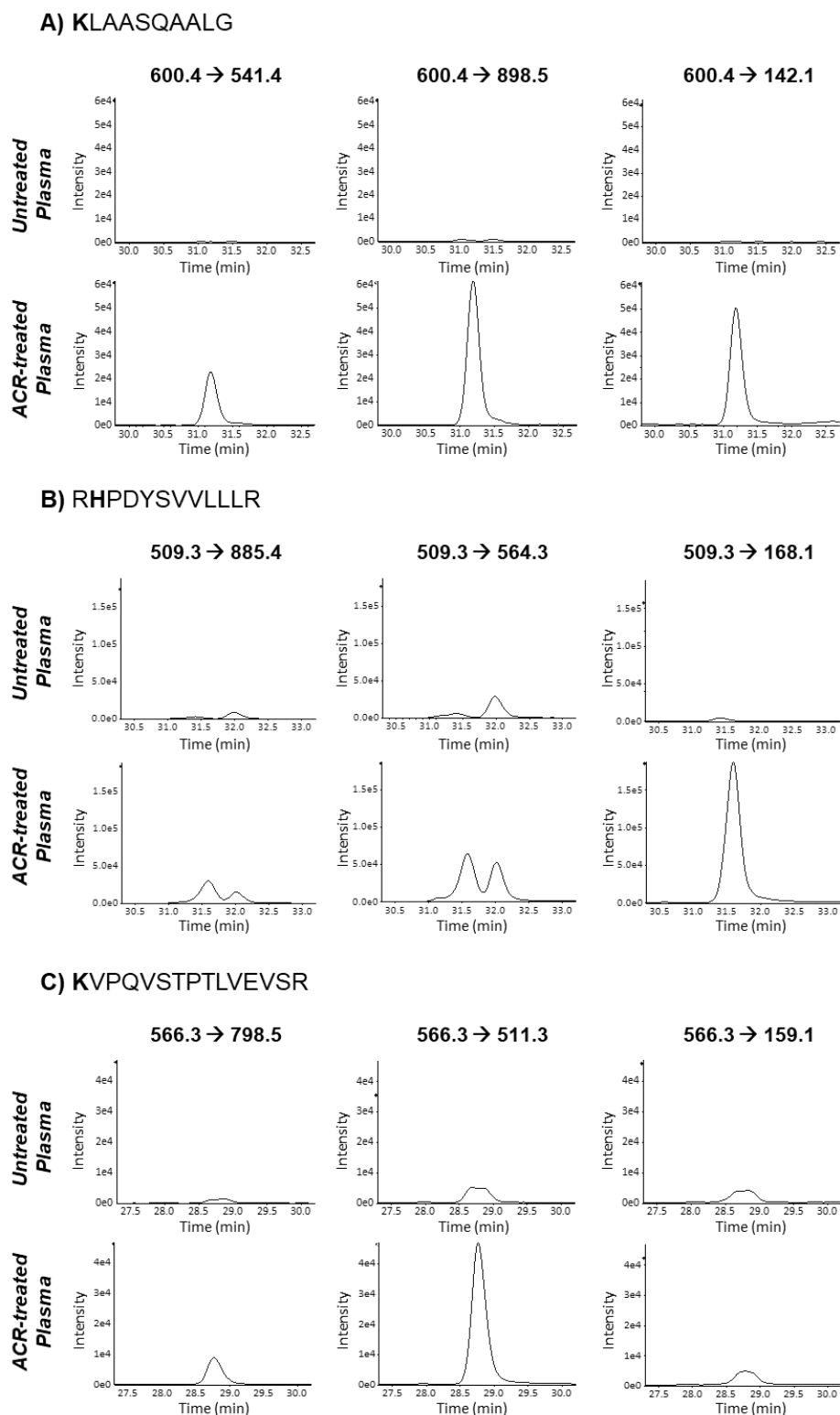
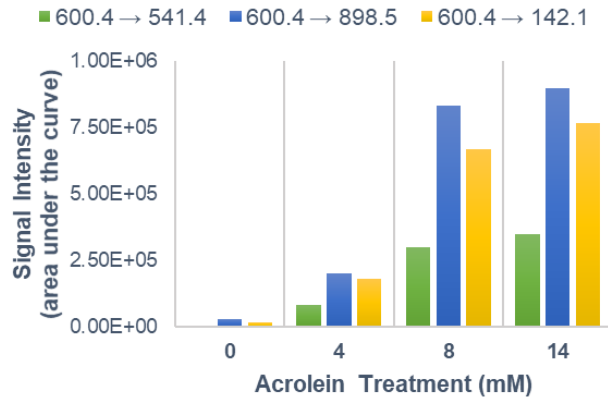


**Figure 2.14. Multiple reaction monitoring (MRM) for the identification of three human serum albumin peptides modified by acrolein in human plasma.** Untreated and treated human plasma with ACR at 8 mM for 2 hours. KLAASQAALG modified on lysine residue (A), RHPDYSVLLLR modified on histidine residue (B) and KVQPQVSTPTLVEVSR modified on the lysine residue (C).

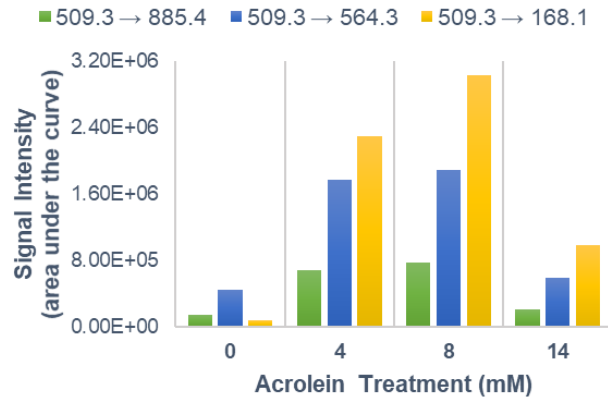


The same MRM method was tested to detect acrolein-modified human serum albumin peptides in plasma after different acrolein concentration treatments. **Figure 2.15** shows a plot of the area under the curve as the signal intensity for the peaks detected of each modified-peptide transition after plasma being treated with acrolein at 4, 8 or 14 mM. The transitions studied were sensitive to changes in the acrolein concentration treatment and different amounts of the modified peptides were detected in the plasma. Transitions for KLVAASQAALG were detected with the lowest intensity for 4 mM while 8 and 14 mM produced the highest intensity signals and at very similar levels (**Figure 2.15A**). The transitions 600.4 → 898.5 and  $m/z$  600.4 → 142.1 showed the best signal intensity out of the three tested for this peptide. Interestingly for RHPDYSVLLLLR, the transitions 509.3 → 885.4 and 509.3 → 564.3 were detected at the same levels for both 4 and 8 mM (**Figure 2.15B**). Only the transition 509.3 → 168.1 detected the increase of this modified peptide between these treatments. The lowest signal intensity detected for all of this peptide transitions were detected after the 14 mM treatment. The transition 566.3 → 511.3 for KVPQVSTPTLVEVSR detected an increase in this modified peptide at 8 and 14 mM in comparison with the control, however the signal for 14 mM was lower than for 8 mM (**Figure 2.15C**). The other two transitions showed lower intensity signals overall. The transition 566.3 → 159.1 was detected at roughly the same intensity at all concentration treatment and even at the control sample.

### A. KLAASQAALG



### B. RHPDYSVLLLLR



### C. KVPQVSTPTLVEVSR

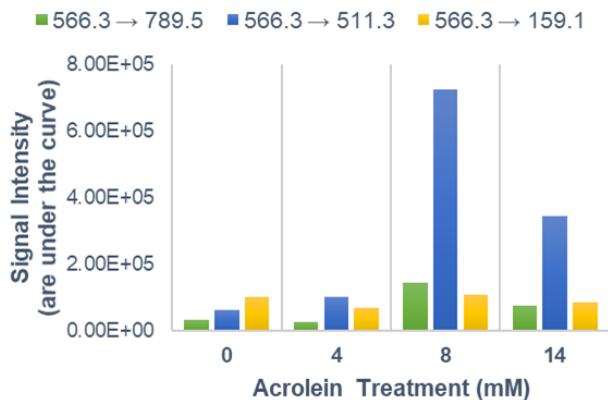


**Figure 2.15. MS/MS signal intensities produced by three human serum albumin peptides identified in human plasma after treatment with different concentrations of acrolein (0 mM, 4 mM, 8 mM and 14 mM). Two transitions for peptide-specific product ions (green and blue) and one transition for residue and modification-specific report ion (yellow). KLAASQAALG modified on lysine residue (A), RHPDYSVLLLLLR modified on histidine residue (B) and KVPQVSTPTLVEVSR modified on the lysine (C). (n=1).**

## 2.4. Discussion

In this study, the modification of proteins by two aldehydes, acrolein and 4-hydroxyhexenal, was evaluated as a model of lipoxidation adducts that may occur in inflammatory diseases. The first aim was to map the sites of modification using LC-MS/MS and identify potential diagnostic ions for adducts with different amino acid residues. To ensure extensive adduct formation and to allow a better MS characterisation of the adducts formed, high and non-physiological concentrations of the aldehydes were used, even though it has been suggested that local levels of aldehydes can be higher than plasma levels [303]. Acrolein modifications were found in 5 lysozyme and 11 HSA peptides and were predominantly formed by Michael addition reactions with cysteine, histidine and lysine amino acid residues, based on the mass increases of 56 Da or 58 Da for unreduced or reduced forms respectively, despite the potential for this aldehyde also to form Schiff's base adducts. Additionally, 5 diagnostic ions for acrolein adducts with cysteine, histidine and lysine were consistently observed in the MS/MS spectra of modified peptides. HHE modifications were found in 14 HSA peptides, with adducts identified on cysteine, lysine, histidine and arginine residues, based on the mass increase of 114 Da or 96 Da for Michael addition and Schiff base, respectively. In addition, 8 potential diagnostic ions for HHE adducts with lysine, arginine and histidine were observed.

The bottom-up proteomic approach allowed identification of 8 lysozyme residues modified by acrolein: Cys6, Cys30, Cys64, Cys76, Cys80, Lys96, Cys155 and Lys116, which fitted well with the 8 acrolein molecules found covalently bound per lysozyme by intact protein analysis. For HSA, mainly histidine and lysine residues were found to be modified: His67, Lys137, His146, Lys262, Lys276, His288, His338, Lys414, Lys525 and Lys574. The high number of cysteines modified in lysozyme is likely to result from the reduction prior to reaction with the acrolein. This also confirms that free cysteine residues are highly susceptible to acrolein modification. For HSA the reduction was omitted and since only one single cysteine (Cys34) is in the free thiol form, modifications of lysine and histidine were consequently more prevalent. The tryptic peptide containing the HSA free cysteine was challenging to detect, as it is a long peptide that gives low ion intensity. Some of the peptides identified contained missed cleavages owing to modification of lysine residues, which could complicate relative quantification against untreated samples due to generation of different peptides. A number of the lysines and histidines observed to be modified have been reported to be susceptible to electrophilic attack, and the occurrence of acrolein-protein adducts has previously been reported both *in vitro* and *in vivo* [74], including studies of acrolein modification of albumin [304]. The same bottom-up proteomic approach was used to identify 12 HSA residues modified by HHE: Cys75, Cys124, Lys137, Cys245, His247, Cys265, Cys279, His288, Cys360, Arg410, His464 and Cys477. Two residues were found

to be modified by both aldehydes (Lys137 and His288), suggesting highly susceptibility of these to lipoxidation.

HSA is highly abundant, and its modification might be seen as a defence mechanism to prevent the damage of other critical and less abundant proteins. However, it is still important to consider the potential physiological consequences of lipoxidation, as human serum albumin has many biological functions that could as well be affected by modification. For example, His67 was readily modified by acrolein, and is one of the residues contributing to the zinc binding site on albumin [20, 305, 306]. Zinc is required for essential intra and extracellular enzymes function. The zinc site on albumin is formed by the side chains of His67 and Asn99 from domain I, and His247 and Asp249 from domain II [305]. So modification on any of these residues could disrupt zinc binding to and transport by albumin. As decreased binding of zinc can affect fatty acid binding to albumin [307], this modification could result in increased levels of fatty acids in the blood and contribute to plasma lipid changes in cardiovascular diseases and diabetes. While acrolein was found to modify many relevant residues, under physiological conditions the profile of the modifications could be different. The data presented here, and previous literature suggest that the cysteine residues would be major sites of modification [285, 308, 309]. Furthermore, the sequence coverage obtained was incomplete (typically 80-85%) and some potential modification sites, such as the N-terminal, were not covered; hence no conclusions can be drawn about these sites. Nevertheless, this shows the importance of identifying the correct location of protein modifications and understand their relevance to disease.

A major aim of the study was to identify the diagnostic ions for the aldehyde adducts that could subsequently be used in targeted mass spectrometry approaches such as multiple reaction monitoring (MRM), or to confirm peptide identifications. At lower  $m/z$  range of the MS/MS spectra, immonium and related internal fragmentation ions specific to amino acids present in the peptides can be observed; these ions are potential MS/MS reporter ions for modified amino acid residues. From the MS/MS spectra of the modified tryptic peptides, several potential diagnostic ions for the acrolein (Figure 2.9) and for HHE (Figure 2.11) modifications were identified. While protein-acrolein adducts have been extensively studied previously [308, 310, 311], the focus was on finding these reporter ions since it appears that there are no specific studies of this kind aiming to improve the detection of these modifications. The success of the application of these reporter ions on novel detection methods corresponds to the second aim of this chapter and it is discussed in detail below.

In summary, the first aim has provided new data on the sites of modification in two model proteins by acrolein and HHE. It has also identified novel diagnostic fragment ions for acrolein and HHE adducts of cysteine, lysine, histidine and arginine. This study shows the power of combined use of direct infusion and LC-MS/MS to identify the type, the number

and the location of protein adducts. The MS approaches described here could also be applied to study other types of adducts as biomarkers of lipoxidation in cells and tissues under pathophysiological conditions. The acrolein diagnostic ions were used in targeted mass spectrometry approaches, such as multiple reaction monitoring, to identify and quantify aldehyde adducts.

For the second aim of the study in this chapter, an MRM approach was developed to detect albumin-acrolein adducts in human plasma. The success of developing any MRM method depends upon selection of the most appropriate peptides and their respective transitions. Transitions were designed based on MS/MS data resulting from bottom-up analysis of acrolein-treated HSA. To ensure that the MRM method could be applied to biological samples, multiple transitions were established per peptide owing to the complexity of human plasma [211]. The  $m/z$  of the modified peptide was set as the precursor ion. Ions from the b and y type fragmentation chosen based on the highest intensity fragmentation ions present in the MS/MS spectra [312], as well as the report ions for acrolein modification, were used as the product ions. The bottom-up data used to choose these ions was acquired on a Q-TOF while the MRM data was acquired on a triple quadrupole, which could explain why some of the transitions did not work as well to detect the modifications with the MRM method [300, 312]. No peptide containing modified cysteine was used in the MRM method, as cysteine gives weak immonium ion signals and consequently its corresponding report ion did not work well in this method development. Two of the three peptides used in the method (RHPDYSVLLLLR and KVPQVSTPTLVEVSR) contained at least one proline residue and it has been suggested that peptides containing this residue are able to produce higher intensity MS/MS signals facilitating their detection [313]. The three peptides used were shown to be selective and provided good intensity peaks indicating highly sensitive detection of HSA-acrolein modifications.

After the method development performed on *in vitro* modified HSA, this was tested on *in vitro* acrolein-treated plasma. Previous studies reported that due to the large variety of proteins present in plasma, the MRM approach detected a large amount of noise and interference, and better results were obtained when the MRM method was run on plasma-extracted albumin instead of the whole plasma [314]. However, for our method, no sample preparation was used apart from plasma dilution before treatment and the method proved to be sensitive with minimal background noise.

One issue detected in the plasma but not in the HSA data was the double peak detected by the transitions  $509.3 \rightarrow 885.4$  and  $509.3 \rightarrow 564.3$  for RHPDYSVLLLLR. This might mean that another precursor ion with the same mass  $m/z$  509.3 is also producing the same product ions. However, this does not interfere with the identification of the modified peptide

because another transition was used in parallel using the reporter ion  $m/z$  168.1, which has previously been shown to be selective for acrolein-histidine modification. This confirmed the retention time consequently identifying which of the two peaks correspond to our peptide of interest.

One hypothesis tested with this method was that increasing the concentration of acrolein treatment on HSA, would consequently increase the level of acrolein modifications. However, this hypothesis was not confirmed. This could be due to the level of acrolein-induced albumin crosslinking that occurs during the different treatments. Unfortunately, crosslinking was not studied, and this could not be confirmed. Acrolein protein-protein cross-linking has been previously studied [315, 316], including in proteins such as Hsp90 which has a role in the response to oxidative stress [317], but none of these were studied using mass spectrometry, as opposed to the interchain cross-linking of DNA mediated by acrolein which has been studied by MALDI-TOF [318, 319]. The same hypothesis could possibly explain why at 8 mM acrolein treatment similar or slightly higher intensity peaks were detected than at 14 mM treatment for the peptides RHPDYSVLLLLR and KLAASQAALG. This could be because acrolein modifications at His338 and Lys574 are more likely to induce crosslinks than modifications at Lys414, and therefore there would be fewer of these modified peptides resulting from enzymatic digestion. However, without further studies, it is not possible to confirm this hypothesis, and the evidence supporting the formation of acrolein-induced albumin crosslinking is a limitation of this work.

A thorough validation process of the transitions used in this method would be desirable to be able to accurately quantify the level of acrolein-albumin adducts. For example, the samples would need to be spiked with a known concentration peptide to serve as an internal standard [300]. Once the transitions are accurately validated using *in vitro* acrolein-treated plasma from healthy volunteers, it would be ideal to test it with plasma from patients with a pathophysiological conditions known to result in increased acrolein-albumin adducts such as cardiovascular disease, type 2 diabetes mellitus, Alzheimer's disease and brain infarction [314, 320] to fully validate the method. Unfortunately, there was not enough time to source such samples and carry out further investigation.

In conclusion, it is evident that an MRM approach for acrolein-albumin adducts has the potential to become a robust method with further validation. Many pathophysiological conditions result in increased levels of oxidative stress, and other RCS-albumin adducts as biomarkers for oxidative stress have repeatedly been suggested in recent years [302, 314]. The lack of sensitive, specific and validated analytical assays has held back progress in the use of these adducts as biomarkers of oxidative stress. LC-MS/MS analysis, specially targeted methods as MRM, provide a promising solution to this need for sensitive and highly specific measurements of RCS-albumin adducts. The method developed in this chapter has

identified successful and promising MRM transitions, specially the novel transitions using report ions which proved to be highly selective for acrolein modification. This provided an approach that could potentially be used in the future for detection of acrolein-albumin adducts in human plasma, for example from diabetic patients or lung cancer since acrolein is a major component of tobacco smoke.

## **Chapter 3. Synthesis of 2-chlorohexadecanal and its adduction to proteins**



### 3.1. Introduction

In inflammation, neutrophils are activated and release numerous bioactive and anti-microbial molecules, including partially reactive oxygen species such as hydrogen peroxide. Hydrogen peroxide is a substrate of the enzyme myeloperoxidase (MPO), which in the presence of chloride ion produces hypochlorous acid (HOCl) [139, 321], a strong oxidizing and chlorinating agent. HOCl is primarily responsible for the microbicidal action of neutrophils but during chronic inflammation it is able to react with host proteins, nucleic acids and lipids [322]. Plasmalogens, which contain a vinyl ether bond, are particularly susceptible to reaction with HOCl, resulting in the production of free  $\alpha$ -chloroaldehydes [142, 143]. Plasmalogens are a subclass of phospholipids found in many cells but are particularly enriched in phagocytes such as neutrophils [323].  $\alpha$ -chloroaldehydes have previously been reported to accumulate in activated human neutrophils and monocytes [138, 324] and to be elevated in human aortic atherosclerotic plaques [147]. Although  $\alpha$ -chloroaldehydes are produced during neutrophil activation, the mechanism by which they have an impact on cell function remains to be resolved. The biological activity attributed to  $\alpha$ -chloroaldehydes may be mediated through metabolism to  $\alpha$ -chloro carboxylic acids, which have been reported to induce apoptosis [325]. However,  $\alpha$ -chloro aldehydes are likely to cause direct cellular effects due to their reactive aldehyde group and  $\alpha$ -chlorinated carbon. A potential mechanism by which  $\alpha$ -chloroaldehydes could cause impact in cell function is by forming reversible Schiff base adducts with amines in proteins [326].

The HOCl oxidation of plasmenylcholine (16:0/18:1) results in formation of lysophosphatidylcholine (0:0/18:1) and 2-chlorohexadecanal (2-ClHDA), by far the most studied  $\alpha$ -chloroaldehyde [138, 146]. 2-ClHDA is known to be involved in pro-inflammatory and cell death pathways, making it important to understand the mechanisms underlying such roles [151, 152]. Therefore, it is important to understand its metabolism and cellular impact. 2-ClHDA has been reported to contribute to atherosclerosis and cardiac dysfunction [147, 327] suggesting that this chloroaldehyde in particular is relevant in inflammatory diseases. Additionally, it has been reported to activate cyclooxygenase-2 (COX-2), which is highly expressed in atherosclerotic lesions, via an NF- $\kappa$ B mediated pathway [151]. MPO is also highly expressed in neuroinflammatory diseases, such as Parkinson's and Alzheimer's diseases, in comparison with normal brain [328, 329], and 2-ClHDA has been reported to affect brain function by induction of blood-brain barrier dysfunction (BBB). This was shown in primary brain microvascular endothelial cells (BMVEC) on treatment with MPO-H<sub>2</sub>O<sub>2</sub>-Cl, and in a mouse model, neutrophils released MPO into the cerebrovasculature, induced decrease of brain plasmalogen content, formation of 2-ClHDA, increased BBB permeability and activated the MAPK cascade in response to systemic lipopolysaccharide (LPS) administration [148, 330]. Previous studies suggest that 2-ClHDA

causes brain damage by covalent modification of proteins, which impairs function and triggers responses associated with oxidative stress [331]. PARK7 (DJ-1), which protect cells from oxidative stress, has been identified as a prime target of 2-ClHDA in brain [331]. Additionally, DJ-1 has also been reported to form adducts with other electrophilic aldehydes, such as HNE and these adducts were found increased in blood from Parkinson's disease patients when compared with healthy controls [332].

2-ClHDA undergoes redox metabolism via the fatty acid-fatty alcohol cycle, resulting in the corresponding alcohol or carboxylic acid [333]. The oxidation to 2-chlorohexadecanoic acid (2-ClHA) from 2-ClHDA is dependent on fatty aldehyde dehydrogenase (FALDH) and has been demonstrated both in isolated human neutrophils and *in vivo* systems [150, 333]. 2-ClHA does not show the neutrophil chemoattractant properties of 2-ClHDA [138] and its generation from 2-ClHDA might be considered as a protective pathway. However, 2-HDA was found to accumulate in activated monocytes and to induce apoptosis through mechanisms involving H<sub>2</sub>O<sub>2</sub> release and ER stress, in monocytic and macrophagic cell lines, as well as primary human monocytes [325].

Pre-treatment of monocytes with glutathione (GSH) shown to ameliorate the production of H<sub>2</sub>O<sub>2</sub> induced by 2-ClHA and reduce the caspase 3 activity, PARP cleavage and CHOP expression [325]. GSH is responsible for detoxification of endogenous and exogenous potentially toxic electrophiles due to its nucleophilic thiol, which can react with unsaturated and halogenated carbons [334, 335]. The  $\alpha$ -chlorinated carbon of 2-ClHDA was shown to react with the nucleophilic thiol of GSH, resulting in a peptidoaldehyde (FALD-GSH) which has been found in activated neutrophils and in plasma of a mouse arthritis model [199]. LC-MS/MS [336] confirmed the structure of the adduct, which is formed from nucleophilic attack at the  $\alpha$ -chlorinated carbon by the thiol with loss of chlorine [199]. The dihydrochalcone-type polyphenol phloretin has also been shown to be able to attenuate the cellular effect of 2-ClHDA, providing protection against BBB dysfunction, apoptosis and ATP depletion [152]. The structure of the adduct of phloretin and 2-ClHDA was confirmed by NMR, and biological experiments demonstrated that the adduct did not alter cell function, so this can therefore, be considered a detoxification pathway [337].

2-chlorohexadecanal is not commercially available, thus its synthesis is necessary prior to any study on its effect on proteins. Recent studies have used the for reaction of 1-O-hexadec-enyl-glycerol-3-phosphocholine with HOCl followed by lipid extraction and HPLC purification to obtain 2-chlorohexadecanal [151]. This approach proved to be time consuming and relatively expensive. In this study, two alternative approaches were tested. First, a multi-step reaction was evaluated, consisting of: 1) synthesis of hexadecanal from hexadecanol by Corey-Suggs oxidation [338]; 2) acetal protection of the hexadecanal using trimethylorthoformate to protect the aldehyde from nucleophilic attack during chlorination;

3) chlorination via manganese catalysed chlorination with trimethylsilylchloride; 4) deprotection the 2-chloro-methylacetal hexadecanal by mild acid hydrolysis. This was also time consuming, although it would allow synthesis of reasonable quantities of the chloroaldehyde, and so an alternative one-pot method was investigated using trichloroisocyanuric acid (TCCA) as the oxidizing and chlorinating agent with TEMPO (2,2,6,6-tetramethylpiperidine 1-oxyl) as a catalyst [339]. All reaction products were characterized by  $^1\text{H}$  NMR.

Liquid chromatography coupled to tandem mass spectrometry was used to investigate protein modifications by 2-chlorohexadecanal. As for chapter 2, lysozyme (14,306 Da), which is rich in lysine and cysteine residues, and human serum albumin (66,437 Da), the most abundant human plasma protein were used as model proteins. Non-physiologically high concentrations of 2-chlorohexadecanal were used to ensure adduct formation as the aim was to generate adducts in reasonable abundance in order to characterize the modified amino acids and identify potential reporter ions for these modifications which are preferably amino acid- and modification-specific and, which could be used to develop targeted methods such as SRM or MRM for the identification of these adducts in clinical samples.

## 3.2. Material and Methods

### 3.2.1. Multi-step synthesis of hexadecanal from hexadecanol

#### 3.2.1.1. Synthesis of hexadecanal (Corey-Suggs oxidation)

Into a three-necked round bottom flask, under positive pressure of nitrogen gas, 123.63 mmol (17.9 g) of pyridinium chlorochromate (PCC) dissolved in 150 mL of dry dichloromethane (DCM) was added. The mixture was stirred for 15 min at room temperature, then 82.49 mmol (13.4 g) of hexadecanol dissolved in 50 mL of dry DCM was added in one portion. The mixture immediately turned black. It was left to stir for 1.5 hours at room temperature after which 150 mL of dry diethyl ether was added, and a black tarry precipitate formed [338]. The solution was filtered under gravity and the black precipitate was washed with dry diethyl ether and wash filtered. The filtrate was then filtered for a second time using a sintered funnel loaded with 30g of Florisil<sup>®</sup> to remove fine particulates. The Florisil<sup>®</sup> was then washed 2 x 30 mL with petroleum ether 60-80/diethyl ether (90:10). The organic extracts were evaporated under vacuum and the resulting off-white powder was dried in a desiccator. The reaction was monitored by TLC (silica gel 60 F<sub>254</sub>, Merck, Darmstadt, Germany) using pet ether 60-80/ether (90:10) as solvent and the retention factor (Rf) for the starting material was 0.1 and for the final product was 0.37.

#### 3.2.1.2. Synthesis of dimethylacetal hexadecanal (protection)

4.19 mmol of hexadecanal (1 g) from the previous reaction and 8.21 mmol (900  $\mu$ L) of trimethylorthoformate (TMOF) were dissolved in 20 mL of dry methanol. 4.65 mmol of *p*-toluene sulfonic acid (0.8 g) was then added. The mixture was stirred under reflux for 4 h at 70 °C. The reaction was then diluted with 20 mL of pentane, washed with 10 mL of 0.5% NaOH solution and the aqueous phase extracted with 3 x 10 mL of pentane. The organic phases were combined and dried over MgSO<sub>4</sub>. The solvent was evaporated under vacuum to obtain the hexadecanal methyl acetal as a white solid. The reaction was monitored by TLC using n-hexane/ethyl acetate (95:5) as solvent and the Rf of the final product was 0.56.

#### 3.2.1.3. Synthesis of 2-chloro-methylacetal hexadecanal (chlorination)

MnCl<sub>2</sub> (1.5 mmoles, 0.339 g) was weighed into a flask with 10 mL of acetonitrile and methanol (50:50) and the mixture stirred until the MnCl<sub>2</sub> was completely dissolved. MnO<sub>2</sub> (3.1 mmoles, 0.527 g) and the methyl acetal (3.5 mmoles, 1.14 g) from the reaction above were added and the mixture immediately turned black. The stirred mixture was refluxed at 40 °C for 15 minutes before trimethylsilylchloride (TMSCl) (14.4 mmoles, 3.1 g) was poured into the mixture in one portion. The reaction was left to reflux for 42 hours and then it was

diluted with 20 mL of hexane. The mixture was diluted with 20 mL of CH<sub>2</sub>Cl<sub>2</sub> and the precipitated removed by filtration. The organic phase was washed with 10 mL of 1.5 % NaOH solution. The aqueous layer was then extracted with 2 x 10 mL of hexane, and the organic phases were combined, dried over MgSO<sub>4</sub> and then evaporated under vacuum. The reaction was monitored by TLC using pet ether 60-80/dichloromethane (70:30) as solvent and the R<sub>f</sub> of the final product was 0.28.

#### **3.2.1.4. Acid hydrolysis of 2-chloro-methylacetal hexadecanal (deprotection)**

To 1.25 mmol (400 mg) of 2-chloro-methylacetal hexadecanal dissolved in 5 mL of anhydrous CH<sub>2</sub>Cl<sub>2</sub> were added 2.5 mL of 50:50 trifluoroacetic acid (TFA) and water (v/v). The reaction was stirred at 37 °C for 48 hours, after which it was diluted with 20 mL of CH<sub>2</sub>Cl<sub>2</sub> and washed three times with 20 mL of an aqueous 5% NaHCO<sub>3</sub> solution. The aqueous phase was re-extracted with CH<sub>2</sub>Cl<sub>2</sub> (3 x 20 mL) and the combined organic phases were dried over MgSO<sub>4</sub> evaporated in vacuum. The reaction was monitored by TLC using hexane/dichloromethane (50:50) as solvent and the R<sub>f</sub> of the final product was 0.59.

### **3.2.2. Direct conversion of alcohol into chloroaldehyde**

#### **3.2.2.1. First attempt**

Hexadecanol (4.12 mmol, 1 g) was dissolved in 20 mL of dichloromethane. 3.3 mmol (0.78 g) of trichloroisocyanuric acid (TCCA) and 0.3 mmol (0.0415 g) of TEMPO (catalyst) were added to the reaction which was left stirring for one hour at room temperature. The product was filtered twice, and a white powder was formed. Reaction was monitored by TLC using hexane/dichloromethane (50:50) as solvent. The R<sub>f</sub> of the starting material was 0.32 and for the final product was 0.79. Product was characterized by <sup>1</sup>H NMR.

#### **3.2.2.2. Second attempt**

Hexadecanol (0.5 mmol, 121.2 mg) and TEMPO (0.03 mmol, 4.69 mg) were dissolved in 5 mL dichloromethane. The mixture was cooled to 0 °C. TCCA (0.5 mmol, 116.2 mg) was added in small portions while stirring. The reaction was left to stir for 10 minutes at 0 °C. The reaction was then stirred for additional 30 minutes at room temperature while being monitored by TLC using hexane/dichloromethane (50:50) as solvent. The retention factor (R<sub>f</sub>) for the starting material was 0.25 and for the final product was 0.68. Pentane was added and the mixture filtered. The filtrate was then washed three times with 20 mL of water, dried over MgSO<sub>4</sub> and concentrated under vacuum. The product obtained was a yellow oil that was characterized by <sup>1</sup>H NMR.

### 3.2.3. <sup>1</sup>H NMR analysis

<sup>1</sup>H NMR experiments were performed at room temperature on a Bruker spectrometer operating at 400 MHz with a 5mm PABBO probe. Spectra were acquired with an 8012.82 Hz spectral width, 296.6 K data points, a 1s relaxation delay (d1) and 16 scans. Data processing was performed using MestReNova (Mnova NMR) programme, version 8.1 (Mestrelab Research, California, USA). Chemical shifts are given in ppm. The chemical shifts were referenced internally to the TMS signal at 0.00ppm. Splitting pattern abbreviations are s, singlet; d, doublet; t, triplet; m, multiplet.

### 3.2.4. GC-FID analysis

GC-FID analysis was performed using an Agilent HP-5 column (30m, 0.32mm i.d., 0.25µm) with an Agilent Technologies 7829A gas chromatograph. The analysis of the multistep reaction was performed with the injector at 250 °C and an isothermal analysis with the oven kept at 260 °C with an analysis time of 2 minutes. The analysis of the direct conversion products was performed as previously described by Wacker, B.K. *et al* [336]. The injector and the transfer lines were kept at 250 °C. The GC oven was kept at 150 °C for 3.5 minutes and increase the temperature at a rate of 25 °C /min to 300 °C. This temperature was held for an additional 5 minutes.

### 3.2.5. Treatment of model proteins with 2-chlorohexadecanal *in vitro*

Lysozyme and human serum albumin (1 mg/mL) were first reduced with 100 mM DTT for 30 minutes as described in Section 2.2.2. Synthesized 2-chlorohexadecanal was added to the protein at treatment concentrations of 8 and 16 mM and allowed to react for 2 hours at room temperature. To stabilize adducts, NaBH<sub>4</sub> was added to the reaction to a final concentration of 5 mM and left for 1 hour at room temperature.

### 3.2.6. Liquid Chromatography-Mass Spectrometry (LC-MS) Analysis

Peptides were separated and analysed using an Ultimate 3000 system (Thermo Scientific, Hempstead, UK) coupled to a 5600 TripleTOF (ABSciex, Warrington, UK). The analysis was performed as previously described by Verrastro *et al.*, 2016 [298] and as detailed in section 2.2.6.

### 3.2.7. Database Search

The Mascot® probability-based search engine (Matrix Science, London, version 2.4.0) was used to interrogate the SwissProt 2017-07 primary database. LC-MS .wiff files of each sample were searched for protein identification and oxidative post-translational

modifications (oxPTMs). For protein identification, variable modifications of methionine oxidation and carbamidomethyl cysteine were used. For the analysis of the lipoxidation products, the initial searches additionally used a variable modification list including 2-chlorohexadecanal reduced adducts at 258.9 Da and 222.4 Da for arginine, lysine and histidine amino acid residues and at 240.4 Da for cysteine amino acid residue. Other parameters for the searches were as follows: Enzyme: Trypsin; Peptide tolerance:  $\pm 0.6$  Da; MS/MS tolerance:  $\pm 0.6$  Da; Peptide charge state: +2, +3; Max Missed cleavages: 1; #13C: 0; Quantitation: None; Instrument: ESI-QUAD-TOF; Data format: Mascot Generic; Experimental mass values: Monoisotopic; Taxonomy: Chordata. All data identifying modifications were manually validated before inclusion.

### 3.3. Results

#### 3.3.1. Multi-step reaction synthesis of 2-chlorohexadecanal

While the aim was to characterize the modification by chloroaldehydes of proteins using the proteomic approach described in chapter 2,  $\alpha$ -chloroaldehydes are not commercially available and its synthesis was required prior all the other experiments. 2-chlorohexadecanal has been the most studied  $\alpha$ -chloroaldehyde as it is a biological product of the reaction of HOCl with plasmenylcholine (16:1/18:0). The first approach to the synthesis of 2-chlorohexadecanal was a multi-step reaction that started with the oxidation of hexadecanol to hexadecanal following the Corey-Suggs protocol [338] using pyridinium chlorochromate (PCC), a readily available, stable reagent, that oxidizes a wide variety of alcohols to carbonyl compounds with high efficiency (**Figure 3.1**).

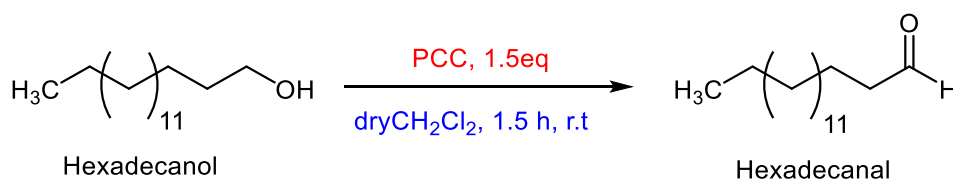


**Figure 3.1.** Corey-Suggs oxidation of hexadecanol to hexadecanal using pyridinium chlorochromate as catalyst.

The reaction was monitored by thin-layer chromatography (TLC) and the retention factor (Rf) for the starting material was 0.1 while for the product was 0.37. The reaction yield was 97.7%. A proton nuclear magnetic resonance ( $^1\text{H}$  NMR) spectrum was also obtained in order to confirm the structure of the starting material (**Figure 3.2A**) and the product (**Figure 3.2B**).



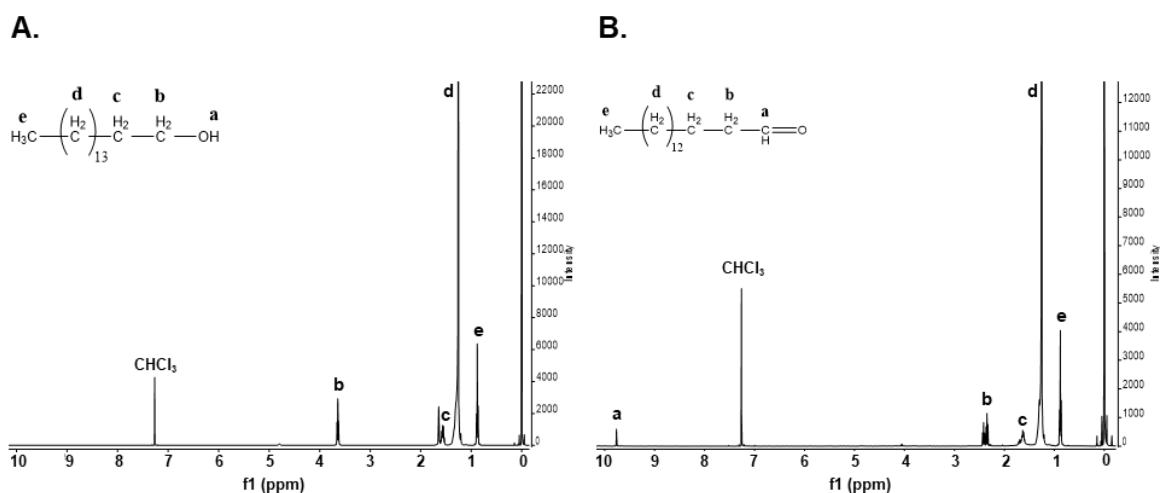


**Figure 3.2.**  $^1\text{H}$  NMR spectrum of the starting material hexadecanol (**A**) and the product of its oxidation, hexadecanal (**B**). A-  $^1\text{H}$  NMR: 3.63 ppm (2H, t,  $\text{CH}_2$ ); 1.56 ppm (2H, m,  $\text{CH}_2$ ); 1.28 ppm (26H, m,  $\text{CH}_2$ ); 0.88 ppm (3H, t,  $\text{CH}_3$ ). B-  $^1\text{H}$  NMR: 9.77 ppm (1H, t,  $\text{C}(=\text{O})\text{H}$ ); 2.40 ppm (2H, m,  $\text{CH}_2$ ); 1.63 ppm (2H, m,  $\text{CH}_2$ ); 1.28 ppm (24H, m,  $\text{CH}_2$ ); 0.88 ppm (3H, t,  $\text{CH}_3$ ). Internal reference (TMS) at 0.0 ppm.

The  $^1\text{H}$  NMR analysis confirmed that the product obtained was hexadecanal. The peak at 7.3 ppm corresponds to chloroform, the solvent used. The peak lower in the field (higher frequency), observed at 9.7 ppm was only observed in **Figure 3.2B** has a singlet and corresponds to the proton in the aldehydic group ( $\text{RC}(=\text{O})\text{H}$ ). This confirms that the oxidation from the alcohol to aldehyde occurred. The protons identified as **b** are closer to the electronegativity of the oxygen than the remaining protons and therefore appear at lower field (2.3 ppm) than the remaining protons. The protons identified as **e** appear as a triplet at 0.9 ppm and correspond to the terminal methyl group. The area of the multiplet peak identified as **c** confirms that it corresponds to the remaining 22 protons in the structure.

While the next step could be chlorination of hexadecanal, the carbonyl group would be vulnerable, so it needs to be protected. This is most easily achieved through formation of the dimethyl acetal. This was formed by reaction of hexadecanal with trimethyl orthoformate (TMOF) in methanol and using p-toluenesulfonic acid (pTSA) as organic acid catalyst. The final product was hexadecanal dimethyl acetal (**Figure 3.3**).

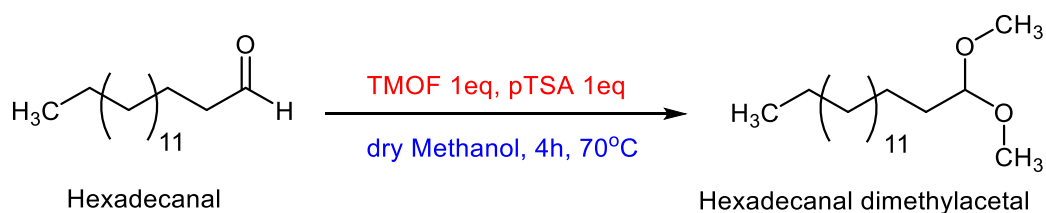


**Figure 3.3.** Introduction of a protective group to hexadecanal by trimethyl orthoformate (TMOF) in methanol and using p-toluenesulfonic acid (pTSA) as catalyst, resulting in hexadecanal dimethyl acetal.

The reaction was monitored by thin-layer chromatography (TLC) and the retention factor (Rf) for the product was 0.56, and the reaction yield was 94.7%. A proton nuclear magnetic resonance ( $^1\text{H}$  NMR) spectrum was also obtained in order to confirm the structure of the final product (**Figure 3.4**).

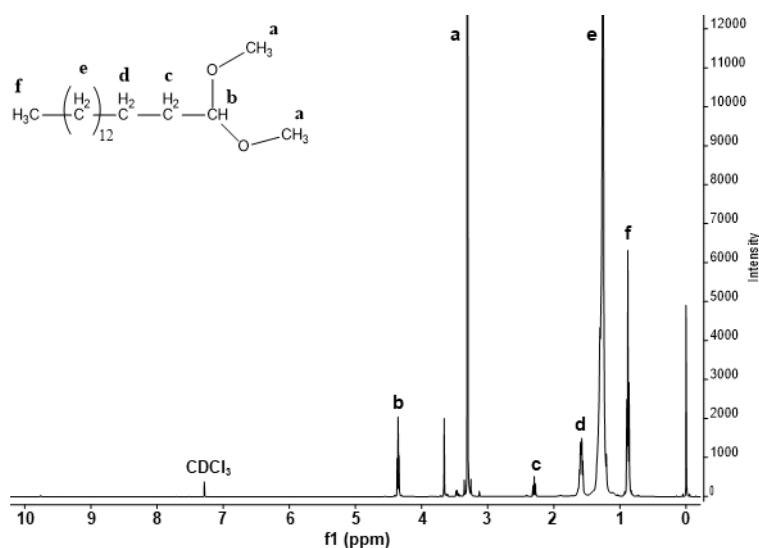


**Figure 3.4.**  $^1\text{H}$  NMR spectrum of hexadecanal dimethyl acetal, product of the reaction of hexadecanal with TMOF in the presence of pTSA.  $^1\text{H}$  NMR: 4.36 ppm (1H, t, (OR')CH(OR'')); 3.31 ppm (6H, s, OCH<sub>3</sub>); 2.30 ppm (2H, td, CH<sub>2</sub>); 1.59 ppm (2H, tt, CH<sub>2</sub>); 1.26 ppm (24H, m, CH<sub>2</sub>); 0.88 ppm (3H, t, CH<sub>3</sub>). Internal reference (TMS) at 0.0 ppm.

The main differences between starting material and final product were the disappearance of the proton in the aldehydic group (the peak previously observed at approximately 9 ppm), and appearance of the protons from the methyl groups of the acetal identified as **a** in **Figure 3.4**. The area of the peak at 3.3 ppm corresponds to 6 protons and confirms the formation of the protecting group. The peak at lower field that appeared at 4.4 ppm as a triplet (**b**) corresponds to the proton on the carbon adjacent to the two oxygen atoms increasing the electronegativity. The remaining protons in the structure were explained above since these did not change during this reaction. Again, the peak at 7.3 ppm corresponds to deuterated chloroform.

With the aldehyde group protected, the next step was the alpha chlorination of the dimethylacetal. The chlorinating agents used were manganese chloride ( $\text{MnCl}_2$ ) and manganese oxide ( $\text{MnO}_2$ ), in a mixture of acetonitrile and methanol. Trimethylsilyl chloride (TMSCl) was used as catalyst. The final product was 2-chloro-hexadecanal dimethyl acetal (**Figure 3.5**).

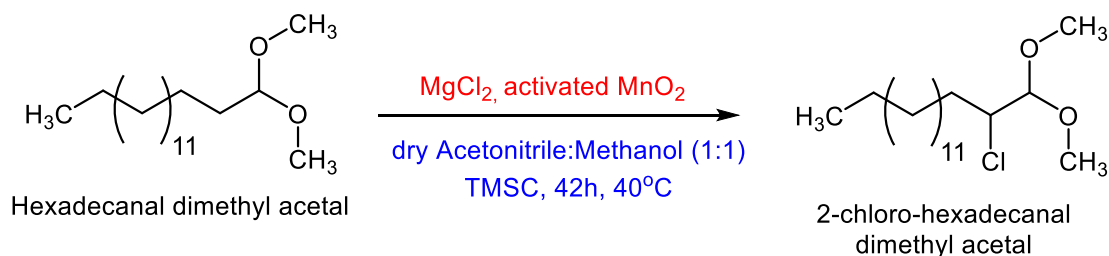


**Figure 3.5.** Chlorination reaction of hexadecanal dimethyl acetal to a 2-chloro-aldehyde dimethyl acetal, using manganese chloride ( $\text{MnCl}_2$ ) and manganese oxide ( $\text{MnO}_2$ ), in a mixture of acetonitrile and methanol, and trimethylsilyl chloride (TMSCl) as catalyst.

The reaction was monitored by thin-layer chromatography (TLC) and the retention factor (Rf) for the product was 0.28. It was not possible to determine the reaction yield as the required product was obtained in low amount and in a mixture with other components. A proton nuclear magnetic resonance ( $^1\text{H}$  NMR) spectrum was also obtained in order to confirm the structure of the different products **Figure 3.6**.

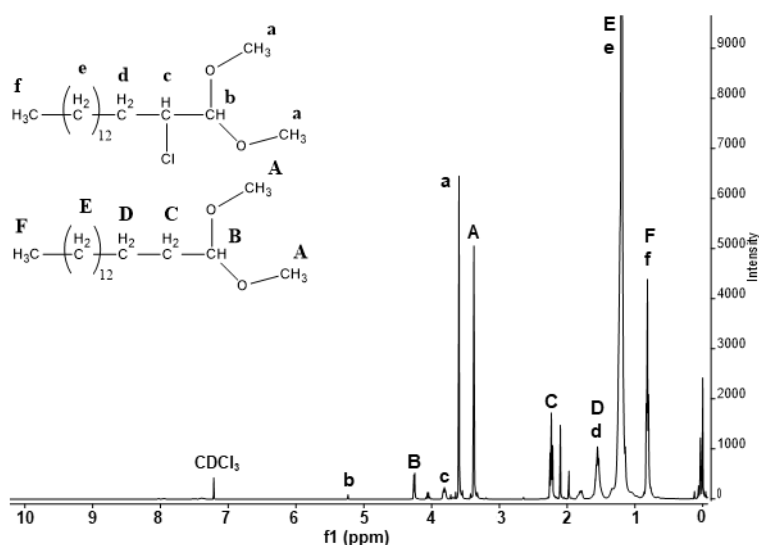


**Figure 3.6.**  $^1\text{H}$  NMR spectrum of 2-chlorohexadecanal dimethyl acetal, the product of the chlorinating of hexadecanal dimethyl acetal.  $^1\text{H}$  NMR: a- 3.61 ppm (6H, s,  $\text{OCH}_3$ ); b- 5.23 ppm (1H, d,  $(\text{OR}')\text{CH}(\text{OR}'')$ ); c- 3.82 ppm (1H, m,  $\text{CHCl}$ ); d- 1.55 ppm (2H, m,  $\text{CH}_2$ ); e- 1.20 ppm (24H, m,  $\text{CH}_2$ ); f- 0.82 ppm (3H, t,  $\text{CH}_3$ ); A- 3.38 ppm (6H, s,  $\text{OCH}_3$ ); B- 4.25 ppm (1H, t,  $(\text{OR}')\text{CH}(\text{OR}'')$ ); C- 2.25 ppm (2H, m,  $\text{CH}_2$ ). Internal reference (TMS) at 0.0 ppm.



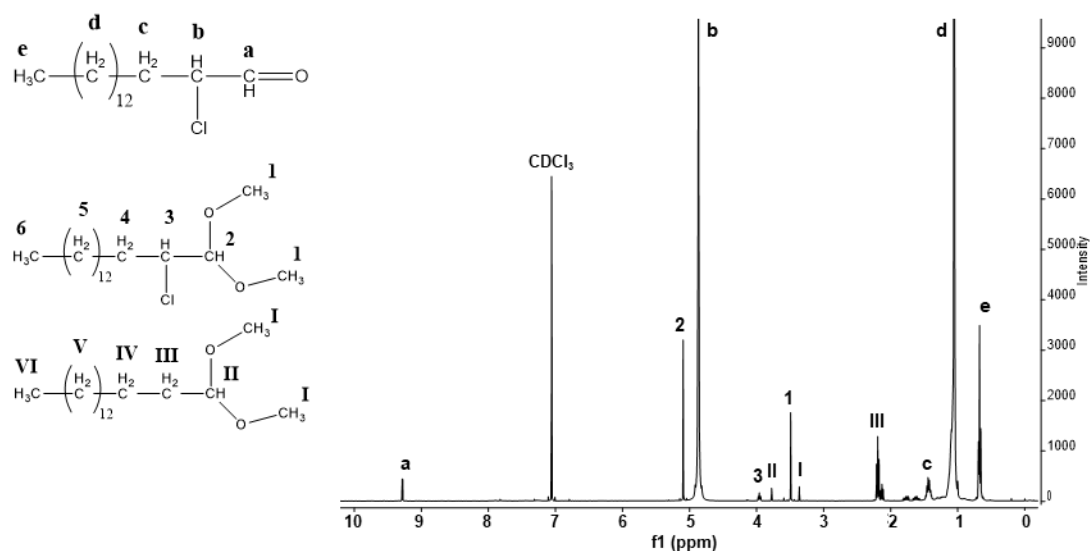
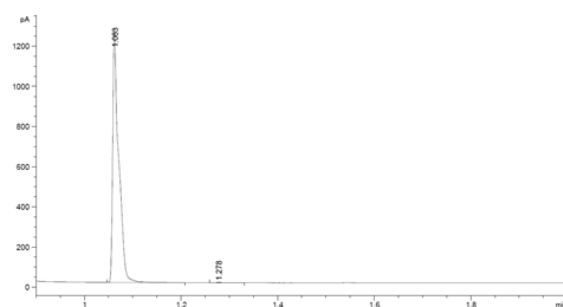


**Figure 3.8.**  $^1\text{H}$  NMR spectrum of 2-chlorohexadecanal, the product of TFA acid hydrolysis reaction.  $^1\text{H}$  NMR: a- 9.28 ppm (1H, d, C(=O)H); b- 4.89 ppm (1H, m, CHCl); c- 1.45 ppm (2H, m, CH<sub>2</sub>); d- 1.06 ppm (24H, m, CH<sub>2</sub>); e- 0.68 ppm (3H, t, CH<sub>3</sub>). 1- 3.49 ppm (6H, s, CH<sub>3</sub>); 2- 5.10 ppm (1H, d, OCH); 3- 3.96 ppm (1H, m, CHCl). I- 3.36 ppm (6H, s, CH<sub>3</sub>); II- 3.77 ppm (1H, t, OCH); III- 2.19 ppm (2H, m, CH<sub>2</sub>). Internal reference (TMS) at 0.0 ppm.

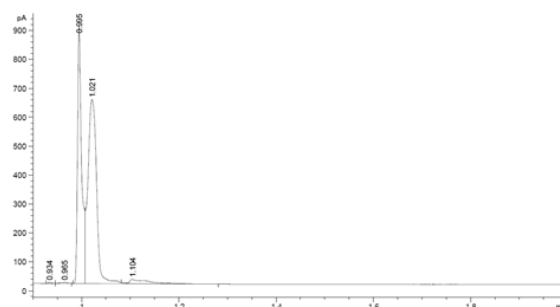
The acid hydrolysis deprotects the aldehydic groups and the appearance of a doublet at 9.3 ppm (**a**) confirm this. Similarly to the previous reaction, the identification of the peaks **a** and **b** was crucial for the product identification, the latter being identified at 4.8 ppm. Many other peaks appeared in the spectra and these were identified as starting material, 2-chlorohexadecanal dimethyl acetal and hexadecanal dimethyl acetal, the two products from the previous reaction and already described above. This confirms that the acid hydrolysis, similarly to the chlorination, was not complete.

GC-FID analysis of hexadecanol and hexadecanal separately allowed their retention time to be determined as 6.3 min and 5.9 min, respectively (**Figure 3.9A** and **Figure 3.9B**). GC-FID analysis of the acid hydrolysis product confirmed the presence of 7.4 % of hexadecanol, 1.8 % of hexadecanal, 60.7 % of 2-chlorohexadecanal, and 30 % of unknown impurities, possibly the dimethylacetal or chlorinated dimethylacetal from previous reactions(**Figure 3.9C**).

### A. Hexadecanol



### B. Hexadecanal



### C. Acid Hydrolysis Product

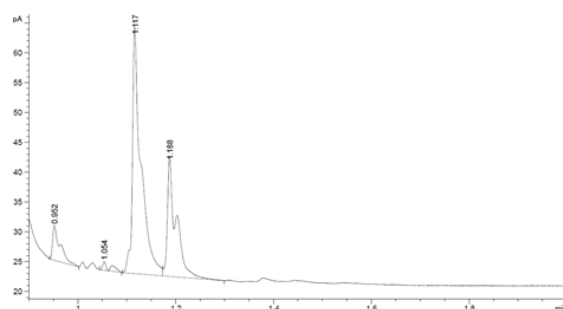


**Figure 3.9. GC-FID spectra of 2-chlorohexadecanal as a product of acid hydrolysis, the last step of a multi-step reaction.** GC data acquired with an isothermal analysis at 260 °C for 2 minutes. A – hexadecanol (1.06 min, 99.9%); B – hexadecanal (0.99 min, 37.9%; 1.02 min, 58.5%); C – product of the acid hydrolysis (0.95 min, 7.4%; 1.05 min, 1.8 %, 1.12 min, 60.7 %; 1.19 min, 30%).

### 3.3.2. Direct conversion of hexadecanol to hexadecanal and 2-chloro-hexadecanal

Although the  $\alpha$ -chloroaldehyde was obtained in reasonable overall yield using the approach above, the synthesis was time-consuming due to the number of steps required, and the product was impure and obtained in low overall yield. Other approaches were evaluated for the synthesis of the aldehyde by the direct conversion of the primary alcohol to the corresponding  $\alpha$ -chloroaldehyde [339-341]. The method developed by Jing et al [339] for the direct conversion of primary and secondary alcohols into the corresponding aldehydes using trichloroisocyanuric acid, serving both as stoichiometric oxidant and  $\alpha$ -halogenating reagent was used to produce  $\alpha$ -chlorohexadecanal from hexadecanol and two different attempts were made as described below.

#### 3.3.2.1. First Attempt at Direct Synthesis of 2-chloro-hexadecanal

The first attempt to the direct conversion of hexadecanol to 2-chlorohexadecanal used trichloroisocyanuric acid (TCCA) as the oxidizing and chlorinating agent and TEMPO as catalyst (**Figure 3.10**). Hexadecanol was dissolved in  $\text{CH}_2\text{Cl}_2$ , TCCA and TEMPO were added at room temperature, and the reaction was left stirring for one hour. The reaction was initially orange, and after 45 minutes became yellow and after one hour was white. By filtration, an off-white powder was removed to obtain a colorless solution.

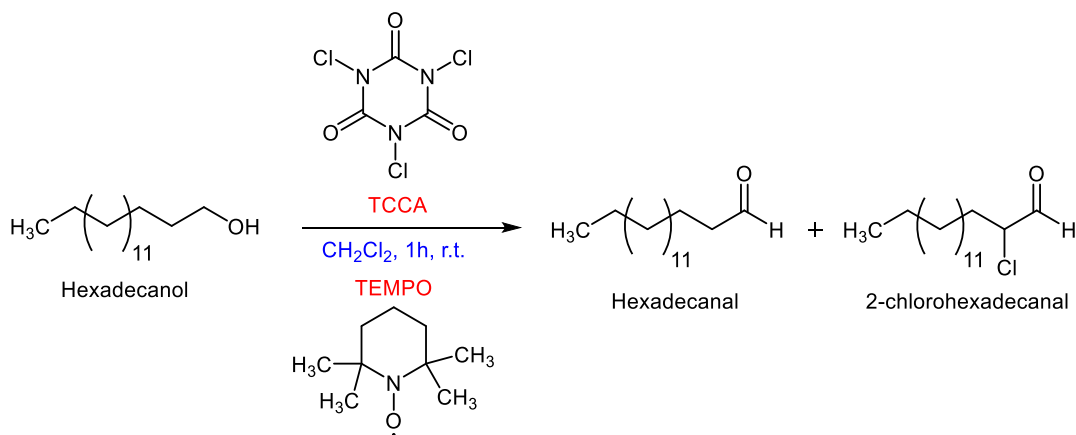


**Figure 3.10.** First attempt at the direct conversion of hexadecanol to  $\alpha$ -chlorohexadecanal and hexadecanal.

The reaction was monitored by thin-layer chromatography (TLC) and the retention factor (Rf) for the starting material was 0.32 and for the final product was 0.79. A proton nuclear magnetic resonance ( $^1\text{H}$  NMR) spectrum was also obtained in order to confirm the structure of the final product in (**Figure 3.11**).

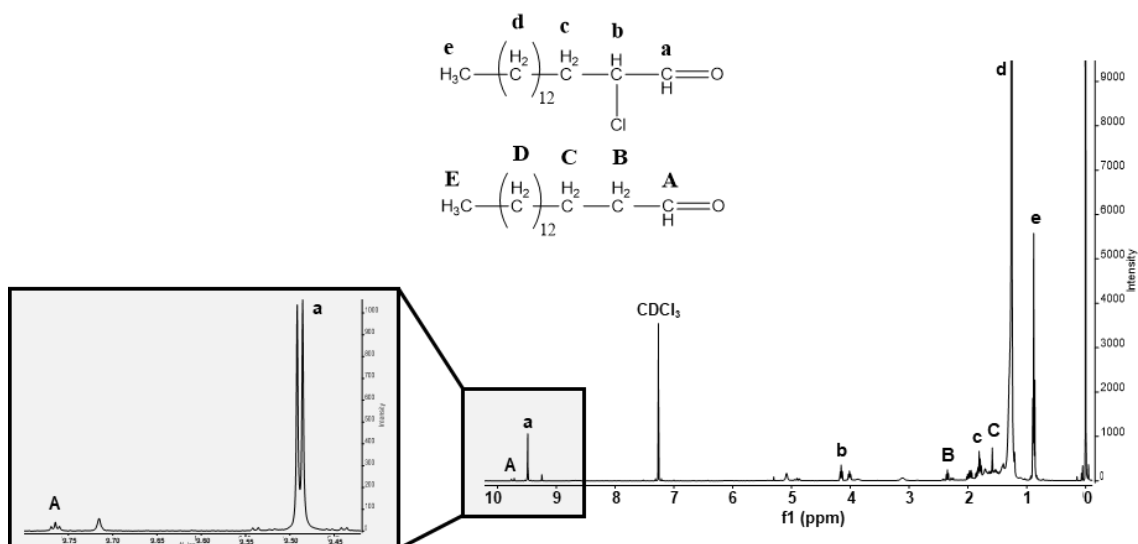
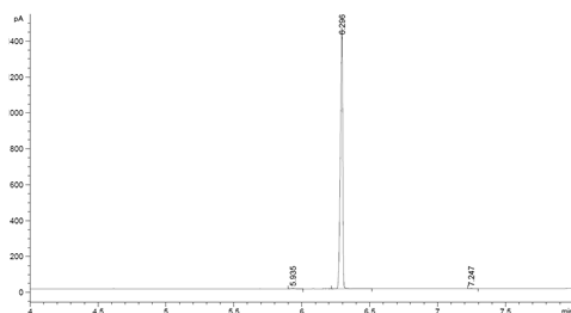


**Figure 3.11.  $^1\text{H}$  NMR spectrum of 2-chlorohexadecanal, the product of direct conversion from hexadecanol (1<sup>st</sup> approach).**  $^1\text{H}$  NMR: a- 9.5 ppm (1H, d, C(=O)H); b- 4.2 ppm (1H, m, CHCl); c- 1.8 ppm (2H, m, CH<sub>2</sub>); d- 1.3 ppm (24H, m, CH<sub>2</sub>); e- 0.9 ppm (3H, t, CH<sub>3</sub>). A- 9.7 ppm (1H, t, C(=O)H); B- 2.4 ppm (2H, m, CH<sub>2</sub>); C- 1.6 ppm (2H, m, CH<sub>2</sub>). Internal reference (TMS) at 0.0 ppm.

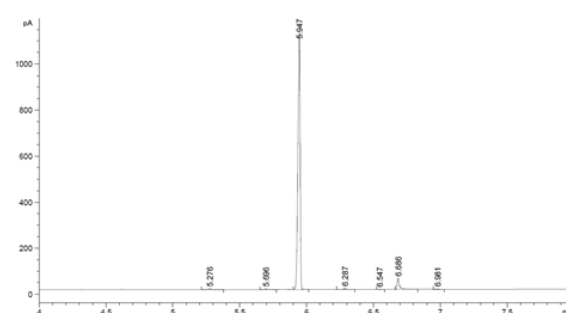
The direct conversion comprises of two simultaneous reactions, oxidation of the alcohol and chlorination of the alpha carbon. The oxidation alone produces hexadecanal, for which the protons were identified from **A** to **E** in **Figure 3.11**, and from the oxidation and chlorination results in 2-chlorohexadecanal, protons from which were identified form **a** to **e**. The main difference between both products and the starting material is the appearance of peak at around 9 ppm corresponding to the protons from the aldehydic group. The protons from the aldehyde appear as a triplet at 9.7 ppm, while the protons from the  $\alpha$ -chloroaldehyde appear as a doublet at 9.5 ppm. The protons in the  $\alpha$ -carbon of the 2-chlorohexadecanal (**b**) appear at higher field to the protons in the  $\alpha$ -carbon of the hexadecanal (**B**) due to electronegativity of the chlorine. GC-FID analysis (**Figure 3.12**) confirmed the presence of 9.5% of hexadecanol, 8 % of hexadecanal and 59.1 % of 2-chlorohexadecanal.



### A. Hexadecanol



### B. Hexadecanal



### C. Direct conversion product

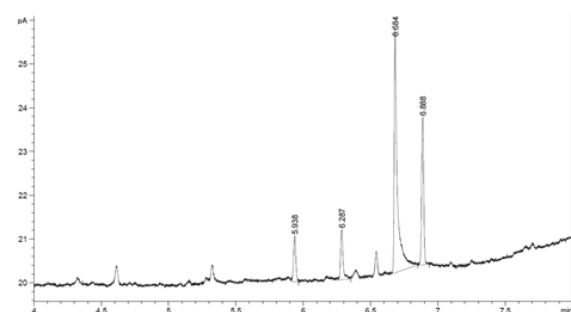


**Figure 3.12. GC-FID spectra of 2-chlorohexadecanal as a product of direct conversion from hexadecanol.** GC data acquired with a gradient starting from 150 °C to 300 °C at a rate of 25 °C/min, total run time of 14.5 minutes. A – hexadecanol (6.3 min, 99.7 %); B – hexadecanal (5.9 min, 93.9 %); C – product of the direct conversion (5.9 min, 8%; 6.3 min, 9.5 %; 6.7 min, 59.1 %; 6.9 min, 23.4 %).

### 3.3.2.2. Second Attempt at Direct Synthesis of 2-chloro-hexadecanal

The second approach to the direct conversion of hexadecanol to hexadecanal and 2-chlorohexadecanal still used trichloroisocyanuric acid (TCCA) as the oxidizing and chlorinating agent and TEMPO as catalyst (**Figure 3.13**). Hexadecanol and TEMPO were dissolved in  $\text{CH}_2\text{Cl}_2$  and cooled to  $0\text{ }^\circ\text{C}$  prior to addition of TCCA, and the mixture was stirred for 10 minutes at  $0\text{ }^\circ\text{C}$ . The reaction was then allowed to warm to room temperature and stirred for another 30 minutes. After filtration, a yellow oil was obtained.

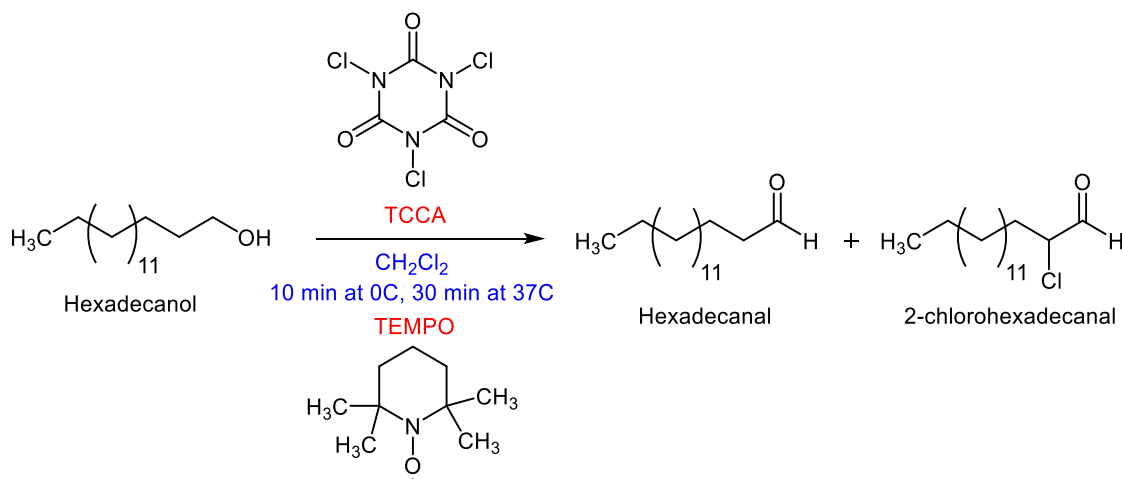


**Figure 3.13.** Second attempt at the direct conversion of hexadecanol to  $\alpha$ -chlorohexadecanal and hexadecanal.

The reaction was monitored by thin-layer chromatography (TLC) and the retention factor ( $R_f$ ) for the starting material was 0.25 and for the final product was 0.68. The reaction yield was 64%. A proton nuclear magnetic resonance ( $^1\text{H}$  NMR) spectrum was also obtained in order to confirm the structure of the final product in **Figure 3.14**.

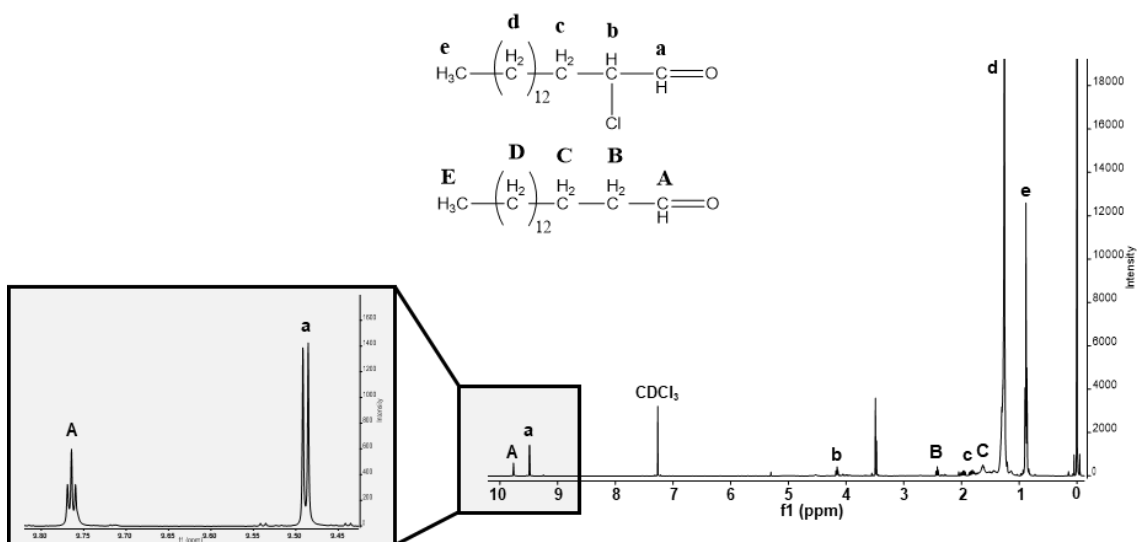


**Figure 3.14.  $^1\text{H}$  NMR spectrum of 2-chlorohexadecanal, the product of direct conversion from hexadecanol (2<sup>nd</sup> approach).**  $^1\text{H}$  NMR: a- 9.5 ppm (1H, d, C(=O)H); b- 4.2 ppm (1H, m, CHCl); c- 1.8 ppm (2H, m, CH<sub>2</sub>); d- 1.3 ppm (24H, m, CH<sub>2</sub>); e- 0.9 ppm (3H, t, CH<sub>3</sub>). A- 9.7 ppm (1H, t, C(=O)H); B- 2.4 ppm (2H, m, CH<sub>2</sub>); C- 1.6 ppm (2H, m, CH<sub>2</sub>). Internal reference (TMS) at 0.0 ppm.

The analysis of this spectra was the same described previously for Figure 3.11 since the expected final products were the same. Hexadecanal protons were identified from **A** to **E** and 2-chlorohexadecanal protons from **a** to **e**. The protons from the aldehyde appear as a triplet at 9.7 ppm while the protons from the  $\alpha$ -chloroaldehyde appear as a doublet at 9.5 ppm. The protons in the  $\alpha$ -carbon of the 2-chlorohexadecanal (**b**) appear upfield due to the combination of oxygen and chlorine electronegativity. The remaining protons upfield were not affected during this reaction and were less affected by the electronegativity thus appearing at lower frequency. GC-FID analysis (**Figure 3.15**) confirmed the presence of 1.7 % of hexadecanol, 5.7 % of hexadecanal and 60.9 % of 2-chlorohexadecanal.

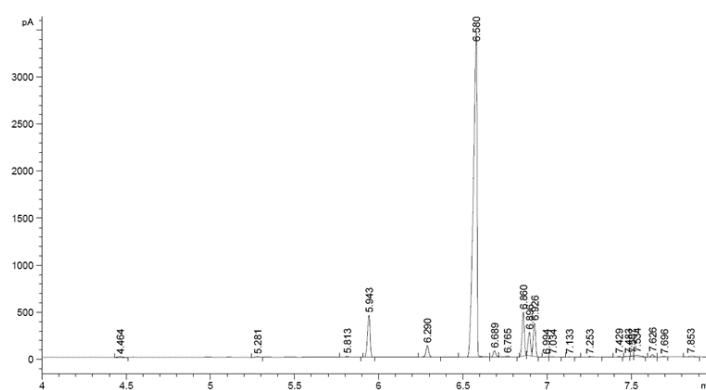


**Figure 3.15. GC-FID spectra of 2-chlorohexadecanal as a product of direct conversion from hexadecanol.** GC data acquired with a gradient starting from 150 °C to 300 °C at a rate of 25 °C/min, total run time of 14.5 minutes. Three peaks were identified: hexadecanal at 5.9 min, 5.7%; hexadecanol at 6.3 min, 1.7%, 2-chlorohexadecanal at 6.7 min, 60.9%. Other three peaks at around 6.9 min with a total of 12.3% were identified as unknown impurities.

### 3.3.3. Lipoxidation of lysozyme by 2-chloro-hexadecanal

Biomolecules exposed to reactive chlorine species and the chlorination of plasmemyl phospholipids results, among other reaction products, in  $\alpha$ -chloroaldehydes. These aldehydes are known to be involved in cellular process such as apoptosis [342]. Therefore, it is important to study the modification of proteins by  $\alpha$ -chloroaldehydes. A recent study demonstrated using LC-MS/MS the 2-chlorohexadecanal modification of glutathione, indicating that the field is slowly starting to move forward [199]. Consequently, the next step of the study was to react the synthesized  $\alpha$ -chloroaldehyde with two model proteins, lysozyme and human serum albumin, and characterize its modifications.

Lysozyme was incubated with 8 or 16 mM of 2-chlorohexadecanal for 2, 4 or 24 hours, after which the products were reduced and stabilised by the addition of sodium borohydride ( $\text{NaBH}_4$ ) at 5 mM final concentration. A bottom-up proteomic approach was carried out as described in chapter 3. The native and the aldehyde-treated lysozyme were separated by 15% SDS-PAGE (**Figure 3.16**), before the gel bands were cut for tryptic digestion and the peptides analysed by LC-MS/MS.

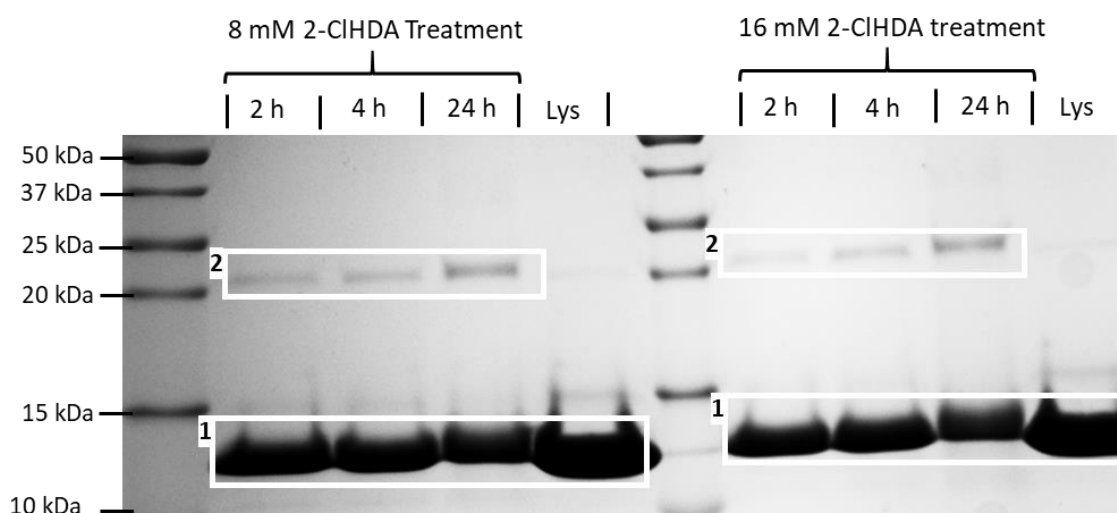


**Figure 3.16.** SDS-PAGE (denaturing gel electrophoresis) results for lysozyme untreated and treated with 8 mM or 16 mM 2-chloro-hexadecanal (2-ClHDA) for 2, 4 or 24 hours. Gel stained with Coomassie blue staining. The highlighted sections boxed in white were cut for further analysis.

This approach allowed the identification of 2 peptides from lysozyme modified by 2-chlorohexadecanal, based on the peptides' molecular weight, mass/charge ratio and charge of the peptide ion, ion score and LC retention time (**Table 3.1**). The mass of the adduct suggested that 2-chlorohexadecanal reacted by Schiff base formation with additional loss of HCl (**Appendix 1**). Both arginine (Arg, R) and lysine (Lys, K) residues were also found to be modified, with the modified residues being identified as Arg5 and Lys13.

**.Table 3.1. Modification of lysozyme by hexadecanal and 2-chloro-hexadecanal**

Treatment	Sequence coverage	Modified Residues	Lysozyme modified peptides (a <sup>b</sup> )	Theoretical mass of modified peptide	Observed mass of modified peptide	m/z (charge)	Ion score	Rt (min)
2 hours 8 mM	82 %	Arg5	V <sub>2</sub> FG <sup>R</sup> + <sup>222</sup> CELAAAMK <sub>13</sub>	1516.89	1517.15	506.7 (3+)	52	29.17
		Lys13	C* <sub>6</sub> ELAAAM* <sup>K</sup> + <sup>222</sup> R <sub>13</sub>	1286.75	1286.79	644.4 (2+)	38	50.64
4 hours 8 mM	82 %	Arg5	V <sub>2</sub> FG <sup>R</sup> + <sup>222</sup> CELAAAMK <sub>13</sub>	1516.89	1517.13	506.7 (3+)	58	30.82
		Lys13	C* <sub>6</sub> ELAAAM* <sup>K</sup> + <sup>222</sup> R <sub>13</sub>	1286.75	1286.79	644.4 (2+)	50	51.05
2 hours 16 mM	82 %	Arg5	V <sub>2</sub> FG <sup>R</sup> + <sup>222</sup> CELAAAMK <sub>13</sub>	1516.89	1517.16	506.7 (3+)	63	29.01
		Lys13	C* <sub>6</sub> ELAAAM* <sup>K</sup> + <sup>222</sup> R <sub>13</sub>	1286.75	1286.80	644.4 (2+)	65	50.94
4 hours 16 mM	82 %	Lys13	C* <sub>6</sub> ELAAAM* <sup>K</sup> + <sup>222</sup> R <sub>13</sub>	1286.75	1286.80	644.4 (2+)	64	51.14
24 hours 16 mM	82 %	Lys13	C* <sub>6</sub> ELAAAM* <sup>K</sup> + <sup>222</sup> R <sub>13</sub>	1285.75	1286.80	644.4 (2+)	52	50.86

a (subscript) – amino acid position in the mature protein for the start and end residues.

b (superscript) – mass difference corresponding to the modification on the affected residue (shown in red).

Initially MASCOT software was used to identify peptides modified by 2-chlorohexadecanal, and each potential modification was confirmed by manual analysis of MS/MS spectrum as in the example shown in **Figure 3.17** for the peptide CELAAAMKR modified on Lys13. Similarly to the work described in section 2.3.1, the MS/MS spectra were analysed in the search for diagnostic ions of these modifications. It was possible to identify the modified lysine immonium ion at  $m/z$  323 Da when this amino acid residue was found modified and the proposed structure is shown in **Figure 3.18**. This ion, being amino acid- and aldehyde-specific, is a good candidate for a diagnostic fragmentation ion for 2-ClHDA-lysine modifications and could be used for the development of targeted methods, such as MRM and precursor ion scanning.

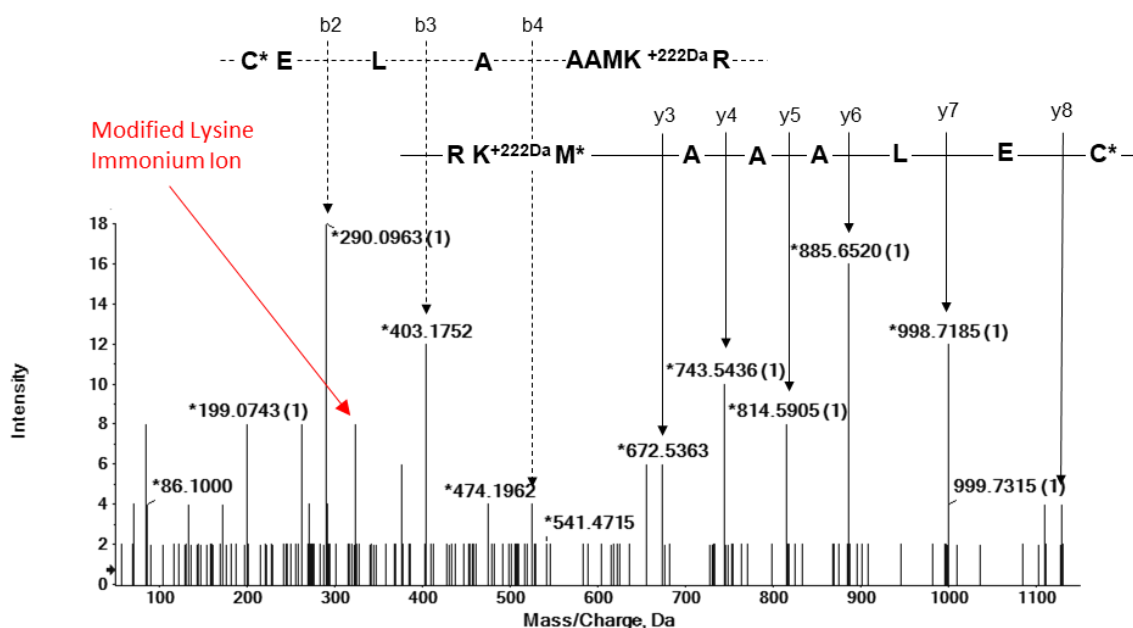


**Figure 3.17.** MS/MS spectra of lysozyme tryptic peptide. CELAAAMKR modified on a lysine residue by 2-chlorohexadecanal by Schiff base formation with loss of HCl followed by NaBH<sub>4</sub> reduction (+ 222 Da). The y and b ions indicated by the arrows confirm the peptide sequence and the modification on the cysteine residue. Immonium ions for hexadecanal-modified lysine found at  $m/z$  323 Da.

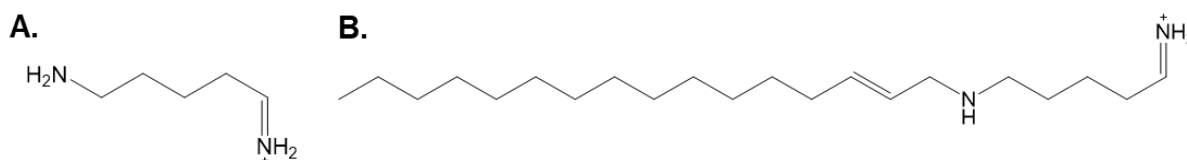


**Figure 3.18.** Proposed structure for the reporter ion observed at  $m/z$  323 Da. A) structure of the lysine residue immonium ion ( $m/z$  101.1 Da). B) structure of the 2-ClHDA-lysine reporter ion ( $m/z$  323 Da).

### 3.3.4. Lipoxidation of human serum albumin by 2-chloro-hexadecanal

Human serum albumin is the most abundant protein in human blood and therefore is subject to constant post translational modifications (PTMs), so the effect of 2-chlorohexadecanal on this protein was assessed. HSA was incubated with 8 or 16 mM of 2-ClHDA for 2, 4 or 24 hours before these samples were separated by 15% SDS-PAGE (**Figure 3.19**) and the bands highlighted were cut out, digested with trypsin and the tryptic peptides analysed by LC-MS/MS.

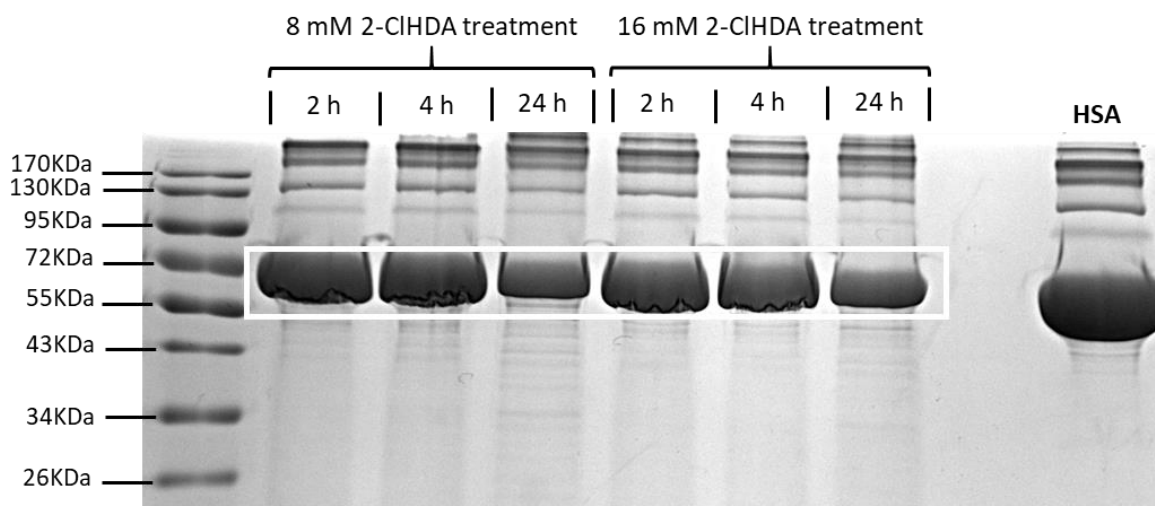


**Figure 3.19.** SDS-PAGE (denaturing gel electrophoresis) results for human serum albumin untreated and treated with 8 mM or 16 mM 2-chloro-hexadecanal for 2, 4 or 24 hours. Gel stained with Coomassie blue staining. The highlighted sections boxed in white were cut for further analysis.

This approach allowed the identification of 3 peptides from HSA modified by 2-chlorohexadecanal (**Table 3.2**). The mass of the adducts suggest that 2-chlorohexadecanal reacted by Schiff base formation with additional loss of HCl, the same as was observed for lysozyme in 3.3 (**Appendix 1**). Only lysine (Lys, K) residues were found to be modified: these were Lys257, Lys499 and Lys549. Initially MASCOT software was used to identify peptides modified by 2-chlorohexadecanal, and each potential modification was confirmed by manual analysis of MS/MS spectrum. Diagnostic fragmentation ions for 2-ClHDA-lysine modification were not detected.

**Table 3.2. Modification of human serum albumin by hexadecanal and 2-chloro-hexadecanal.**

Treatment	Sequence coverage	Modified Residues	HSA modified peptides (a <sup>b</sup> )	Theoretical mass of modified peptide	Observed mass of modified peptide	m/z (charge)	Ion score	Rt (min)
2 hours 8 mM	82 %	Lys257	<sup>250</sup> AEFAEVS <sup>K+222</sup> LVTDLTK <sub>264</sub>	1872.12	1872.03	625.1 (3+)	30	51.33
4 hours 8 mM	73 %	Lys499	<sup>497</sup> VTK <sup>+222</sup> CCTESLVNR <sub>508</sub>	1573.89	1574.20	525.7 (3+)	34	35.23
24 hours 8 mM	81 %	Lys549	<sup>549</sup> K <sup>+222</sup> QTALVELVK <sub>558</sub>	1349.93	1349.82	675.9 (2+)	53	43.25
4 hours 16 mM	81 %	Lys549	<sup>549</sup> K <sup>+222</sup> QTALVELVK <sub>558</sub>	1329.93	1349.82	675.9 (2+)	48	43.23

a (subscript) – amino acid position in the mature protein for the start and end residues.

b (superscript) – mass difference corresponding to the modification on the affected residue (shown in red).



### 3.4. Discussion

The work described in this chapter had two main aims, firstly to test different synthesis protocols for  $\alpha$ -chloroaldehydes, and find alternatives to the methods currently used, and secondly to characterize the adducts of the synthetic aldehyde with proteins by LC-MS/MS. Previous studies have assessed the biological effects of 2-chlorohexadecanal for which the synthesis of the aldehyde was required. The mostly used methods included the reaction of 1-O-hexadec-enyl-glycerol-3-phosphocholine with HOCl and HPLC purification [151]. This method is time consuming and expensive. Therefore, less time-consuming alternatives were tried.

In this study, two other approaches were tested. First, a multi-step reaction, which included hexadecanol oxidation to hexadecanal followed by acetal derivatisation, chlorination and finally deprotection to obtain 2-chlorohexadecanal. This chain of reactions took one week of work overall, therefore also being time consuming and not showing an improvement to the other method mentioned above. Additionally, these reactions require the use of harmful chemicals such as TFA and pTSA, both corrosive and irritant, TMOF and TMSC, both flammable, and PCC which is carcinogenic. This chain of reaction allowed us to obtain in the end 60.7 % of 2-chlorohexadecanal, with 7.4 % of hexadecanol and 1.8 % of hexadecanal still present as well as 30 % of unknown impurities. As a result of the poor yield, presence of impurities that were hard to remove and the use of PCC, two attempts were made to use an alternative method to directly convert hexadecanol into hexadecanal and 2-chlorohexadecanal, according to the method of Jing *et al.* [339]. This reaction used TCCA as an oxidizing and chlorinating agent and TEMPO as a catalyst. In the first attempt, all reaction components were dissolved in  $\text{CH}_2\text{Cl}_2$  and left stirring for one hour at room temperature. The  $^1\text{H}$  NMR analysis confirmed the presence of hexadecanal and 2-chlorohexadecanal and the GC-FID analysis confirmed the presence of 9.5% of hexadecanol, 8% of hexadecanal, 59.1% of 2-chlorohexadecanal, and 23.4% of unknown impurities. This reaction was already a good alternative, taking only one hour and decreasing the amount of unknown impurities in comparison with the multi-step reaction. However, a second attempt was made to try to improve the hexadecanal/2-chlorohexadecanal ratio and decrease the percentage of impurities. In the second attempt, hexadecanol and TEMPO were firstly dissolved in  $\text{CH}_2\text{Cl}_2$  and cooled to 0 °C, then TCCA was added and left stirring for 10 minutes, after which the reaction was warmed to 37 °C and left stirring for another 30 minutes. In this attempt, pentane was added to the reaction before filtration, which being a non-polar solvent promoted the precipitation of pentane insoluble compounds, removing some of the impurity as 2-ClHDA due to the long carbon chain is non-polar and therefore soluble. The resulting oil was characterized by  $^1\text{H}$  NMR

and although the product yield was not greatly increased, the amount of unidentified impurities was lower. According to the GC-FID data, the changes made for the second attempt decreased the amount of hexadecanol, hexadecanal and unknown impurities in the final product, while slightly increasing the amount of 2-chlorohexadecanal. Nevertheless, both attempts at the direct conversion of hexadecanol to 2-chlorohexadecanal represent a good alternative to current methods used, as they are less time consuming and use fewer harmful chemicals, improving time spent with the synthesis as well as health and safety of the experiments. This finding will help the research on this particular aldehyde move forward since its synthesis can be quicker and still with satisfactory quality. Another method that could have been tested to synthesize 2-chlorohexadecanal was the direct organocatalytic asymmetric  $\alpha$ -chlorination of aldehydes from Halland *et al.* which has also been reported to be a quick method that synthesizes  $\alpha$ -chloroaldehydes with good yield within one hour reaction [343].

The modification of two proteins by 2-chlorohexadecanal was evaluated as a model of lipoxidation adducts that may occur in inflammatory disease. The aim was to characterize these modifications using LC-MS/MS and identify potential diagnostic ions for adducts of 2-chlorohexadecanal with different amino acid residues. While the physiological concentration of 2-ClHDA ranges between 25 to 30  $\mu$ M [148, 330], higher concentrations were used to ensure adducts were formed. 2-ClHDA modifications were identified on 2 lysozyme and 3 human serum albumin peptides, all with a mass increase of 222.2 Da corresponding a Schiff's base formation between the carbonyl from the aldehyde and the amine from lysine, followed by reduction of imine by sodium borohydride (**Figure 3.20A**). This is a mild reducing agent therefore the unsaturation on the carbon chain was not reduced. Duerr *et al* previously reported the 2-ClHDA-thiol adduct to occur by nucleophilic attack to the  $\alpha$ -chlorinated carbon with the adduct formed retaining the carbonyl group [199] and corresponding to a mass shift of 240.25 Da in its reduced form (**Figure 3.20B**), however no modifications were detected on cysteine residues. Condensation of thioamides with  $\alpha$ -halocarbonyl compounds confirms that the thiol group reacts with the  $\alpha$ -halogenated carbon while the amine group reacts with the carbonyl group [344]. Similarly, 2-chloroaldehydes react differently with the thiol group in cysteines and the amine group in lysines. This justifies the different mechanism of adduction reported in this thesis and the mechanism reported by Duerr *et al* [199]. While the adduct resulting in a same mass shift of 22.2 Da can also be achieved by hexadecanal-lysine modification (**Figure 3.20C**), the samples were reduced and therefore there is a higher probability of this mass difference being a result of a reduced form of 2-ClHDA-lysine adduct rather than the unreduced form of the hexadecanal-lysine adduct.

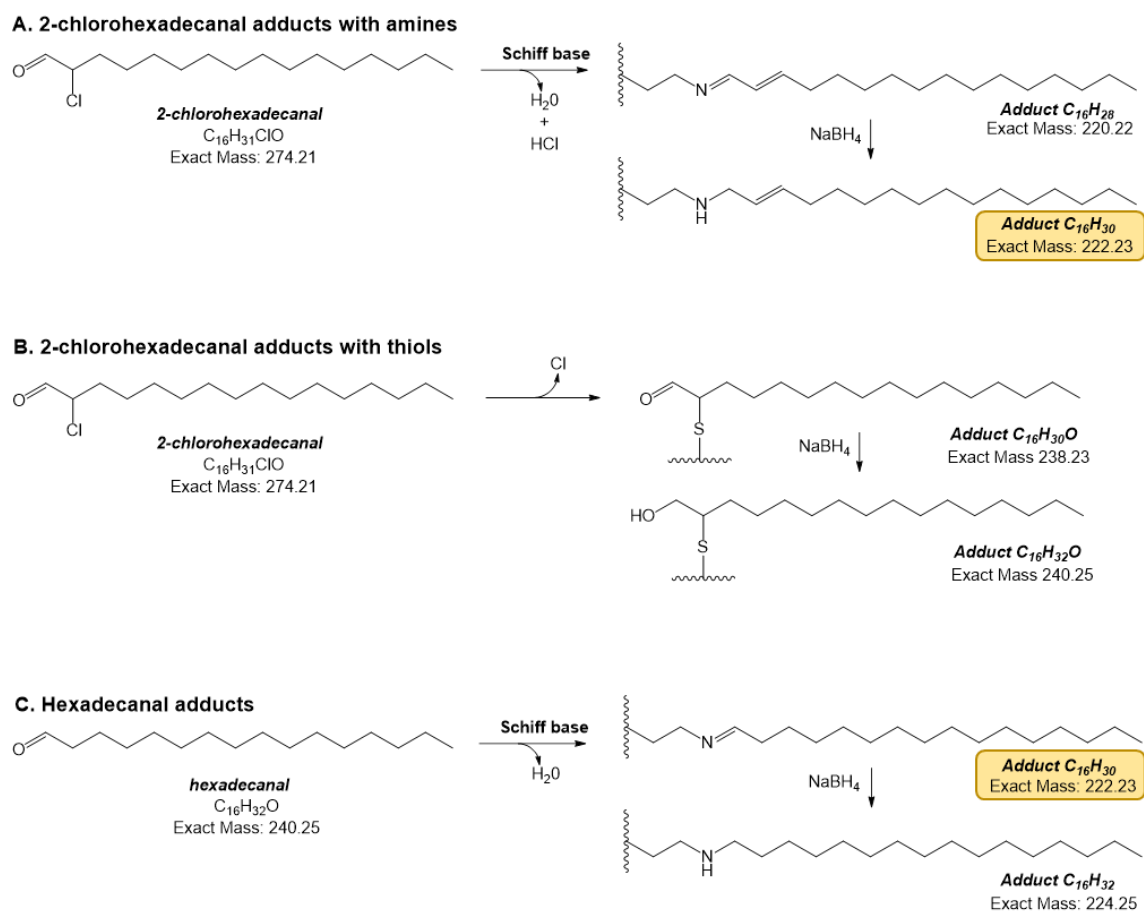


**Figure 3.20. Structure of unreduced and reduced hexadecanal and 2-chlorohexadecanal adducts.** (A) 2-Chlorohexadecanal adducts with amines by Schiff base formation followed by imine reduction but not the carbon chain unsaturation; (B) 2-Chlorohexadecanal adducts with thiol (cysteine residue) by nucleophilic attack of C-Cl followed by reduction of the remaining carbonyl; (C) Hexadecanal adduct with amine by Schiff base formation followed by imine reduction.

The bottom-up proteomic approach allowed the identification of 2 modified lysozyme residues: Arg5 and Lys13. For HSA only lysine residues were found to be modified: Lys257, Lys499 and Lys549. The proteins were not reduced prior to the 2-CIHDA treatment as explained in chapter 3, meaning that the cysteine residues were in disulphide bonds and therefore not available for modification. This might explain why no 2-CIHDA-cysteine adducts were detected, even though these have been previously reported by another group in work using glutathione [199]. A major aim of the study was to identify diagnostic ions for the 2-CIHDA adducts that could later be used in targeted mass spectrometry approaches, multiple reaction monitoring (MRM) or precursor ion scanning (PIS). MS/MS spectra contain immonium ions that are specific to amino acid residues present in the peptide and these ions are potential MS/MS reporter ions for modified amino acid residues. One diagnostic ion was detected for 2-CIHDA-lysine modification at  $m/z$  323. While protein-acrolein adducts

have been previously reported, it appears that there aren't any specific studies of reporter ions that could be used for this type of modifications. None of the HSA amino acid residue positions found modified have been previously reported modified by lipoxidation. Nevertheless, this approach allowed us to identify some protein modifications by 2-CIHDA and mostly important to provide reporter ions that could be relevant in disease diagnostic method development.

In summary, this study has provided a novel approach to 2-chlorohexadecanal synthesis able to obtain the product in an hour saving time and consumables in research. It also provided novel data on modification in two model proteins by 2-CIHDA and has identified a novel diagnostic ion for 2-CIHDA-lysine adduct that can be used in targeted mass spectrometry approaches to identify and quantify these adducts in biological or clinical complex samples.

## **Chapter 4. Chromatography methods for separation of proteins modified by short-chain aldehydes**

#### 4.1. Introduction

The analysis of the proteome of an organism is a difficult challenge due to the dynamic range of protein concentrations [345, 346]. Genetic information processing increases protein variation through mutations, polymorphisms and alternative splicing. Protein isoforms have high sequence similarity and arise either from the same gene family or from polymorphisms [347]. A single gene can code for multiple proteins due to alternative mRNA splicing, resulting in multiple protein forms with different peptide sequences [348]. However, protein isoforms can also be generated from separate genes such as actin and pyruvate kinase isoforms [349, 350]. Each protein isoform can be expressed in different tissues being therefore associated with different roles. However, for some isoforms their roles are still not completely understood and post translational modification (PTMs) can add extra differences to the complexity of the cellular proteome, which itself can change in response to different stimuli. Therefore, a comprehensive characterization of all of these isoforms is important to improve diagnosis and treatment of diseases such different types of cancer where protein biomarkers are important [351, 352].

A wide variety of methods can be used for protein study, yet mass spectrometry approaches are distinctively suited to handle the complexity of proteomics [248]. There are two strategies for protein analysis by MS: bottom-up and top-down approaches. The bottom-up proteomics approach involves proteins being chemically or enzymatically digested prior to peptide analysis by MS [353]. The identification of the peptides is performed by analysis of their fragmentation pattern, which identifies the protein and characterizes and localizes possible PTMs, usually by comparison to databases [353, 354]. However, different isoforms may produce peptides with the same sequence, making this approach a disadvantage for isoform investigation. Other disadvantages of the bottom-up approach are the limited dynamic range of MS analysis, which only allows peptides present at higher relative abundance to be analysed but misses information regarding low abundant proteins, as several peptides might not be specific to a single protein and regions of the protein sequence might not be covered so information on possible PTMs is unavailable. The top-down approach corresponds to intact protein analysis by MS in which intact protein ion masses are measured followed by fragmentation without prior digestion [355]. This approach facilitates a complete characterization of protein isoforms, as well as PTMs by the shift caused to the protein mass. Several applications have been reported for this proteomic approach, including the interpretation of the “histone code” by characterizing the combination of multiple modifications such as acetylation, methylation and phosphorylation [235, 356, 357] and the characterization of biotherapeutic molecules such as monoclonal antibodies [239, 358]. Even though top-down analysis has been shown to be a powerful tool, the throughput for proteome analysis still needs improvement. Recent advances in the

chromatographic methods, MS instrumentation, dissociation methods and data processing software have greatly improved intact protein analysis [359, 360]. The development of soft ionization techniques such as electrospray ionization (ESI) revolutionized protein and peptide analysis using MS [209], particularly by the ability to couple MS with liquid chromatography (LC).

The separation of peptides and proteins is a key step in both top-down and bottom-up MS approaches. Liquid chromatography is one of the most common methods for small molecule separation, which consists of differential partitioning of analytes between a liquid mobile phase and a stationary phase. Intact protein analysis using LC coupled to MS provides information on the accurate mass of the protein, relative abundance of its isoforms, PTMs localization and combination of any other modifications on the protein [361, 362]. Each of these applications requires upfront separation. Reverse-phase chromatography (RPLC) has been widely used for intact protein analysis due to its compatibility with ESI-MS. The aqueous solvent mixtures used in RPLC are compatible with ESI-MS and the additives such as formic acid or trifluoroacetic acid improve not only the chromatographic peak shape but also provides a source of protons. Nevertheless, other separation methods can separate proteins based on their structure, mass, charge or presence of modifications such as size exclusion chromatography (SEC) and ion exchange chromatography (IEX).

RPLC uses non-polar stationary phase and polar mobile phase and therefore hydrophilic analytes elute first. Several stationary phases can be used, with alkyl chains linked to porous silica particles being the most common, where shorter chains such as C4 are generally used since proteins show strong retention on long chains (e.g. C8, C18) [361]. However, derivatized nonporous silica (NPS) particles and superficially porous particles containing a nonporous silica core and a porous shell have also been reported to be suitable for protein work [233, 363, 364]. For this study, a polymeric reversed-phase material (resin based on a hydrophobic supermacroporous polymer) was used, which offered high-resolution separation of intact proteins with increased mechanical strength (stable at extreme pH and high temperature), high efficiency with low carry-over and high throughput. In RPLC the retention of proteins is also affected by the size of the particles, the pressure, the temperature and the composition of the mobile phase [365-367].

Ion exchange chromatography (IEX) is a non-denaturing separation technique which separation relies on the differences in the charge of the analytes. Changes in protein charge cause by modifications may affect the separation. Protein separation by IEX depends on the protein interaction with the charged stationary phase and a salt-gradient is usually applied for elution [232, 368]. Proteins are eluted in order of increasing binding charge, which closely correlates with their isoelectric point (pI). Employing a pH gradient instead of a salt-gradient can be a useful alternative to separate proteins with small changes in pI. In

this method, proteins' net charges are modified during the gradient and proteins elute at their pI. The proteins suitable to be separated using this technique would depend on the pH range of the gradient. The choice of the eluent to be used is also important, so usually a mixture of amine buffering species and weak acids are chosen to create the gradient [369, 370]. The advantage of a pH gradient is the low concentration of salt used, which allows on-line coupling to mass spectrometry [371]. This method has been mainly applied to separation and characterization of biopharmaceuticals like monoclonal antibodies [372]. In addition, it has also been used to separate protein isoforms. The use of both cation exchange chromatography (CEC) and anion exchange chromatography (AEC) have been reported for intact protein analysis when coupled to RPLC, which not only increases the fractionation but also desalts the samples prior to MS analysis. For example, the *Escherichia coli* proteome was studied by two-dimensional separation using CEC coupled to on-line RPLC [373] and AEC coupled to RPLC-MS [374]. A few years later, a similar method using AEC-RPLC was applied to top-down analysis of human leukocytes proteome in order to implement this technique in clinical studies [375]. IEC can also be applied to separation of HSA isoforms, which are known to be a biomarker of age [376]. The analysis of HSA isoforms started with a mixed-mode anion exchange-hydrophobic interaction chromatography, which is commonly used to assess the redox state of HSA [377]. However, this technique was not coupled to mass spectrometry, thus limiting the information provided by the method. Later, different HSA isoforms were separated by their pI using a pH gradient method and an anion exchange column, and fractions were collected for further analysis by RPLC-MS [378]. More recently, non-denaturing ion exchange chromatography methods coupled on-line to native mass spectrometry were developed for monoclonal antibodies [379], interferon- $\beta$  [380] and HSA isoforms characterization [381]. The use of MS-compatible salts allows the direct detection and characterization by MS, which could easily be applied for clinical diagnosis purposes.

The separation methods described above have been used to separate protein isoforms resulting from post-translational modifications such as deamidation, glycation and phosphorylation but as yet have not been applied for separation of lipoxidation products. Lipoxidation is more commonly analysed by bottom-up approaches that allow the modifications to be localized and characterized by mass spectrometry [217]. RPLC is usually used for separation of lipoxidized proteins since the oxidized lipid modification increases the hydrophobicity of the proteins. The same modifications can also change the protein net charge and therefore IEC could also be applied for lipoxidized protein separation.

The aim of the work reported in this chapter was to test different chromatographic methods for protein isoform and oxPTM separations and ion exchange chromatography by



pH gradient and reverse-phase chromatography were the methods used. Additionally, the same modified proteins were analysed by bottom-up approach to localize and characterize these modifications. Comparison between trypsin digestion protocols and data processing software for peptide analysis was also performed.

## **4.2. Material and Methods**

### **4.2.1. Materials**

Water (Optima LC-MS grade) and ammonium formate (LC-MS grade) were obtained from Fisher Scientific (Schwerte, Germany). Formic acid (LC-MS grade), ammonium acetate, acetic acid, human serum albumin and human serum plasma were purchased from Sigma-Aldrich (Sigma-Aldrich, Munich, Germany). 4-Hydroxy-2-trans-nonenal (HNE) and 4-Hydroxy-2-trans-hexenal (HHE) were purchased from Cayman Chemicals.

### **4.2.2. Treatment of proteins with aldehydes in vitro**

Ubiquitin, insulin and human serum albumin (100 $\mu$ M) were modified by two different aldehydes. 4-hydroxy-hexenal (HHE) and 4-hydroxy-nonenal (HNE) were added to the protein solution at a 1:10 (protein: aldehyde) molar ratio and allowed to react for 2 hours at room temperature. To stabilize adducts, NaBH<sub>4</sub> was added to a final concentration of 25 mM and left to react for 1 hour at room temperature.

### **4.2.3. Ion Exchange Chromatography (IEC)**

UHPLC separation was performed on Thermo Scientific Vanquish UHPLC System equipped with a binary pump, an autosampler and a column compartment. A binary solvent system was used, in which eluent A consisted of 10 mM ammonium acetate and 10 mM ammonium formate and eluent B of 10 mM acetic acid and 10 mM formic acid. Proteins (25  $\mu$ L; each sample in technical triplicate) were loaded onto an anion exchange column (ProPac SAX-10, 2 x 50 mm) at 0% B and eluted using a gradient: ramp from 0% to 60% B during 10 minutes followed by an isocratic gradient at 100% for 1 min. Together with an equilibration time of 9 min, the samples were injected every 20 min. The pH range of the gradient was 2.9-6.5. Proteins (25  $\mu$ L; each sample in technical triplicate) were loaded onto a cation exchange column (MabPac SCX-10 RS 5  $\mu$ m, 2.1 x 50 mm) at 0% B and eluted using a gradient: ramp from 0% to 75% B for 10 min followed by an isocratic gradient at 100% for 4 min. Together with an equilibration time of 11 min, the samples were injected every 25 min. The pH range of the gradient was 5.3-10.9. For both methods, the column temperature was set to 25 °C and the flow rate to 400  $\mu$ L/min.

### **4.2.4. Reverse Phase Chromatography**

UHPLC separation was performed on Thermo Scientific Vanquish UHPLC System equipped with a binary pump, an autosampler and a column compartment. A binary solvent system was used, in which eluent A consisted of 0.1% of formic acid in water and eluent B of 0.1% of formic acid in acetonitrile. Proteins (5  $\mu$ L; each sample in technical triplicate) were

loaded onto a reverse phase column (MabPac RP 4  $\mu\text{m}$ , 2.1 x 50 mm) at 0% B and eluted using a gradient: ramp from 0% to 40% B for 4 min, then isocratic gradient at 40% B for 2 min followed by 1 minute at 100% B. Together with an equilibration time of 3 min, the samples were injected every 10 min. Column temperature was set to 50 °C and the flow rate to 600  $\mu\text{L}/\text{min}$ . Peptides (5  $\mu\text{L}$  from 20  $\mu\text{M}$  solution; each sample in technical triplicate) were loaded onto a reverse phase column (Acclaim VANQUISH C18 2.2 $\mu$ , 2.1 x 250 mm) at 10% B and eluted using a gradient: ramp from 10% to 45% B for 13 min followed by an isocratic gradient at 90% B for 2 min. Together with an equilibration time of 5 min, the samples were injected every 20 min. Column temperature was set to 35 °C and the flow rate to 250  $\mu\text{L}/\text{min}$ .

#### **4.2.5. Mass Spectrometry for intact protein analysis**

A Q Exactive HF mass spectrometer (Thermo Fisher Scientific, Bremen, Germany) using a HESI source was operated in Full MS HMR mode for HSA and in Protein mode for the other two proteins. Every sample was measured in technical triplicates in positive ion mode. Ion source parameters were the following: Source Voltage: 3.6 kV; Ion transfer tube temperature: 320°C; Sheath Gas: 30 arbitrary units; Aux Gas: 15 arbitrary units; vaporizer temperature: 100°C. The Orbitrap mass analyser was operated in high mass resolution (HMR) mode at a resolution setting of 15,000 and in Protein mode at a resolution setting of 60,000 for  $m/z$  200 in full-scan mode (scan range: 2000–6000  $m/z$  automatic gain control target: 3e6; max. injection time: auto (needed to be changed in at least 500 ms, 10 microscans). The S-Lens RF level was set to 150%.

#### **4.2.6. Mass Spectrometry for peptide analysis**

A Q Exactive HF mass spectrometer (Thermo Fisher Scientific, Bremen, Germany) using a HESI source was operated in data-dependent acquisition (DDA) mode. Every sample was measured in technical triplicates in positive ion mode. Ion source parameters were the following: Source Voltage: 3.6 kV; Ion transfer tube temperature: 320°C; Sheath Gas: 30 arbitrary units; Aux Gas: 15 arbitrary units; vaporizer temperature: 100°C. The Orbitrap mass analyser was operated at a resolution setting of 120,000 for  $m/z$  200 in full-scan mode (scan range: 350–2000  $m/z$  automatic gain control target: 3e6; max. injection time: auto (needed to be changed in at least 500 ms, 10 microscans) and at a resolution setting of 30,000 for  $m/z$  200 in the Top10 DDA MS/MS mode (HCD, Stepped Normalized Collision Energy: 30  $\pm$  10 eV; Isolation Width: 1.0 Da; Activation Q: 0.2; Activation Time: 10 ms; automatic gain control target: 1e5; max. injection time: 100 ms; Intensity threshold: 5e4 counts) with dynamic exclusion for 10 s and in profile mode.

#### **4.2.7. In-gel digestion**

The reaction products from 4.2.2. were separated by 12.5 % SDS-polyacrylamide gel electrophoresis (section 2.2.5) followed by staining with Coomassie blue to visualize the bands prior to further processing. Bands present in the gel were then excised and tryptic digestion was performed according to Verrastro et al., 2016 [298]. The peptide extracts were dried for storage and resuspended in 0.1% formic acid in water prior to MS analysis.

#### **4.2.8. SMART Digestion**

Samples were diluted to 2 mg/mL (protein). Then 150  $\mu$ L SMART Trypsin Buffer was added to the SMART digest vials, followed by 50  $\mu$ L of sample (100  $\mu$ g). Samples were incubated at 70 °C with mixing at 1400 rpm. The tubes were incubated for different digestion times according to the protein size. Following trypsin digestion, samples were centrifuged for 2 minutes at 4600 g and the supernatants placed in a fresh tube. Reduction of disulphide bonds was carried out with DTT, final concentration 10 mM, for 30 minutes in the dark.

#### **4.2.9. Data processing**

The software BioPharma Finder 3.1 (Thermo Fisher Scientific) was used for peptide mapping analysis and to match them to the primary sequence of each protein (Uniprot entries: Insulin, P01315; Ubiquitin, P0CG48; HSA, P02768). Allowed variable modifications were methionine oxidation, Cys carbamidomethylation and HNE- or HHE-carbonylation on Cys, Lys, Arg and His to form Michael addition or on Lys and Arg to form base Schiff base adducts (respectively characterized by an isotopic delta mass equal to 114.14 Da, 93.13 Da and 78.11 Da for HHE, and 156 and 138 for HNE). Furthermore, the following key processing parameters were set such as mass tolerance  $\pm$  10 ppm, relative abundance threshold 10%, charge state range 2-10.

### 4.3. Results

#### 4.3.1. Protein separation by ion exchange chromatography

An anion exchange chromatography method was used to separate protein within a pH range of 2.9 to 6.5. It was important to know the isoelectric point (pI) of each protein being separated with this method, since it should fit within this pH range. The pI corresponds to the pH at which the net charge on the protein is zero, meaning that the protein is no longer interacting with the column and elutes. The proteins used were insulin (pI 5.35), ubiquitin (pI 6.79) and human serum albumin (pI 4.7) and their AEC base peak chromatograms are shown in **Figure 4.1**.

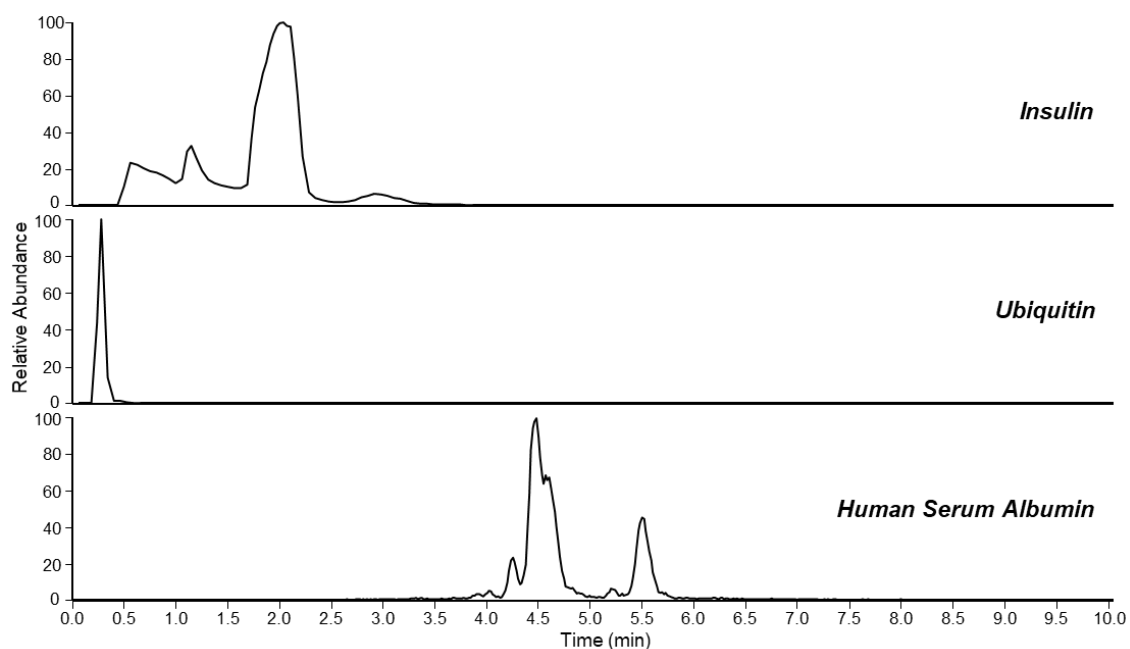


**Figure 4.1. Base peak chromatograms resulting from anion exchange chromatography separation of different protein isoforms.** Retention time 0.0 to 10.0 minutes. Protein used were insulin, ubiquitin and human serum albumin

This chromatographic method was able to separate different isoforms for insulin as well as for human serum albumin, since the base peak chromatograms above show multiple peaks corresponding to different protein isoforms. The same was not observed for ubiquitin, for which only one peak eluted. Insulin and ubiquitin both started eluting early reflecting higher PIs whereas HAS did not elute until later. These proteins were then treated with 4-hydroxy-hexenal (HHE) or 4-hydroxy-nonanal (HNE) and the same chromatographic method was used to separate the proteins upon treatment (**Figure 4.2**).

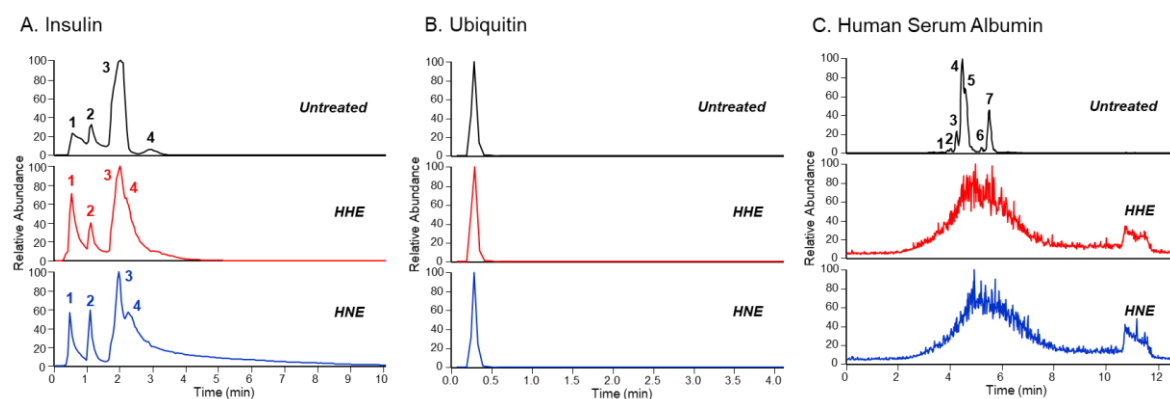


**Figure 4.2. Base peak chromatograms from anion exchange chromatography separation of untreated and HHE or HNE treated protein.** A-insulin; B-ubiquitin; C-human serum albumin. Retention times varying from 0.0 to 14.0 minutes. Untreated samples data in black, HHE treatment data in red and HNE treatment in blue. Each peak was assigned a number for later identification.

Treated and untreated forms of the same protein were not separated by the AEC method used, since no new peaks were detected upon treatment or a change in retention time detected. However, in **Figure 4.2A** it was possible to observe a tailing of the peaks for the treated samples. In fact, the isoform eluting between 2 and 4 minutes showed what seems to be two peaks with low resolution. This effect was not observed for ubiquitin (**Figure 4.2B**) which continue to correspond to only one peak even upon aldehyde treatment. In turn, human serum albumin showed a quite complex chromatogram upon treatment possibly due to the high amount of modifications and distinct peaks were no longer observed (**Figure 4.2C**). Nevertheless, the analysis of the MS data confirmed the presence of the HHE and HNE modifications on the proteins by the increase in the protein mass corresponding to the insertion of these aldehydes either by Michael addition or by Schiff base formation (**Figure 4.3**).

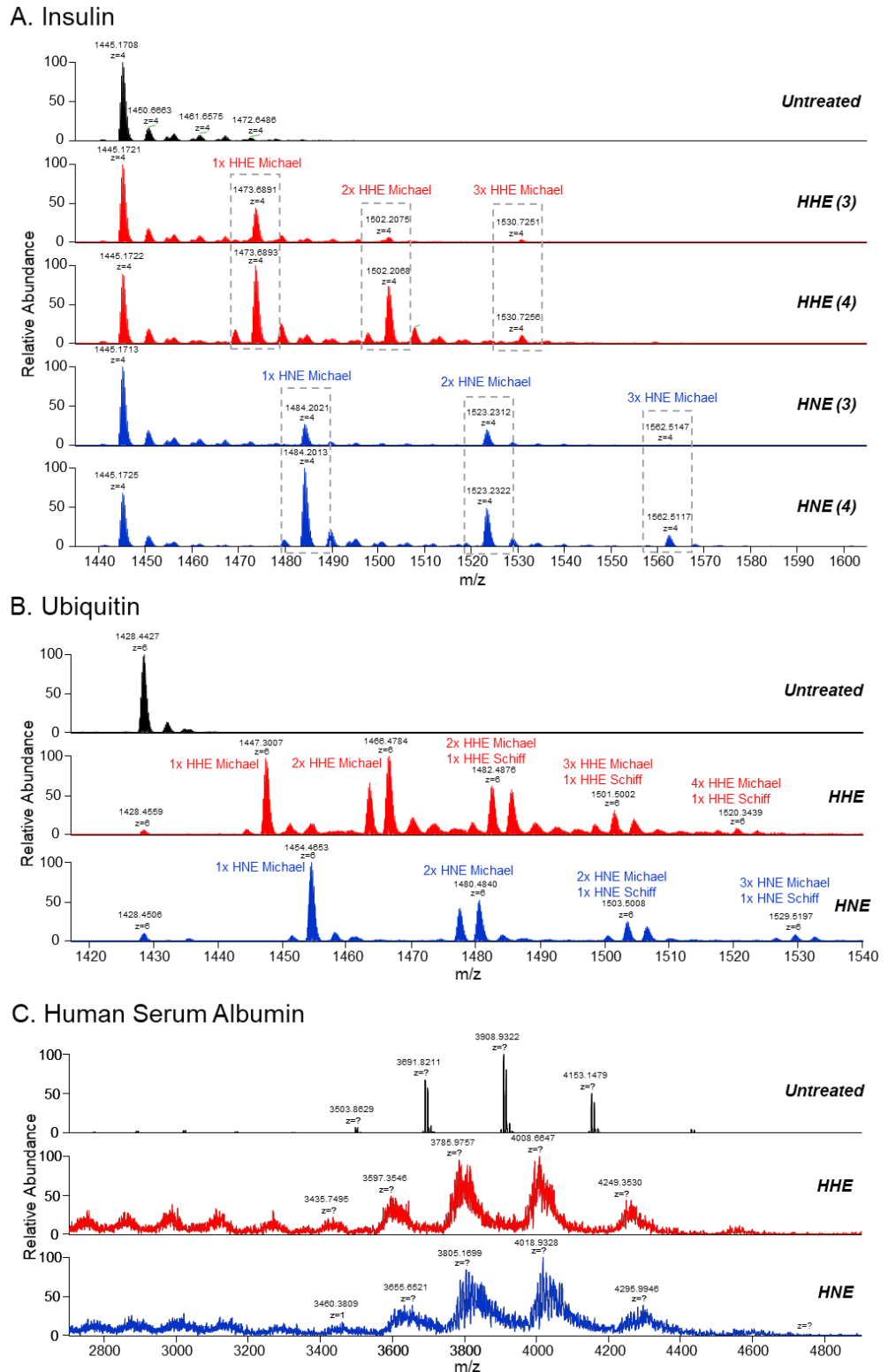


**Figure 4.3. MS spectra of untreated or HHE/HNE-treated intact protein separated by AEC.** The spectra correspond to the peaks in Figure 4.2 and these are labelled with the same number as the corresponding chromatographic peak. (A) Insulin ( $z=4+$ ), isoform in peaks 3 and 4 from Figure 2 are shown; (B) Ubiquitin ( $z=6+$ ), MS data from single peak in chromatogram.; (C) HSA, MS data from peak at highest relative abundance and for aldehyde-treated samples, the same retention time was selected. Untreated samples data in black, HHE treatment data in red and HNE treatment in blue.

The untreated insulin was identified at  $m/z$  1445.17 (charge 4+). The covalent adducts with the aldehydes were confirmed by the insertion of one ( $m/z$  1473.689), two ( $m/z$  1502.207) or three ( $m/z$  1530.725) HHE molecules or one ( $m/z$  1484.202), two ( $m/z$  1523.231) or three ( $m/z$  1562.514) HNE molecules (**Figure 4.3A**). Comparison between the two spectra for the same treatment showed an increase in the extension of modification by an increase in the relative abundance of the modified species in the second spectrum (higher retention time). This demonstrated that the method was able to separate slightly insulin with different extent of aldehyde modification. The untreated ubiquitin was identified at  $m/z$  1428.44 (charge 6+). Upon treatment, a total of up to 5 covalent adducts were confirmed for HHE and up to 4 were confirmed for HNE, including Michael addition and Schiff base formation, corresponding to a mass increase of 114.07 Da and 96.06 Da for HHE and 156.12 Da and 138.10 Da for HNE respectively. The highest covalent modification corresponded to the insertion of four HHE molecules by Michael addition and one by Schiff base resulting in the  $m/z$  1520.344, or the insertion of three HNE molecules by Michael addition and one by Schiff base resulting in the  $m/z$  1529.519. For HSA, due to the larger protein size, it was not possible to determine the charge envelop and therefore no specific modifications could be reported from this data.

In order to separate protein isoforms with higher pI, a cation exchange chromatographic (CEC) method was tested with a pH range of 5.3 to 10.9. The proteins tested were the same as for AEC and the base peak chromatograms for insulin (pI 5.35), ubiquitin (pI 6.79) and human serum albumin (pI 4.7) are shown in **Figure 4.4**.

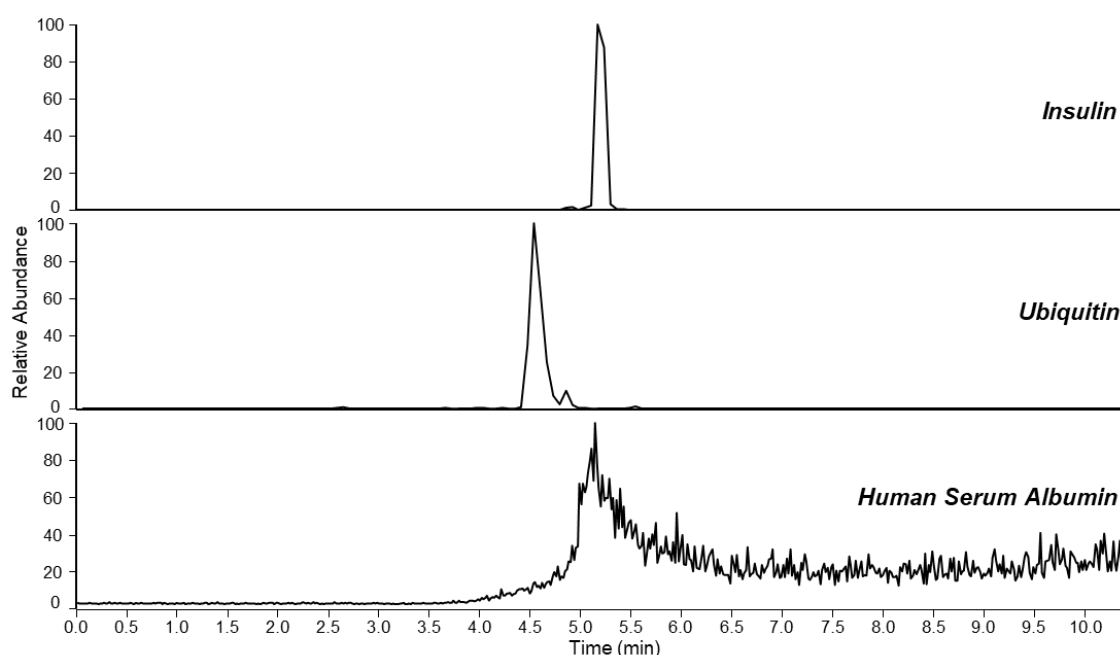


**Figure 4.4. Base peak chromatograms resulting from cation exchange chromatography separation of different protein isoforms.** Retention time was 0.0 to 10.0 minutes. Protein used were insulin, ubiquitin and human serum albumin.



CEC was not able to separate insulin isoforms, in contrast to what was previously observed for AEC; however, the retention of this protein in this chromatography was 5 minutes, which was longer than with AEC. On the other hand, CEC was found to be more suitable for ubiquitin separation than AEC; two peaks were observed confirming the separation of different isoforms with retention times of 4.5 and 4.9 minutes. Human serum albumin, with a lower pI than the other proteins tested, was not separated by CEC, since no clear peaks were observed in the chromatogram. Similarly to the experiment described above, these proteins were treated with 4-hydroxy-hexenal (HHE) or 4-hydroxy-nonenal (HNE) and the modified proteins were then separated by CEC (**Figure 4.5**).

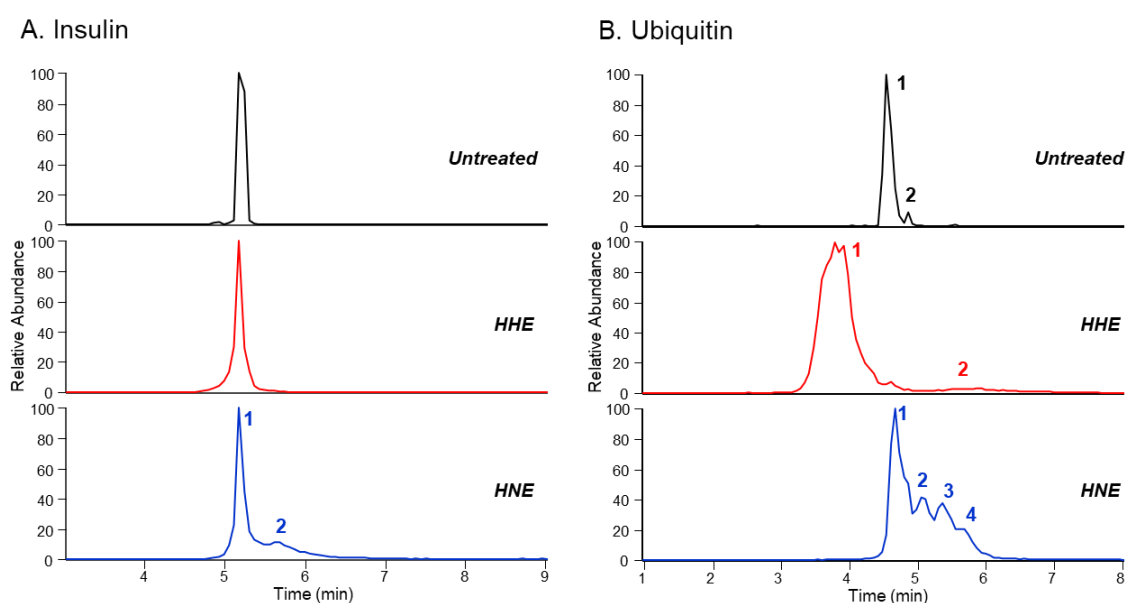
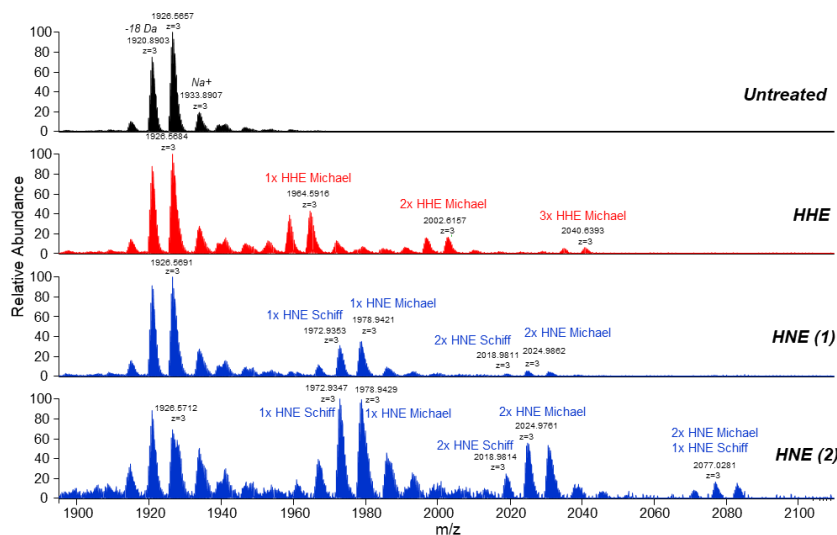


**Figure 4.5. Base peak chromatograms from cation exchange chromatography separation of untreated and HHE or HNE treated protein. A-insulin; B-ubiquitin.** Retention times varied from 1.0 to 9.0 minutes. Untreated samples data in black, HHE treatment data in red and HNE treatment in blue. Each peak was assigned a number for later identification.

The aldehyde treatment did not change the retention time of insulin; upon HHE treatment, it still only one peak was present in the chromatogram, while HNE treatment resulted in the detection of two peaks showing some separation. In case of ubiquitin, HHE treatment changed the retention time of the protein resulting in earlier elution. In contrast, HNE treatment of ubiquitin resulted in four peaks in the chromatogram with increasing retention time in comparison with the untreated ubiquitin. HSA results are not shown since the untreated samples did not present good separation with this method. **Figure 4.6** shows the MS spectra of each peak identified in the chromatograms above, which are identified by the numbering alongside the spectra.

### A. Insulin



### B. Ubiquitin

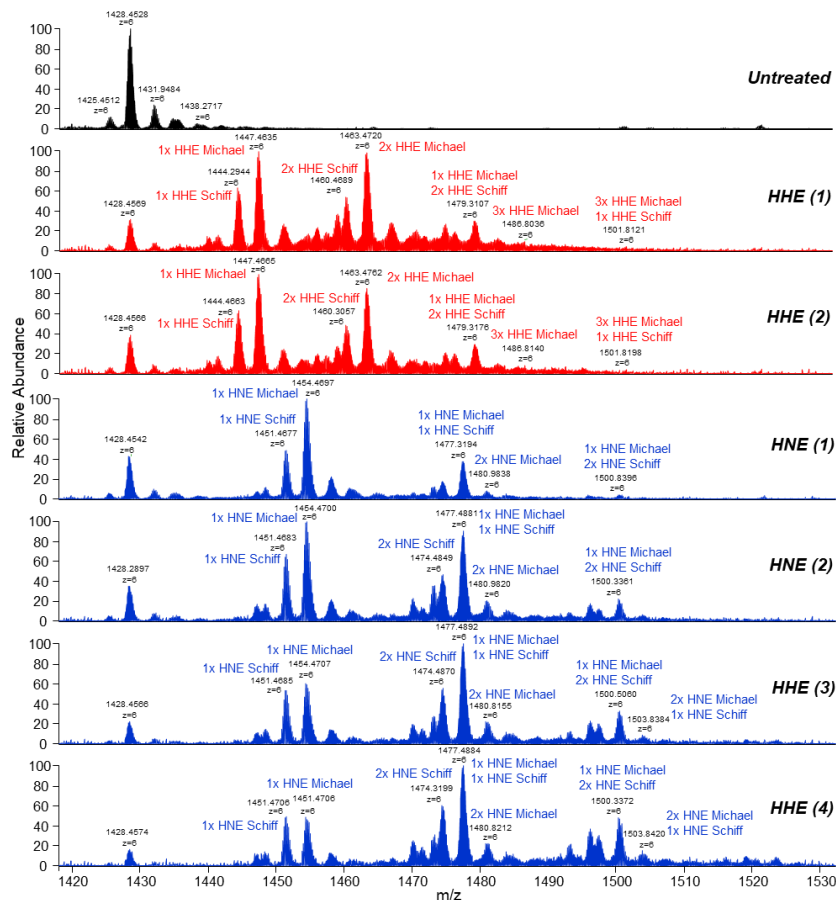


**Figure 4.6. MS spectra of untreated or HHE/HNE-treated intact protein separated by CEC.** The spectra correspond to the peaks in Figure 4.5 and these are labelled with the same number as the corresponding chromatographic peak. (A) Insulin ( $z=3+$ ), MS data for single chromatogram peak for untreated and HHE-treated and for the two peaks for HNE-treated; (B) Ubiquitin ( $z=6+$ ), MS data from the single peak 1 for untreated protein, peaks 1 and 2 for HHE-treated protein and peaks 1, 2, 3 and 5 for HNE-treated protein. Untreated samples data in black, HHE treatment data in red and HNE treatment in blue.

The untreated insulin was identified at  $m/z$  1926.5657 (charge state 3+). In **Figure 4.6A**, the MS data for HHE-modified insulin corresponds to the single peak in **Figure 4.5A** and the HHE covalent adducts were confirmed by the insertion of one ( $m/z$  1964.5916), two ( $m/z$  2002.6157) or three ( $m/z$  2040.6393) HHE molecules by Michael addition. Also in **Figure 4.5A** two peaks were observed after HNE-treatment and therefore in **Figure 4.6A** two spectra are shown corresponding to each chromatographic peak. The HNE covalent adducts were confirmed by the insertion of one ( $m/z$  1978.9421) or two ( $m/z$  2024.9862) HNE molecules by Michael addition and one ( $m/z$  1972.9353) or two ( $m/z$  2018.9811) HNE molecules by Schiff-base reaction. Additionally  $m/z$  2077.0281 was also observed with the highest retention time peak and was identified as the insertion of 3 HNE molecules, two by Michael addition and one by Schiff-base reaction. The MS data confirmed the separation by CEC of insulin with different extent of aldehyde modification. The peak with the highest retention time was shown to correspond to higher amount of insulin HNE-modification. In **Figure 4.6B**, the untreated ubiquitin was identified at  $m/z$  1428.4528 (charge 6+), and these MS data correspond to peak 1 in **Figure 4.5B**. Up to 4 HHE molecules and 3 HNE molecules were found to be covalently linked to ubiquitin, identified by the masses described above for **Figure 4.3B**. For HHE-treated ubiquitin, two peaks were observed in the chromatogram and comparison of the MS data of each peak did not show differences in the amount of protein modification. On the other hand, comparison of the spectra for each HNE-treated ubiquitin chromatographic peak showed a decrease in untreated protein relative abundance and an increase in the extent of HNE modification with the increase in retention time. This observation is in accordance to the results from insulin, showing the ability to separate proteins with different degrees of modification by cation exchange chromatography, as the aldehyde modification alters the protein's pI, resulting in later elution from the column. HSA data was not shown since no conclusions could be obtained from it.

#### 4.3.2. Intact protein separation by reverse phase chromatography

In order to assess which chromatography method would better suit the separation of lipoxidized proteins, a reverse phase (RP) chromatography method was used to separate untreated as well as HHE or HNE-treated insulin, ubiquitin and human serum albumin (the same samples used for ion exchange chromatography described in **4.3.1**). This separates proteins according to their hydrophobicity, starting as hydrophilic followed by a gradient increasing in hydrophobicity. Due to the solvents used, intact protein analysis by RP corresponds to the denatured forms of the proteins, in contrast to the native non-denaturing ion exchange chromatography. **Figure 4.7** shows the base peak chromatograms obtained for untreated and treated proteins by reverse phase chromatography.

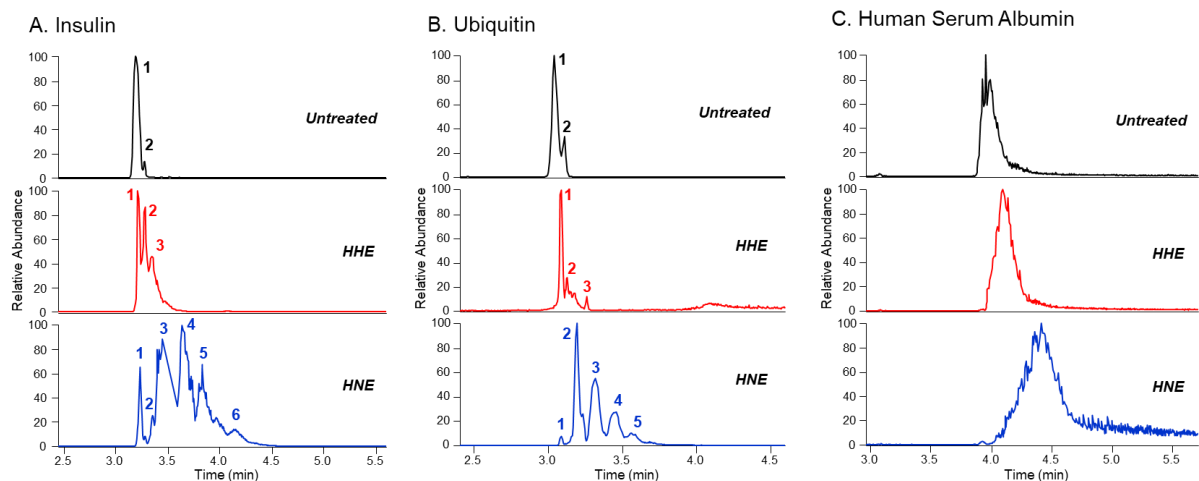
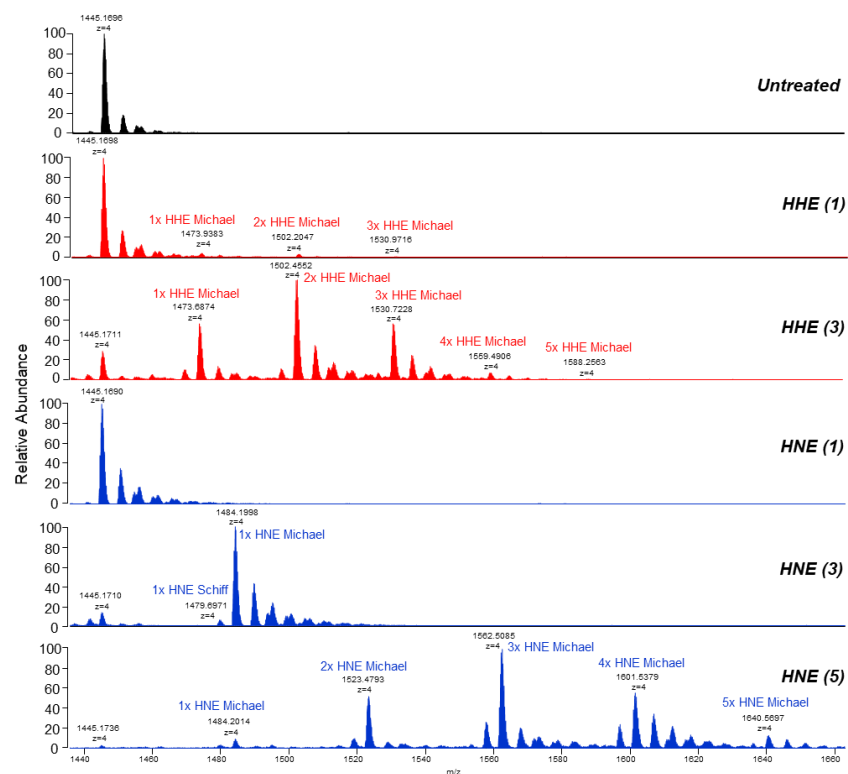


**Figure 4.7. Base peak chromatograms from reverse phase chromatography separation of untreated and HHE or HNE treated protein. A-insulin; B-ubiquitin; C-HSA.** Retention times varying from 2.5 to 5.5 minutes. Untreated samples data in black, HHE treatment data in red and HNE treatment in blue. More than one peak was observed in each chromatogram; therefore a number was assigned for later identification.

For all the proteins tested, it was observed that the aldehyde modification changed their retention time, reflecting increased hydrophobicity. For insulin, 3 peaks were detected after HHE treatment and 6 after HNE treatment. The same effect was observed for ubiquitin with three peaks and five peaks detected upon HHE and HNE respectively. For HSA, no distinct and resolved peaks were observed but it was still possible to observe the shift in retention time after aldehyde modification. The MS shown in **Figure 4.8** helped with the identification and characterization of the species in each of these peaks. HSA data are not shown for the same reason as stated previously.

### A. Insulin



### B. Ubiquitin

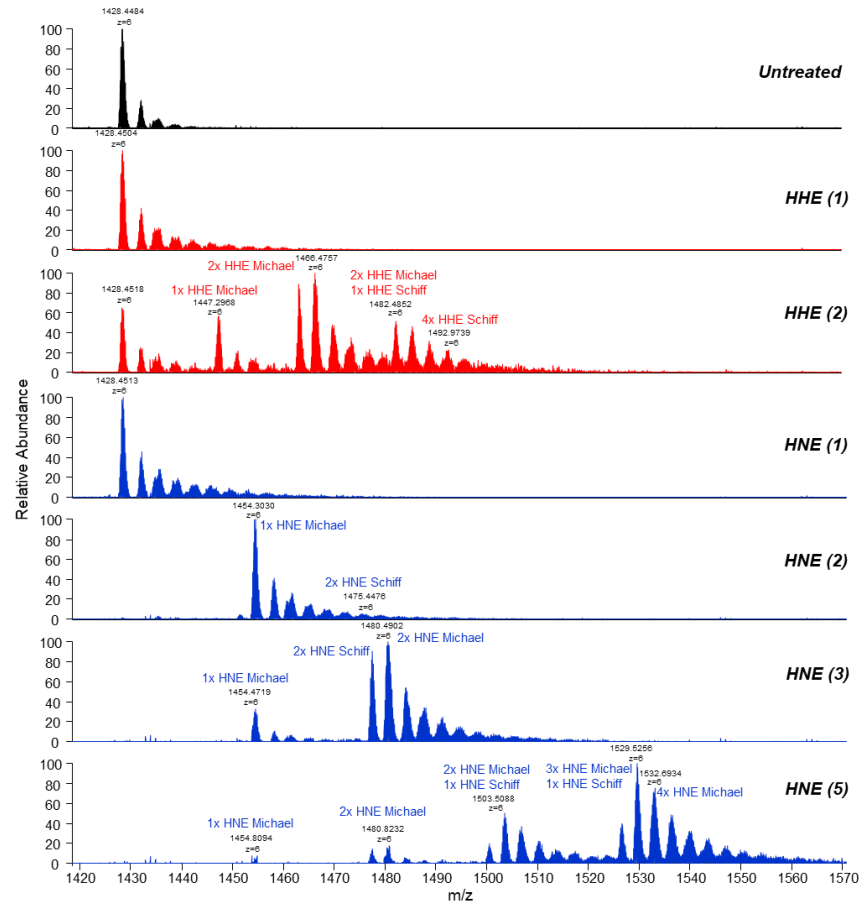


**Figure 4.8. MS spectra of untreated or HHE/HNE-treated intact protein separated by reverse phase chromatography.** The spectra correspond to the peaks in Figure 4.7 and these are labelled with the same number as the corresponding chromatographic peak. A-Insulin (z=4+), MS data shown for peak 1 for untreated, peaks 1 and 3 for HHE-treated and peaks 1, 3 and 5 for HNE-treated; B-Ubiquitin (z=6+), MS data shown for peak 1 for untreated, peaks 1 and 2 for HHE-treated and peaks 1, 2, 3 and 5 for HNE-treated. Untreated samples data in black, HHE treatment data in red and HNE treatment in blue.

Compared to the native peak at  $m/z$  1445.1696 (charge 4+) for insulin and at  $m/z$  1428.4484 (charge 6+) for ubiquitin, increased  $m/z$  for the modifications were observed. MS data analysis showed that the distinct peaks separated by RPLC demonstrated in **Figure 4.7** correspond to different degree of modification of the protein with the highly modified proteins eluting later. This observation was confirmed for both HHE and HNE. These results shown reverse phase chromatography to be able to separate unmodified from modified protein as well as separation of proteins by the extent of modification, thus being a better choice than the ion exchange chromatography methods described in **4.3.1.** for lipoxidized proteins separation.

### **4.3.3. Comparison between protein digestion methods**

A bottom-up approach was also used to localize and characterize the HHE and HNE modifications to insulin, ubiquitin and human serum albumin. The same samples were digested into peptides by two different protocols for comparison. The first method tested was the commonly used in-gel digestion method where an SDS polyacrylamide gel was run and the band of interest cut and digested with trypsin to obtain peptides. The second method used was the SMART Digest™ Trypsin Kit from Thermo, which has been reported to be a significant improvement over in-solution digestion methods requiring less than 60 minutes to achieve full digestion, whereas usually it would take up to 24 hours and the reduction in the number of chemicals used resulted in cleaner samples [382]. After MS data was acquired, the analysis was performed using Biopharma Finder. The protein sequence coverage obtained was dependent on the digestion method used (**Table 4.1**).

**Table 4.1. Sequence coverage of insulin, ubiquitin and human serum albumin.** Proteins were digested by in-gel or SMART trypsin digestion, and peptide MS analysis performed using Biopharma Finder.

Sequence Coverage (%)						
Proteins	Untreated		HHE-treated		HNE-treated	
	In-Gel	SMART	In-Gel	SMART	In-Gel	SMART
Insulin	-	7.4	-	6.5	-	6.5
Ubiquitin	72.4	51.3	94.7	60.5	94.7	40.8
HSA	79.3	59.7	90.6	78.1	92.5	70.8

The percentage of protein sequence coverage was shown to be dependent on the digestion method and on the aldehyde treatment. Using biopharma finder, the sequence coverage for proteins digested by in-gel trypsin digestion was slightly higher than by SMART digest for three proteins tested. Additionally, both aldehyde treatments decreased the percentage of sequence coverage when samples were digested by SMART digest but the same was not observed for in-gel digestion samples, for which the percentage of sequence coverage showed a 20% increase upon treatment. This bottom-up approach allowed for the localization and characterization of the HHE and HNE modifications on ubiquitin and human serum albumin and the results are reported in **Table 4.2** and **Table 4.3**, respectively. The peptides were identified based on their molecular weight, mass/charge ratio and charge of the peptide ion and LC retention time. Results for insulin are not shown in the tables below, because data was only acquired for SMART digestion.

**Table 4.2. Modification of ubiquitin by HHE or HNE.** Peptides obtained by in-gel (G) or SMART (S) trypsin digestion and MS data was analysed by Biopharma Finder.

Modified Residues	Ubiquitin modified peptides (a <sup>b</sup> )	Mass of modified peptide	m/z (charge)	Rt (min)	Digestion Protocol
<b>4-hydroxy-hexenal (HHE)</b>					
His68	E <sub>64</sub> STLH <sup>+114</sup> LVLRL <sub>72</sub>	1180.6825	394.568 (3+)	8.39	G S
His68	E <sub>64</sub> STLH <sup>+96</sup> LVLRL <sub>72</sub>	1162.6708	582.343 (2+)	9.98	G S
His68	E <sub>64</sub> STLH <sup>+78</sup> LVLRL <sub>72</sub>	1144.6608	573.338 (2+)	10.40	G
<b>4-hydroxy-nonenal (HNE)</b>					
His68	E <sub>64</sub> STLH <sup>+156</sup> LVLRL <sub>72</sub>	1222.7278	612.371 (2+)	10.48	G
His68	E <sub>64</sub> STLH <sup>+138</sup> LVLRL <sub>72</sub>	1204.7179	603.366 (2+)	11.88	G S

**Table 4.3. Modification of human serum albumin by HHE or HNE.** Peptides obtained by in-gel (G) or SMART (S) trypsin digestion and MS data was analysed by Biopharma Finder.

Modified Residues	HSA modified peptides (a <sup>b</sup> )	Mass of modified peptide	m/z (charge)	Rt (min)	Digestion Protocol
<b>4-hydroxy-hexenal (HHE)</b>					
His3	DAH <sup>+114</sup> KSEVAHR	1262.6368	421.887 (3+)	3.23	S
Lys4	DAH <sup>+114</sup> KSEVAHR	1262.6368	421.886 (3+)	3.12	S
His9	SEVAH <sup>+114</sup> R	811.4183	406.716 (2+)	3.25	S
Lys12	FK <sup>+114</sup> DLGEENFK	1339.6661	670.840 (2+)	6.80	S
Lys12	FK <sup>+96</sup> DLGEENFK	1321.6554	441.559 (3+)	6.80	S
His67	SLH <sup>+114</sup> TLFGDK	1130.5974	377.873 (3+)	8.37	G S
Cys75	LC <sup>+96</sup> TVATLR	971.5478	486.781 (2+)	7.88	G S
Cys101	NEC <sup>+114</sup> FLQHK	1131.5392	566.777 (2+)	6.35	G S
Cys101	NEC <sup>+114</sup> FLQHKDDNPNLPR	2052.9702	685.665 (3+)	6.58	G S
Cys124	LVRPEVDVMC <sup>+96</sup> TAFHDNEETFLKK	2816.3889	568.087 (5+)	9.45	S
His128	LVRPEVDVMCTAFH <sup>+114</sup> DNEETFLKK	2834.3984	710.108 (4+)	9.45	S
His146	RH <sup>+114</sup> PYFYAPELFFAK	2012.0592	672.028 (3+)	11.70	S



Cys177	AAC <sup>+96</sup> LLPK	810.4671	406.241 (2+)	7.79	G
Arg186	LDEL <sup>R+114</sup> DEGK	1187.6028	396.875 (3+)	4.89	G
Lys190	LDEL <sup>R</sup> DEG <sup>K+114</sup> ASSAK	1631.8389	544.954 (3+)	4.05	S
Cys200	<sup>C+96</sup> ASLQK	744.3839	373.199 (2+)	5.86	S
Lys212	AF <sup>K+96</sup> AWAVAR	1114.6284	372.550 (3+)	7.50	S
Arg218	AWAVAR <sup>R+114</sup> LSQR	1270.7145	636.365 (2+)	7.38	S
Cys265	YI <sup>C+114</sup> ENQDSISSK	1499.6815	750.848 (2+)	6.24	G S
Cys265	YI <sup>C+96</sup> ENQDSISSK	1481.6710	741.843 (2+)	6.24	G S
Cys289	SH <sup>C+114</sup> IAEVENDEMPADLPSLAADFVESK	3030.3918	1011.472 (3+)	11.54	G S
Arg338	R <sup>H+114</sup> PDYSVLLLLR	1580.9049	791.460 (3+)	9.49	S
Lys378	VFDEF <sup>K+114</sup> PLVEEPQNLIK	2158.1587	720.728 (3+)	10.46	S
Cys392	QN <sup>C+114</sup> ELFEQLGEYK	1713.7913	857.903 (2+)	10.14	S
Cys392	QN <sup>C+96</sup> ELFEQLGEYK	1695.7797	848.897 (2+)	10.14	S
Arg410	FQNALL <sup>V<sup>R+114</sup></sup> YTK	1465.8291	489.617 (3+)	8.33	S
Arg410	FQNALL <sup>V<sup>R+96</sup></sup> YTK	1447.8217	483.614 (3+)	8.83	S
Lys414	<sup>K+114</sup> VPQVSTPTLVEVSR	1752.9985	878.008 (2+)	7.62	S
Lys432	NLG <sup>K+114</sup> VGSK	915.5395	458.777 (2+)	3.26	S
Lys432	NLG <sup>K+96</sup> VGSK	897.5287	449.772 (2+)	3.27	S
Arg485	<sup>R+96</sup> PCFSALEVDETYVPK	1948.9631	650.996 (3+)	9.07	G S
Cys487	RPC <sup>+114</sup> FSALEVDETYVPK	1966.9724	656.999 (3+)	9.07	S
Lys525	<sup>K+114</sup> QTALVELVK	1241.7596	621.887 (2+)	7.71	S
Lys525	<sup>K+96</sup> QTALVELVK	1223.7491	408.924 (3+)	7.76	S
Cys567	ADDKET <sup>C+114</sup> FAEEGKK	1683.7666	562.263 (3+)	4.82	G
<b>4-hydroxy-nonenal (HNE)</b>					
His9	SEVA <sup>H+156</sup> R	853.4664	427.740 (2+)	5.01	G S
His67	SL <sup>H+156</sup> TLFGDK	1172.6442	587.329 (2+)	10.70	S
His128	LVRPEVDVMCTAF <sup>H+156</sup> DNEETFLK	2748.355	917.460 (3+)	11.62	S
Arg186	LDEL <sup>R+156</sup> DEGK	1229.6497	410.890 (3+)	7.98	G S
Cys265	YI <sup>C+156</sup> ENQDSISSK	1541.7289	771.872 (2+)	9.05	G S

Lys276	LK <sup>+156</sup> ECC <sup>+57</sup> EKPLLEK	1644.8835	549.302 (3+)	7.74	G
Cys289	SHC <sup>+156</sup> IAEVENDEMPADLPSLAADFVESK	3072.4399	1025.488 (3+)	12.45	S
His338	RH <sup>+156</sup> PDYSVVLLLR	1622.9518	812.483 (2+)	10.70	S
His338	H <sup>+156</sup> PDYSVVLLLR	1466.8524	489.958 (3+)	12.14	S
Cys392	QNC <sup>+156</sup> ELFEQLGEYK	1755.8402	879.429 (2+)	11.95	S
Arg410	FQNALLVR <sup>+156</sup> YTK	1507.8785	754.947 (2+)	10.36	S
Arg410	FQNALLVR <sup>+138</sup> YTK	1489.8680	745.941 (2+)	10.59	G S
Lys414	K <sup>+156</sup> VPQVSTPTLVEVSR	1795.0471	599.356 (3+)	8.97	S
Lys432	NLGK <sup>+138</sup> VGSK	939.5760	470.795 (2+)	6.99	S
Lys432	NLGK <sup>+156</sup> VGSK	957.5867	479.801 (2+)	6.99	S
His440	H <sup>+156</sup> PEAK	736.4120	369.213 (2+)	4.84	S
Arg485	R <sup>+138</sup> PCFSALEVDETYVPK	1991.0093	664.677 (3+)	10.73	S
Arg485	R <sup>+156</sup> PCFSALEVDETYVPK	2009.0183	671.015 (3+)	10.72	S
Cys487	RPC <sup>+156</sup> FSALEVDETYVPK	2009.0215	671.015 (3+)	10.58	S
Lys525	K <sup>+156</sup> QTALVELVK	1283.8062	428.943 (3+)	9.42	S
Lys525	K <sup>+138</sup> QTALVELVK	1265.7961	422.939 (3+)	9.52	S
Cys567	ADDKETC <sup>+156</sup> FAEEGKK	1725.8132	576.278 (3+)	7.20	G

With this bottom-up proteomic approach only one histidine residue (His68) could be identified on insulin modified by both HHE and HNE, either by Michael addition or by Schiff-base formation, and independently from the digestion protocol used. For HSA, the analysis was more complex due to the protein size. A total of 27 amino acid residues were found to be modified by HHE, while 17 amino acid residues were found to be modified by HNE. Most of these residues were cysteine (Cys) and lysine (Lys) but histidine (His) and arginine (Arg) modifications were also detected. Some residues, for example Lys12, Cys75, Cys101, Cys124, Lys190, Cys200, Lys212, Arg218 and Lys378, were found to be exclusively modified by HHE, while the residues Lys276 and His440 were exclusively modified by HNE.

In contrast to the sequence coverage observations, comparison of the two digestion approaches in terms of modified peptides detection showed that SMART digest, even though it had lower sequence coverage, allowed the detection of more modified peptides, either by HHE or HNE (**Figure 4.9**). Around 60-70% of peptides found to be modified were produced from SMART digest while under 10% were produced by in-gel digestion. Only 20-30% of the peptides listed in **Table 4.3** were generated by both digestion approaches.

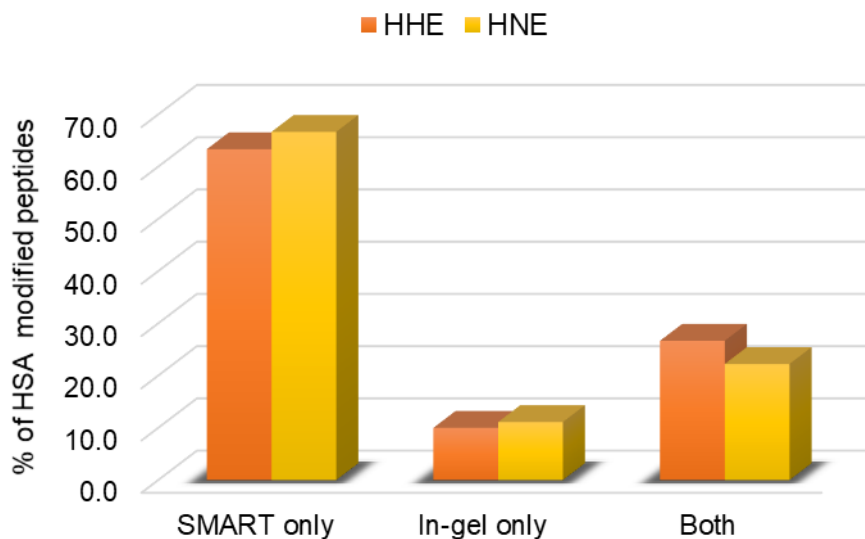


**Figure 4.9. Percentage of HSA modified peptides detected after SMART and In-gel digestion.**

#### 4.4. Discussion

Selection of the appropriate chromatography for LC-MS analysis of lipoxidized proteins is a key step in proteomics specially in intact protein analysis. The diversity of proteins in shape, size or charge result in different interaction with column affecting its elution. Protein lipoxidation increases its complexity, hydrophobicity and charge resulting in a different interaction with chromatographic columns. The aim of the study reported in this chapter was to compare different chromatography methods for the separation of untreated protein isoforms as well as aldehyde-modified proteins. Three methods were tested: anion exchange, cation exchange and reverse phase chromatography. The proteins used to test the methods were insulin, ubiquitin and human serum albumin, either untreated or HHE/HNE-treated. The ion exchange methods presented in this study were based on a pH gradient using ammonium acetate and ammonium formate as the high pH eluent and acetic acid and formic acid as the low pH eluent. For these methods, the isoelectric point of each protein was important since the elution from the column would depend on the protein net charge, being eluted from the column once the pH from the mobile phase met the protein pI leaving it with neutral net charge. The ion exchange methods tested worked better for native protein isoform separation than lipoxidized proteins. It was hypothesized that these methods could be used to separate lipoxidized proteins since the oxidized lipid modifications could change the net charge of a protein. However, only cation exchange chromatography was able to distinctively separate HNE-modified ubiquitin and insulin, while MS data confirmed the modified proteins eluting slightly later than unmodified, no clear separation was observed at any other condition. Anion exchange chromatography was able to separate several isoforms of insulin and human serum albumin, the two proteins for which the PIs fit within the pH range of the gradient used. These observations confirm that each IEC method should be tailored to the pI of the protein of interest. However, for an ion exchange method to be coupled on-line to mass spectrometry, the choice of buffers needs to be compatible. This limits the buffers that can be used and therefore limiting the pH ranges that can be covered and consequently the proteins that are suitable for separations using these methods. Therefore, the anion exchange chromatography method used in this study shown interesting preliminary results in human serum albumin isoform separation which could potentially be applied to a clinical purpose. This method showed the same degree of separation with a similar HSA isoforms chromatogram as previously reported by Leblanc *et al* , which used a salt-gradient instead of pH gradient method for HSA isoforms separation [381]. Even though both methods were able to separate the isoforms and are both suitable for on-line coupling to MS, the pH gradient described in this chapter is quicker (20 min) when compared to theirs (80 min), which makes it more appealing for a potential clinical application. In contrast, this method was not able to separate lipoxidized HSA as

this was so heavily modified that no distinct peaks were observed. The proteins were modified on a 1:10 ratio so possibly a 1:1 ratio of modification would improve the separation of lipoxidized HSA. In conclusion, this chapter shows that the anion exchange chromatography method could be an easy and rapid tool for clinical application for HSA isoform separation and further validation of this method should be conducted with clinical samples. For example, plasma from diabetic or Alzheimer's disease patients could be used to validate the method as for these the glycosylated isoforms of human serum albumin have been suggested as a biomarker [383, 384]. It was also possible to observe that the separation was easier for smaller proteins rather than large, for which multiple charges can influence the separation but most importantly the MS analysis. To improve this limitation, a middle down approach could have been applied for larger proteins such as human serum albumin [385]. On the other hand, reverse-phase chromatography showed to be the best separation method tested for lipoxidized-protein separation. The aldehyde modification on the proteins caused a change in hydrophobicity, causing a change in retention time and allowing for the modified-proteins to be separated, not only according to the different degrees of modification but also separated unmodified from modified protein. Reverse-phase chromatography is the commonly used method for intact protein analysis and here it was shown to be the best for quick separation of lipoxidized proteins. Even though ion exchange chromatography is being proposed as a good alternative to reverse phase in other applications than lipoxidation, such as basic drugs determination [386], the fact that this is not coupled to mass spectrometry does not limit the solvents that can be used and potentially improves the application of this method. However, for lipoxidized protein analysis, the coupling to MS for characterization is essential and ion exchange is not as good as reverse-phase chromatography for separation of these.

Bottom-up LC-MS/MS analysis of insulin, ubiquitin and HSA were performed to localize the oxPTM hotspots of these proteins. In order to obtain the peptides, the samples were digested by in-gel or SMART digestion. The latest corresponds to a kit from Thermo which consists of an improved in-solution trypsin digestion in which trypsin is linked to beads and digests the proteins with an easy and quick protocol that obtains peptides in minutes. Additionally, it requires less sample manipulation since no reduction or alkylation is necessary. On the other hand, for in-gel digestion, more sample preparation is required such as to run a denaturing gel (SDS-PAGE), as the protein is cleaved into peptides in the later steps, which can take up to 2 days. In terms of sequence coverage, in-gel digestion shown higher percentage than SMART digestion, possibly due to less sample complexity and better detection of the fewer peptides present. However, a higher number of modification hotspots were identified using the later. While in-solution and in-gel digestion are two well-used approaches to prepare a bottom-up proteomic sample, in-gel digestion

has several advantages including simplification of samples of greater complexity before mass spectrometry analysis potentially contributing to the higher sequence coverage observed [216, 387]. In-solution digestion have the advantage of being a straightforward method where fewer things can go wrong. Additionally, it requires less protein and the peptides extraction efficiency is higher, which might justify the higher number of modification hotspots identified [388, 389]. Several amino acid residues were found to be modified by HHE and HNE, including some lysine, histidine and cysteine residues which have been previously reported modified by short-chain aldehydes [217]. However, in contrast to previous studies [286], the HSA cys34 was not found to be modified by either of the aldehyde treatments used in this study. This might be due to the size of the tryptic peptide containing this residue, which could give low ion intensity making its detection challenging.

In conclusion, the study reported in this chapter demonstrated that ion exchange chromatography methods are rising as a good alternative for protein separation and here it was shown to be the best specifically in isoform separation. This could then be potentially used in clinical applications where isoform separation is relevant for example in the assessment of glycosylated isoforms of human serum albumin in diabetes. However, reverse phase chromatography remained the better method for lipoxidized proteins separation in agreement to previous studies, and the quick method reported here showed promising preliminary results in separation of proteins by degree of modification, and therefore potential application of this to investigate degree of lipoxidized proteins in human plasma as a diagnosis tool for inflammatory diseases.

**Chapter 5. Short-chain lipid peroxidation products form covalent adducts with pyruvate kinase and inhibit its activity in vitro and in breast cancer cells**

## 5.1. Introduction

Tumour cells, as other highly proliferative cells, show upregulation of aerobic glycolysis, also known as the Warburg effect [270, 390]. They are also known to have altered redox balance, with higher cellular levels of reactive oxygen species as well as increased antioxidant concentrations [390, 391], and this pro-oxidative status is a requirement for their proliferative state through changes in metabolic reprogramming [391, 392]. These changes may be achieved by modulation of enzymatic activities, as many enzymes in glycolysis are sensitive to cellular redox balance, including glyceraldehyde-3-phosphate dehydrogenase (GAPDH), pyruvate kinase M2 (PKM2), and phosphofructokinase (PFK) [393]. For example, the oxidation of the cysteine residue in the catalytic site of GAPDH leads to inhibition of its activity [394-396]. PFK can be regulated under oxidative stress by modifications of PFKFB3, which catalyzes the formation of fructose-2,6-bisphosphate, a potent allosteric inhibitor of PGFK, as modification of PFKFB3 on a cysteine residue located near the substrate binding pocket and cause decrease in its catalytic activity [397]. However, few studies have been conducted on the effect of oxidative stress on pyruvate kinase.

Pyruvate kinase is the last enzyme of glycolysis and catalyses the conversion of phosphoenolpyruvate and ADP to pyruvate and ATP. It has been suggested to be a key player in the Warburg effect, since its activity can be modulated by allosteric regulation in tumour cells. Tumours, and other proliferating cells, have higher expression of the PKM2 isoform which is subject to allosteric regulation and lower activity compared to the non-allosteric PKM1 isoform found in the majority of tissues [398, 399]. While PKM1 exists in the active tetrameric form, PKM2 occurs in equilibrium between monomer, dimer and the active tetramer [398]. This can be regulated by a wide variety of molecules, for example, the upstream glycolytic metabolite fructose-1,6-bisphosphate (F1,6BP), which stabilizes the tetramer, and in its absence PKM2 activity drops to 4% [400-402]. Owing to its complement of nucleophilic amino acids such as cysteine residues, pyruvate kinase can also be inhibited by oxidants such as H<sub>2</sub>O<sub>2</sub> [401, 403, 404]. Even though this modification is reversible and can be recovered with a reducing agent, oxidation of pyruvate kinase can affect substrate binding, binding of allosteric regulators or multimerization [405]. Thus, oxidation has been suggested as a mechanism for inhibiting pyruvate kinase, for example in lung cancer cells [403]. It has been proposed that inhibition of pyruvate kinase leads to rerouting of glycolytic intermediates into the pentose phosphate pathway in order to generate NADPH and maintain reduced glutathione levels, facilitating cell survival in a pro-oxidative status [406]. In fact, accumulation of PEP has been shown to stimulate the pentose phosphate pathway by a feedback loop in the eukaryotic model *S. cerevisiae* [407]. Such metabolomic changes allow tumour cells to meet the increased biosynthetic demands for antioxidants, lipids and nucleotides, promoting tumour growth [399, 408].



While hydrogen peroxide or peroxyxynitrite can affect glycolytic enzymes directly, more reactive oxidants such as hydroxyl radicals can damage other cellular components such as lipids and cause lipid peroxidation. Oxidation of polyunsaturated fatty acids results in a wide range of products including short-chain aldehydes that are reactive and can cause covalent modifications of proteins [20, 31]. This process is known as lipoxidation and can occur via formation of Schiff's base or Michael adducts on nucleophilic amino acids including lysine, histidine or cysteine [409, 410], as described in chapter 1. These adducts have been shown to occur both *in vitro* and *in vivo*, and links to inflammatory diseases such as atherosclerosis and Alzheimer's disease have also been reported [410].

The 6-carbon aldehyde 4-hydroxyhexenal (HHE) is one of the major lipid peroxidation products of  $\omega$ -3 PUFAs; it has very comparable reactivity to HNE, usually referred to as the the most toxic of this class of lipid oxidation product, and therefore of potential importance in disease [113]. The 3-carbon compound malondialdehyde (MDA) is the most studied aldehyde [411] and as it is bifunctional it has the potential to crosslink proteins [129]. Acrolein is another 3-carbon aldehyde more commonly associated with tobacco smoke and processed foods [412], but which can also occur as a breakdown product of lipid peroxidation [74]. Acrolein is highly reactive, and it has been associated apoptosis and disruption of inflammation and antioxidant defence regulation [71, 80]. These aldehydes, an in particular HNE, have been suggested to have both pro-tumorigenic and anti-cancer effects depending on their levels. Aldehyde adducts with proteins and DNA can be mutagenic and carcinogenic [413], and have been reported to inhibit cell proliferation and angiogenesis as well as inducing differentiation and apoptosis in tumor cell lines [414]. Despite the known links between lipoxidation and cancer, little attention has been focused on the study of lipid peroxidation-derived aldehydes on glycolytic enzymes involved in the Warburg effect. GAPDH appears to be particularly susceptible to lipoxidation and it has been reported to be modified by HNE *in vitro* [163] and by acrolein in mouse carcinoma cells treated in culture [272, 415, 416]. In another study, the sites and mechanism of GAPDH modification by acrylamide, acrolein and methylvinyl ketone were compared [417]. Acrylamide caused the greatest inhibition of the enzyme activity and it was directly related with the modification on Cys152, located in the GAPDH active site. In contrast, lipoxidation of pyruvate kinase is still largely unexplored with only one study reporting the potential for HNE and its di-carbonyl analogue 4-oxononenal (ONE) to inactivate PKM2 [273].

In view of the gap in knowledge on the interactions of short chain reactive aldehydes with pyruvate kinase, we investigated the modification of this protein by acrolein, malondialdehyde and 4-hydroxyhexenal using LC-MS/MS to map the sites of modification following treatment *in vitro*. We then determined the effects of these treatments on PKM2 activity, both *in vitro* and in the cultured cell line MCF-7, and assessed their impact on cell viability, with the aim of

determining the potential of different aldehydes reactivity to contribute to metabolic remodelling via PKM2. The metabolic changes in the cell line MCF-7 caused by acrolein were also assessed by  $^1\text{H}$  NMR in collaboration with the University of Birmingham.

## 5.2. Material and Methods

### 5.2.1. Synthesis of 4-hydroxy-2(E)-hexenal

4-hydroxy-2(E)-hexenal (HHE) was a kind donation from and was obtained by cross-metathesis between acrolein and 1-penten-3-ol with Hoveyda-Grubbs catalyst in good yield (68%), following the two published procedures [418, 419]. <sup>1</sup>H NMR (300 MHz, Aceton-d<sub>6</sub>) δ 9.57 (d, J = 7.9 Hz, 1H), 6.96 (dd, J = 15.6, 4.4 Hz, 1H), 6.22 (ddd, J = 15.6, 7.9, 1.7 Hz, 1H), 4.32 (ddt, J = 9.5, 6.7, 3.2 Hz, 1H), 4.22 (d, J = 4.9 Hz, 1H), 1.83 – 1.42 (m, 2H), 0.94 (t, J = 7.4 Hz, 3H) ; <sup>13</sup>C NMR (75 MHz, Aceton-d<sub>6</sub>) δ 193.1, 160.3, 130.3, 71.3, 29.2, 8.9.

### 5.2.2. Treatment of pyruvate kinase with aldehydes in vitro

Pyruvate kinase from rabbit muscle (EC2.7.1.40) was prepared at 2.5 mg/mL in phosphate buffer (7 mM sodium phosphate monobasic and 10 mM disodium phosphate dibasic, pH7.4) and treated with acrolein (ACR), malondialdehyde (MDA) (prepared via acid hydrolysis of 1,1,3,3-tetramethoxypropane) or 4-hydroxy-2(E)-hexenal (HHE) at 2 μM, 10 μM, 20 μM, 38 μM, 100 μM, 200 μM, 380 μM, 500 μM, 760 μM, 1mM or 5 mM, and allowed to react for 10 minutes, 30 minutes, 1 hour, 2 hours or 4 hours at 37 °C. Following the reaction, to stabilize any adducts sodium borohydride (NaBH<sub>4</sub>) was added to the reaction to a final concentration of 5 mM and the reaction left for a further 30 minutes at room temperature. This step was omitted when the treated pyruvate kinase was used immediately in the enzymatic activity assay.

### 5.2.3. Cell culture and aldehyde treatment

MCF-7 cells were cultured in DMEM (Gibco, UK) supplemented with 10% fetal bovine serum (FBS), 100 U/mL penicillin and 100 μg/mL streptomycin in a humidified incubator at 37 °C and 5% CO<sub>2</sub>. For each aldehyde treatment, cells were seeded into new flasks at a cell density of 10<sup>6</sup> /mL and 10x stock solutions of ACR, MDA or HHE in phosphate buffered containing 0.9% NaCl pH 7.4 were added to the culture media to give final concentrations of 2, 10, 20, 100 or 200 μM and incubated for 2, 4 or 24 hours. Biological triplicates were performed.

### 5.2.4. XTT cell viability assay

MCF-7 cells were cultured in a 96-well plate at 10<sup>5</sup> cells per well. The treatments with aldehydes were performed at the concentrations and times described above. XTT [2,3-bis-(2-methoxy-4-nitro-5-sulfophenyl)-2H-tetrazolium-5-carboxanilide] was dissolved in sterile medium to a final concentration of 1 mg/mL. A 10 mM solution PMS (*N*-methyl dibenzopyrazine methyl sulfate) solution was prepared in phosphate buffer saline (PBS). Immediately prior the

start of the assay, 10  $\mu\text{L}$  of PMS was added to 4 mL of XTT solution; 25  $\mu\text{L}$  of PMS/XTT mixture was added to each well and the plate incubated in the dark for 2 h at 37  $^{\circ}\text{C}$  before reading the absorbance at 450 nm. The assay was performed with both technical and biological triplicates.

#### **5.2.5. Cell harvesting, lysis and protein concentration assessment**

Cells were harvested using pre-warmed trypsin-EDTA solution followed by centrifugation at 150 g for 5 min at 4  $^{\circ}\text{C}$  and lysed in lysis buffer (50 mM Tris-HCl pH 7.5, 1 mM EDTA, 150 mM NaCl, 1% Triton X-100) supplemented immediately prior to usage with cComplete™ EDTA-free Protease Inhibitor Cocktail (Sigma Aldrich, UK) according to the manufacturer's instructions. After 15 minutes incubation on ice, the samples were centrifuged at 17,000 g for 2 minutes and the supernatant (cytosolic extract) was retained. The total protein concentration was determined by the Bradford assay using Pierce™ Coomassie Plus Assay Reagent (ThermoFisher Scientific, UK) in a 96-well plate: 5  $\mu\text{L}$  of sample or standard per well were mixed with 250  $\mu\text{L}$  of Coomassie reagent and after 10 mins the absorbance was read at 595 nm. Samples were analysed for enzymatic activity immediately.

#### **5.2.6. Pyruvate kinase activity assays**

Pyruvate kinase activity was measured using a coupled assay using the pyruvate-dependent conversion of NADH to NAD<sup>+</sup> by lactate dehydrogenase as the reporter. For analysis of the effects on pyruvate kinase *in vitro*, 5  $\mu\text{L}$  of the aldehyde-treated pyruvate kinase (equivalent to 1U) were added to a cuvette containing 30  $\mu\text{L}$  of 45 mM adenosine 5'-diphosphate (ADP), 30  $\mu\text{L}$  of 45 mM phosphoenolpyruvate (PEP), 30  $\mu\text{L}$  of 6.6 mM  $\beta$ -nicotinamide adenine dinucleotide reduced form (NADH) and 5  $\mu\text{L}$  of 200 U/mL lactate dehydrogenase (LDH) in 900  $\mu\text{L}$  of 50 mM imidazole-HCl buffer pH 7.6, to give a final volume of 1 mL. The reaction at 25  $^{\circ}\text{C}$  was monitored at 340 nm for 10 minutes and the initial rate of reaction in  $\mu\text{mol}$  NADH utilized /min was calculated. For analysis of pyruvate kinase activity following cell treatments, the cytosolic extract was substituted for the commercial pyruvate kinase preparation.

#### **5.2.7. Protein in-solution digestion**

To 100  $\mu\text{L}$  of aldehyde-treated pyruvate kinase prepared as described above, 100  $\mu\text{L}$  of RapiGest SF (Waters, UK) were added and the solution vortexed. DTT was then added to a final concentration of 5 mM and the reaction incubated at 60  $^{\circ}\text{C}$  for 30 minutes. Cysteine alkylation was then performed by adding iodoacetamide to a final concentration of 15 mM and incubating in the dark for 30 min at room temperature. Trypsin (Trypsin Gold, Mass Spectrometry Grade, Promega, Southampton, UK) was added to a final concentration of 7

µg/mL and the samples were incubated overnight at 37 °C. To prepare samples for LC/MS, trifluoroacetic acid (TFA) was added to a final concentration of 0.5% and the reaction incubated at 37 °C for 45 min, during which time a precipitate formed. Acid-treated samples were centrifuged at 13000 rpm for 10 min then the supernatant carefully transferred to another tube and dried in a centrifugal evaporator and stored dry at -20 °C. Samples were resuspended in H<sub>2</sub>O/acetonitrile (98%/2%), 0.1% formic acid prior to MS analysis.

#### **5.2.8. Cellular extract in-gel digestion**

MCF-7 cells were grown as described in 2.4, but in 75 cm<sup>2</sup> flasks. Cells were harvested by trypsinization and resuspended at 2x10<sup>6</sup> cells/mL in DMEM containing penicillin, streptomycin and 10% bovine calf serum. For each treatment, 5 mL of cells were seeded in a 25 cm<sup>2</sup> flask, topped up with 4.5 mL of medium, and treated with 0.5 mL of a 10x stock of acrolein to yield final concentrations of 10 or 200 µM. At the end of the treatment, cells were harvested and extracted as described in 2.6. Extracts of 1x10<sup>7</sup> cells were run on a 7.5% denaturing polyacrylamide gel followed by in-gel digestion of the bands corresponding to pyruvate kinase according to a previously described protocol [217]. The resulting tryptic peptides were analysed by LC-MS/MS as described for the treatments in vitro.

#### **5.2.9. Liquid Chromatography-Tandem Mass Spectrometry (LC-MS/MS) Analysis**

Peptides were separated and analysed using an Ultimate 3000 system (Thermo Scientific, Hemel Hempstead, UK) coupled to a 5600 TripleTOF (ABSciex, Warrington, UK). The analysis was performed as previously described [298] and as detailed in section 2.2.6.

#### **5.2.10. Database Searches**

The Mascot® probability based search engine (Matrix Science, London, version 2.4.0) was used to interrogate the SwissProt 2019\_03primary database. LC-MS .wiff files of each sample were searched for protein identification and oxidative post-translational modifications(oxPTMs). For protein identification, variable modifications of methionine oxidation and carbamidomethyl cysteine were used. For the analysis of the lipoxidation products, the initial searches additionally used a variable modification list including reduced and unreduced ACR(mass changes of 56.06 Da, 58.08 Da, 40.06 Da, 94.11 Da, 56.06 Da,76.09 Da), MDA (mass changes of 54.05 Da, 56.06 Da, 134.13 Da,36.03 Da and 26.04 Da) or HHE (mass changes of 114.14 Da, 93.13 Da,78.11 Da) adducts at cysteine, lysine and histidine residues. Other parameters for the searches were as follows: Enzyme: Trypsin; Peptide tolerance: ± 0.6 Da; MS/MS tolerance: ± 0.6 Da; Peptide charge state:+2, +3; Max Missed cleavages: 1; #13C: 0; Quantitation: None; Instrument: ESI-QUAD-TOF; Data

format: Mascot Generic; Experimental mass values: Monoisotopic; Taxonomy: Chordata. All data identifying modifications were manually validated before inclusion

#### **5.2.11. Protein structure visualization using PyMOL**

The PyMOL Molecular Graphics System (Version 1.2r3pre, Schrödinger, LLC) was used for molecular visualization of the crystal structure of pyruvate kinase. The .pdb file containing the known crystal structure of PKM from rabbit muscle (P11974) and from Human (P14618) were downloaded from Uniprot. Backbone structures and space filling modules were created using the dropdown menus available on PyMOL. Hydrophobicity mapping was performed using the script called "Color h". This script colours the amino acid residues based on the Eisenberg hydrophobicity scale [420].

#### **5.2.12. Glycolysis Stress Test with Seahorse XF Extracellular Flux Analyzer**

The Glycolytic Stress Test was used to monitor cellular glycolysis upon acrolein treatment. Prior to the assay, the cartridge was hydrated with calibrate solution in a non-CO<sub>2</sub> incubator at 37 °C. On the day of the assay, the XF Glycolysis Stress Test Assay Medium was prepared as non-buffered DMEM XF Base Medium supplemented by 2 mM L-glutamine. The lack of buffer is critical to detect pH changes. Cells were seeded to a 24-well XF Cell Culture Microplate plate at 20,000 cells/well and treated with 2, 10 or 100 µM for 2 hours. Meanwhile, the glucose, oligomycin, and 2-deoxy-D-glucose were left at room temperature for 15 min, diluted to 10mM and loaded into the cartridge. After the treatment, the media was removed, the cells were washed with non-buffered DMEM medium, the assay medium was added, and the plate incubated in a non-CO<sub>2</sub> incubator at 37 °C for 1 hour. During the assay, glucose was injected first to a final concentration of 1 µM and cells catabolize it through glycolysis producing protons causing an increase in the extracellular acidification rate (ECAR). The second injection was oligomycin, to a final concentration of 1 µM, which inhibits mitochondrial ATP production and drives the cells to a maximum glycolytic capacity. Finally, 2-DG was injected to a final concentration of 1 µM inhibiting glycolysis and confirming that the ECAR generated in the assay is due to glycolysis. After the experiment, the protein concentration in each well was measured by Bradford Assay and ECAR values were normalized to protein concentration. The Seahorse XF Glycolysis Stress Test Report Generator automatically calculated the Seahorse XF Glycolysis Stress Test parameters and exported them as an Excel file.

#### **5.2.13. NMR sample preparation**

Samples were prepared according to Saborano, R. *et al.* [275]. MCF-7 cells were grown as described in **2.4** to 80% confluency. To achieve optimal reproducibility, the metabolite

extraction from the MCF-7 cell line was performed with ice-cold solvents to reduce all metabolic processes. Initially the cells were washed 2-3 times with ice cold PBS to remove residual media, then 400  $\mu$ L of cold methanol was added to immediately quench metabolism. Cells were scraped off the flask and the solution transferred to a glass vial, followed by chloroform extraction to obtain and separate the organic and polar phase. Briefly, 200  $\mu$ L of chloroform were added, followed by 30 seconds vortex and the addition of further 200  $\mu$ L of chloroform and 300  $\mu$ L of water. After vortex, samples were left on ice for 10 minutes, followed by centrifugation for 10 minutes at 4000 rpm and the polar layer was then transferred to a clean tube and dried under vacuum for later NMR analysis.

#### 5.2.14. NMR acquisition and analysis

All data collection and data analysis were performed in collaboration with University of Birmingham and according to Saborano, *et al.* [275]. Data collection was carried out using a Bruker 600MHz Avance III spectrometer using a 1.7mm cryoprobe. Dried polar metabolites were re-suspended in sodium phosphate buffer in 90% water and 10% D<sub>2</sub>O (0.1 mol/L, pH 7.00) containing 3-trimethylsilyl-2,2,3,3-d<sub>4</sub>-propionate (TMSP) as an internal chemical shift standard, to acquire 1D <sup>1</sup>H NMR spectra. 1D <sup>1</sup>H-NOESY spectra were collected at 298 K with a 12 ppm spectral width, 32k data points and 128 scans. Spectra were processed using Metabolab [421] programmes within Matlab, version R2017b (MathWorks, Massachusetts, United State). Prior to Fourier transformation, each free induction decay (FID) was zero-filled to 65536 points and multiplied by an exponential function equivalent to a 0.3 Hz line broadening. All spectra were aligned on TMSP, a spline baseline correction was applied, the water and TMSP regions were excluded and Probabilistic Quotient Normalization (PQN) was applied to account for dilution of complex biological mixtures. Resonances were assigned using Chenomx 8.1 spectral database (Alberta, Canada, 2015), and comparing with the chemical shifts in the Human Metabolome Database (HMDB) [422].

#### 5.2.15. Statistical analysis

Data were analysed with Graph Pad Prism using one-way ANOVA for single time point (**Figure 5.4**, **Figure 5.5** and **Figure 5.7**) and using two-way ANOVA for multiple time point (**Figure 5.6** and **Figure 5.10**), both with Dunnett's multiple comparisons test, comparing the values of each treated sample to the mean of the untreated control, normalized to 100%. Two-way ANOVA with Dunnett's multiple comparison test was also used for **Figure 5.14** to compare the values of each metabolite in treated sample to the untreated control. Data are shown as averages  $\pm$  SEM.

## 5.3. Results

### 5.3.1. Identification and mapping of lipoxidation on pyruvate kinase

An LC-MS/MS bottom-up approach was used to investigate the *in vitro* modification of pyruvate kinase by ACR, MDA and HHE in order to map the sites of modification. Each peptide found modified by comparison to a database using the MASCOT<sup>®</sup> software was confirmed by *de novo* sequencing of the MS/MS spectrum [217] (examples for each aldehyde are shown in **Figure 5.1**). Following this approach, 11 acrolein-modified peptides, 10 HHE-modified peptides and 9 MDA-modified peptides were identified based on their peptide molecular weight, mass/charge ratio and charge of the peptide ion, MS/MS ion score and LC retention time (**Table 5.1**). The majority of the identified adducts occurred on lysine and cysteine residues, although some histidine adducts were identified. The mapping of the modified residues onto the enzyme 3D structure is shown in **Figure 5.2**. Pyruvate kinase showed different susceptibility to modification by each aldehyde as the residues modified were substantially different. ACR and HHE are both  $\alpha,\beta$ -unsaturated aldehydes, therefore a similar profile of modification was expected. However, HHE formed adducts on Cys152, Lys188, Lys247, His379 that were not detected with acrolein, whereas acrolein uniquely modified Lys66, Lys166, Lys207 and His464. MDA gave a rather different profile, as only lysine adducts were identified, and modifications on Lys115, Lys224 and Lys270 were unique to this aldehyde. Only Lys393 and Lys475 were consistently identified as modified by all three aldehydes.



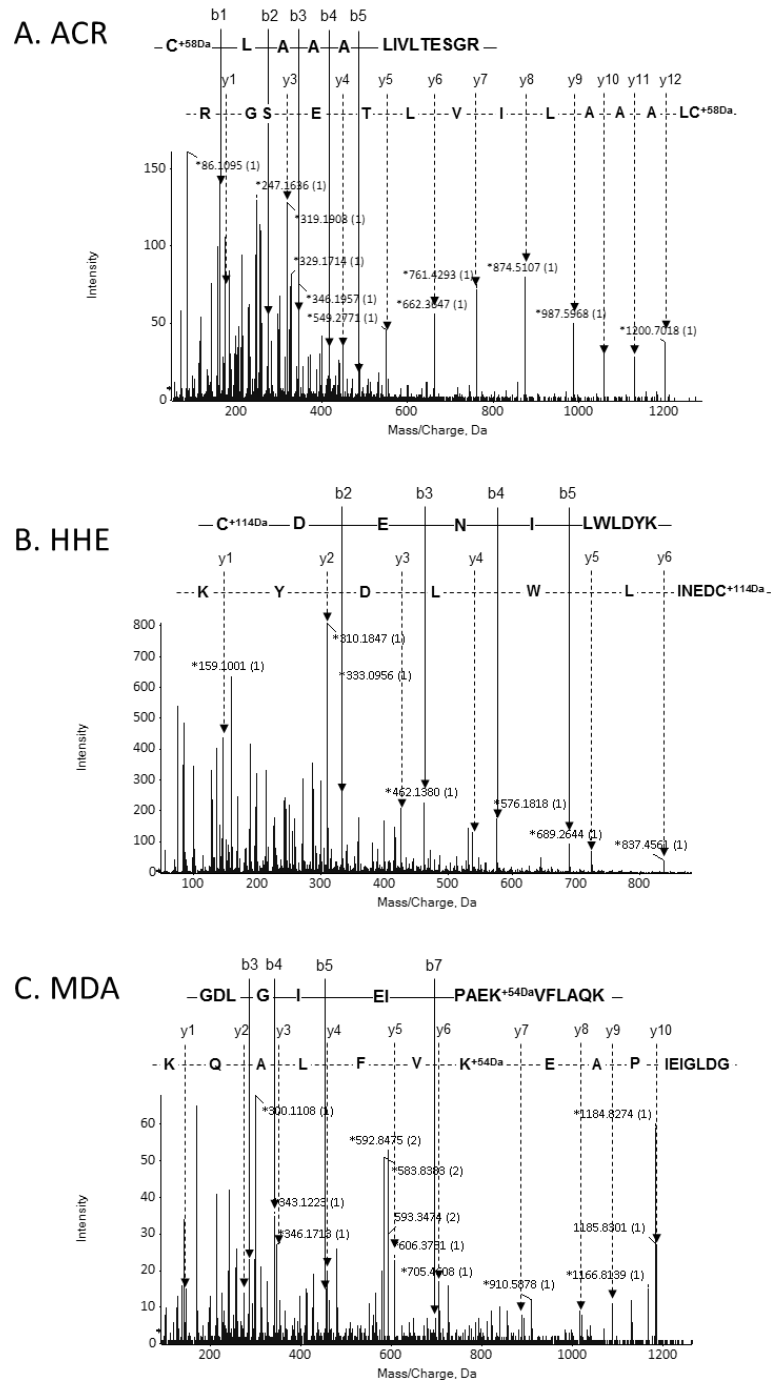


**Figure 5.1. MS/MS spectra of modified pyruvate kinase tryptic peptides.** LC-MS/MS was carried out as described in the experimental section, and peptides identified by Mascot searches as containing adducts were manually validated. (A) CLAAALIVL TESGR modified on the cysteine residue by acrolein forming a Michael adduct; (B) Michael adduct of HHE of the cysteine residue of CDENILWLDYK; (C) GDLGIEIPAEKVFLAQK modified by MDA as a Schiff's base on lysine. The y and b ions indicated by the arrows confirm the peptide sequence and the modification on the cysteine or lysine residues respectively. Figure from [423].

**Table 5.1. Pyruvate kinase residues modified after 10 min treatment at high aldehyde concentrations *in vitro*.**

Modified Residues	Pyruvate kinase modified peptides (a <sup>b</sup> )	Theoretical mass of modified peptide	Observed mass of modified peptide	m/z (charge)	Ion score	Rt (min)	Aldehyde treatment			
							38 μM	380 μM	760 μM	5 mM
<b>Acrolein</b>										
Cys49	<b>SB</b> 44NTGIIC <sup>+56</sup> TIGPASR <sub>56</sub>	1357.70	1357.83	679.9 (2+)	52	27.76	-	-	-	✓
Cys49	<b>MA</b> 44NTGIIC <sup>+58</sup> TIGPASR <sub>56</sub>	1359.72	1359.84	680.9 (2+)	54	27.69	-	✓	✓	✓
Lys66	<b>MA</b> 63EMIK <sup>+58</sup> SGMNVAR <sub>73</sub>	1292.66	1292.81	431.9 (3+)	16	21.87	-	-	✓	✓
Lys166	<b>MA</b> 163NIC <sup>+K+58</sup> VVDVGSK <sub>173</sub>	1275.68	1275.81	638.9 (2+)	13	21.94	-	-	✓	✓
Lys207	<b>SB</b> 207K <sup>+40</sup> GVNLPGAAVDLPAVSEK <sub>224</sub>	1804.01	1804.19	602.4 (3+)	62	31.00	-	-	-	✓
Cys326	<b>MA</b> 320AGKPVIC <sup>+58</sup> ATQMLESMIK <sub>336</sub>	1876.98	1876.17	626.7 (3+)	19	52.72	-	-	-	✓
Cys358	<b>MA</b> 343AEGSDVANAVLDGADC <sup>+58</sup> IMLSGETAK <sub>367</sub>	2494.16	2494.37	832.5 (3+)	37	49.48	✓	-	-	-
Lys367	<b>MA</b> 343AEGSDVANAVLDGADC <sup>+58</sup> IMLSGETAK <sup>+58</sup> GDYPLEAVR <sub>376</sub>	3551.67	3551.99	889.0 (4+)	26	47.52	-	✓	-	-
Lys393	<b>MA</b> 393K <sup>+58</sup> LFELAR <sub>400</sub>	1062.61	1062.72	532.4 (2+)	27	29.34	-	-	✓	✓
Lys393	<b>SB</b> 393K <sup>+40</sup> LFELAR <sub>400</sub>	1060.59	1060.63	531.3 (2+)	9	21.87	-	-	✓	✓
Cys423	<b>MA</b> 423C <sup>+58</sup> LAAALIVLTESGR <sub>436</sub>	1473.82	1473.96	737.9 (2+)	89	51.53	-	-	-	✓
His464	<b>SB</b> 462QAH <sup>+40</sup> LYR <sub>467</sub>	826.44	826.51	414.3 (2+)	21	21.03	✓	-	-	-
Cys474	<b>MA</b> 468GIFPVVC <sup>+58</sup> K <sub>475</sub>	975.55	975.63	460.8 (2+)	31	30.97	✓	✓	✓	✓
Lys475	<b>MA</b> 468GIFPVVC <sup>+K+58</sup> DPVQEAWAEDVDLR <sub>489</sub>	2599.30	2599.51	867.5 (3+)	57	53.72	-	-	✓	✓
<b>4-hydroxy-hexenal</b>										
Cys152	<b>SB</b> 152C <sup>+96</sup> DENILWLDYK <sub>162</sub>	1506.71	1506.86	754.44 (2+)	24	39.35	-	✓	✓	✓
Cys152	<b>MA</b> 152C <sup>+114</sup> DENILWLDYK <sub>162</sub>	1524.72	1524.72	763.43 (2+)	72	33.52	✓	✓	✓	✓
Lys188	<b>MA</b> 187QK <sup>+114</sup> GPDFLVTEVENGGFLGSK <sub>206</sub>	2235.14	2235.34	746.12 (3+)	17	35.84	-	-	-	✓
Lys247	<b>SB</b> 247K <sup>+96</sup> AADVHEVR <sub>255</sub>	1119.60	1119.73	374.25 (3+)	27	18.23	-	-	-	✓

Cys326	<b>SB</b>	<sup>320</sup> AGKPVIC <sup>+96</sup> ATQMLESMIKKPRPTR <sub>342</sub>	2650.45	2650.72	531.15 (5+)	14	38.00	-	-	-	✓
Cys326	<b>MA</b>	<sup>320</sup> AGKPVIC <sup>+114</sup> ATQMLESMIKKPRPTR <sub>342</sub>	2668.46	2668.72	445.79 (6+)	13	29.35	-	-	-	✓
Cys358	<b>MA</b>	<sup>343</sup> AEGSDVANAVLDGADC <sup>+114</sup> IMLSGETAK <sub>367</sub>	2550.18	2550.42	851.15 (3+)	36	36.37	-	✓	✓	✓
His379	<b>MA</b>	<sup>377</sup> MQH <sup>+114</sup> LIAR <sub>383</sub>	981.54	981.64	491.83 (2+)	13	19.81	-	-	✓	✓
His391	<b>MA</b>	<sup>384</sup> EAEAAMFH <sup>+114</sup> R <sub>392</sub>	1174.54	1174.67	392.56 (3+)	10	21.82	-	-	-	✓
Lys393	<b>MA</b>	<sup>393</sup> K <sup>+114</sup> LFEELAR <sub>400</sub>	1118.63	1118.72	560.37 (2+)	26	29.38	-	✓	✓	✓
Cys423	<b>SB</b>	<sup>423</sup> C <sup>+96</sup> LAAALIVLTESGR <sub>436</sub>	1529.85	1529.98	765.99 (2+)	76	40.94	✓	✓	✓	✓
Cys474	<b>MA</b>	<sup>468</sup> GIFPVVC <sup>+114</sup> K <sub>475</sub>	975.55	975.62	488.82 (2+)	26	28.22	-	-	✓	✓
Lys475	<b>MA</b>	<sup>468</sup> GIFPVVCK <sup>+114</sup> DPVQEAWAEDVDLR <sub>489</sub>	2599.29	2599.49	867.50 (3+)	85	33.83	-	-	-	✓

#### Malondialdehyde

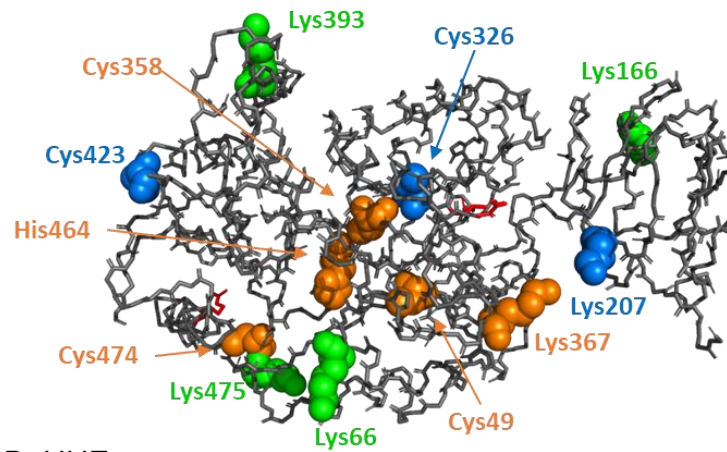
Lys115	<b>SB</b>	<sup>93</sup> TATESFASDPILYRPVAVALDTK <sup>+54</sup> GPEIR <sub>120</sub>	3070.59	3070.81	768.71 (4+)	42	34.07	-	✓	-	✓
Lys135	<b>SB</b>	<sup>126</sup> GSGTAEVELK <sup>+54</sup> K <sub>136</sub>	1171.61	1171.52	391.51 (3+)	52	18.74	-	✓	✓	-
Lys188	<b>SB</b>	<sup>187</sup> QK <sup>+54</sup> GPDFLVTEVENGGFLGSK <sub>206</sub>	2175.08	2175.21	726.08 (3+)	94	34.69	✓	✓	✓	✓
Lys207	<b>SB</b>	<sup>207</sup> K <sup>+54</sup> GVNLPGAAVDLPAVSEK <sub>224</sub>	1817.99	1818.03	607.02 (3+)	70	28.67	✓	✓	✓	✓
Lys224	<b>SB</b>	<sup>208</sup> GVNLPGAAVDLPAVSEK <sup>+54</sup> DIQDLK <sub>230</sub>	2402.27	2402.45	801.82 (3+)	87	33.97	-	✓	✓	✓
Lys270	<b>SB</b>	<sup>267</sup> IISK <sup>+54</sup> IENHEGVR <sub>278</sub>	1447.78	1447.74	483.59 (3+)	82	23.05	-	-	-	✓
Lys305	<b>SB</b>	<sup>295</sup> GDLGIEIPA EK <sup>+54</sup> VFLAQK <sub>311</sub>	1881.03	1881.08	628.03 (3+)	48	34.80	-	-	-	✓
Lys393	<b>SB</b>	<sup>393</sup> K <sup>+54</sup> LFEELAR <sub>400</sub>	1058.58	1058.57	530.29 (2+)	37	27.85	✓	✓	✓	✓
Lys475	<b>SB</b>	<sup>468</sup> GIFPVVC* <sup>K+54</sup> DPVQEAWAEDVDLR <sub>489</sub>	2596.26	2596.49	866.50 (3+)	72	36.79	✓	✓	✓	✓

a (subscript) – amino acid position in the mature protein

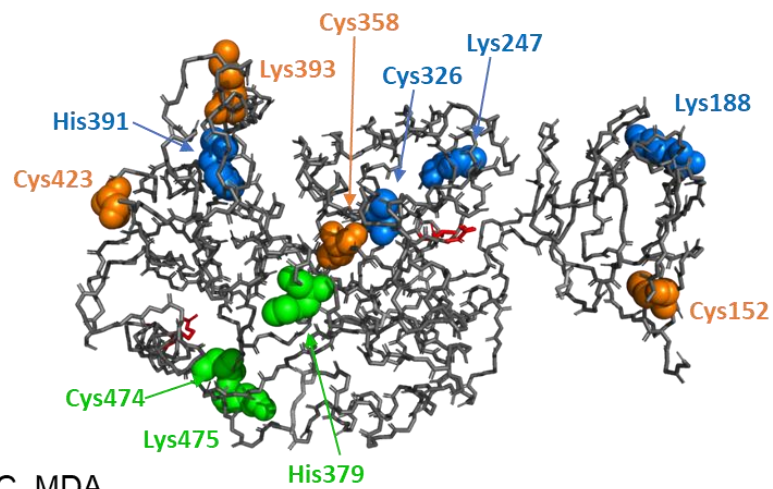
b (superscript) - mass difference corresponding to the modification

Michael adduction (MA) or Schiff-base formation (SB)

A. ACR



B. HHE



C. MDA

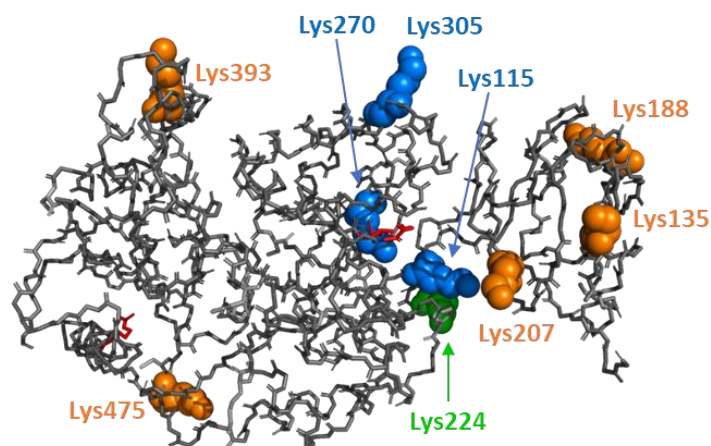


**Figure 5.2. Mapping of lipoxidation adducts to the crystal structure of pyruvate kinase.** Backbone structure with modified residues indicated in space-fill form, showing the location of adducts of acrolein (A), HHE (B) and MDA (C). The modified residues are color-coded with orange indicating those found only at 380  $\mu$ M, green for those found additionally at 760  $\mu$ M and blue for ones found additionally at 5 mM. Figure from [423].

The identified modifications were also mapped onto space-filling models mapped for hydrophobicity of the solvent-accessible surface to evaluate if the hydrophobicity may affect the location of the modification. The surface hydrophobicity is indicated in red in **Figure 5.3**; no clear correlation was identified between the hydrophobicity and the site of modification. Nonetheless, it was observed that acrolein was able to penetrate more readily into narrow pockets in the enzyme in comparison to HHE.

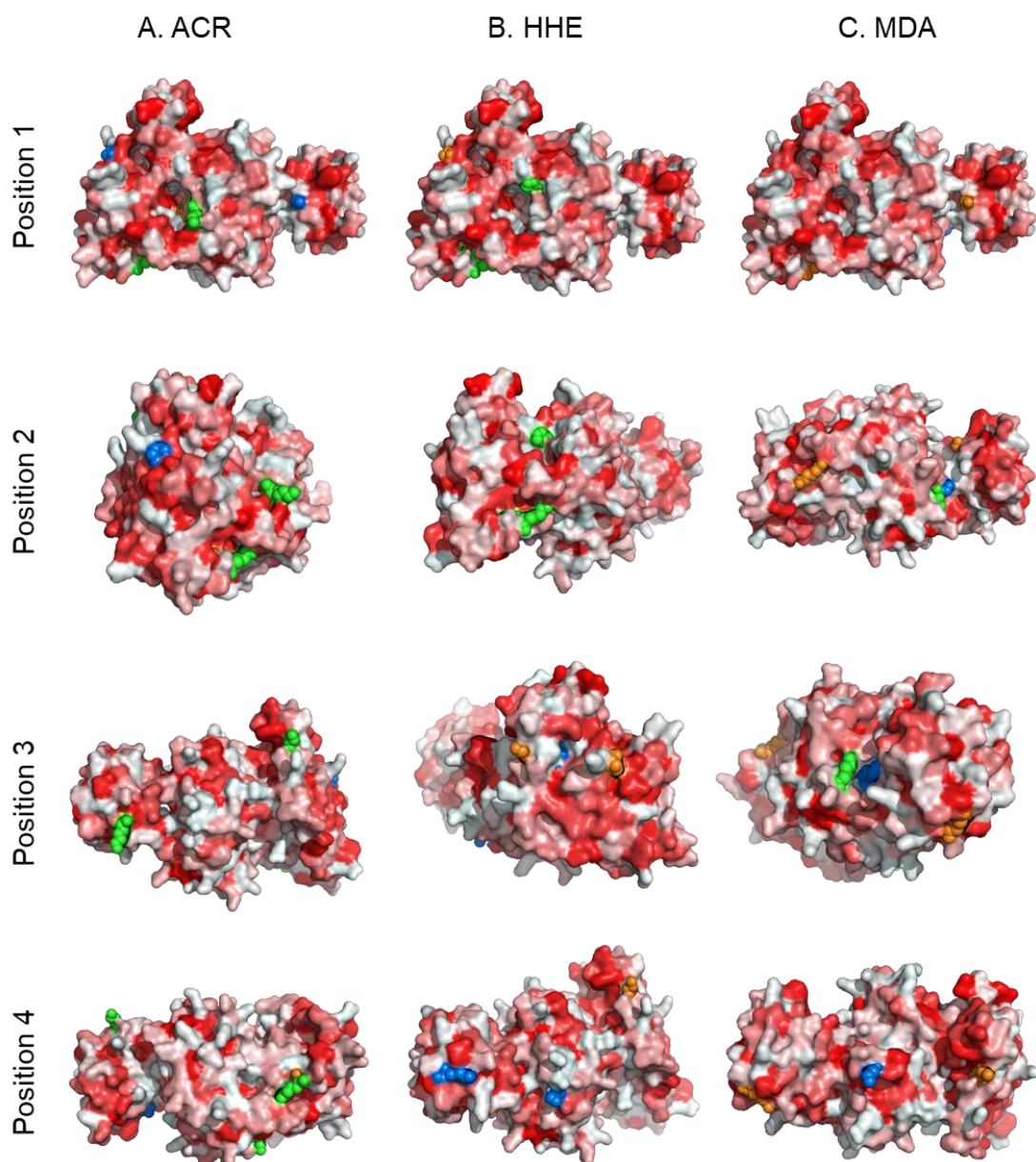
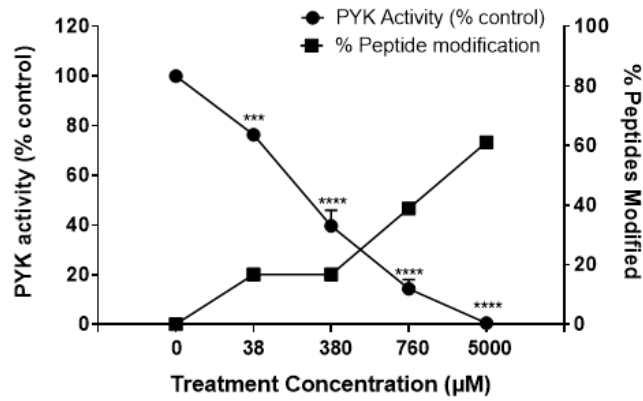


**Figure 5.3. Space filling models of pyruvate kinase showing surface hydrophobicity and sites of adduction at high aldehyde concentrations.** Surface views with increasing hydrophobicity shown in darker red. The location of adducts of acrolein (A), HHE (B) and MDA (C) are shown color-coded with orange indicating those found only at 380  $\mu\text{M}$ , green for those found additionally at 760  $\mu\text{M}$  and blue for ones found additionally at 5 mM. Figure from [423].

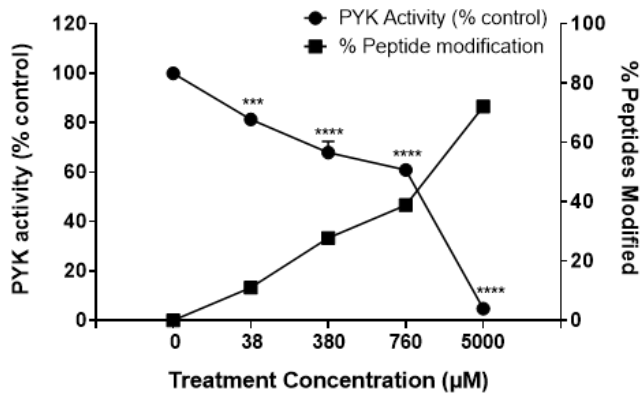
### 5.3.2. Inhibition of pyruvate kinase activity following treatment *in vitro*

The effect of the same treatment time and concentrations on pyruvate kinase activity were determined *in vitro* by a coupled spectrophotometric assay. It is worth noting that the isoform used for the *in vitro* study was PKM1 from rabbit muscle. A significant dose-dependent effect on the activity of pyruvate kinase was observed for all acrolein and HHE treatments. In contrast, MDA at lower concentration had no effect and an impact on the activity was only observed at the highest concentration of 5 mM. The activity of pyruvate kinase as percentage of control and the number of modified peptides detected as a percentage of the total number of modifiable tryptic peptides in the protein are shown in **Figure 5.4**. A clear inverse relationship between the enzymatic activity and the number of modifications can be seen. HHE gave the highest maximum number of modified peptides, followed by acrolein, and MDA was the lowest, reflecting the fact that only lysine residues can be modified by MDA. However, at 380  $\mu$ M treatment, MDA actually gave a higher percentage of modified peptides than the other two aldehydes.

### A. ACR



### B. HHE



### C. MDA

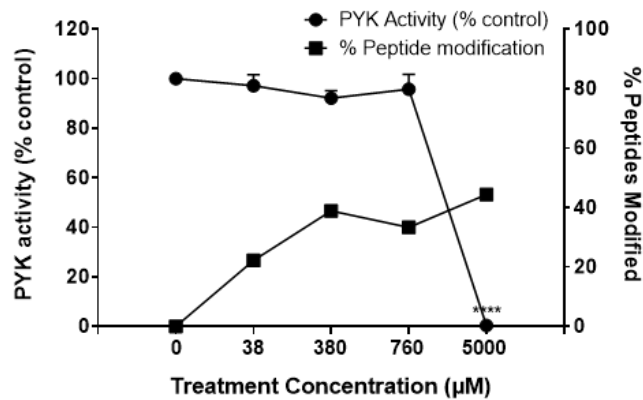


**Figure 5.4. Inverse relationship between the dose-dependent effect of aldehydes on the activity of pyruvate kinase in vitro and the percentage of modified pyruvate kinase peptides identified.** Pyruvate kinase was treated with 38 μM, 380 μM, 760 μM and 5 mM final concentrations of acrolein, 4-hydroxy-hexenal or malondialdehyde for 10 minutes before the assessment of its activity by spectrophotometric assay of NADH oxidation at 340 nm (n=4; Mean ± SEM; \* p<0.1 \*\* p<0.01 \*\*\* p<0.001 \*\*\*\* p<0.0001). Peptide modification was determined from the total number of modified peptides as a % of the total modifiable peptides in the sequence. Figure from [423].



The concentration range of aldehydes used for mapping of the sites of modification was significantly higher than the concentrations that have been measured for these aldehydes in their free form in plasma. Hence, the effects of a wider range of treatment concentrations, that included physiological (2  $\mu\text{M}$ ) to pathophysiological (20-100  $\mu\text{M}$ ) concentrations, on pyruvate kinase activity were tested (**Figure 5.5**). It can be seen that acrolein caused a dose-dependent decrease in the activity of pyruvate kinase, with 70% activity at 100  $\mu\text{M}$  and 200  $\mu\text{M}$ , 40% at 500  $\mu\text{M}$  and 10% at 1 mM treatment, corresponding to substantially more inhibition than either of the other aldehydes.

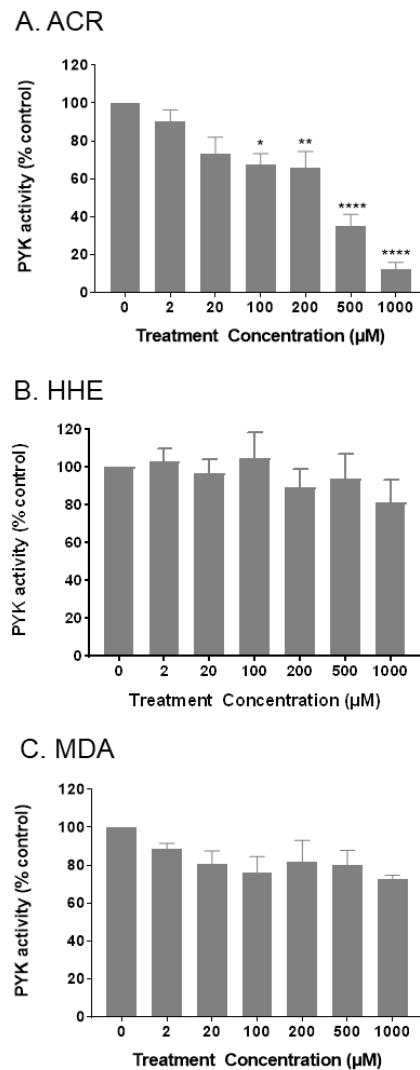


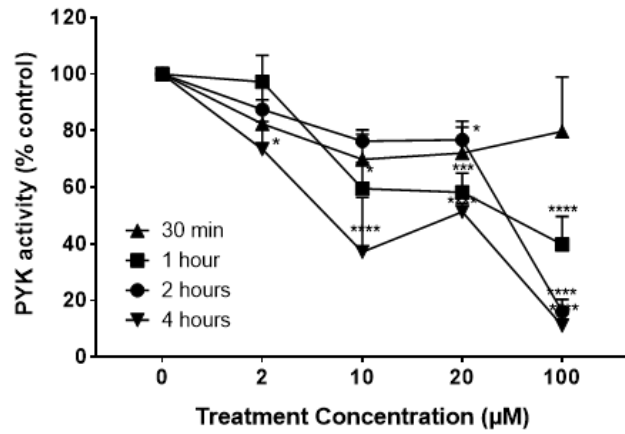
**Figure 5.5. Dose-dependent effect of short treatments with acrolein, 4-hydroxy-hexenal and malondialdehyde on the activity of in-vitro pyruvate kinase.** Pyruvate kinase was treated with 2  $\mu\text{M}$ , 20  $\mu\text{M}$ , 100  $\mu\text{M}$ , 200  $\mu\text{M}$ , 500  $\mu\text{M}$  and 1 mM of each aldehyde for 10 minutes before the assessment of its activity (n=3; Mean  $\pm$  SEM; \* p<0.1 \*\* p<0.01 \*\*\* p<0.001 \*\*\*\* p<0.0001). Figure from [423].

### 5.3.3. The effect of longer treatment times on activity and lipoxidation of pyruvate kinase

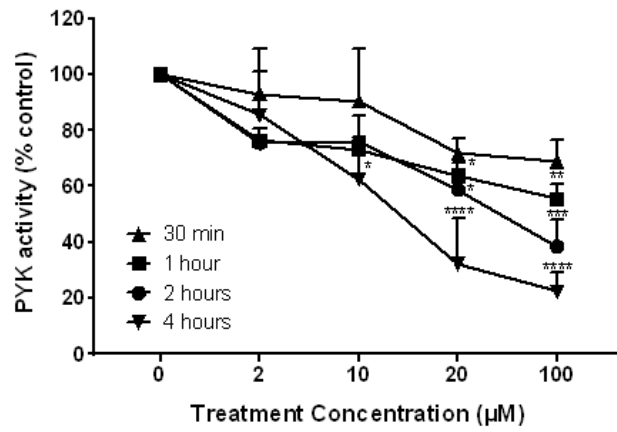
It was noted that the treatment concentrations required to cause significant inhibition were high, and it was hypothesized that this might relate to the very short incubation times tested initially (10 minutes), despite the fact that the reaction of acrolein with protein was expected to be rapid. Therefore, further experiments were carried out with longer incubations of 30 minutes to 4 hours with the lower range of concentrations for each aldehyde (**Figure 5.6**).

In general, longer incubations resulted in more extensive inhibition of activity showing a time-dependent trend for acrolein and HHE treatments. Acrolein above 10  $\mu\text{M}$  caused significant effect on the activity after 1 hour reaction with only 40% activity remaining in the 100  $\mu\text{M}$  treatment. Increasing the time of reaction to 2 hours caused a decrease in activity to approximately 20% at the same concentration, and further inhibition was observed with 4 hours reaction. At 10  $\mu\text{M}$  acrolein, a known pathophysiological concentration [269, 424], only 40% remaining activity was observed after 4 hours reaction. In the case of HHE, a treatment concentration of 100  $\mu\text{M}$  caused a time-dependent effect on the activity, with 70% remaining after 30 mins, 55% after 1 hour, 40% after 2 hours and 30% after 4 hours. The 4 hour treatment also showed a significant dose-dependent effect. Comparing the two aldehydes, acrolein caused more inhibition of pyruvate kinase activity. MDA did not show a clear dose or time-dependent effect on the activity; however, significant inhibition was observed at all concentrations following a 2 hour treatment.

### A. ACR



### B. HHE



### C. MDA

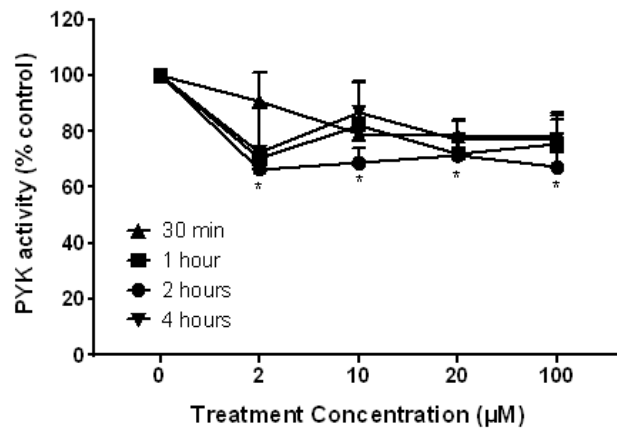


**Figure 5.6. Effect of longer treatments with acrolein, 4-hydroxy-hexenal and malondialdehyde on the activity of pyruvate kinase in vitro.** Pyruvate kinase was treated with 2 µM, 10 µM, 20 µM and 100 µM of each aldehyde for 30 minutes, 1 hour, 2 hours or 4 hours before the assessment of its activity (n=3; Mean ± SEM; \* p<0.1 \*\* p<0.01, \*\*\* p<0.001 and \*\*\*\* p<0.0001). Figure from [423].

The same bottom-up LC-MS/MS approach from **3.1** allowed the identification of 10 peptides modified by acrolein and 4 peptides modified by HHE after 4 hour treatments (**Table 5.2**). Mostly the same adducts were observed after 2 hour treatments (**Table 5.3**), with the exception of three residues, Lys166, Lys207 and His391, which were only found at 4 hours and two residues, Lys188 and His464, which were only found at 2 hours. Apart from MDA where no adducts could be detected, all the amino acid residues found modified with the longer and lower treatment were ones already identified in **Table 5.1** after shorter time and higher concentration treatments.

**Table 5.2. Pyruvate kinase residues modified after 4 hours treatment with low concentrations of aldehydes.**

Modified Residues	Pyruvate kinase modified peptides (a <sup>b</sup> )	Theoretical mass of modified peptide	Observed mass of modified peptide	m/z (charge)	Ion score	Rt (min)	Aldehyde treatment (4 hours)					
							2 μM	10 μM	20 μM	100 μM	200 μM	
<b>Acrolein</b>												
Cys49	<b>MA</b> 44NTGIIC <sup>+58</sup> TIGPASR <sub>56</sub>	1359.72	1359.61	680.81 (2+)	80	15.97	-	✓	✓	✓	✓	
Cys152	<b>MA</b> 152C <sup>+58</sup> DENILWLDYK <sub>162</sub>	1468.69	1468.58	735.29 (2+)	91	19.57	✓	✓	✓	✓	✓	
Lys166	<b>MA</b> 163NIC*K <sup>+58</sup> VVDVGSK <sub>173</sub>	1275.68	1275.57	426.19 (3+)	26	11.56	-	-	-	-	✓	
Lys207	<b>MA</b> 207K <sup>+58</sup> GVNLPGAAVDLPVSEK <sub>224</sub>	1822.02	1821.83	608.28 (3+)	16	16.21	-	-	-	-	✓	
Lys207	<b>MA</b> 207K <sup>+96</sup> GVNLPGAAVDLPVSEK <sub>224</sub>	1860.04	1859.89	620.97 (3+)	44	16.47	-	-	-	-	✓	
Cys358	<b>MA</b> 343AEGSDVANAVLDGADC <sup>+58</sup> IMLSGETAK <sub>367</sub>	2494.16	2493.97	832.33 (3+)	118	21.22	-	-	-	✓	✓	
His391	<b>MA</b> 384EAEAAMFH <sup>+58</sup> R <sub>392</sub>	1118.52	1118.41	373.81 (3+)	46	11.64	-	-	-	-	✓	
Lys393	<b>MA</b> 393K <sup>+58</sup> LFELAR <sub>400</sub>	1062.61	1062.51	355.18 (3+)	37	14.66	-	-	-	-	✓	
Lys393	<b>MA</b> 393K <sup>+96</sup> LFELAR <sub>400</sub>	1100.62	1100.52	367.84 (3+)	39	14.83	-	-	-	-	✓	
Cys423	<b>MA</b> 423C <sup>+58</sup> LAAALIVLTESGR <sub>436</sub>	1473.82	1473.71	737.86 (2+)	108	20.72	-	✓	✓	✓	✓	
Cys474	<b>MA</b> 468GIFPVVC <sup>+58</sup> K <sub>475</sub>	919.52	919.44	460.72 (2+)	47	17.13	-	✓	✓	✓	✓	
Lys475	<b>MA</b> 468GIFPVVC*K <sup>+58</sup> DPVQEAWAEDVDLR <sub>489</sub>	2543.27	2543.10	848.71 (3+)	103	19.99	-	-	-	✓	✓	
<b>4-hydroxy-2-hexenal</b>												
Cys152	<b>SB</b> 152C <sup>+96</sup> DENILWLDYK <sub>162</sub>	1506.71	1506.61	754.31 (2+)	18	22.46	-	-	-	-	✓	
Cys152	<b>MA</b> 152C <sup>+114</sup> DENILWLDYK <sub>162</sub>	1524.72	1524.59	763.30 (2+)	46	20.12	✓	✓	✓	✓	✓	
Cys423	<b>MA</b> 423C <sup>+114</sup> LAAALIVLTESGR <sub>436</sub>	1529.85	1529.72	765.87 (2+)	77	22.37	✓	✓	✓	✓	✓	
Cys474	<b>MA</b> 468GIFPVVC <sup>+114</sup> K <sub>475</sub>	975.55	975.44	488.73 (2+)	26	16.76	-	-	✓	✓	✓	
Lys475	<b>MA</b> 468GIFPVVC <sup>+114</sup> DPVQEAWAEDVDLR <sub>489</sub>	2599.29	2599.11	867.38 (3+)	91	18.97	-	-	✓	✓	✓	
<b>Malondialdehyde</b>												
<i>No modifications detected</i>												

---

a (subscript) – amino acid position in the mature protein  
b (superscript) - mass difference corresponding to the modification  
Michael addition (MA) or Schiff-base formation (SB)

**Table 5.3. Pyruvate kinase residues modified after 2 hours treatment with low concentrations of aldehydes**

Modified Residues	Pyruvate kinase modified peptides (a <sup>b</sup> )	Theoretical mass of modified peptide	Observed mass of modified peptide	m/z (charge)	Ion score	Rt (min)	Aldehyde treatment (2 hours)					
							2 $\mu$ M	10 $\mu$ M	20 $\mu$ M	100 $\mu$ M	200 $\mu$ M	
<b>Acrolein</b>												
Cys49	<b>MA</b> <sub>44</sub> NTGI <b>C</b> <sup>+58</sup> TIGPASR <sub>56</sub>	1359.72	1359.62	680.82 (2+)	81	16.41	✓	✓	✓	✓	✓	
Cys152	<b>MA</b> <sub>152</sub> <b>C</b> <sup>+58</sup> DENILWLDYK <sub>162</sub>	1468.69	1468.59	735.30 (2+)	95	19.92	✓	✓	✓	✓	✓	
Lys188	<b>SB</b> <sub>187</sub> <b>QK</b> <sup>+40</sup> GPDFLVTEVENGGFLGSK <sub>206</sub>	2161.11	2160.92	721.31 (3+)	67	21.15	-	-	✓	✓	✓	
Cys358	<b>MA</b> <sub>343</sub> AEGSDVANAVLDGAD <b>C</b> <sup>+58</sup> IMLSGETAK <sub>367</sub>	2494.16	2493.99	832.34 (3+)	105	21.57	-	-	✓	✓	✓	
Lys393	<b>MA</b> <sub>393</sub> <b>K</b> <sup>+58</sup> LFELAR <sub>400</sub>	1062.61	1062.52	532.27 (2+)	27	15.07	-	-	-	-	✓	
Cys423	<b>MA</b> <sub>423</sub> <b>C</b> <sup>+58</sup> LAAALIVLTESGR <sub>436</sub>	1473.82	1473.72	737.87 (2+)	87	21.15	✓	✓	✓	✓	✓	
His464	<b>SB</b> <sub>462</sub> QAH <sup>+40</sup> LYR <sub>467</sub>	826.44	826.34	414.18 (2+)	15	10.37	-	-	-	-	✓	
Cys474	<b>MA</b> <sub>468</sub> GIFPV <b>V</b> <b>C</b> <sup>+58</sup> K <sub>475</sub>	919.52	919.44	460.73 (2+)	48	17.48	-	✓	✓	✓	✓	
Lys475	<b>MA</b> <sub>468</sub> GIFPV <b>V</b> <b>C</b> <sup>+58</sup> <b>K</b> DPVQEAWAEDVDLR <sub>489</sub>	2543.27	2543.10	848.71 (3+)	129	20.14	-	-	-	✓	✓	
<b>4-hydroxy-2-hexenal</b>												
Cys152	<b>MA</b> <sub>152</sub> <b>C</b> <sup>+114</sup> DENILWLDYK <sub>162</sub>	1524.72	1524.59	763.30 (2+)	85	20.23	✓	✓	✓	✓	✓	
Cys423	<b>MA</b> <sub>423</sub> <b>C</b> <sup>+114</sup> LAAALIVLTESGR <sub>436</sub>	1529.85	1529.71	765.87 (2+)	95	20.20	✓	✓	✓	✓	✓	
Cys474	<b>MA</b> <sub>468</sub> GIFPV <b>V</b> <b>C</b> <sup>+114</sup> K <sub>475</sub>	975.55	975.44	488.73 (2+)	22	16.96	-	-	✓	✓	✓	
Lys475	<b>MA</b> <sub>468</sub> GIFPV <b>V</b> <b>C</b> <sup>+114</sup> <b>K</b> DPVQEAWAEDVDLR <sub>489</sub>	2599.29	2599.09	867.37 (3+)	70	19.94	-	-	✓	✓	✓	
<b>Malondialdehyde</b>												
<i>No modifications detected</i>												

a (subscript) – amino acid position in the mature protein

b (superscript) - mass difference corresponding to the modification

Michael addition (MA) or Schiff-base formation (SB)

As observed for shorter treatment times, there was an inverse relationship between enzyme activity and percentage of peptides modified for longer treatments, although the total level of modification was significantly lower for these lower treatment concentrations (Figure 5.7).

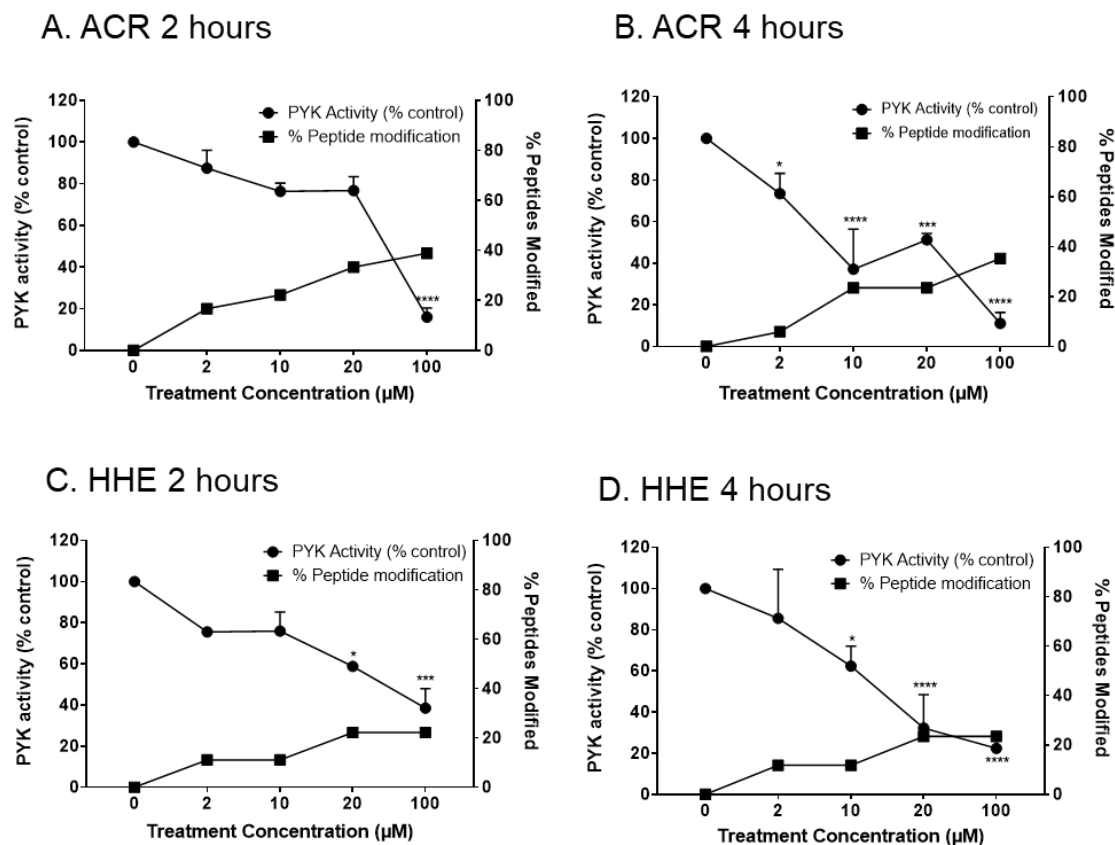
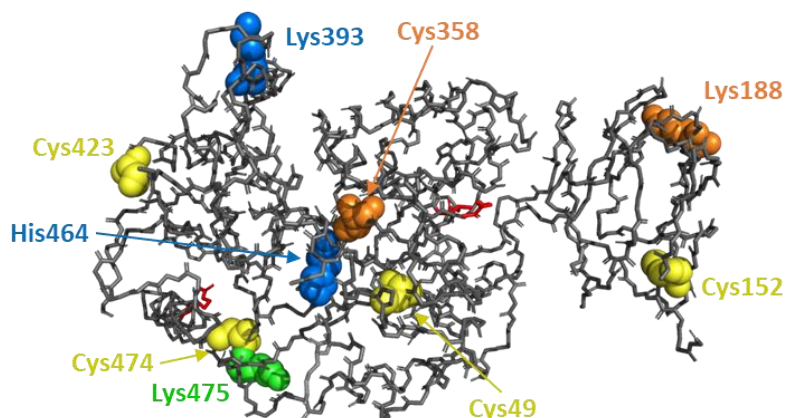


**Figure 5.7. Inverse relationship between the dose-dependent effect of aldehydes on the activity of pyruvate kinase in vitro and the percentage of modified pyruvate kinase peptides identified.** Pyruvate kinase was treated with 2 μM, 10 μM, 20 μM and 100 μM of each aldehyde for 2 hours or 4 hours before the assessment of its activity (n=3; Mean ± SEM; \* p < 0.1 \*\* p < 0.01, \*\*\* p < 0.001 and \*\*\*\* p < 0.0001). Figure from [423].

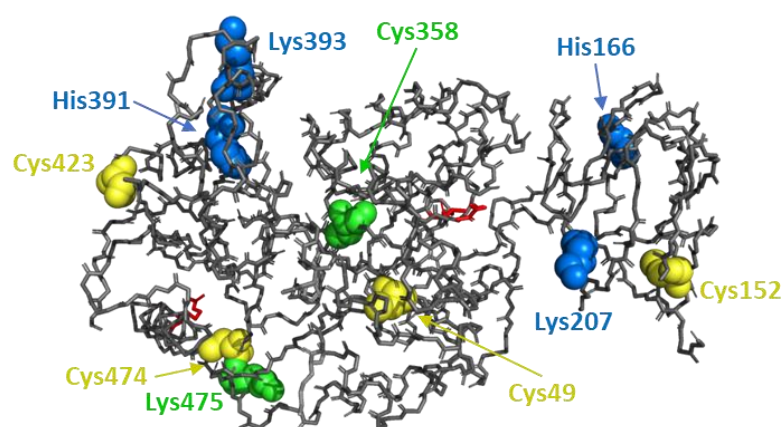
The sites of modifications for these treatments were also mapped to the 3D structure and are shown in Figure 5.8, where it can be seen that cysteine residues were the most sensitive to both acrolein and HHE modification. These were also mapped onto the hydrophobicity models (Figure 5.9) but once again no obvious correlation between the sites of modification and hydrophobicity was apparent.



A. ACR (2 hours)



B. ACR (4 hours)



C. HHE (2 and 4 hours)

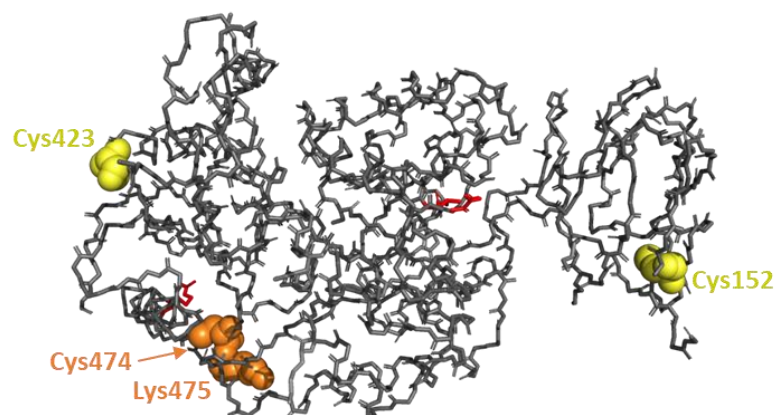


**Figure 5.8. Mapping of lipoxidation adducts formed at low concentrations for 4 h treatments.** Backbone structure with modified residues indicated in space-fill form, showing the location of adducts of acrolein at 2 h (A); acrolein at 4 h (B) and HHE at both time points (C). The modified residues are color-coded with yellow indicating those found only at 10  $\mu\text{M}$ , orange for those found additionally at 20  $\mu\text{M}$ , green for those found additionally at 100  $\mu\text{M}$  and blue for ones found additionally at 200  $\mu\text{M}$ . Figure from [423].

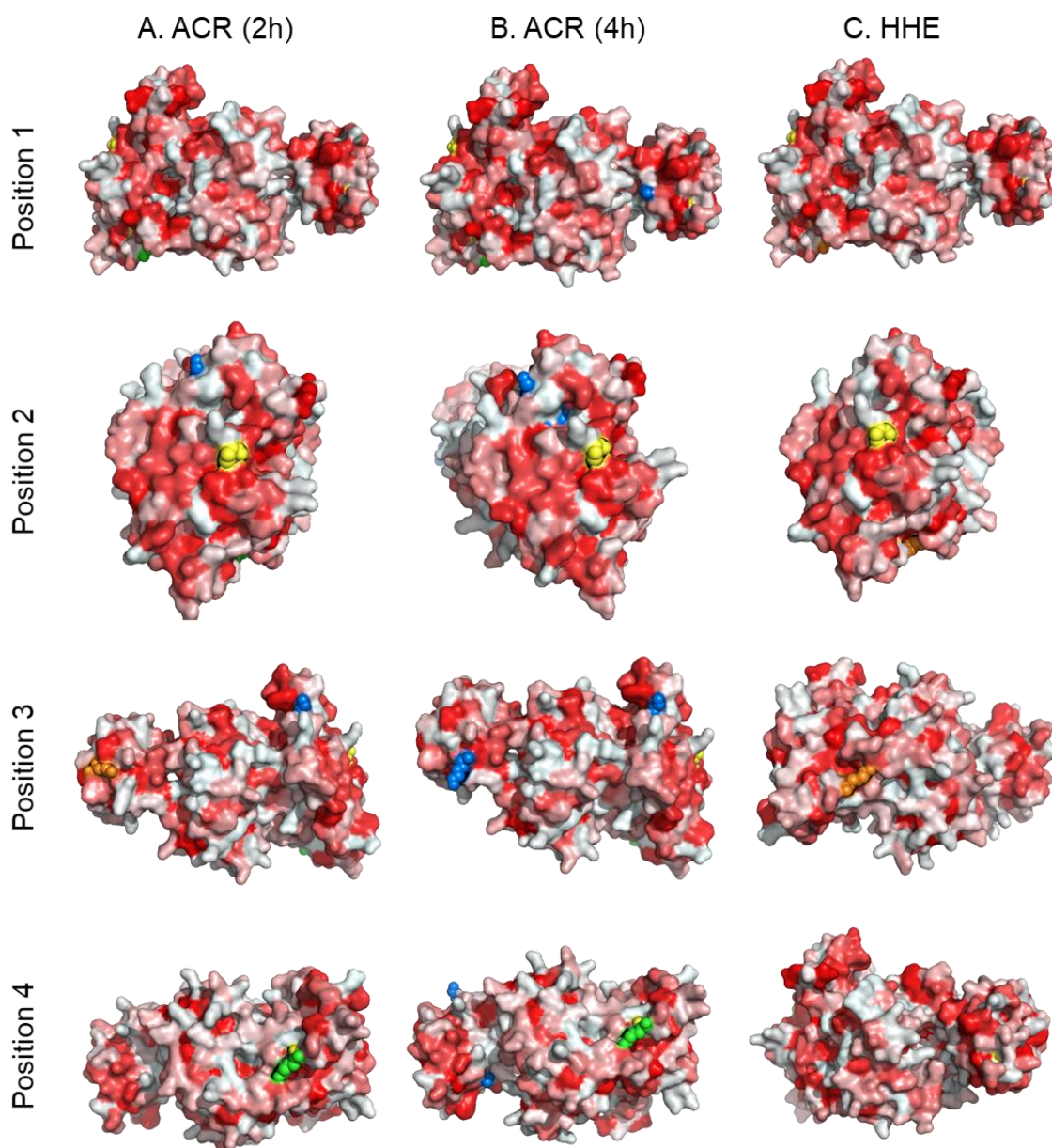


**Figure 5.9. Space filling models of pyruvate kinase showing surface hydrophobicity and sites of adduction at low treatment concentrations.** Surface views with hydrophobicity mapped in red and showing the location of adducts of acrolein (A), HHE (B) and MDA (C). The modified residues are color-coded with yellow indicating those found only at 10  $\mu\text{M}$ , orange for those found additionally at 20  $\mu\text{M}$ , green for those found additionally at 100  $\mu\text{M}$  and blue for ones found additionally at 200  $\mu\text{M}$ . Figure from [423].

#### 5.3.4. Comparison of aldehyde effects on MCF-7 cell pyruvate kinase activity and cell viability

To investigate the ability of the aldehydes to cause inhibition of pyruvate kinase in a cellular environment, MCF-7 cells were treated in culture with aldehydes and their impact on extractable pyruvate kinase activity and cell viability was tested. The data here presented was acquired in collaboration with two placement students. These results are published, and the students contribution was acknowledged as second and third authors [423].

Cells were treated with the lower range of concentration tested *in vitro* for acrolein, MDA and HHE for 2 hours or 24 hours (**Figure 5.10**). Two hour treatments at 10  $\mu\text{M}$  acrolein inhibited the activity of pyruvate kinase to 20% of control (**Figure 5.10A**), while higher concentration treatments had a more severe effect on the activity of the enzyme. Interestingly, cellular pyruvate kinase activity seemed to be less sensitive to 24-hour acrolein treatment with 2-10  $\mu\text{M}$  acrolein, although at higher concentrations the effect was very similar to 2 hours. In contrast, the cell viability showed a slightly different response to treatments at the two time points. Neither treatment time with acrolein caused significant loss of cell viability until concentrations of 100  $\mu\text{M}$  (**Figure 5.10B**). HHE caused a similar, though more gradual, decrease in the enzymatic activity. The 2 h treatment at 10  $\mu\text{M}$  inhibited the activity of pyruvate kinase to 60% of control (**Figure 5.10C**) and higher concentration treatments caused an even more severe effect. Similar to acrolein, pyruvate kinase activity seemed to be less sensitive to 24-hour HHE treatment at all concentrations, but in contrast with acrolein, these treatments only caused a maximum of 20% of loss in cell viability even at higher concentration treatments (**Figure 5.10D**). The effect of MDA on the cellular pyruvate kinase activity was similar to, though smaller than HHE (**Figure 5.10E**). While the concentration-dependent loss of activity appeared greater for the 2 hour treatment, MDA caused no significant loss of viability at any concentration or time point, in contrast with the other two aldehydes tested, especially ACR (**Figure 5.10F**).

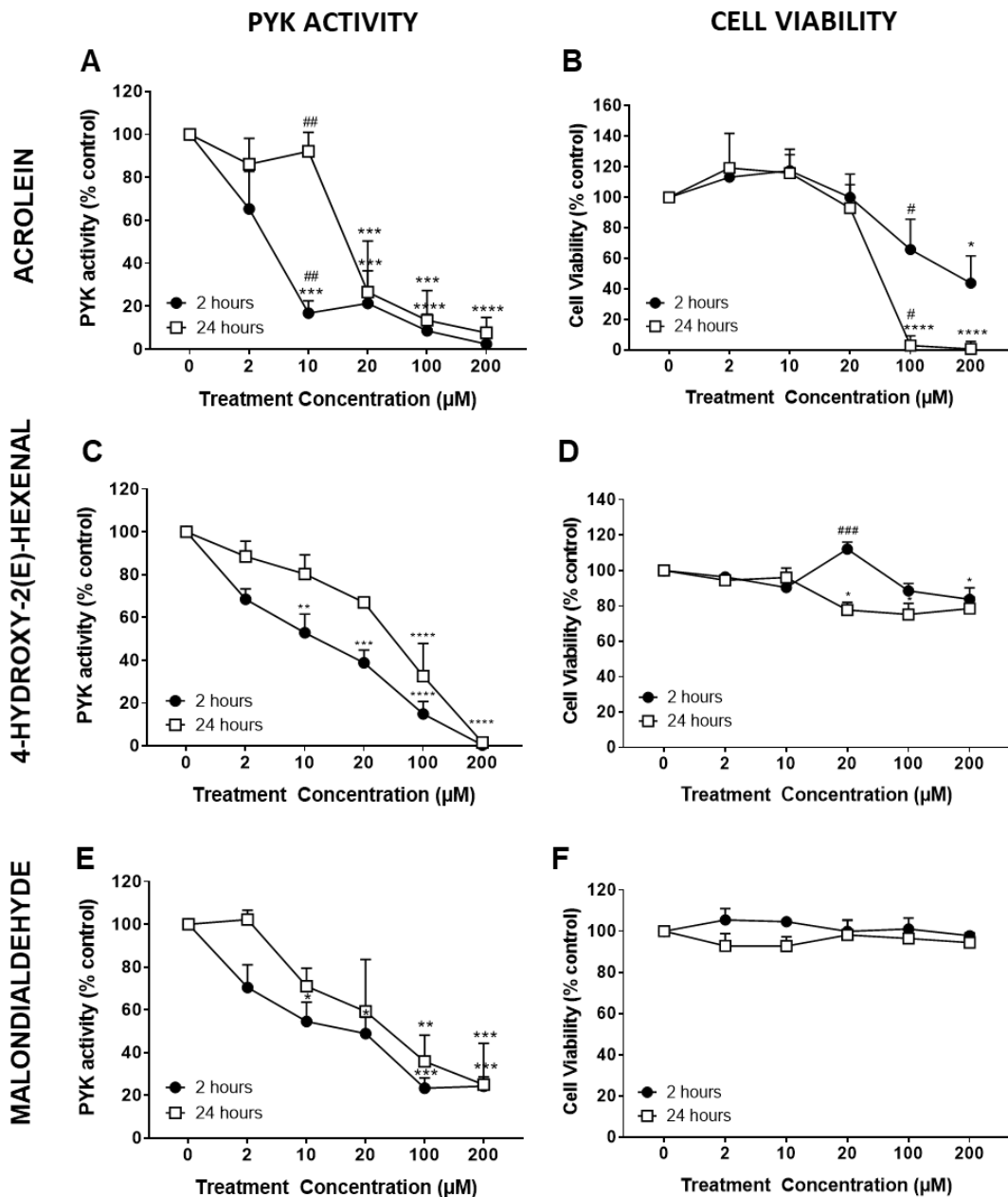


**Figure 5.10. Dose- and time-dependence of aldehyde treatment on the activity of pyruvate kinase and viability of aldehyde-treated MCF-7 cells.** Pyruvate kinase activity is shown on the left for acrolein (A), 4-hydroxyl-2(E)-hexenal (C) and malondialdehyde (E), while cell viability is shown on the right: acrolein (B), 4-hydroxyl-2(E)-hexenal (D) and malondialdehyde (F). Cells were treated with 2 μM, 10 μM, 20 μM, 100 μM and 200 μM of each aldehyde for 2 hours or 24 hours before proteins were extracted and 10 μg of extract were used for pyruvate kinase activity to be assessed. Cell viability assays were performed with n=3 for MDA and HHE and n=4 for ACR (Mean ± SEM; \* p<0.1 \*\* p<0.01, \*\*\* p<0.001 and \*\*\*\* p<0.0001). \* Comparison between treatments and control for each incubation time. # comparison between incubation times. Figure from [423] (This data was acquired by the co-authors Tanzim Ahmed and Will L Dann and used in this thesis with their permission).

LC-MS/MS analysis of the cell extracts after 10  $\mu\text{M}$  and 200  $\mu\text{M}$  acrolein treatment allowed for modifications of cellular pyruvate kinase to be mapped. Although the sequence coverage was low, modifications on Cys152 and Cys358 were detected (**Table 5.4** and **Figure 5.11**). This data agrees with the data from the *in vitro* treatments, where it was identified that these residues were highly susceptible to adduct formation.

**Table 5.4. Pyruvate kinase residues modified after treatment of MCF-7 cells with acrolein**

Treatment	Sequence coverage	Modification	Modified amino acid	Peptide	Ion Score
200 $\mu\text{M}$ 24h	29%	ACR (+58Da)	Cys152	CDENILWLDYK	61
200 $\mu\text{M}$ 2h	32%	ACR (+58Da)	Cys152	CDENILWLDYK	42
10 $\mu\text{M}$ 24h	47%	-	-	-	-
10 $\mu\text{M}$ 2h	51%	ACR (+56Da)	Cys358	AEGSDVANAVLDGAD $\underline{\text{C}}$ IMLSGETAK	82
Control 2h	49%	none	-	-	-
Control 24h	56%	none	-	-	-

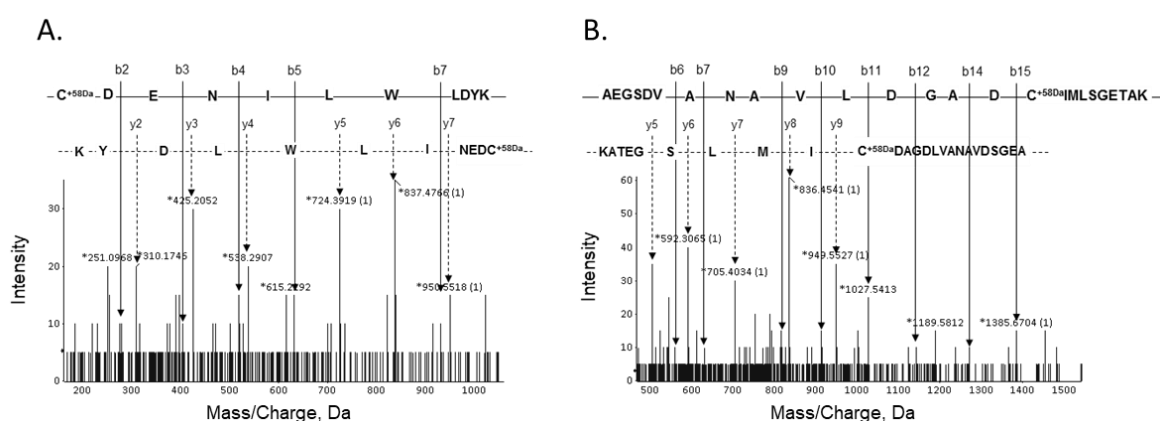


**Figure 5.11. MS/MS spectra of different pyruvate kinase tryptic peptide from MCF-7 cellular extracts.**  $\underline{\text{C}}$ DENILWLDYK (A) and AEGSDVANAVLDGAD $\underline{\text{C}}$ IMLSGETAK (B) modified on a cysteine residue by ACR. The y and b ions indicated by the arrows confirm the peptide sequence and the modification on the cysteine residue. Figure from [423].

### 5.3.5. Acrolein effect on the MCF-7 cells metabolism

The previous sections suggest pyruvate kinase activity to be inhibited in cell by treatment with acrolein. To assess the effect of the treatment on glycolysis, the extracellular acidification rate (ECAR) was measured through real-time and live cell analysis upon 2 hours of acrolein treatment, using a Seahorse XF Analyzer. **Figure 5.12** shows the ECAR profile for MCF-7 cells untreated (control) and acrolein treatment at different concentrations.

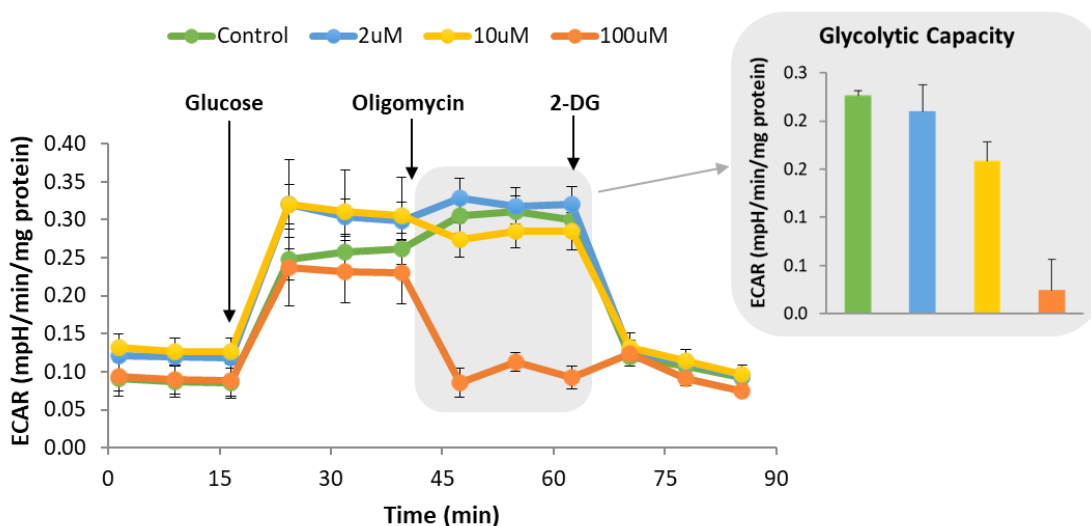


**Figure 5.12. Extracellular acidification rate (ECAR) profile of untreated and acrolein-treated MCF-7.** Cells were treated with 2, 10 or 100  $\mu$ M acrolein prior to the assay. Addition of glucose at 15 min promoted glycolysis and the acidification increase by release of protons ( $H^+$ ) by the cells. Oligomycin inhibits ATP synthase, driving glycolysis to its maximum rate. Later, a competitive inhibitor of glucose (2-DG) is added to shut down glycolysis.

Upon acrolein treatment, a dose-dependent decrease on the glycolytic capacity was observed. Glycolytic capacity is the maximum ECAR reached by a cell after addition of oligomycin which effectively shuts down oxidative phosphorylation and drives the cell to use glycolysis to its maximum capacity.

To further investigate the effect of the inhibition of pyruvate kinase in a cellular metabolism, the metabolomic profile of MCF-7 cells was analysed before and after acrolein treatment. **Figure 5.13** shows the standard  $^1\text{H}$  NMR spectrum of the metabolites extract from MCF-7 cells, where a multitude of signals was detected, reflecting the complex sample composition.

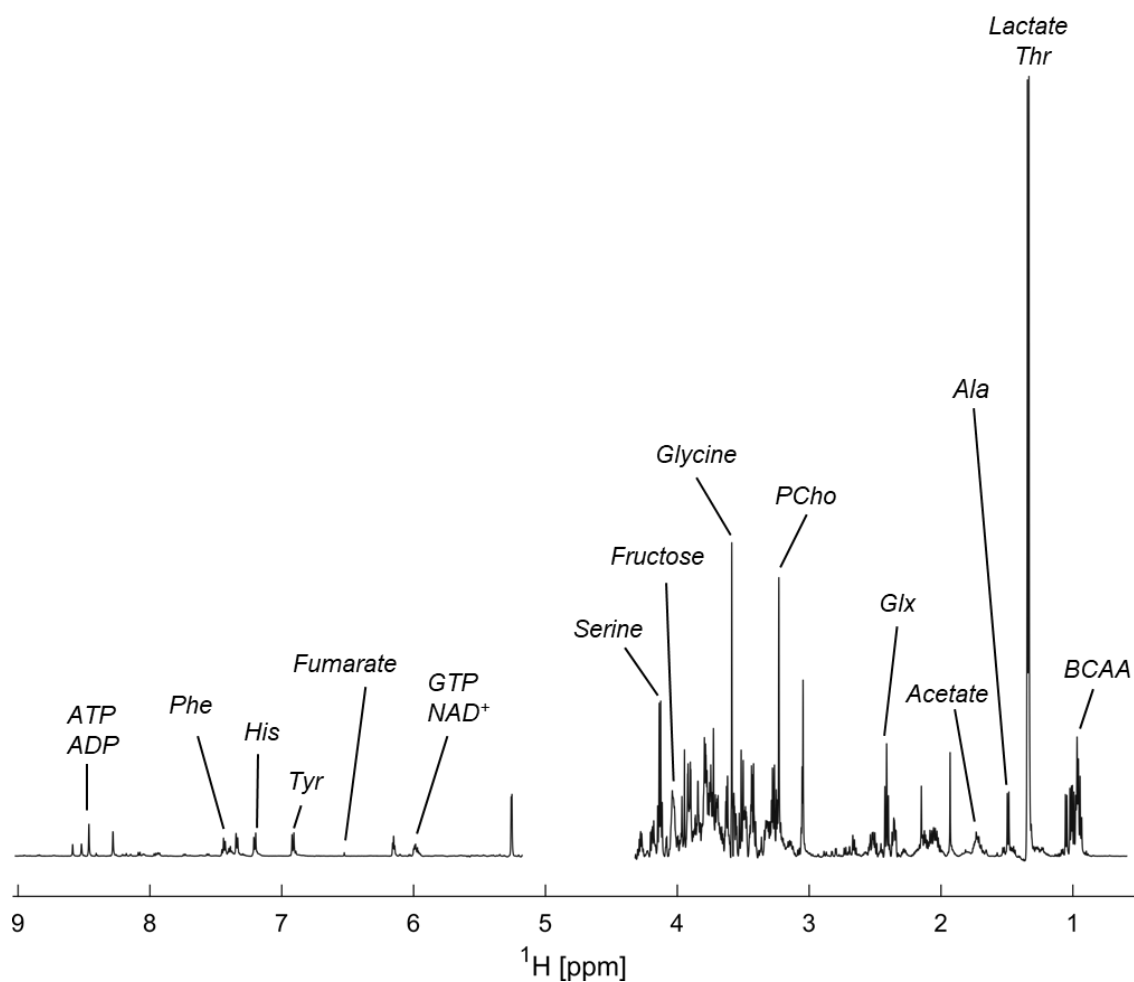


**Figure 5.13. Representative  $^1\text{H}$  NMR spectrum of the metabolome of MCF-7 cells.** Some assignments are indicated: three-letter codes are used for amino acids, ADP - adenosine diphosphate, ATP - adenosine triphosphate, BCAA - branched chain amino acids, NAD - nicotinamide adenine dinucleotide, PCho - phosphocholine.

The low frequency region ( $\delta$  0-3) shows resonances from several amino acids including the branched chain amino acids, alanine, threonine and glutamate, as well as organic acids such as lactate and acetate. In the mid-frequency region ( $\delta$  3-5.5) additional metabolites were detected, including glycine, choline-containing compounds, fructose and serine. The high-frequency region ( $\delta$  5.5-9) is characterized by signals arising from aromatic amino acids such as phenylalanine and tyrosine, organic acids such as fumarate and nucleotides such as ADP, ATP and NAD<sup>+</sup>. It is worth noting the high intensity of the peak corresponding to lactate in the low frequency region, which is likely to occur as these are cancer cells and therefore known to convert most of glucose to lactate regardless of the availability of O<sub>2</sub> (the Warburg effect) [270]. In total, 27 compounds were identified in the cells providing significant information on the metabolic composition and setting the basis for interpreting the effect of acrolein exposure. MCF-7 cells were exposed to 2  $\mu$ M, 10  $\mu$ M and 100  $\mu$ M acrolein for 2 and 24 hours followed by metabolites extraction for analysis. The concentrations and time range of the treatments were chosen based on the cell viability results presented in **Figure 5.10**. **Figure 5.14** shows the <sup>1</sup>H NMR spectra for two hour exposure to acrolein at the three different concentrations tested and its corresponding control (non-exposed).



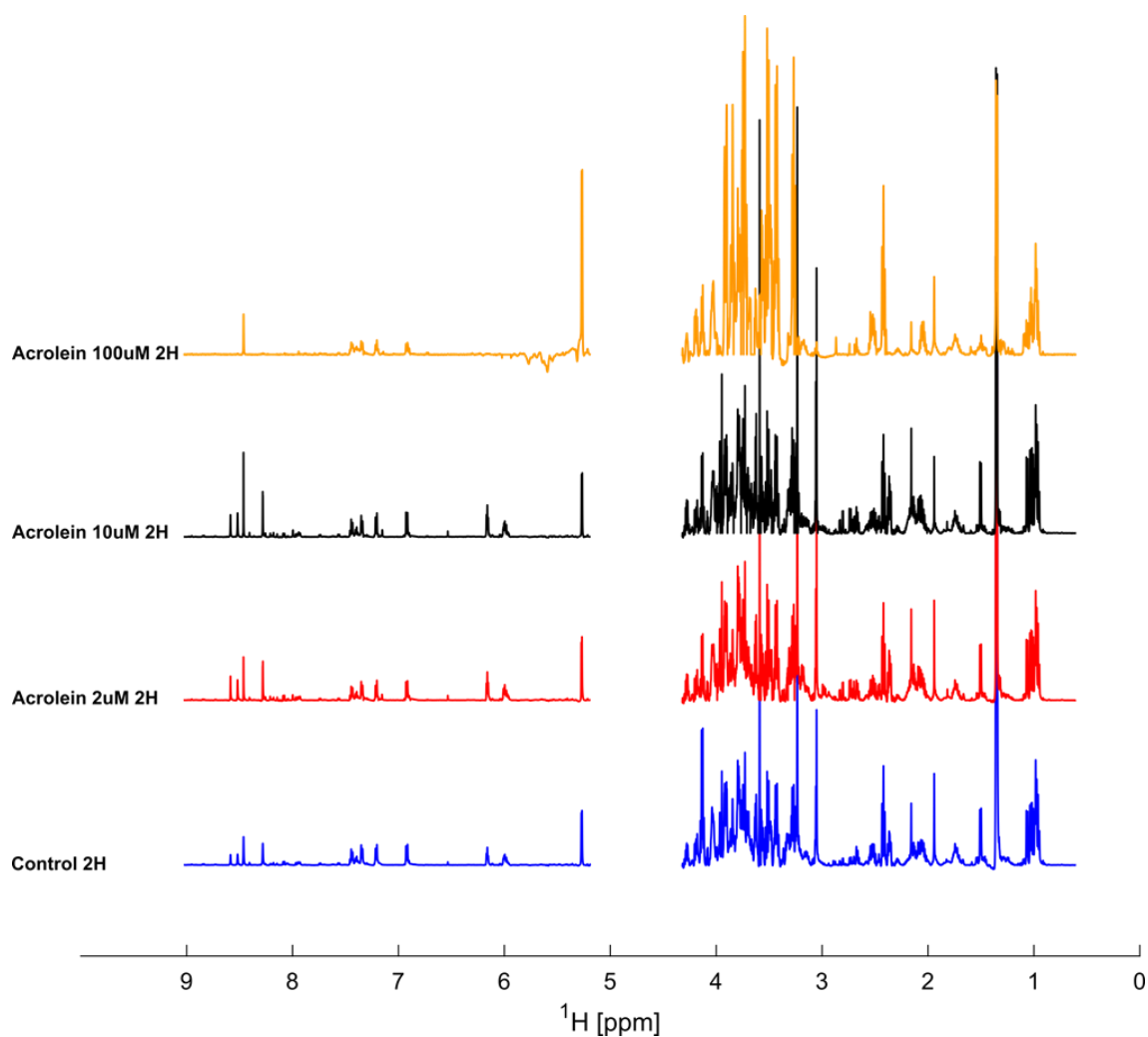


**Figure 5.14.**  $^1\text{H}$  NMR spectra of the metabolome of MCF-7 cells untreated and upon treatment with  $2\ \mu\text{M}$ ,  $10\ \mu\text{M}$  and  $100\ \mu\text{M}$  acrolein for two hours.

A visual comparison of the four spectra allows for some differences to be proposed, such as a decrease in the levels of lactate, glutamate and fumarate in the exposed cells. Additionally, these spectra demonstrate that acrolein caused the metabolome of MCF-7 cells to change in a concentration-dependent manner, with higher concentrations causing stronger effects. To better evaluate the effect of acrolein on the metabolome at different concentrations and times of treatment, the peaks from the spectra were integrated and the intensity of 18 metabolites is shown in **Figure 5.15**. The metabolites chosen for integration were based on the non-ambiguity of their identification, no overlap with other peaks on the spectrum and a good signal to noise ratio of their corresponding peak.

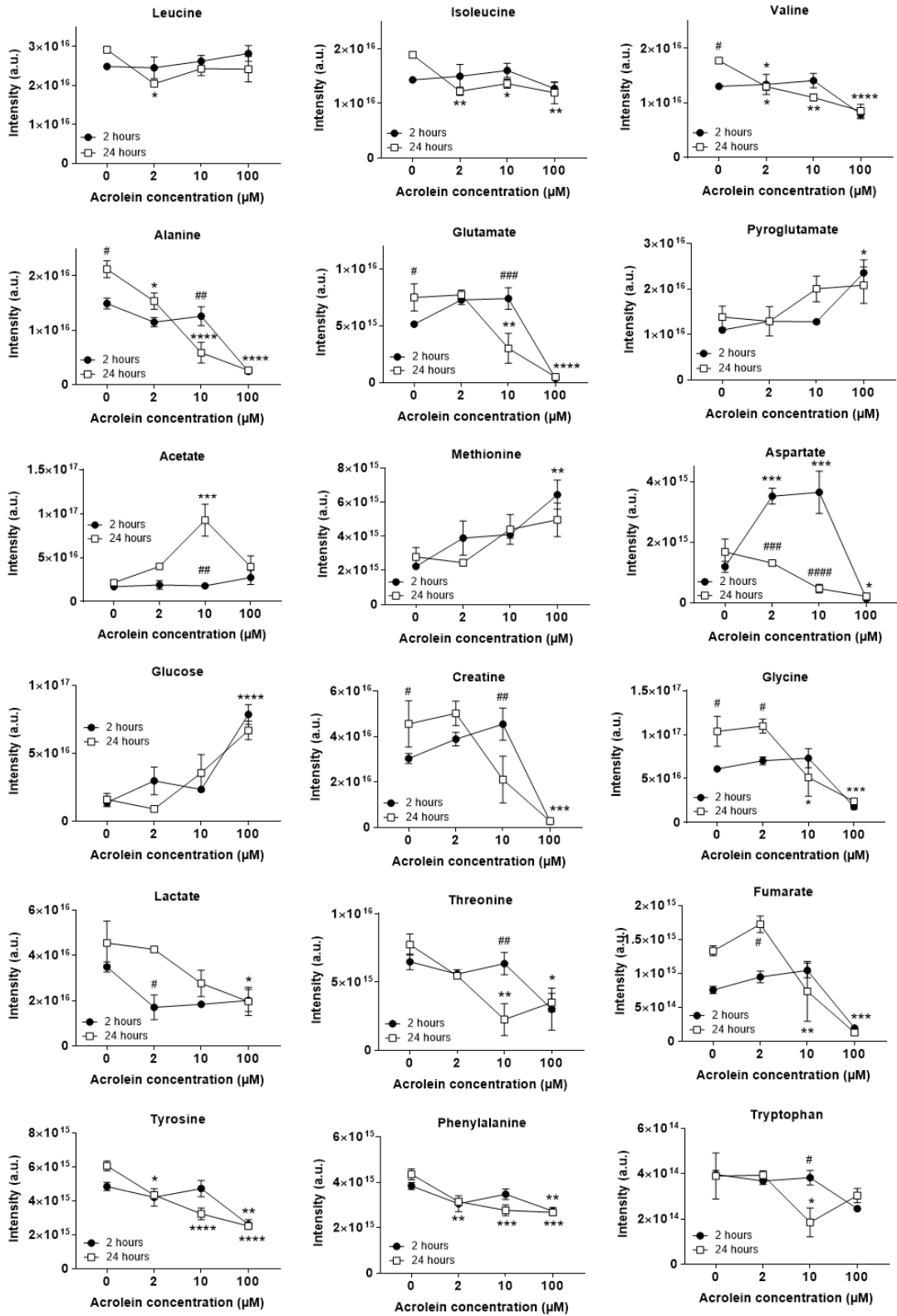


**Figure 5.15. Dose and time-dependence of acrolein treatment on the metabolism of MCF-7 cells.** Cells were exposed to 2 μM, 10 μM and 100 μM of acrolein for 2 hours or 24 hours followed by metabolites extraction and analysed by <sup>1</sup>H NMR. (n=3; Mean ± SEM; \* p<0.1 \*\* p<0.01 \*\*\* p<0.001 \*\*\*\* p<0.0001). \* Comparison between treatments and control for each incubation time. # comparison between incubation times.

The metabolome analysis showed that there was a concentration- and time-dependent effect of acrolein in the cellular metabolism including metabolites from glycolysis, the TCA cycle and amino acid metabolism. At 2h of exposure to  $\mu\text{M}$  acrolein, valine and phenylalanine were lower than in the control. A higher concentration of 10  $\mu\text{M}$  acrolein showed further decrease in valine and an increase in aspartate, while for phenylalanine and all the other metabolites no changes were observed. However, 100  $\mu\text{M}$  acrolein completely changed the cellular metabolism with pyroglutamate, methionine and glucose higher than the control, and almost all of the other metabolites identified were lower than the control including alanine, glutamate, aspartate, glycine, lactate, threonine and fumarate. The profile at 24 hours was similar, but a more pronounced metabolic response was apparent for almost all metabolites at this time-point. Aspartate was observed to be lower than the control at 24 hours, in contrast to 2 hours. Also for 2  $\mu\text{M}$  acrolein, it was observed that there was an increase in lactate, and for 10  $\mu\text{M}$  acrolein the levels of threonine were lower for the 24 hour treatment in comparison to the 2 hour. Additionally, alanine and glutamate decreased more steeply after the 24 hour treatments.

#### 5.4. Discussion

Pyruvate kinase is an important regulatory enzyme in glycolysis, and changes in its expression level, isoform profile and activity have been linked to the switch to aerobic glycolysis in cancer and proliferating cells [350]. Cancer cells also have an altered redox status [392] leading to increased lipid peroxidation and the formation of electrophilic short-chain carbonyl species, but previously there have been few studies of the effects of these carbonyl species on pyruvate kinase. To address this question, the inhibition of pyruvate kinase activity was measured following treatment with acrolein, HHE and MDA *in vitro*, and the formation of protein-aldehyde adducts was monitored by LC-MS/MS. A clear inverse relationship was observed between the extent of adduct formation and the activity of pyruvate kinase for all three aldehydes, and acrolein was found to cause the greatest inhibition. MDA had no significant effect until much higher concentrations were used, probably due to its chemistry that only allows for reaction with lysines to form Schiff's base adducts. However, like the other aldehydes, it can also cause cross-linking.

The mass spectrometry analysis of the profiles of modification showed different susceptibility of pyruvate kinase residues to each aldehyde. The extent of inhibition was dependent on the length of incubation and the treatment concentration, with longer treatments causing loss of activity at lower and physiological concentrations, suggesting that reversibility of these adducts was not a significant factor. Pyruvate kinase extracted from treated cells showed higher susceptibility to modification, indicated by a greater loss of activity at lower concentration than found *in vitro*, and no correlation with the loss of cell viability was observed, suggesting that the loss of activity is not due to general cell dysfunction. It has been reported previously that tumour cells can survive and proliferate with very low pyruvate kinase activity [425], supporting the suggestion that loss of pyruvate kinase activity does not result in cell death. The susceptibility of individual residues to modification varied according to the aldehyde, and even ACR and HHE, which are both  $\alpha,\beta$ -alkenals, showed different modification profiles. Although there were six common residues (Cys326, Cys358, Lys393, Cys423, Cys474, Lys475) modified by these aldehydes following short treatments at higher concentrations, there were also several differences. This may be due to the smaller size of acrolein and a corresponding ability to access more buried residues, such as Cys49, Lys207 and His464. Some additional residues modified by HHE seemed to be surface accessible, including Lys188 and Lys247, and it is unclear why these were not adducted by acrolein; mapping of the surface hydrophobicity did not suggest that modification with the longer or shorter aldehydes correlated strongly with this factor. The only overlap between the three aldehydes were the modifications on Lys393 and Lys475. It is important to note that other modifications might have been present but not detected by the methods used, such as cross-linking.

It is important to attempt to understand the potential functional effects of the identified modifications on different residues. Two of the cysteine residues found modified by acrolein and HHE have been previously reported to be modified by oxidation [405] or electrophilic attack by HNE and ONE [273]. While Cys326 was only modified at higher concentration, Cys358 was modified at lower concentration. Cys326 is buried in the tetramer form but accessible in the monomeric form, and a modification at this site could prevent the reformation of the active tetramer [405], or destabilize the intact tetramer. In PKM1 this residue is protected, which is likely to account for the requirement of a high concentration of aldehyde to detect its modification. Cys358 is located close to the substrate binding site, and has previously been reported to regulate pyruvate kinase activity by oxidation, promoting tumour growth and survival in a pro-oxidative cellular status [403]. Cys423 was another cysteine residues shown to be sensitive to ACR and HHE adduct formation, which together with Cys152. Cys423 is located at the subunit interface, and a modification on this residue could also potentially destabilize the tetrameric form. Cys424 plays a role in protein-protein interaction and allosteric regulation by F-2,6-bP, and has been reported to be modified by electrophilic carbonyl species [273]. However, this residue is only present in the PKM2 isoform and therefore was not found modified in the *in vitro* study described here. Lysine residues can also be modified, and it is important to understand their role in the enzyme activity. For example, Lys305 was found modified at the highest MDA treatment and modification of this residue by acetylation had been reported to reduce pyruvate kinase activity by lowering the affinity for PEP, or triggering the degradation of the enzyme itself under nutrient-deplete conditions [426].

The inverse relationship between pyruvate kinase activity and the percentage of modified peptides observed suggests that the accumulation of adducts, rather than a modification on a specific residue, contributes to conformational change leading to major loss of activity. However, the modification on a single residue cannot be discounted as a possible cause of the loss in activity. For instance, losses in activity were observed at 38  $\mu\text{M}$  acrolein and HHE after 10 mins and 10  $\mu\text{M}$  after 4 hour treatments, thus the adducts detected on these conditions (Cys 152, Cys358, Cys423, His 464, Cys474) are most likely to be involved. The fact that MDA did not cause an inhibition of activity on short treatments, but the modification of many lysines were still detected by LC-MS/MS, suggests that none of these residues are essential for the normal functioning of the enzyme. Instead these residues may well be acting as surface decoys for modification to prevent oxidative damage to more critical residues. The eventual loss of activity above 1 mM MDA is probably a result of conformational changes and unfolding of the protein, rather than modification on specific amino acid residues. Nevertheless, lysine residues have been reported to be involved in the regulation of pyruvate kinase, for example Lys433 can interact with phosphotyrosine-

containing proteins leading to the inhibition of the enzyme by release of F-1,6-bP [427-429]. On the other hand, proteolysis has also been shown to be inhibited by crosslinking of lysine residues on enzymes [55].

The extractable pyruvate kinase activity in the human breast cancer cell line MCF-7 was found to be extremely susceptible to cellular acrolein treatment, with more than 80% loss of activity after 2 hours of 10  $\mu$ M acrolein, in contrast to an inhibition of about 30% *in vitro* with the same treatment. MDA also had a much stronger inhibitory effect on cellular pyruvate kinase, compared to the minimal effect on activity *in vitro*, whereas the effects of HHE *in vitro* and *in vivo* were similar. It is important to note that the treatments *in vitro* and in cells cannot be directly compared, as the *in vitro* worked was carried out using the PKM1 form from rabbit muscle, whereas the MCF-7 cells have been shown to mainly contain the PKM2 isoform [430]. PKM2 can be allosterically regulated and readily dissociates into dimers or monomers with much lower activity, in contrast to PKM1 which is found constitutively in the active, tetrameric form. Despite the large number of different proteins in cells, pyruvate kinase was highly susceptible to inactivation by the aldehyde treatment. However, it is not clear which mechanism, irreversible modification, increased degradation or decreased synthesis of the enzyme, lead to the loss of activity. Previous studies on HNE and ONE using click chemistry followed by shot-gun proteomics identified isoforms M1, M2 and R as susceptible to lipoxidation [431], and another study reported PKM2 to be modified by the same compounds in human colorectal carcinoma (RK) cells [273]. These observations support the hypothesis that the loss in activity is related to direct pyruvate kinase modification by the aldehydes.

Interestingly, for all treatments the loss of activity at low treatment concentrations was less pronounced after 24 hours than 2 hours, which suggest that during longer treatment defence mechanisms are activated by the cell to overcome the loss of activity. In fact, pyruvate kinase has a relatively high turnover rate with half-life of 0.7 days [432], which could explain the recovery of enzyme activity at 24 hours at lower concentrations of aldehyde, although this turnover rate was not measured under the lipoxidative stress conditions of the experiments described in this thesis. It is also known that electrophilic modification of proteins, by HNE or analogues, signals for protein degradation and recycling by the 20S proteasome [433]. However, high concentration treatments can cause cross-linking [434] and protein aggregation, which inhibits the proteasome and leads to cell death [435].

During transformation of cells to a tumorigenic phenotype, pyruvate kinase isoforms and activity have been reported to change in order to switch to aerobic glycolysis (the Warburg effect) [398], resulting in an increase in the production of lactate by glucose-dependent pathways. This study suggests that oxidative modification can also change PKM2 activity

and consequently cause changes in metabolic response. It has been suggested that inhibition of pyruvate kinase causes a backing-up of metabolites in glycolysis as far as glucose-6-phosphate, leading to an increased flux through the pentose phosphate pathway that facilitates antioxidant defence and the synthesis of nucleotides [406]. Despite the low activity of pyruvate kinase, cancer cells are still able to maintain high lactate production, so it was suggested that rather than complete inhibition of pyruvate kinase, PKM2 has a high  $K_m$  for PEP which results in a different flux through glycolysis supporting both lactate production and pentose phosphate pathway [436]. However, pyruvate kinase is highly susceptible to oxidative and electrophilic attack, and there is evidence of elevated levels of oxidants and antioxidants in cancer [437]. This is supported by the data presented in this study as well as others [273, 403, 405, 407]. In the case of inhibition by electrophilic species, it seems likely that increased flux through the pentose phosphate pathway and altered metabolic state increases protein synthesis and maintains cellular functioning.

The decrease in the glycolytic capacity of the cells upon acrolein treatment, confirms the data discussed above suggesting that upon treatment the cellular glycolysis is reduced, and cells switch their metabolism for cell survival and proliferation. Additionally, an NMR based metabolomics approach was used to confirm these changes in the cellular metabolic state. As discussed above, acrolein decreased the activity of pyruvate kinase and consequently the amount of pyruvate being produced through glycolysis. However, the treatments did not show any effect on the cell viability until 100  $\mu\text{M}$  acrolein was reached suggesting that the cells were changing their metabolism and surviving despite the decrease in pyruvate kinase activity. The results of the metabolome analysis showed that acrolein induced changes in amino acid, energy and oxidative stress-related metabolism. The decrease in pyruvate generated from glucose metabolism resulted in utilization of alternative pathways to overcome this, since pyruvate is crucial in cancer cells for conversion into lactate required for invasion and metastasis [438]. This hypothesis was confirmed by no statistically significant differences being observed in the amount of lactate after treatments, where only 100  $\mu\text{M}$  acrolein after 24 hours was able to induce a decrease. The reduced pyruvate kinase activity was compensated for in MCF-7 cells by the production of pyruvate and macromolecules via glucose independent pathways. It has been reported that alanine consumption is increased when pyruvate levels decrease [439], and the decrease in alanine and glutamate observed at 24 hours treatment suggests that these could be being used by the MCF7 cells to fuel the tricarboxylic acid (TCA) cycle, lipid metabolism and to be converted to pyruvate [440]. Another alternative is for pyruvate to be produced from tyrosine, which itself can be produced from phenylalanine [441], and both of these aromatic amino acids showed a significant decrease at 24 hours treatment, suggesting that this may be another pathway which the cells are using to overcome the

lack of pyruvate generation from glucose. Tyrosine can also be converted to fumarate [442], but the decrease in the levels of fumarate observed suggests that this pathway is not being activated, or that fumarate is readily being converted into other metabolites. In fact, cancer cells tend to favour the conversion of pyruvate into lactate rather than using the TCA cycle, so the use of aromatic amino acids to produce pyruvate over supporting the TCA cycle might be expected. A limitation of this metabolomic approach was that no metabolites from the pentose phosphate pathway were detected, so no inferences can be made from these results on whether metabolism is directed towards this pathway. However, accumulation of glucose was not observed, except at the highest acrolein concentration, suggesting that glucose was still being used despite the inhibition of pyruvate kinase.

Several other amino acids were found to vary in response to acrolein in addition to the ones mentioned above, and these different amino acids are involved in different metabolic pathways. For example, valine is metabolised to carbohydrates, leucine to fats and isoleucine to both. After acrolein treatment, isoleucine, valine and threonine were found significantly decreased after 24 hours, which could be an indicator either of their metabolism towards protein synthesis or to form a series of coenzyme A compounds that can be further oxidized for use in the TCA cycle in the forms of acetyl and succinyl CoA [443], contributing to the energy metabolism. Another amino acid found to vary upon acrolein treatment was glycine, which significantly decreased at 24 hours in an acrolein concentration-dependent manner. Glycine is the simplest amino acid and can be utilized for the biosynthesis of glutathione, creatine, nucleic acids and uric acid [444], suggesting that its decrease might be link with the production of antioxidant defences. In fact, the simultaneous decrease of glycine and glutamate at 10  $\mu$ M and 100  $\mu$ M at 24 hours might suggest an increase in the biosynthesis of glutathione in order to provide protection against the oxidative stress generated [445] and to promote the detoxification of acrolein [446, 447]. GSH-ACR adducts have been previously detected in B16-BL6 mouse melanoma cells exposed to cigarette smoke extract [448] and these adducts were promptly reduced and excreted to the extracellular fluid resulting in the detoxification of acrolein. The same group showed that this mechanism of detoxification of acrolein also occurs in non-cancerous cells [449]. The decrease in glutamate might also be related to the increase in pyroglutamate, an analogue of glutamate produced by the loss of a water molecule [450]. Even though its biological role is still not completely understood, free pyroglutamate is known to have a role in osmoprotection and its *de novo* synthesis usually occurs in response to osmotic stress [451]. Pyroglutamate also has an anti-diabetic effect in type 2 diabetes suggesting a role in lipid metabolism, although the mechanism is still not clear [452]. Figure 5.16 summarises the metabolic changes described above for better visualization and understanding.



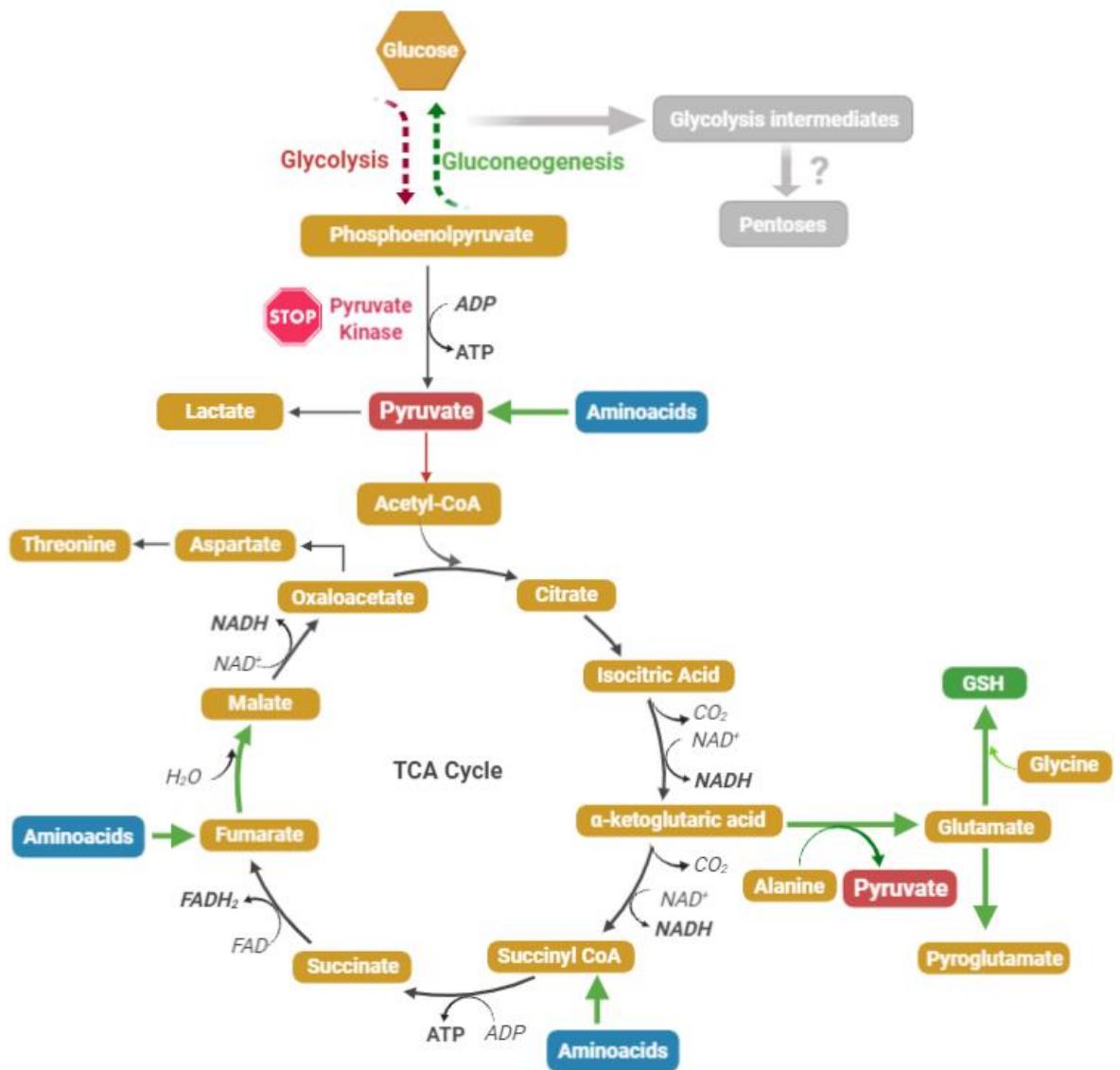


**Figure 5.16. Cellular glycolysis and TCA cycle metabolism.** Diagram representing the metabolic changes detected by <sup>1</sup>H NMR and summarizing the changes discussed above. Green arrows represent the most active reactions according to the observed changes in the levels of each metabolite. These point to a change in metabolism to compensate the loss of pyruvate kinase by promoting pyruvate formation through amino acids and fuelling the TCA cycle metabolism via other ways other than glycolysis. The channelling of glycolysis intermediates into the pentose phosphate pathway was studied and is presented in grey.

All of the metabolic changes discussed above, either for compensation of lower production of pyruvate from glucose or increase in antioxidant defences, were all detected significantly after 24 hour treatments but not after 2 hours, which strengthens the hypothesis of time being needed to activate these defence mechanisms, and also justifies the reduced loss of activity after 24 hours. It is also worth noting that the treatments presented in this study reflect an acute acrolein exposure allowing the cells to adapt to the treatment; a chronic exposure such as in inflammatory disease might show a different metabolic response.

In summary, this study has provided novel data on the susceptibility of the key glycolytic enzyme pyruvate kinase to modification by 3 aldehydes with different chemical reactivities: acrolein (an alkenal), HHE (a hydroxyalkenal), and MDA (a dicarbonyl), and has shown that they cause differential inhibition of activity both *in vitro* and in a breast cancer cell line. Pyruvate kinase in MCF-7 cells was extremely susceptible to inhibition and modification by acrolein, which is a carcinogen present in tobacco smoke as well as a product of lipid peroxidation. Metabolomic analysis of MCF-7 cells upon acrolein treatment revealed a cellular metabolic change that could suggest an additional mechanism by which this compound may contribute to tumorigenesis.

**Chapter 6. Effect of reactive short-chain aldehydes on intermediate filaments network organization**

## 6.1. Introduction

The cytoskeleton is the principal machinery responsible for maintaining cell shape and mechanics. It is commonly divided in terms of its functional subsystems into actin filaments (AFs), microtubules (MTs), and intermediate filaments (IFs), according to their size and protein content. However, recent studies show that key cellular functions such as cell division are dependent on strong crosstalk between all three subsystems [453, 454].

Microtubules are the largest type of filament (about 25 nm in diameter) and are made of  $\alpha/\beta$ -tubulin heterodimers, which assemble into a polar, cylindrical structure in the presence of GTP [455]. This is responsible for cell shape, organelle positioning, cell polarity and segregation of chromosomes during cell division [456]. The different functional specialization can be acquired by interaction with microtubules-associated proteins (MAPs) but also by the “tubulin code” which consists of a combination of differential expression of  $\alpha$ - and  $\beta$ -tubulin isotypes and tubulin post-translational modifications [457, 458]. Actin is the most abundant protein in many cells and the component of microtubules. Humans have three genes for  $\alpha$ -actin, one gene for  $\beta$ -actin, and two genes for  $\gamma$ -actin [459]. Actin has a strong tendency to polymerize into filaments, which consist of two strands of subunits in right-handed helices staggered by half the length of an actin monomer (2.7 nm) [460, 461]. These are responsible for providing structure and support to internal movements, including interaction with myosin motor proteins [462], intracellular transport [463], cellular structure [464], muscle contraction [465] and cytokinesis [466].

Intermediate filaments are made of filamentous proteins that have no known enzymatic activity but have a conserved substructure necessary for their self-assembly into intermediate filaments (which are about 10 nm diameter). The various intermediate filaments provide each cell type with a unique cytoskeletal network, which can be considered as ‘identity cards’ for cell and tissue differentiation [467]. This extensive cytoplasmic network connects the cell cortex to intracellular organelles, conferring an advantage for intermediate filaments in coordinating cell activities [468]. Intermediate-filament proteins can be divided into five types on the basis of primary and gene structure, assembly properties and tissue distribution. Keratins (types I and II) form necessary heteropolymers in epithelial cells, while vimentin, desmin, glial fibrillary acidic protein (GFAP) and peripherin (type III) form homopolymer intermediate filaments. Neurofilament proteins (type IV) include three neurofilament subunits (NF-L, NF-M and NF-H), as well as nestin, syncoilin and  $\alpha$ -internexin. Lastly, the nuclear intermediate filaments (type V) consist of protein lamin A, B1, B2 and C [454, 469].

Vimentin is a coiled-coil protein composed mainly of  $\alpha$ -helical regions linked by connecting segments. Even though a crystal structure for the full-length monomeric or tetrameric vimentin is not yet available, molecular modelling proposes that monomers

assemble into parallel dimers first, which in turn associate antiparallely into tetramers resulting in the structural units for polymerization [470]. These forms robust filaments extended from the nuclear periphery to the cell membrane, and are therefore responsible for several cell activities, including organelle positioning, cell migration and adhesion, and cell signalling [471-476]. Vimentin filaments are able to interact with signalling proteins and are known to bind to phosphorylated ERK, modulating MAPK cascade signaling [477]. Due to such important roles, vimentin has critical implications in pathophysiological conditions. It is recognized as an active factor in cancer [478] and as an autoantigen in rheumatic fever and rheumatoid arthritis [479, 480]. Additionally, it is involved in wound healing and consequent excessive scarring [481, 482], and has a facilitating role in viral infections [483, 484]. The assembly of the vimentin network is regulated by interaction with microtubules and their associated proteins [454, 485]. Under stress conditions, post-translational modifications such as phosphorylation, nitrosylation or carbonylation may also be involved in the regulation of vimentin network [486-489].

In a pathophysiological environment, cells increase the production of oxidants such as hydrogen peroxide, which can directly affect proteins or generate more reactive compounds such as hydroxyl radicals that can cause damage to cellular components, as well as lipid peroxidation. Short-chain aldehydes are one of the many products of the peroxidation of lipids and due to their high reactivity can cause covalent modifications and crosslink of proteins, altering their structure and consequently function [20, 31]. Lipoxidation can occur via Schiff's base formation with lysine residues or formation of Michael adducts on histidine, cysteine or lysine residues [281] and its products have been found in inflammatory diseases such as atherosclerosis and Alzheimer's disease [282]. The lipid peroxidation product 4-hydroxynonenal (HNE) is by far the most studied however other aldehydes deserve some consideration [490]. The 6-carbon 4-hydroxyhexenal (HHE) is one of the major lipid peroxidation products of  $\omega$ -3 polyunsaturated fatty acids (PUFAs) with comparable reactivity to HNE [113]. The 3-carbon compound malondialdehyde (MDA) is the most studied in parallel with HNE and due to its bifunctionality has the potential to crosslink proteins [104, 129]. Another 3-carbon aldehyde is acrolein, more commonly associated with tobacco smoke [31], it is highly reactive, especially with thiol groups of proteins, and it has been associated with apoptosis, inflammation and antioxidant defence regulation [71, 80].

Intermediate filaments are highly sensitive to oxidative and electrophilic stress, and their proteins such as vimentin, GAFP and lamin have been previously reported as direct targets not only of oxidation and nitrosylation as stated above but also of lipoxidation [491-493]. MDA and glyoxal (GO) have been shown to play a role in fibrosis and impaired wound-healing processes mediated by vimentin disruption and deciliation [494]. The smoke component acrolein was reported to target vimentin and cause cross-linking in lung cells

[495] and vimentin network rearrangement/disruption in human gingival fibroblasts [496]. More recently, the pre-incubation *in vitro* wildtype vimentin with HNE before polymerization was shown to result in shorter filaments. This effect was slightly attenuated by mutation of the residue Cys328, required for polymerization,; however, the levels of total adducts detected by western blot did not change since HNE could form adducts with other residues such as histidine and lysine [497]. In fact, it has been previously reported that Cys328 is required for the normal function of vimentin under resting conditions and for its plasticity in response to oxidative stress. The dual function of the single cysteine residue on vimentin is related to its modulation by zinc levels. Zinc was shown to regulate vimentin polymerization and cysteine modification, suggesting that this specific residue has a zinc binding role on vimentin [498]. Lipoxidation of the single cysteine residue Cys328 by cyclopentenone prostaglandins (cyPG), a reactive lipid type generated by inflammation, has been previously reported. This covalent adduct between the lipid and Cys328 caused a rearrangement of the vimentin network [492, 499].

As yet, there have been no comparative studies of Cys328-mediated effects of different small aldehydes on vimentin. Therefore the aim of this study was to address the importance of Cys328 in vimentin organization, by comparison of the network upon treatment of cells expressing wildtype vs cells expressing mutant Cys328S with acrolein, malondialdehyde and 4-hydroxyhexenal. Moreover, the ability of the vimentin network to reorganize 24 hours after treatment with acrolein and malondialdehyde was also assessed by overnight monitoring of the vimentin network organization.

## **6.2. Material and Methods**

### **6.2.1. Cell culture and aldehyde treatment**

Adrenal carcinoma SW13/cl.2 cells are a well-known model for vimentin cellular studies due to their lack of cytoplasmic intermediate filaments [500]. These cells allow for the effects of vimentin to be studied without interference from the endogenous protein. Cells were cultured in p100 dishes in DMEM with 10% (v/v) fetal bovine serum (FBS) and antibiotics (100 U/ml penicillin and 100 µg/ml streptomycin). For network visualization, cells were co-transfected with RFP//vimentin plasmids, expressing untagged vimentin plus GFP-vimentin for time-lapse microscopy. SW13/cl.2 cells untransfected or stably transfected with RFP//vimentin wild type (wt) or RFP//vimentin C328S mutant, have been described previously [498]. For time-lapse experiments, transient transfections were carried out in p35 dishes divided in 4 compartments at 70% confluence using Lipofectamine 2000. Briefly, 1 µg of DNA (0.8 µg of RFP//vim wt and 0.2 µg of GFP-vimentin wt) and 3 µL of Lipofectamine were used per dish. Transfections were carried out in medium without antibiotics for 48 h. Imaging of live cells was performed 48 h after transfection. For single-point experiments, treatments were carried out in serum free medium and cells were seeded into a 12-well with glass coverslip plate. Cells at 80% confluence were treated with 10 µM ACR or HHE, or 30 µM MDA for 1, 2 or 24 hours. These concentrations have been previously reported as pathophysiological levels in human plasma. Aldehydes were prepared as a 10x stock in water and filtered with 0.22 µm filter unit (Merk Millipore, Cork, Ireland) for sterilization, before being added to the cells for treatment. For time-lapse microscopy, the treatments were added immediately before the visualization for monitoring of the effect.

### **6.2.2. Fluorescence microscopy and cell imaging**

Cells treated with the different compounds were visualized by confocal microscopy on Leica SP2 or SP5 microscopes. Images were acquired every 0.5 µm and single sections or overall projections are shown, as indicated. For immunofluorescence, cells were fixed with 4% (w/v) paraformaldehyde for 25 min at room temperature, permeabilized with 0.1% (v/v) Triton-X100 in PBS and blocked with 1% (w/v) BSA in PBS. Antibodies were used at 1:200 dilution in blocking solution. For the detection of full-length vimentin the V9 antibody was employed. Filamentous actin (f-actin) was stained with Phalloidin-Alexa568 (Molecular Probes) following the manufacturer's instructions. Nuclei were counterstained with DAPI (3 µg/ml). Measurements of cell area were obtained with ImageJ. Time-lapse microscopy was carried out in a multidimensional microscopy system Leica AF6000 LX in a humidified 5% CO<sub>2</sub> atmosphere at 37 °C. Green fluorescence and differential interference contrast (DIC) images were recorded.

### **6.2.3. Statistical analysis**

All experiments were performed at least three times. The results are presented as mean values and the error bars are the standard error of the mean (mean  $\pm$  SEM). Two-way analysis of variance (ANOVA) was used with the Dunnett's correction to evaluate significant differences among samples. A value of  $P < 0.05$  was considered to be statistically significant. Statistical analysis was performed using GraphPad Prism 7 software.



### 6.3. Results

#### 6.3.1. Effect of short-chain aldehydes on vimentin network by confocal microscopy

The aim of this chapter was to evaluate the effect of the lipid peroxidation products short-chain aldehydes on the intermediate filaments network. The main filament studied in was vimentin, which is responsible for cell structure and organelle positioning. Therefore, SW-13/cl.2 cells expressing wildtype vimentin were treated with 10  $\mu$ M acrolein, 10  $\mu$ M 4-hydroxyhexenal and 30  $\mu$ M malondialdehyde, and the effect on the vimentin network was assessed by confocal microscopy. **Figure 6.1** shows the overlay channels of the immunofluorescence for vimentin in green and for nuclei in blue for the 3 time points and the three aldehydes tested.

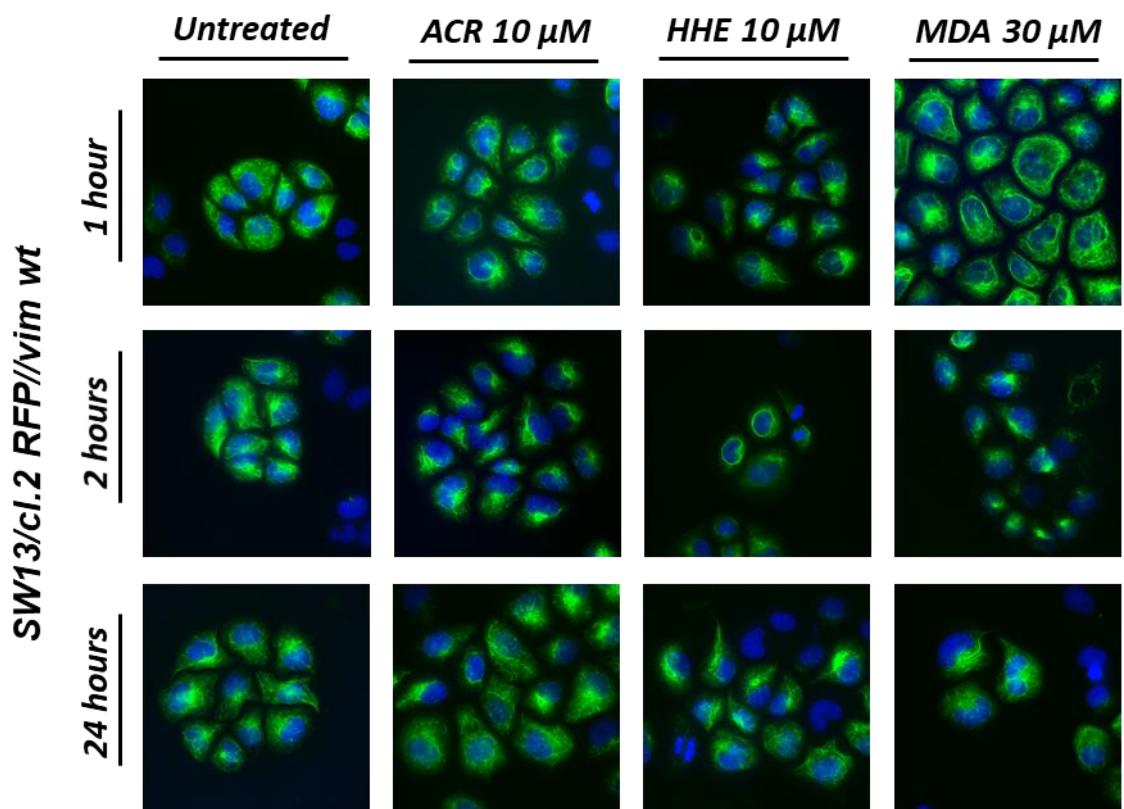


**Figure 6.1.** Effect of acrolein, 4-hydroxyhexenal and malondialdehyde on vimentin organization in cells. SW13/cl.2 cells stably transfected with RFP//vimentin wt were treated with 10  $\mu$ M ACR and HHE and 30  $\mu$ M MDA for 1, 2 or 24 hours after which cells were fixed and vimentin network analysed by immunofluorescence. Scale bars, 20  $\mu$ m. V9 antibody detected vimentin (green) and nuclei were counterstained with DAPI (blue).

All aldehydes tested caused a disorganization the vimentin filament network resulting in an accumulation around the nucleus. This effect was particularly evident for the 2 hours treatment, even though it was also observed for the other two time points. A small recovery of this network appears to occur 24 hours after the treatments. In order to assess these changes in the vimentin network better and investigate vimentin accumulation/aggregation, the vimentin and actin networks were compared (**Figure 6.2**).

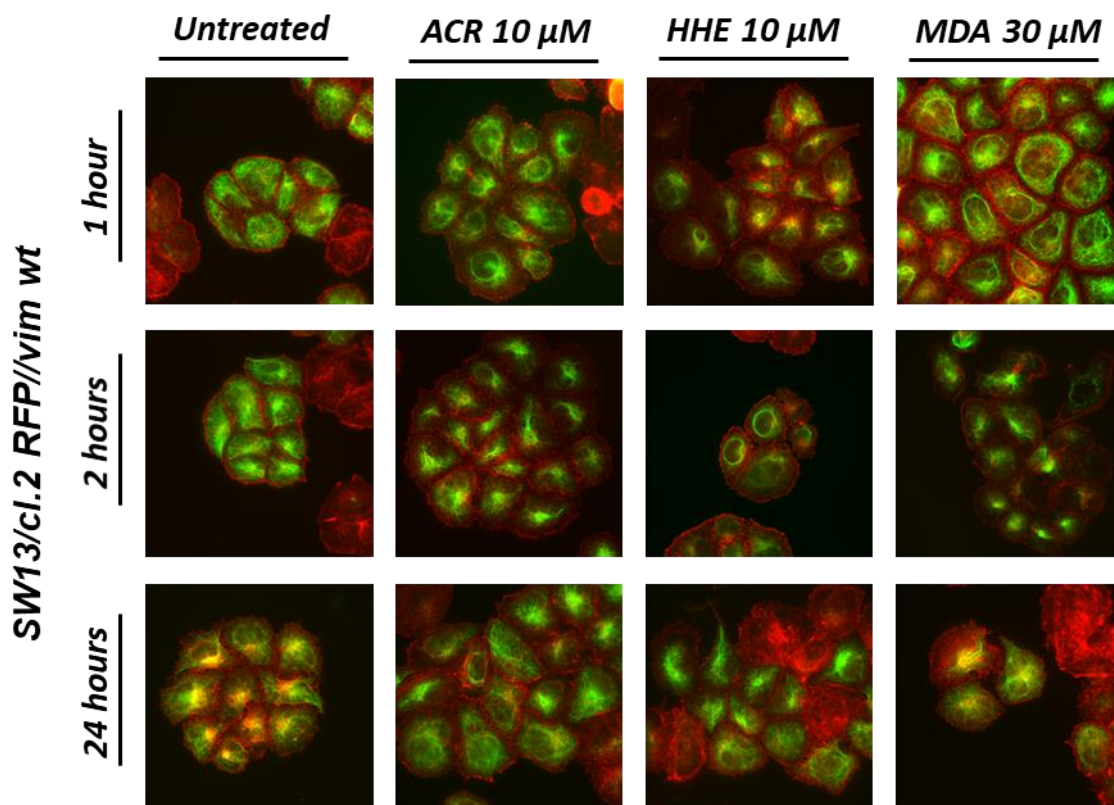


**Figure 6.2. Comparison of actin and vimentin networks organization after acrolein, 4-hydroxyhexenal and malondialdehyde treatment.** SW13/cl.2 cells stably transfected with RFP//vimentin wt were treated with 10 μM ACR and HHE and 30 μM MDA for 1, 2 or 24 hours, after which cells were fixed and the vimentin network analysed by immunofluorescence. Scale bars, 20 μm. V9 antibody (1:200) detected vimentin (green) and filamentous actin was stained with Phalloidin-Alexa568 (red).

The actin network helped to outline the cells and therefore assess the area covered by the vimentin network. While for the control samples the vimentin seemed to occupy almost the whole cell, after the treatments it was possible to observe an aggregation of this filament and consequently that it appeared to occupy less area within the cell. After 2 hours treatment this aggregation was very clear when compared with the control for the same time point. After only 1 hour of treatment the same effect can be observed, although to a smaller extent. For better quantification of this effect, the area of actin was used as the area of the whole cell and the ratio vimentin/actin was calculated (**Figure 6.3**). All conditions tested

were found to be statistically different from their respective controls (**Figure 6.3A**). After 1 hour treatment, HHE appeared to cause the most accumulation of the vimentin network, while for acrolein 2 hours appeared most effective, although no statistically significant differences were confirmed between the different aldehydes at any time point. **Figure 6.3B** shows the same percentages represented as % of control, where the ratio for each control was set as 100% and all the other percentages calculated accordingly. This was performed to perceive more clearly the differences between conditions. Statistically significant differences were only observed for acrolein between the time points of 1 and 2 hours. Even though no statistical difference was observed between 24 hours and the other time points, a trend suggests a small recovery of the vimentin network overnight.

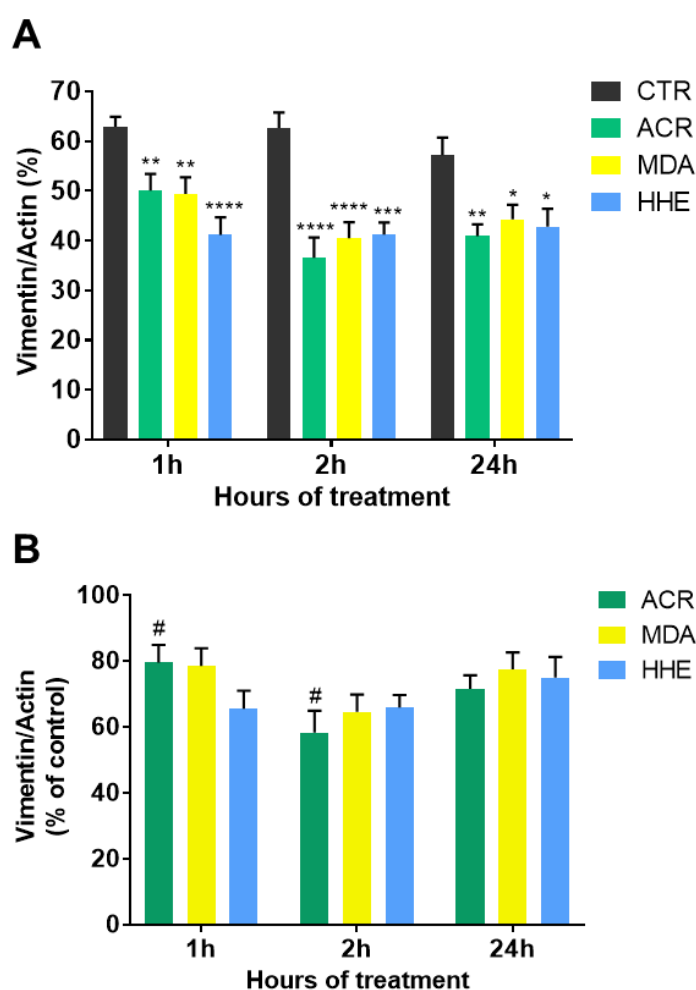


**Figure 6.3. Relative quantification of vimentin cell distribution.** Variance in vimentin/actin ratio to assess the effect of the aldehyde's treatment on the vimentin network. (A) vimentin/actin ratio expressed in percentage for control (no treatment), ACR at 10  $\mu$ M, MDA at 30  $\mu$ M and HHE 10  $\mu$ M; (B) vimentin/actin ratio normalized as percentage of control, comparison between time points. (n=9; Mean  $\pm$  SEM; \*  $p < 0.1$ , \*\*  $p < 0.01$ , \*\*\*  $p < 0.001$  and \*\*\*\*  $p < 0.0001$ ) \* Comparison of conditions with control; # comparison between conditions.

### 6.3.2. Mutation of Cys328 confers protection from lipoxidation on the vimentin network

To assess the importance of the only cysteine residue in the vimentin amino acid sequence, a same cell line with mutant vimentin was used in which the cysteine residue on the position 328 was substituted by a serine, described as C328S throughout the chapter. **Figure 6.4** shows the overlap of the immunofluorescence for vimentin and for nuclei for the 3 time points and the three aldehydes tested on this mutant cell line.

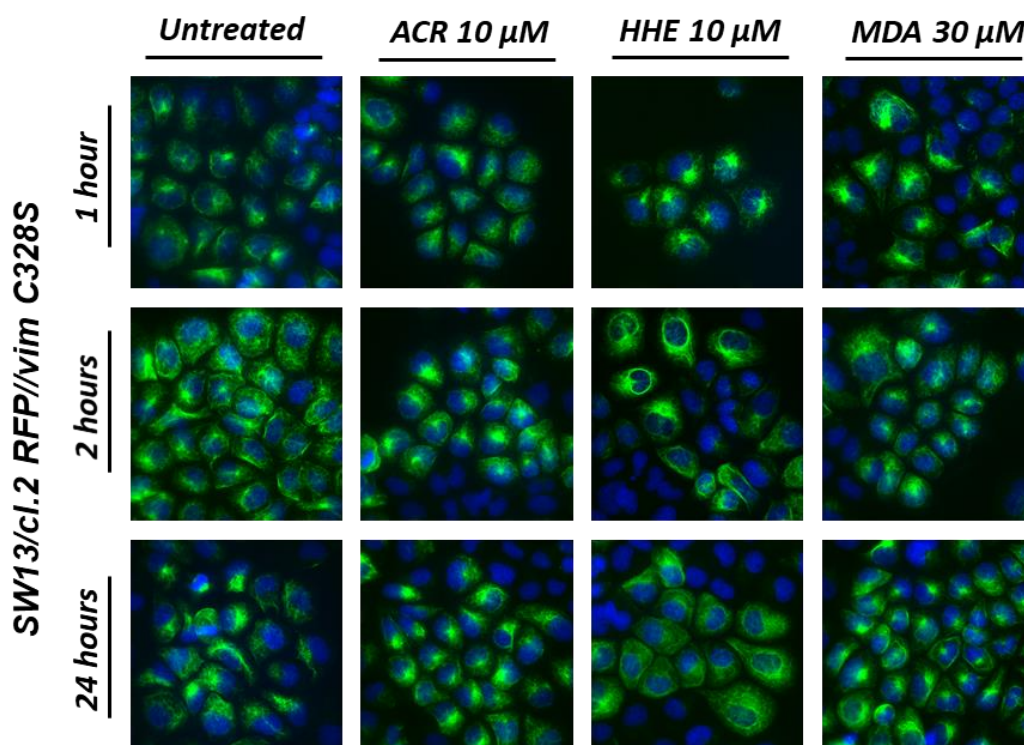


**Figure 6.4. Effect of acrolein, 4-hydroxyhexenal and malondialdehyde on vimentin organization in cells.** SW13/cl.2 cells stably transfected with RFP//vimentin Cys328Ser (C328S) were treated with 10 μM ACR and HHE and 30 μM MDA for 1, 2 or 24 hours after which cells were fixed and vimentin network analysed by immunofluorescence. Scale bars, 20 μm. V9 antibody (1:200) detected vimentin (green) and nuclei were counterstained with DAPI (blue).

The vimentin network of the control samples from the mutant cell line already shows some degree of disruption when compared with the control samples from **Figure 6.3**. An aggregation of vimentin was also observed for this cell line after treatment, although to a smaller extent than the aggregation observed previously for the wild type. Similarly, a small recovery of the network appeared to be happening 24 hours after the treatments and these changes were also investigated by vimentin and actin networks comparison (**Figure 6.5**).

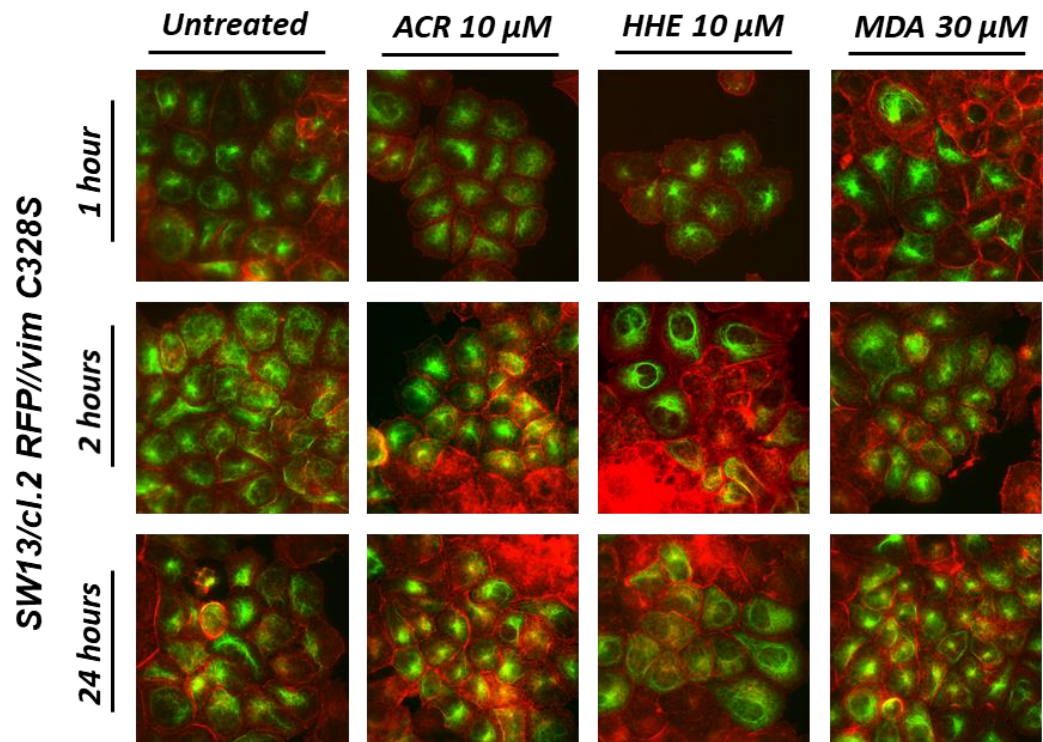
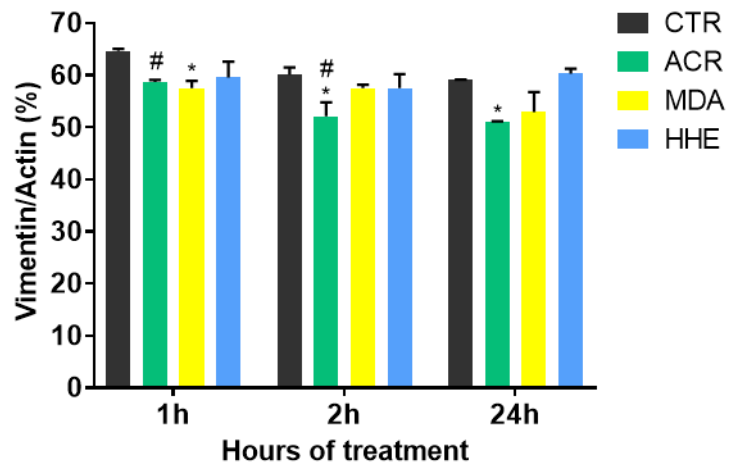


**Figure 6.5. Comparison of actin and vimentin networks organization after acrolein, 4-hydroxyhexenal and malondialdehyde treatment.** SW13/cl.2 cells stably transfected with RFP//vimentin Cys328Ser (C328S) were treated with 10  $\mu\text{M}$  ACR and HHE and 30  $\mu\text{M}$  MDA for 1, 2 or 24 hours, after which cells were fixed and vimentin network analysed by immunofluorescence. Scale bars, 20  $\mu\text{m}$ . V9 antibody detected vimentin (green) and filamentous actin was stained with Phalloidin-Alexa568 (red).

The vimentin network seemed to occupy almost the whole cell in the control samples as well as after the aldehyde treatments. In **Figure 6.5**, some perinuclear accumulation aggregation of vimentin after HHE treatment for 1 and 2 hours was observed. However, these only represent a small group of cells, and other cells in the same plate did not show the same effect (data not shown). So for better determination of this effect and accounting for the three replicates data, the area of actin was used as the area of the whole cell and the ratio vimentin/actin was calculated (**Figure 6.6**). **Figure 6.6A** shows the ratio between vimentin and actin network areas for the mutant cell line. The vimentin C328S mutant showed attenuated responses to the aldehyde treatments, being more resistant to these. When compared with the control samples, only MDA showed a significant effect after 1 hour treatment while ACR showed a significant effect after 2 and 24 hours treatment. Similarly to the wild type (**Figure 6.6B**), only ACR showed a difference between conditions significantly decreasing the ratio after 2 hours when compared with 1 hour treatment. The results indicate that the mutation on the only cysteine residue of vimentin protected the vimentin network from lipoxidation, supported by the smaller changes in the vimentin/actin ratio.

**A. SW13/cl.2 RFP//vim C328S**



**B. SW13/cl.2 RFP//vim wt**

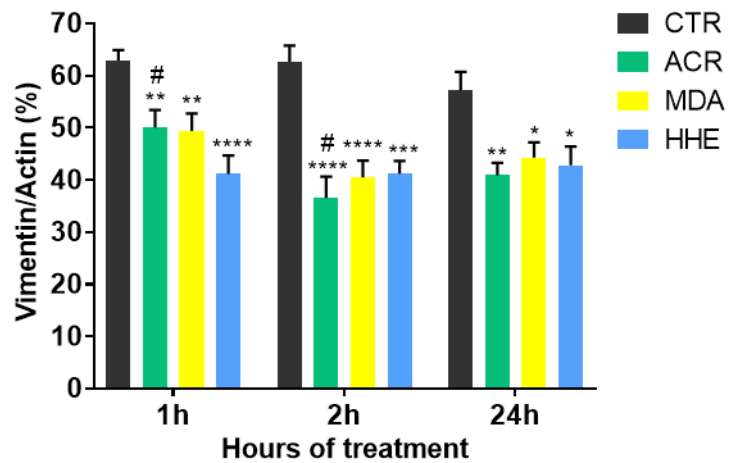


**Figure 6.6. Relative quantification of vimentin cell distribution.** Variance in vimentin/actin ratio to assess the effect of the aldehyde's treatment on the vimentin network. (A) vimentin/actin ratio expressed in percentage for untreated and treated C238S mutant cells; (B) vimentin/actin ratio expressed in percentage for untreated and treated SW13 cell line, which is the same as shown in **Figure 6.3A** for comparison. (n=3; Mean  $\pm$  SEM; \* p<0.1 \*\* p<0.01, \*\*\* p<0.001 and \*\*\*\* p<0.0001) \* Comparison of conditions with control; # comparison between conditions.

### 6.3.3. Monitoring the effect of ACR and MDA treatment by time-lapse microscopy

In order to investigate the possibility that the vimentin network slightly recovered overnight after the treatments (**section 6.3.1**), the effect of ACR and MDA on the vimentin network was assessed by time-lapse microscopy. In this way the same group of cells was monitored throughout the experiment. Micrographs were taken before the treatment was added and after the treatment each 30 minutes for the first 4 hours and then every hour overnight (**Figure 6.7**). The quality of the pictures is lower than the quality in the previous figures because the intensity of the laser and the time of exposure were decreased in order to limit its impact on cell survival. Two different groups of cells were monitored overnight after exposure to 10  $\mu\text{M}$  of acrolein. For both groups of cells, it was clear that the first 4 hours of treatment caused a disorganization of the vimentin network resulting in its accumulation. However, **Figure 6.7A** indicates that the overnight monitoring did not detect a recovery of the vimentin network. In fact, after 8 hours of treatments the cells appeared to be dead. In contrast, in **Figure 6.7B** which monitored a different group of cells, a recovery of the network appeared to occur from 6 to 16 hours after the acrolein treatment was used.

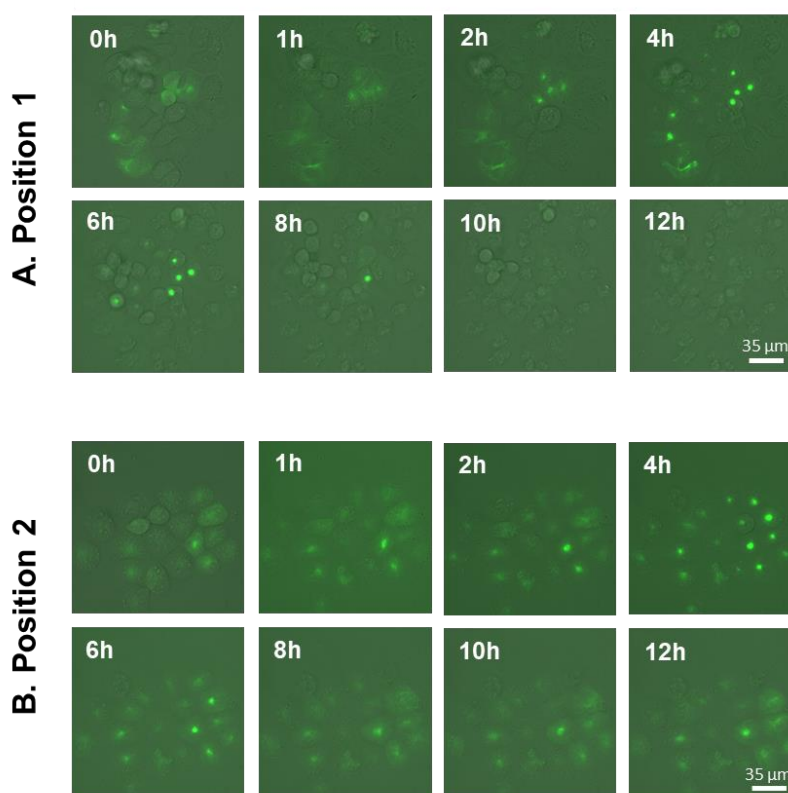


**Figure 6.7. Time-lapse microscopy monitoring of cells treated with 10  $\mu\text{M}$  acrolein.** Micrographs were taken every 30 minutes for the first 4 hours and then every hour overnight. Here are shown the pictures taken 1, 2, 4, 6, 8, 10 and 12 hours after the treatment. Two different positions of the dish, A and B, followed the effect of the same treatment a different group of cells. Micrographs consist of green fluorescence (vimentin) and differential interference contrast (DIC) images overlapped.

The same experiment was performed after cell treatment with 30  $\mu\text{M}$  of malondialdehyde (**Figure 6.8**). Similarly to the effect observed after acrolein treatment, the first four hours after MDA treatment resulted in an accumulation of vimentin that can be observed by the increase in intensity of the green fluorescence. Once again, the recovery of the vimentin network after treatment was not observed overnight. In fact, 10 hours after the treatment it was possible to observe cell death resulting in the release of its content.

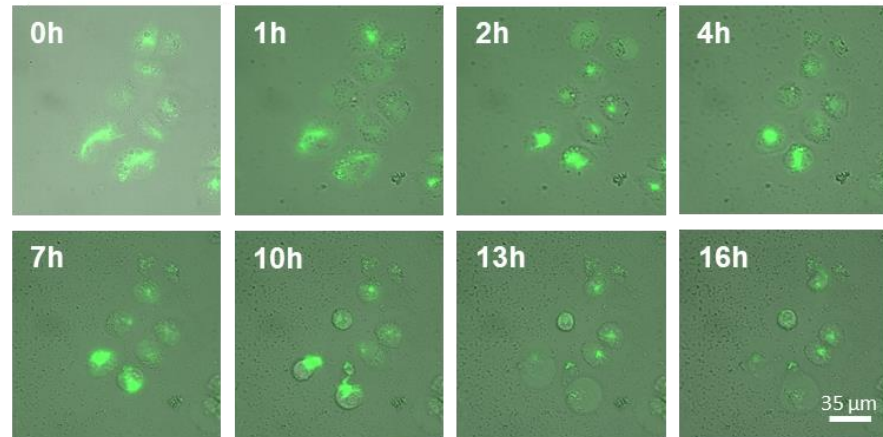


**Figure 6.8. Time-lapse microscopy monitoring of cells treated with 30  $\mu\text{M}$  malondialdehyde.** Micrographs were taken every 30 minutes for the first 4 hours and then every hour overnight. The images taken 1, 2, 4, 7, 10, 13 and 16 hours after the treatment are shown. Micrographs consist of green fluorescence (vimentin) and differential interference contrast (DIC) images overlap.



#### 6.4. Discussion

Vimentin plays a key role in normal functioning of cells and during pathophysiological conditions in addition to its structural function. Among other roles, vimentin is responsible for organelle positioning and facilitates wound repair [498]. This protein is also known to be a critical sensor for oxidative stress and a target for lipoxidation by electrophilic lipids [488, 498]. Due to the lack in studies on the Cys328-mediated effect of short-chain aldehydes on vimentin, the main aim of the study reported in this chapter was to assess the effect of acrolein, malondialdehyde and 4-hydroxyhexenal in vimentin network organization as well as determine the importance of the only cysteine residue in the vimentin sequence. The concentration of each aldehyde used has previously been reported as a pathophysiological concentration of these free aldehydes in human plasma or serum [31, 269]. The cell line used was the SW13/cl.2 cells stably transfected with RFP//vimentin wild type (wt). The mutant cell line RFP//vimentin C328S was used to investigate the role of the cysteine residue Cys328 in the lipoxidation of vimentin, and RFP//vimentin wt plus GFP-vimentin wt transfection was used for time-lapse experiments.

The results show that treatment of cells with reactive aldehydes results in morphological alterations of the network including a marked reorganization and accumulation around the nucleus. All aldehydes showed the ability to reduce the area of vimentin in the cell, an indication of its aggregation around the nucleus. In fact, the juxtannuclear condensation of cytoplasmic intermediate filaments like vimentin upon treatment with unsaturated carbonyl species has previously been reported [493, 498]. Intermediate filament remodelling can be a mediator of cell damage or a mechanism of defence, therefore the biological implications of the lipoxidation-associated aggregation is still not completely understood. Acrolein and HNE showed to cause the highest vimentin aggregation. Juxtannuclear aggregation of vimentin filament caused by lipoxidation has been previously described in fibroblasts and in epithelial cells after acrolein and HNE, respectively [496, 497]. Moreover, mutation of Cys328 resulted in protection against the lipoxidation effect and only acrolein was able to cause a slight aggregation of vimentin overnight. Cys328 is the only cysteine residue on vimentin and it has been reported to be susceptible to modification by reactive aldehydes such as HNE in biological systems [489]. The results in this chapter confirmed Cys328 as a major target of lipoxidation since its mutation to serine conferred protection. Mutation of this cysteine has showed protection against other electrophilic species [492, 498, 499] and demonstrated Cys328 to be a hot spot for posttranslational modifications in vimentin [497, 501, 502]. Cysteine residues are commonly susceptible to modification on several protein apart from vimentin [493, 503]. Filament disruption upon lipoxidation is not just an issue with vimentin. Other intermediate filaments, for example GFAP, have been reported to show the same effect on the network upon lipoxidation and this protein also has a conserved cysteine

residue Cys294 which plays a crucial role in organization and assembly of the filaments [493]. Overall, these studies confirm that these conserved cysteine residues in intermediate filaments are sensors for stress and its mutation confers protection against oxidative stress.

In early experiments there was some evidence of a trend to cellular recovery of vimentin network at 24 hours, even though the data were not significantly different. However, in this experiment, different groups of cells were studied for each time point. To overcome this limitation, a time-lapse experiment was set up in order to follow the same cells and monitor the changes in vimentin overnight after treatment. During the first four hours the juxtannuclear aggregation was confirmed, however the time lapse microscopy approach did not confirm the recovery of the network overnight and cell death was observed. The cell death might be caused by phototoxicity resulting from cumulative exposure, as little cell death was observed in the end-point experiments, even though the intensity of the laser and its phototoxicity were taken into consideration when planning the experiment parameters and a lower intensity and short exposure times of the laser were chosen [504]. Moreover, these aldehyde concentrations were not supposed to be cytotoxic as described in **section 5.3.4**. The phototoxicity of the laser was confirmed by observation under the microscope of the cells that were not being monitored overnight, which were confirmed to be alive. To overcome this limitation, future experiments should be performed by monitoring the cells only once every two hours, for example after the first four hours, to reduce the exposure time of the laser to the cells. As information on the first 4 hours has now been obtained, this would not need to be reported in a time lapse experiment, decreasing the exposure of the cells to the laser and increasing the probability of observing vimentin recovery.

In conclusion, this study demonstrated the effect of electrophilic modification by short-chain reactive aldehydes on vimentin network organization and localization in cells. The observed aggregation of vimentin around the nucleus could be associated with cell dysfunction and therefore connected to pathophysiological conditions such as aging, inflammatory diseases and cancer. A limitation of this study was the lack of MS data to support the hypothesis of Cys328 being a target of lipoxidation. Therefore, MS analysis of the extractable vimentin from this cell lines would strengthen the data presented in this chapter.

## **Chapter 7. Conclusion**

## 7.1. General discussion

The oxidative modification of lipids containing polyunsaturated fatty acids results in a wide diversity of reactive products, including short-chain aldehydes, which are highly reactive and able to modify proteins. Lipoxidation products generated at lower levels can be related to have a signaling role and activate antioxidant defences. However, at higher levels these have been linked to many inflammatory diseases, thus their study, as potential biomarkers of inflammation, is important. Mass spectrometry-based methods are a key tool in proteomic research but there is still a need to improve the detection methods for lipoxidation adducts, as these are extremely challenging to detect due to their relative low abundance. In this project, a bottom-up approach was able to map aldehyde modifications on human serum albumin. However, the incomplete sequence coverage detected by LC-MS could be improved in order to obtain information on the modification status of other residues that were not covered, for example Cys34 which is a major target for modification in HSA and several studies and methods have been developed with focus on its detection. The sequence coverage can possibly be improved by combination of different proteases to digest the protein generating smaller peptides and allowing the detection of Cys34, since using trypsin digestion only the peptide containing this residue was too long and gave low ion intensity. Protein-protein cross-linking has also previously been shown to occur through acrolein modification, including in proteins such as Hsp90, which has a role in the response to oxidative stress. However, a limitation of the work reported in this thesis is the lack of mass spectrometry analysis of protein crosslinking adducts even though these were possibly observed by SDS-PAGE where bands corresponding to double or three times the mass of protein in study were observed. It would have been interesting to conduct a study by LC-MS/MS for mapping and characterization of these crosslinks and determine hotspots for their occurrence in proteins such as human serum albumin.

Regardless, the tandem mass spectrometry approach used allowed for the detection of potential diagnostic ions for adducts of aldehydes with nucleophilic amino acid residues such as cysteine, histidine, lysine and arginine. Five diagnostic ions for acrolein and eight for 4-hydroxyhexenal adducts with human serum albumin were consistently observed in the MS/MS spectra of modified peptides. The diagnostic ions for acrolein modification were then used in the development of a multiple reaction monitoring MS-based approach focused on their detection in complex biological samples. The transitions  $600.4 \rightarrow 142.1$  and  $509.3 \rightarrow 168.1$ , which include the reporter ions for lysine and histidine modification respectively, were shown to be successful in the detection of acrolein-albumin adducts as their signal was detected exclusively in acrolein-treated samples, both for *in vitro* modified human serum albumin and human plasma. Therefore the novel MRM method developed identified promising transitions for acrolein-albumin adduct detection and proved to be

highly selective for acrolein modification. Previously reported targeted methods developed for albumin modification detection required protein extraction from plasma due to interference from other proteins [314]; however, for the method described here, sample preparation was kept to a minimum by only diluting the plasma and the transitions were detected with minimal background noise. Further validation of this targeted method using clinical samples is still necessary to understand its potential application in the detection of acrolein-albumin adducts in case of disease, such as from type 2 diabetes mellitus patients [505], Alzheimer's disease or any type of cancer, with lung cancer being the most applicable as acrolein is a major component of tobacco smoke. Hopefully the success of this method, developed using the reporter ions described in chapter 2, will encourage other methods to be developed with a similar approach for other protein modifications, including using the other reporter ions reported in this thesis.

Chlorine containing aldehydes have previously been reported to be produced during neutrophil activation and to accumulate, for example, in atherosclerotic plaques [147]. There is still a lack in knowledge on their impact on cell function, as they have the potential to modify proteins and therefore directly cause structural and functional changes. Additionally, their reactivity in comparison with other aldehydes such as those mentioned above, and the products formed after chloroaldehyde modification of proteins is still largely unexplored. An alternative method to directly convert hexadecanol into 2-chlorohexadecanal was proposed on chapter 3, which was less time-consuming and cheaper than current methods used [339]. An MS-based approach allowed the characterization of 2-chlorohexadecanal modification of human serum albumin and consequently the detection of a reporter ion for 2-ClHDA-lysine adducts. Previous studies reported that 2-ClHDA reacts with cysteine residues by nucleophilic attack on C-Cl retaining the carbonyl group [199]. However, the mass of the lysine residue reported in this thesis corresponds to the Schiff-base formation with additional loss of HCl, showing that analysis of 2-chloroaldehyde adducts is more complex than other aldehydes, due to the different types of modifications that can arise depending on the amino acid residue modified. Further analysis of 2-ClHDA adducts by MS is needed to confirm the sensitivity of the reporter ion  $m/z$  323 to detect 2-ClHDA-lysine adducts. In addition, the purity of the synthetic 2-ClHDA could be improved by flash chromatography or HPLC for extraction of the chloroaldehyde and removal of impurities that could interfere with future experiments. For example, to assess the cellular effect of 2-ClHDA it is important that its purity is high to ensure that the effects observed are due to chloroaldehyde treatment instead of its impurities. In the work reported in chapter 3, the synthetic 2-ClHDA was reacted with human serum albumin for mapping and characterization of its modifications, however other properties of this aldehydes could be

explored apart from its reactivity with proteins such as antimicrobial inspired by the properties of other chlorine containing compounds as hypochlorous acid (HOCl).

Proteomic analysis is challenging due to the dynamic range of proteins and mass spectrometry approaches are distinctively suited to handle this complexity [345]. However, upfront separation is required for mass spectrometry application in the study of protein isoforms and localization of post-translational modifications, for example [361, 362]. Therefore, chromatographic coupling as a separation technique for peptides and proteins is a key step in mass spectrometry analysis, and liquid chromatography is the most common method for small molecule separation. Anion exchange chromatography turned out to be the best separation method tested for protein isoform separation with, for example, up to seven isoforms being separated for human serum albumin. The pH gradient used produced a similar separation pattern to a previously reported salt-gradient for HSA isoform separation [381], but the method described in this thesis was able to separate these isoforms in  $\frac{1}{4}$  of the time required by the previous method, increasing its potential for a clinical application. Even though anion exchange chromatography showed promising results as a quick alternative for human serum albumin isoform separation, this separation method should now be validated for plasma samples from healthy volunteers, to determine its potential to separate albumin isoforms in a complex sample and understand the sample preparations required for the success of this separation. After these have been established, the method should be tested to quantify different protein isoforms in case of diseases, for example to quantify the different glycosylated isoforms of albumin in diabetic patients as these could be used as a prognosis tool. The choice of the right separation method is important for the characterization of intact proteins for mass spectrometry, improving their detection and allowing the diagnosis of different diseases such as cancer, where distinction between isoforms is vital [352]. Ion exchange chromatography has been proposed as a good alternative to reverse phase [386], but for lipoxidized protein separation it was observed that reverse-phase chromatography was still the best method as it was able to separate HHE and HNE-modified proteins with different degrees of modification, as well as separating unmodified from modified protein. This level of separation was not obtained with ion exchange chromatography. The intact protein MS analysis was powerful for identification of modification in small proteins such as insulin and ubiquitin, however for larger proteins such as human serum albumin for which multiple charges can influence the MS analysis. So, the separation and top-down analysis of large proteins turned out to be a major challenge and new approaches could be used, such as the middle-down proteomic approach, for the full characterization of PTMs on human serum albumin. This approach has been previously successfully applied for other large molecules characterization such as monoclonal antibodies [239].

Due to their ability to directly modified proteins, short-chain aldehydes are been proposed as compounds able to change protein structure and function, and therefore having a role in the onset of several diseases such as cancer. Despite this known link between lipoxidation and cancer, little attention has been focused on the study of the effect of aldehydes on glycolytic enzymes involved in the modulation of the cancer metabolism into aerobic glycolysis [270, 390]. Some studies have reported aldehyde modification of GAPDH, both *in vitro* and in mouse models [163, 272, 506], but lipoxidation of pyruvate kinase is still largely unexplored, with only one study reporting its inactivation by HNE and ONE [273]. To understand to effects of acrolein, HHE and MDA on pyruvate kinase, the PKM1 was modified *in vitro* and several hotspots for modification were found by LC-MS/MS to be at or close to the active and the allosteric sites, which might explain the loss of enzymatic activity observed. The effect of the same aldehydes on cellular pyruvate kinase (PKM2) found this enzyme to be highly susceptible to modification, and its activity was inhibited under pathophysiological concentrations in a time- and dose-dependent manner, with acrolein appearing to be the most toxic of the aldehydes tested. Some of the modifications mapped *in vitro* were also detected by MS on the pyruvate kinase extracted from these cells. An altered cellular metabolism upon exposure to acrolein was observed to counteract the decrease in pyruvate being produced, suggesting that this aldehyde may contribute to mechanisms of tumorigenesis via pyruvate kinase inhibition. In fact, acrolein is a major component in tobacco smoke and this could be one of its mechanisms of action as a carcinogen. Further experiments should be conducted on a non-cancerous cell line in order to study the ability of acrolein, and other aldehydes, to switch the cell metabolism to a cancerous state and better understand the underlying mechanisms.

In contrast, intermediate filaments have no known enzymatic activity but their extensive cytoplasmatic network confers on them a role in coordinating cell activities [468]. Vimentin is an intermediate filament that is able to interact with signaling proteins and have critical contribution in pathophysiological conditions as cancer [477]. Under stress conditions, post-translational modifications of vimentin such as phosphorylation and nitrosylation have been reported to regulate the vimentin network. In particular, the cysteine residue 328 on vimentin is known to be required for its response to oxidative stress [497, 498]. Due to the lack of studies regarding the Cys328-mediated effect of short-chain aldehydes on vimentin organization, this issue was addressed in this thesis with a comparative study of the network upon treatment of cells expressing wildtype or mutant Cys328S with acrolein, HHE and MDA. The three aldehydes were able to cause morphological alterations, including vimentin aggregation around the nucleus, which had also been reported to happen upon treatment with unsaturated carbonyl species [493, 498]. This remodelling of intermediate filaments is usually linked to mediation of cell damage or as a mechanism of defence, but the biological

implication of aldehyde-mediated aggregation is still not completely understood. Cys328 was shown to be a target for lipoxidation as its mutation conferred protection from lipoxidation on the vimentin network. Cysteine residues have been reported as common targets of oxidative modification; nonetheless LC-MS/MS analysis of the cellular protein extract should be performed to confirm the modification of this specific residue in vimentin. For further confirmation that the aggregation of vimentin upon aldehyde treatment was Cys328-mediated, the protein cellular extract should be analysed by LC-MS/MS for mapping of the modification. This would be important not just to confirm cysteine modification but also to find other modified residues that might be relevant for vimentin network assembly.

To note that from all the aldehydes tested in this thesis, acrolein was generally the more modifying and toxic aldehyde. This observation was consistent across the *in vitro* and the different cellular work.

## **7.2. Summary and perspectives**

The research presented in this thesis has provided a novel method for detection of aldehyde adducts, as well as highlighting some of their cellular effects. However, further studies are still required in order to completely understand the effect of these aldehydic short-chain lipid peroxidation products. The lack of sensitive methods for aldehyde-protein adducts has held back progress in the use of these as clinical biomarkers. The development of targeted methods appeared to be promising candidates for application in measurement of aldehyde-albumin adducts in clinical samples due to their selectivity although further optimization would be required for high sensitivity. The improvement of upfront chromatography methods for their separation in combination with these targeted MS methods seems to be the way of moving the field forward.

In summary, the work presented in this thesis has contributed to the mapping of aldehydic short-chain lipid peroxidation products modifications on proteins, the development of novel methods for their detection, and the assessment of their effects on cellular proteins and general metabolism. These cellular changes might underlie pathological conditions such as cancer, diabetes or other inflammatory diseases, and therefore be used as biomarkers for their diagnosis and prognosis. While much work is still needed to fully understand the mechanisms behind these effects, the research presented in this thesis is an important contribution towards a more complete understanding of the role of short-chain reactive aldehydes in disease.



## **Chapter 8. List of References**

- [1] E. Fahy, S. Subramaniam, R.C. Murphy, M. Nishijima, C.R. Raetz, T. Shimizu, F. Spener, G. van Meer, M.J. Wakelam, E.A. Dennis, Update of the LIPID MAPS comprehensive classification system for lipids, *Journal of lipid research* 50 (2009) S9-14.
- [2] The nomenclature of lipids (Recommendations 1976) IUPAC-IUB Commission on Biochemical Nomenclature, *Biochem J* 171(1) (1978) 21-35.
- [3] U.a.S.C. Gogus, n-3 Omega fatty acids: a review of current knowledge, *International Journal of Food Science & Technology* 45(3) (2010) 417-436.
- [4] N.D. Riediger, R.A. Othman, M. Suh, M.H. Moghadasian, A systemic review of the roles of n-3 fatty acids in health and disease, *J Am Diet Assoc* 109(4) (2009) 668-79.
- [5] J.T. Brenna, N. Salem, A.J. Sinclair, S.C. Cunnane, I.S.S.F. International Society for the Study of Fatty Acids and Lipids, alpha-Linolenic acid supplementation and conversion to n-3 long-chain polyunsaturated fatty acids in humans, *Prostaglandins Leukot Essent Fatty Acids* 80(2-3) (2009) 85-91.
- [6] M.S. Ellulu, H. Khaza'ai, I. Patimah, A. Rahmat, Y. Abed, Effect of long chain omega-3 polyunsaturated fatty acids on inflammation and metabolic markers in hypertensive and/or diabetic obese adults: a randomized controlled trial, *Food Nutr Res* 60 (2016) 29268.
- [7] C.N. Serhan, N. Chiang, J. Dalli, The resolution code of acute inflammation: Novel pro-resolving lipid mediators in resolution, *Semin Immunol* 27(3) (2015) 200-15.
- [8] P.C. Calder, Polyunsaturated fatty acids and inflammatory processes: New twists in an old tale, *Biochimie* 91(6) (2009) 791-5.
- [9] H. Harizi, J.B. Corcuff, N. Gualde, Arachidonic-acid-derived eicosanoids: roles in biology and immunopathology, *Trends Mol Med* 14(10) (2008) 461-9.
- [10] J. Lombard, Once upon a time the cell membranes: 175 years of cell boundary research, *Biol Direct* 9 (2014) 32.
- [11] G. van Meer, D.R. Voelker, G.W. Feigenson, Membrane lipids: where they are and how they behave, *Nat Rev Mol Cell Biol* 9(2) (2008) 112-24.
- [12] E.M. Hein, L.M. Blank, J. Heyland, J.I. Baumbach, A. Schmid, H. Hayen, Glycerophospholipid profiling by high-performance liquid chromatography/mass spectrometry using exact mass measurements and multi-stage mass spectrometric fragmentation experiments in parallel, *Rapid Commun Mass Spectrom* 23(11) (2009) 1636-46.
- [13] C. Hunte, S. Richers, Lipids and membrane protein structures, *Curr Opin Struct Biol* 18(4) (2008) 406-11.
- [14] Ü. Coskun, M. Grzybek, D. Drechsel, K. Simons, Regulation of human EGF receptor by lipids, *Proceedings of the National Academy of Sciences* 108(22) (2011) 9044-9048.
- [15] M. Schieber, N.S. Chandel, ROS function in redox signaling and oxidative stress, *Curr Biol* 24(10) (2014) R453-62.
- [16] H. Sies, Oxidative stress: a concept in redox biology and medicine, *Redox Biol* 4 (2015) 180-3.
- [17] M.P. Murphy, How mitochondria produce reactive oxygen species, *Biochem J* 417(1) (2009) 1-13.
- [18] G. Lenaz, The mitochondrial production of reactive oxygen species: mechanisms and implications in human pathology, *IUBMB Life* 52(3-5) (2001) 159-64.
- [19] P. Pacher, J.S. Beckman, L. Liaudet, Nitric oxide and peroxynitrite in health and disease, *Physiol Rev* 87(1) (2007) 315-424.
- [20] A. Reis, C.M. Spickett, Chemistry of phospholipid oxidation, *Biochim Biophys Acta* 1818(10) (2012) 2374-87.
- [21] C.C. Winterbourn, Toxicity of iron and hydrogen peroxide: the Fenton reaction, *Toxicol Lett* 82-83 (1995) 969-74.
- [22] M. Valko, D. Leibfritz, J. Moncol, M.T. Cronin, M. Mazur, J. Telser, Free radicals and antioxidants in normal physiological functions and human disease, *Int J Biochem Cell Biol* 39(1) (2007) 44-84.
- [23] H. Yin, L. Xu, N.A. Porter, Free radical lipid peroxidation: mechanisms and analysis, *Chem Rev* 111(10) (2011) 5944-72.

- [24] K.V. Ramana, S. Srivastava, S.S. Singhal, Lipid Peroxidation Products in Human Health and Disease 2016, *Oxidative Medicine and Cellular Longevity* 2017 (2017) 2.
- [25] T.J. Montine, K.S. Montine, W. McMahan, W.R. Markesbery, J.F. Quinn, J.D. Morrow, F2-isoprostanes in Alzheimer and other neurodegenerative diseases, *Antioxid Redox Signal* 7(1-2) (2005) 269-75.
- [26] J.A. Berliner, J.W. Heinecke, The role of oxidized lipoproteins in atherogenesis, *Free Radic Biol Med* 20(5) (1996) 707-27.
- [27] S.S. Davies, L. Guo, Lipid peroxidation generates biologically active phospholipids including oxidatively N-modified phospholipids, *Chem Phys Lipids* 181 (2014) 1-33.
- [28] V.N. Bochkov, A. Kadl, J. Huber, F. Gruber, B.R. Binder, N. Leitinger, Protective role of phospholipid oxidation products in endotoxin-induced tissue damage, *Nature* 419(6902) (2002) 77-81.
- [29] M.Z. Ashraf, N.S. Kar, E.A. Podrez, Oxidized phospholipids: biomarker for cardiovascular diseases, *Int J Biochem Cell Biol* 41(6) (2009) 1241-4.
- [30] N.A. Porter, S.E. Caldwell, K.A. Mills, Mechanisms of free radical oxidation of unsaturated lipids, *Lipids* 30(4) (1995) 277-90.
- [31] B.C. Sousa, A.R. Pitt, C.M. Spickett, Chemistry and analysis of HNE and other prominent carbonyl-containing lipid oxidation compounds, *Free Radic Biol Med* 111 (2017) 294-308.
- [32] E. Niki, Y. Yoshida, Y. Saito, N. Noguchi, Lipid peroxidation: mechanisms, inhibition, and biological effects, *Biochem Biophys Res Commun* 338(1) (2005) 668-76.
- [33] B. Fuchs, K. Bresler, J. Schiller, Oxidative changes of lipids monitored by MALDI MS, *Chem Phys Lipids* 164(8) (2011) 782-95.
- [34] A.R. Brash, Autoxidation of methyl linoleate: identification of the bis-allylic 11-hydroperoxide, *Lipids* 35(9) (2000) 947-52.
- [35] K.A. Tallman, D.A. Pratt, N.A. Porter, Kinetic products of linoleate peroxidation: rapid beta-fragmentation of nonconjugated peroxy radicals, *J Am Chem Soc* 123(47) (2001) 11827-8.
- [36] W. Jira, G. Spiteller, W. Carson, A. Schramm, Strong increase in hydroxy fatty acids derived from linoleic acid in human low density lipoproteins of atherosclerotic patients, *Chem Phys Lipids* 91(1) (1998) 1-11.
- [37] C.J. Brooks, W.A. Harland, G. Steel, J.D. Gilbert, Lipids of human atheroma: isolation of hydroxyoctadecadienoic acids from advanced aortal lesions, *Biochim Biophys Acta* 202(3) (1970) 563-6.
- [38] J. Rolin, H. Vego, A.A. Maghazachi, Oxidized Lipids and Lysophosphatidylcholine Induce the Chemotaxis, Up-Regulate the Expression of CCR9 and CXCR4 and Abrogate the Release of IL-6 in Human Monocytes, *Toxins* 6(9) (2014) 2840-2856.
- [39] C.E. Ramsden, J.R. Hibbeln, S.F. Majchrzak, J.M. Davis, n-6 Fatty acid-specific and mixed polyunsaturate dietary interventions have different effects on CHD risk: a meta-analysis of randomised controlled trials, *British Journal of Nutrition* 104(11) (2010) 1586-1600.
- [40] V.N. Vangaveti, V.M. Shashidhar, C. Rush, U.H. Malabu, R.R. Rasalam, F. Collier, B.T. Baune, R.L. Kennedy, Hydroxyoctadecadienoic acids regulate apoptosis in human THP-1 cells in a PPAR $\gamma$ -dependent manner, *Lipids* 49(12) (2014) 1181-92.
- [41] H.W. Gardner, Oxygen radical chemistry of polyunsaturated fatty acids, *Free Radic Biol Med* 7(1) (1989) 65-86.
- [42] D. O'connor, E. Mihelich, M. Coleman, Stereochemical course of the autooxidative cyclization of lipid hydroperoxides to prostaglandin-like bicyclic endoperoxides, *Journal of the American Chemical Society* 106(12) (1984) 3577-3584.
- [43] E.S. Musiek, H. Yin, G.L. Milne, J.D. Morrow, Recent advances in the biochemistry and clinical relevance of the isoprostane pathway, *Lipids* 40(10) (2005) 987-94.
- [44] P. Montuschi, P.J. Barnes, L.J. Roberts, Isoprostanes: markers and mediators of oxidative stress, *FASEB J* 18(15) (2004) 1791-800.
- [45] M. Czernska, K. Mikołajewska, M. Zieliński, J. Gromadzińska, W. Wąsowicz, Today's oxidative stress markers, *Med Pr* 66(3) (2015) 393-405.

- [46] L.J. Roberts, J.D. Morrow, Measurement of F(2)-isoprostanes as an index of oxidative stress in vivo, *Free Radic Biol Med* 28(4) (2000) 505-13.
- [47] T. Obata, K. Tomaru, T. Nagakura, Y. Izumi, T. Kawamoto, Smoking and oxidant stress: assay of isoprostane in human urine by gas chromatography–mass spectrometry, *Journal of Chromatography B: Biomedical Sciences and Applications* 746(1) (2000) 11-15.
- [48] G. Davì, M.T. Guagnano, G. Ciabattoni, S. Basili, A. Falco, M. Marinopiccoli, M. Nutini, S. Sensi, C. Patrono, Platelet Activation in Obese Women Role of Inflammation and Oxidant Stress, *JAMA* 288(16) (2002) 2008-2014.
- [49] G. Davì, G. Ciabattoni, A. Consoli, A. Mezzetti, A. Falco, S. Santarone, E. Pennese, E. Vitacolonna, T. Bucciarelli, F. Costantini, F. Capani, C. Patrono, In Vivo Formation of 8-Iso-Prostaglandin F<sub>2α</sub> and Platelet Activation in Diabetes Mellitus, *Circulation* 99(2) (1999) 224-229.
- [50] M.P. Reilly, D. Praticò, N. Delanty, G. DiMinno, E. Tremoli, D. Rader, S. Kapoor, J. Rokach, J. Lawson, G.A. FitzGerald, Increased Formation of Distinct F<sub>2</sub> Isoprostanes in Hypercholesterolemia, *Circulation* 98(25) (1998) 2822-2828.
- [51] D. Praticò, C.M. Clark, V.M. Lee, J.Q. Trojanowski, J. Rokach, G.A. FitzGerald, Increased 8,12-iso-iPF<sub>2α</sub>-VI in Alzheimer's disease: correlation of a noninvasive index of lipid peroxidation with disease severity, *Ann Neurol* 48(5) (2000) 809-12.
- [52] D. Mozaffarian, R. Micha, S. Wallace, Effects on coronary heart disease of increasing polyunsaturated fat in place of saturated fat: a systematic review and meta-analysis of randomized controlled trials, *PLoS Med* 7(3) (2010) e1000252.
- [53] D. Mozaffarian, R.N. Lemaitre, I.B. King, X. Song, H. Huang, F.M. Sacks, E.B. Rimm, M. Wang, D.S. Siscovick, Plasma phospholipid long-chain ω-3 fatty acids and total and cause-specific mortality in older adults: a cohort study, *Ann Intern Med* 158(7) (2013) 515-25.
- [54] L.C. Del Gobbo, F. Imamura, S. Aslibekyan, M. Marklund, J.K. Virtanen, M. Wennberg, M.Y. Yakoob, S.E. Chiuve, L. Dela Cruz, A.C. Frazier-Wood, A.M. Fretts, E. Guallar, C. Matsumoto, K. Prem, T. Tanaka, J.H. Wu, X. Zhou, C. Helmer, E. Ingelsson, J.M. Yuan, P. Barberger-Gateau, H. Campos, P.H. Chaves, L. Djoussé, G.G. Giles, J. Gómez-Aracena, A.M. Hodge, F.B. Hu, J.H. Jansson, I. Johansson, K.T. Khaw, W.P. Koh, R.N. Lemaitre, L. Lind, R.N. Luben, E.B. Rimm, U. Risérus, C. Samieri, P.W. Franks, D.S. Siscovick, M. Stampfer, L.M. Steffen, B.T. Steffen, M.Y. Tsai, R.M. van Dam, S. Voutilainen, W.C. Willett, M. Woodward, D. Mozaffarian, C.f.H.a.A.R.i.G.E.C.F.A.a.O.R.C. (FORCe), ω-3 Polyunsaturated Fatty Acid Biomarkers and Coronary Heart Disease: Pooling Project of 19 Cohort Studies, *JAMA Intern Med* 176(8) (2016) 1155-66.
- [55] J.H. Wu, R. Micha, F. Imamura, A. Pan, M.L. Biggs, O. Ajaz, L. Djousse, F.B. Hu, D. Mozaffarian, Omega-3 fatty acids and incident type 2 diabetes: a systematic review and meta-analysis, *Br J Nutr* 107 Suppl 2 (2012) S214-27.
- [56] E.C. Rizos, E.E. Ntzani, E. Bika, M.S. Kostapanos, M.S. Elisaf, Association Between Omega-3 Fatty Acid Supplementation and Risk of Major Cardiovascular Disease Events: A Systematic Review and Meta-analysis Omega-3 Fatty Acids and Cardiovascular Disease, *JAMA* 308(10) (2012) 1024-1033.
- [57] A. Ismail, G. Bannenberg, H.B. Rice, E. Schutt, D. MacKay, Oxidation in EPA- and DHA-rich oils: an overview, *Lipid Technology* 28(3-4) (2016) 55-59.
- [58] M. Zerouga, W. Stillwell, J. Stone, A. Powner, L.J. Jenki, Phospholipid class as a determinant in docosahexaenoic acid's effect on tumor cell viability, *Anticancer Res* 16(5A) (1996) 2863-8.
- [59] V.P. Yakubenko, K. Cui, C.L. Ardell, K.E. Brown, X.Z. West, D. Gao, S. Stefl, R.G. Salomon, E.A. Podrez, T.V. Byzova, Oxidative modifications of extracellular matrix promote the second wave of inflammation via β<sub>2</sub> integrins, *Blood* 132(1) (2018) 78.
- [60] A.N. Onyango, Small reactive carbonyl compounds as tissue lipid oxidation products; and the mechanisms of their formation thereby, *Chem Phys Lipids* 165(7) (2012) 777-86.
- [61] X. Gu, R.G. Salomon, Fragmentation of a linoleate-derived γ-hydroperoxy-α,β-unsaturated epoxide to γ-hydroxy- and γ-oxo-alkenals involves a unique pseudo-symmetrical diepoxycarbinyl radical, *Free Radic Biol Med* 52(3) (2012) 601-606.

- [62] C. Schneider, N.A. Porter, A.R. Brash, Routes to 4-hydroxynonenal: fundamental issues in the mechanisms of lipid peroxidation, *J Biol Chem* 283(23) (2008) 15539-43.
- [63] C.M. Spickett, The lipid peroxidation product 4-hydroxy-2-nonenal: Advances in chemistry and analysis, *Redox Biol* 1 (2013) 145-52.
- [64] H.-Y. Wu, J.-K. Lin, Determination of Aldehydic Lipid Peroxidation Products With Dabsylhydrazine by High-Performance Liquid Chromatography, *Analytical Chemistry* 67(9) (1995) 1603-1612.
- [65] W.A. Pryor, E. Bermúdez, R. Cueto, G.L. Squadrito, Detection of aldehydes in bronchoalveolar lavage of rats exposed to ozone, *Fundam Appl Toxicol* 34(1) (1996) 148-56.
- [66] M.W. Frampton, W.A. Pryor, R. Cueto, C. Cox, P.E. Morrow, M.J. Utell, Ozone exposure increases aldehydes in epithelial lining fluid in human lung, *Am J Respir Crit Care Med* 159(4 Pt 1) (1999) 1134-7.
- [67] S. Kumar, J. Huang, N. Abbassi-Ghadi, H.A. Mackenzie, K.A. Veselkov, J.M. Hoare, L.B. Lovat, P. Španěl, D. Smith, G.B. Hanna, Mass Spectrometric Analysis of Exhaled Breath for the Identification of Volatile Organic Compound Biomarkers in Esophageal and Gastric Adenocarcinoma, *Ann Surg* 262(6) (2015) 981-90.
- [68] A.D. Watson, N. Leitinger, M. Navab, K.F. Faull, S. Hörkkö, J.L. Witztum, W. Palinski, D. Schwenke, R.G. Salomon, W. Sha, G. Subbanagounder, A.M. Fogelman, J.A. Berliner, Structural identification by mass spectrometry of oxidized phospholipids in minimally oxidized low density lipoprotein that induce monocyte/endothelial interactions and evidence for their presence in vivo, *J Biol Chem* 272(21) (1997) 13597-607.
- [69] C.M. Spickett, A. Reis, A.R. Pitt, Use of narrow mass-window, high-resolution extracted product ion chromatograms for the sensitive and selective identification of protein modifications, *Anal Chem* 85(9) (2013) 4621-7.
- [70] H. Esterbauer, R.J. Schaur, H. Zollner, Chemistry and biochemistry of 4-hydroxynonenal, malonaldehyde and related aldehydes, *Free Radic Biol Med* 11(1) (1991) 81-128.
- [71] J.F. Stevens, C.S. Maier, Acrolein: sources, metabolism, and biomolecular interactions relevant to human health and disease, *Mol Nutr Food Res* 52(1) (2008) 7-25.
- [72] D. Aizenbud, I. Aizenbud, A.Z. Reznick, K. Avezov, Acrolein-an  $\alpha,\beta$ -Unsaturated Aldehyde: A Review of Oral Cavity Exposure and Oral Pathology Effects, *Rambam Maimonides Med J* 7(3) (2016).
- [73] S. Horiyama, M. Kunitomo, N. Yoshikawa, K. Nakamura, Mass Spectrometric Approaches to the Identification of Potential Ingredients in Cigarette Smoke Causing Cytotoxicity, *Biol Pharm Bull* 39(6) (2016) 903-8.
- [74] K. Uchida, M. Kanematsu, Y. Morimitsu, T. Osawa, N. Noguchi, E. Niki, Acrolein is a product of lipid peroxidation reaction. Formation of free acrolein and its conjugate with lysine residues in oxidized low density lipoproteins, *J Biol Chem* 273(26) (1998) 16058-66.
- [75] C. Lambert, J. McCue, M. Portas, Y. Ouyang, J. Li, T.G. Rosano, A. Lazis, B.M. Freed, Acrolein in cigarette smoke inhibits T-cell responses, *J Allergy Clin Immunol* 116(4) (2005) 916-22.
- [76] J. Luo, R. Shi, Acrolein induces axolemmal disruption, oxidative stress, and mitochondrial impairment in spinal cord tissue, *Neurochem Int* 44(7) (2004) 475-86.
- [77] R. Shi, T. Rickett, W. Sun, Acrolein-mediated injury in nervous system trauma and diseases, *Mol Nutr Food Res* 55(9) (2011) 1320-31.
- [78] R. Shi, The dynamics of axolemmal disruption in guinea pig spinal cord following compression, *J Neurocytol* 33(2) (2004) 203-11.
- [79] R.E. Biagini, M.A. Toraason, D.W. Lynch, G.W. Winston, Inhibition of rat heart mitochondrial electron transport in vitro: implications for the cardiotoxic action of allylamine or its primary metabolite, acrolein, *Toxicology* 62(1) (1990) 95-106.
- [80] J.P. Kehrer, S.S. Biswal, The molecular effects of acrolein, *Toxicol Sci* 57(1) (2000) 6-15.
- [81] J. Luo, R. Shi, Acrolein induces oxidative stress in brain mitochondria, *Neurochem Int* 46(3) (2005) 243-52.

- [82] R.A. Vaishnav, I.N. Singh, D.M. Miller, E.D. Hall, Lipid peroxidation-derived reactive aldehydes directly and differentially impair spinal cord and brain mitochondrial function, *J Neurotrauma* 27(7) (2010) 1311-20.
- [83] IARC monographs on the evaluation of the carcinogenic risk of chemicals to humans: some monomers, plastics and synthetic elastomers, and acrolein, *IARC Monogr Eval Carcinog Risk Chem Hum* 19 (1979) 1-513.
- [84] I. Rahman, W. MacNee, Lung glutathione and oxidative stress: implications in cigarette smoke-induced airway disease, *Am J Physiol* 277(6) (1999) L1067-88.
- [85] H. Yao, I. Rahman, Current concepts on oxidative/carbonyl stress, inflammation and epigenetics in pathogenesis of chronic obstructive pulmonary disease, *Toxicol Appl Pharmacol* 254(2) (2011) 72-85.
- [86] S.D. Sithu, S. Srivastava, M.A. Siddiqui, E. Vladykovskaya, D.W. Riggs, D.J. Conklin, P. Haberkzettel, T.E. O'Toole, A. Bhatnagar, S.E. D'Souza, Exposure to acrolein by inhalation causes platelet activation, *Toxicol Appl Pharmacol* 248(2) (2010) 100-10.
- [87] J. Luo, B.G. Hill, Y. Gu, J. Cai, S. Srivastava, A. Bhatnagar, S.D. Prabhu, Mechanisms of acrolein-induced myocardial dysfunction: implications for environmental and endogenous aldehyde exposure, *Am J Physiol Heart Circ Physiol* 293(6) (2007) H3673-84.
- [88] X. Liu, W. Zheng, M.P. Sivasankar, Acute Acrolein Exposure Induces Impairment of Vocal Fold Epithelial Barrier Function, *PLoS One* 11(9) (2016) e0163237.
- [89] S. Uchiyama, K. Ohta, Y. Inaba, N. Kunugita, Determination of carbonyl compounds generated from the E-cigarette using coupled silica cartridges impregnated with hydroquinone and 2,4-dinitrophenylhydrazine, followed by high-performance liquid chromatography, *Anal Sci* 29(12) (2013) 1219-22.
- [90] H. McRobbie, A. Phillips, M.L. Goniewicz, K.M. Smith, O. Knight-West, D. Przulj, P. Hajek, Effects of Switching to Electronic Cigarettes with and without Concurrent Smoking on Exposure to Nicotine, Carbon Monoxide, and Acrolein, *Cancer Prevention Research* 8(9) (2015) 873.
- [91] A. Khlystov, V. Samburova, Flavoring Compounds Dominate Toxic Aldehyde Production during E-Cigarette Vaping, *Environ Sci Technol* 50(23) (2016) 13080-13085.
- [92] S.S. Hecht, S.G. Carmella, D. Kotandeniya, M.E. Pillsbury, M. Chen, B.W.S. Ransom, R.I. Vogel, E. Thompson, S.E. Murphy, D.K. Hatsukami, Evaluation of Toxicant and Carcinogen Metabolites in the Urine of E-Cigarette Users Versus Cigarette Smokers, *Nicotine & Tobacco Research* 17(6) (2014) 704-709.
- [93] S. Stein, Y. Lao, I.Y. Yang, S.S. Hecht, M. Moriya, Genotoxicity of acetaldehyde- and crotonaldehyde-induced 1,N2-propanodeoxyguanosine DNA adducts in human cells, *Mutat Res* 608(1) (2006) 1-7.
- [94] B. Ul Islam, P. Ahmad, G. Rabbani, K. Dixit, Moinuddin, S.A. Siddiqui, A. Ali, Neo-epitopes on crotonaldehyde modified DNA preferably recognize circulating autoantibodies in cancer patients, *Tumour Biol* 37(2) (2016) 1817-24.
- [95] K. Ishino, C. Wakita, T. Shibata, S. Toyokuni, S. Machida, S. Matsuda, T. Matsuda, K. Uchida, Lipid peroxidation generates body odor component trans-2-nonenal covalently bound to protein in vivo, *J Biol Chem* 285(20) (2010) 15302-13.
- [96] S. Haze, Y. Gozu, S. Nakamura, Y. Kohno, K. Sawano, H. Ohta, K. Yamazaki, 2-Nonenal newly found in human body odor tends to increase with aging, *J Invest Dermatol* 116(4) (2001) 520-4.
- [97] A. Hernández-Hernández, J. Sánchez-Yagüe, E.M. Martín-Valmaseda, M. Llanillo, Oxidative inactivation of human and sheep platelet membrane-associated phosphotyrosine phosphatase activity, *Free Radic Biol Med* 26(9-10) (1999) 1218-30.
- [98] T. Ohyashiki, K. Kamata, M. Takeuchi, K. Matsui, Contribution of peroxidation products to oxidative inactivation of rat liver microsomal glucose-6-phosphatase, *J Biochem* 118(3) (1995) 508-14.
- [99] Y. Riahi, G. Cohen, O. Shamni, S. Sasson, Signaling and cytotoxic functions of 4-hydroxyalkenals, *Am J Physiol Endocrinol Metab* 299(6) (2010) E879-86.
- [100] R.J. Schaur, W. Siems, N. Bresgen, P.M. Eckl, 4-Hydroxy-nonenal-A Bioactive Lipid Peroxidation Product, *Biomolecules* 5(4) (2015) 2247-337.

- [101] S. Bacot, N. Bernoud-Hubac, N. Baddas, B. Chantegrel, C. Deshayes, A. Doutheau, M. Lagarde, M. Guichardant, Covalent binding of hydroxy-alkenals 4-HDDE, 4-HHE, and 4-HNE to ethanolamine phospholipid subclasses, *J Lipid Res* 44(5) (2003) 917-26.
- [102] C. Schneider, K.A. Tallman, N.A. Porter, A.R. Brash, Two distinct pathways of formation of 4-hydroxynonenal. Mechanisms of nonenzymatic transformation of the 9- and 13-hydroperoxides of linoleic acid to 4-hydroxyalkenals, *J Biol Chem* 276(24) (2001) 20831-8.
- [103] S. Sasson, Nutrient overload, lipid peroxidation and pancreatic beta cell function, *Free Radic Biol Med* 111 (2017) 102-109.
- [104] A. Ayala, M.F. Muñoz, S. Argüelles, Lipid peroxidation: production, metabolism, and signaling mechanisms of malondialdehyde and 4-hydroxy-2-nonenal, *Oxid Med Cell Longev* 2014 (2014) 360438.
- [105] E.E. Dubinina, V.A. Dadali, Role of 4-hydroxy-trans-2-nonenal in cell functions, *Biochemistry (Mosc)* 75(9) (2010) 1069-87.
- [106] E. López-Bernardo, A. Anedda, P. Sánchez-Pérez, B. Acosta-Iborra, S. Cadenas, 4-Hydroxynonenal induces Nrf2-mediated UCP3 upregulation in mouse cardiomyocytes, *Free Radic Biol Med* 88(Pt B) (2015) 427-438.
- [107] H. Zhang, H.J. Forman, 4-Hydroxynonenal activates Src through a non-canonical pathway that involves EGFR/PTP1B, *Free Radic Biol Med* 89 (2015) 701-7.
- [108] A. Manea, S.A. Manea, A. Todirita, I.C. Albulescu, M. Raicu, S. Sasson, M. Simionescu, High-glucose-increased expression and activation of NADPH oxidase in human vascular smooth muscle cells is mediated by 4-hydroxynonenal-activated PPAR $\alpha$  and PPAR $\beta/\delta$ , *Cell Tissue Res* 361(2) (2015) 593-604.
- [109] X.H. Yu, Y.C. Fu, D.W. Zhang, K. Yin, C.K. Tang, Foam cells in atherosclerosis, *Clin Chim Acta* 424 (2013) 245-52.
- [110] Y. Riahi, N. Kaiser, G. Cohen, I. Abd-Elrahman, G. Blum, O.M. Shapira, T. Koler, M. Simionescu, A.V. Sima, N. Zarkovic, K. Zarkovic, M. Orioli, G. Aldini, E. Cerasi, G. Leibowitz, S. Sasson, Foam cell-derived 4-hydroxynonenal induces endothelial cell senescence in a TXNIP-dependent manner, *J Cell Mol Med* 19(8) (2015) 1887-99.
- [111] J.M. Camarillo, K.L. Rose, J.J. Galligan, S. Xu, L.J. Marnett, Covalent Modification of CDK2 by 4-Hydroxynonenal as a Mechanism of Inhibition of Cell Cycle Progression, *Chem Res Toxicol* 29(3) (2016) 323-32.
- [112] C. Kabuta, K. Kono, K. Wada, T. Kabuta, 4-Hydroxynonenal induces persistent insolubilization of TDP-43 and alters its intracellular localization, *Biochem Biophys Res Commun* 463(1-2) (2015) 82-7.
- [113] F.J. Van Kuijk, L.L. Holte, E.A. Dratz, 4-Hydroxyhexenal: a lipid peroxidation product derived from oxidized docosahexaenoic acid, *Biochim Biophys Acta* 1043(1) (1990) 116-8.
- [114] E.K. Long, M.J. Picklo, Trans-4-hydroxy-2-hexenal, a product of n-3 fatty acid peroxidation: make some room HNE.. *Free Radic Biol Med* 49(1) (2010) 1-8.
- [115] M. Awada, C.O. Soulage, A. Meynier, C. Debard, P. Plaisancié, B. Benoit, G. Picard, E. Loizon, M.A. Chauvin, M. Estienne, N. Peretti, M. Guichardant, M. Lagarde, C. Genot, M.C. Michalski, Dietary oxidized n-3 PUFA induce oxidative stress and inflammation: role of intestinal absorption of 4-HHE and reactivity in intestinal cells, *J Lipid Res* 53(10) (2012) 2069-80.
- [116] A. Ishikado, Y. Nishio, K. Morino, S. Ugi, H. Kondo, T. Makino, A. Kashiwagi, H. Maegawa, Low concentration of 4-hydroxy hexenal increases heme oxygenase-1 expression through activation of Nrf2 and antioxidative activity in vascular endothelial cells, *Biochem Biophys Res Commun* 402(1) (2010) 99-104.
- [117] A. Ishikado, K. Morino, Y. Nishio, F. Nakagawa, A. Mukose, Y. Sono, N. Yoshioka, K. Kondo, O. Sekine, T. Yoshizaki, S. Ugi, T. Uzu, H. Kawai, T. Makino, T. Okamura, M. Yamamoto, A. Kashiwagi, H. Maegawa, 4-Hydroxy hexenal derived from docosahexaenoic acid protects endothelial cells via Nrf2 activation, *PLoS One* 8(7) (2013) e69415.
- [118] M. Guichardant, S. Bacot, P. Molière, M. Lagarde, Hydroxy-alkenals from the peroxidation of n-3 and n-6 fatty acids and urinary metabolites, *Prostaglandins Leukot Essent Fatty Acids* 75(3) (2006) 179-82.

- [119] P. Spiteller, W. Kern, J. Reiner, G. Spiteller, Aldehydic lipid peroxidation products derived from linoleic acid, *Biochim Biophys Acta* 1531(3) (2001) 188-208.
- [120] K. Kawai, K. Matsuno, H. Kasai, Detection of 4-oxo-2-hexenal, a novel mutagenic product of lipid peroxidation, in human diet and cooking vapor, *Mutat Res* 603(2) (2006) 186-92.
- [121] Z. Liu, P.E. Minkler, L.M. Sayre, Mass spectroscopic characterization of protein modification by 4-hydroxy-2-(E)-nonenal and 4-oxo-2-(E)-nonenal, *Chem Res Toxicol* 16(7) (2003) 901-11.
- [122] S.H. Lee, I.A. Blair, Characterization of 4-oxo-2-nonenal as a novel product of lipid peroxidation, *Chem Res Toxicol* 13(8) (2000) 698-702.
- [123] D. Lin, H.G. Lee, Q. Liu, G. Perry, M.A. Smith, L.M. Sayre, 4-Oxo-2-nonenal is both more neurotoxic and more protein reactive than 4-hydroxy-2-nonenal, *Chem Res Toxicol* 18(8) (2005) 1219-31.
- [124] N. Otaki, M. Chikazawa, R. Nagae, Y. Shimozu, T. Shibata, S. Ito, Y. Takasaki, J. Fujii, K. Uchida, Identification of a lipid peroxidation product as the source of oxidation-specific epitopes recognized by anti-DNA autoantibodies, *J Biol Chem* 285(44) (2010) 33834-42.
- [125] J.J. Galligan, K.L. Rose, W.N. Beavers, S. Hill, K.A. Tallman, W.P. Tansey, L.J. Marnett, Stable histone adduction by 4-oxo-2-nonenal: a potential link between oxidative stress and epigenetics, *J Am Chem Soc* 136(34) (2014) 11864-6.
- [126] H. Kasai, K. Kawai, 4-oxo-2-hexenal, a mutagen formed by omega-3 fat peroxidation: occurrence, detection and adduct formation, *Mutat Res* 659(1-2) (2008) 56-9.
- [127] M. Guichardant, B. Chantegrel, C. Deshayes, A. Doutheau, P. Moliere, M. Lagarde, Specific markers of lipid peroxidation issued from n-3 and n-6 fatty acids, *Biochem Soc Trans* 32(Pt 1) (2004) 139-40.
- [128] V. Voitkun, A. Zhitkovich, Analysis of DNA-protein crosslinking activity of malondialdehyde in vitro, *Mutat Res* 424(1-2) (1999) 97-106.
- [129] D. Del Rio, A.J. Stewart, N. Pellegrini, A review of recent studies on malondialdehyde as toxic molecule and biological marker of oxidative stress, Nutrition, metabolism, and cardiovascular diseases : *NMCD* 15(4) (2005) 316-28.
- [130] M. Khoubnasabjafari, K. Ansarin, A. Jouyban, Reliability of malondialdehyde as a biomarker of oxidative stress in psychological disorders, *Bioimpacts* 5(3) (2015) 123-7.
- [131] M. Hecker, V. Ullrich, On the mechanism of prostacyclin and thromboxane A2 biosynthesis, *J Biol Chem* 264(1) (1989) 141-50.
- [132] W.A. Pryor, J.P. Stanley, E. Blair, Autoxidation of polyunsaturated fatty acids: II. A suggested mechanism for the formation of TBA-reactive materials from prostaglandin-like endoperoxides, *Lipids* 11(5) (1976) 370-9.
- [133] S.P. Aubourg, Interaction of malondialdehyde with biological molecules — new trends about reactivity and significance, *International Journal of Food Science & Technology* 28(4) (1993) 323-335.
- [134] L.J. Niedernhofer, J.S. Daniels, C.A. Rouzer, R.E. Greene, L.J. Marnett, Malondialdehyde, a product of lipid peroxidation, is mutagenic in human cells, *J Biol Chem* 278(33) (2003) 31426-33.
- [135] W. Palinski, V.A. Ord, A.S. Plump, J.L. Breslow, D. Steinberg, J.L. Witztum, ApoE-deficient mice are a model of lipoprotein oxidation in atherogenesis. Demonstration of oxidation-specific epitopes in lesions and high titers of autoantibodies to malondialdehyde-lysine in serum, *Arterioscler Thromb* 14(4) (1994) 605-16.
- [136] M. Veneskoski, S.P. Turunen, O. Kummu, A. Nissinen, S. Rannikko, A.L. Levonen, S. Hörkkö, Specific recognition of malondialdehyde and malondialdehyde acetaldehyde adducts on oxidized LDL and apoptotic cells by complement anaphylatoxin C3a, *Free Radic Biol Med* 51(4) (2011) 834-43.
- [137] M.P. Kalapos, Where does plasma methylglyoxal originate from?, *Diabetes Res Clin Pract* 99(3) (2013) 260-71.
- [138] A.K. Thukkani, F.F. Hsu, J.R. Crowley, R.B. Wysolmerski, C.J. Albert, D.A. Ford, Reactive chlorinating species produced during neutrophil activation target tissue



- plasmalogens: production of the chemoattractant, 2-chlorohexadecanal, *J Biol Chem* 277(6) (2002) 3842-9.
- [139] M.B. Lampert, S.J. Weiss, The chlorinating potential of the human monocyte, *Blood* 62(3) (1983) 645-51.
- [140] S. Sugiyama, Y. Okada, G.K. Sukhova, R. Virmani, J.W. Heinecke, P. Libby, Macrophage myeloperoxidase regulation by granulocyte macrophage colony-stimulating factor in human atherosclerosis and implications in acute coronary syndromes, *Am J Pathol* 158(3) (2001) 879-91.
- [141] S.J. Weiss, R. Klein, A. Slivka, M. Wei, Chlorination of taurine by human neutrophils. Evidence for hypochlorous acid generation, *J Clin Invest* 70(3) (1982) 598-607.
- [142] M.C. Messner, C.J. Albert, F.F. Hsu, D.A. Ford, Selective plasmalogen oxidation by hypochlorous acid: formation of lysophosphatidylcholine chlorohydrins, *Chem Phys Lipids* 144(1) (2006) 34-44.
- [143] C.J. Albert, J.R. Crowley, F.F. Hsu, A.K. Thukkani, D.A. Ford, Reactive chlorinating species produced by myeloperoxidase target the vinyl ether bond of plasmalogens: identification of 2-chlorohexadecanal, *J Biol Chem* 276(26) (2001) 23733-41.
- [144] K. Uchida, Protein Lipoxidation, *Lipid Oxidation in Health and Disease* CRC Press 2015 pp. 119-134.
- [145] M.C. Messner, C.J. Albert, J. McHowat, D.A. Ford, Identification of lysophosphatidylcholine-chlorohydrin in human atherosclerotic lesions, *Lipids* 43(3) (2008) 243-9.
- [146] J. Lessig, J. Schiller, J. Arnhold, B. Fuchs, Hypochlorous acid-mediated generation of glycerophosphocholine from unsaturated plasmalogen glycerophosphocholine lipids, *J Lipid Res* 48(6) (2007) 1316-24.
- [147] A.K. Thukkani, J. McHowat, F.F. Hsu, M.L. Brennan, S.L. Hazen, D.A. Ford, Identification of alpha-chloro fatty aldehydes and unsaturated lysophosphatidylcholine molecular species in human atherosclerotic lesions, *Circulation* 108(25) (2003) 3128-33.
- [148] A. Ullen, G. Fauler, H. Köfeler, S. Walzl, C. Nussold, E. Bernhart, H. Reicher, H.J. Leis, A. Wintersperger, E. Malle, W. Sattler, Mouse brain plasmalogens are targets for hypochlorous acid-mediated modification in vitro and in vivo, *Free Radic Biol Med* 49(11) (2010) 1655-65.
- [149] G. Marsche, R. Heller, G. Fauler, A. Kovacevic, A. Nuzskowski, W. Graier, W. Sattler, E. Malle, 2-chlorohexadecanal derived from hypochlorite-modified high-density lipoprotein-associated plasmalogen is a natural inhibitor of endothelial nitric oxide biosynthesis, *Arterioscler Thromb Vasc Biol* 24(12) (2004) 2302-6.
- [150] K.R. Wildsmith, C.J. Albert, D.S. Anbukumar, D.A. Ford, Metabolism of myeloperoxidase-derived 2-chlorohexadecanal, *J Biol Chem* 281(25) (2006) 16849-60.
- [151] M.C. Messner, C.J. Albert, D.A. Ford, 2-Chlorohexadecanal and 2-chlorohexadecanoic acid induce COX-2 expression in human coronary artery endothelial cells, *Lipids* 43(7) (2008) 581-8.
- [152] A. Ullen, G. Fauler, E. Bernhart, C. Nussold, H. Reicher, H.J. Leis, E. Malle, W. Sattler, Phloretin ameliorates 2-chlorohexadecanal-mediated brain microvascular endothelial cell dysfunction in vitro, *Free Radic Biol Med* 53(9) (2012) 1770-81.
- [153] D. Ford, Halogenated Lipids: Products of Peroxidase-Derived Reactive Halogenating Species Targeting Conventional Lipids, *Lipid Oxidation in Health and Disease*, CRC Press 2015, pp. 77-100.
- [154] B.S. Berlett, E.R. Stadtman, Protein oxidation in aging, disease, and oxidative stress, *J Biol Chem* 272(33) (1997) 20313-6.
- [155] Schiff bases: A short review of their antimicrobial activities, *Journal of Advanced Research* 2(1) (2011) 1 - 8.
- [156] T. Tokoroyama, Discovery of the Michael Reaction, *European Journal of Organic Chemistry* 2010(10) (2010) 2009-2016.
- [157] A. Furuhashi, T. Ishii, S. Kumazawa, T. Yamada, T. Nakayama, K. Uchida, N(epsilon)-(3-methylpyridinium)lysine, a major antigenic adduct generated in acrolein-modified protein, *J Biol Chem* 278(49) (2003) 48658-65.

- [158] K. Ichihashi, T. Osawa, S. Toyokuni, K. Uchida, Endogenous formation of protein adducts with carcinogenic aldehydes: implications for oxidative stress, *J Biol Chem* 276(26) (2001) 23903-13.
- [159] M. Alaiz, S. Barragán, Changes induced in bovine serum albumin following interactions with the lipid peroxidation product E-2-octenal, *Chem Phys Lipids* 77(2) (1995) 217-23.
- [160] A. Baker, L. Zidek, D. Wiesler, J. Chmelík, M. Pagel, M.V. Novotny, Reaction of N-acetylglucyllysine methyl ester with 2-alkenals: an alternative model for covalent modification of proteins, *Chem Res Toxicol* 11(7) (1998) 730-40.
- [161] K. Uchida, E.R. Stadtman, Selective cleavage of thioether linkage in proteins modified with 4-hydroxynonenal, *Proc Natl Acad Sci U S A* 89(12) (1992) 5611-5.
- [162] K. Uchida, E.R. Stadtman, Modification of histidine residues in proteins by reaction with 4-hydroxynonenal, *Proc Natl Acad Sci U S A* 89(10) (1992) 4544-8.
- [163] K. Uchida, E.R. Stadtman, Covalent attachment of 4-hydroxynonenal to glyceraldehyde-3-phosphate dehydrogenase. A possible involvement of intra- and intermolecular cross-linking reaction, *J Biol Chem* 268(9) (1993) 6388-93.
- [164] L.M. Sayre, P.K. Arora, R.S. Iyer, R.G. Salomon, Pyrrole formation from 4-hydroxynonenal and primary amines, *Chem Res Toxicol* 6(1) (1993) 19-22.
- [165] M.X. Fu, J.R. Requena, A.J. Jenkins, T.J. Lyons, J.W. Baynes, S.R. Thorpe, The advanced glycation end product, Nepsilon-(carboxymethyl)lysine, is a product of both lipid peroxidation and glycoxidation reactions, *J Biol Chem* 271(17) (1996) 9982-6.
- [166] K.J. Wells-Knecht, E. Brinkmann, J.W. Baynes, Characterization of an Imidazolium Salt Formed from Glyoxal and N.alpha.-Hippuryllysine: A Model for Maillard Reaction Crosslinks in Proteins, *The Journal of Organic Chemistry* 60(20) (1995) 6246-6247.
- [167] U. Schwarzenbolz, T. Henle, R. Haeßner, H. Klostermeyer, On the reaction of glyoxal with proteins, *Zeitschrift für Lebensmitteluntersuchung und -Forschung A* 205(2) (1997) 121-124.
- [168] T. Ishii, S. Kumazawa, T. Sakurai, T. Nakayama, K. Uchida, Mass spectroscopic characterization of protein modification by malondialdehyde, *Chem Res Toxicol* 19(1) (2006) 122-9.
- [169] K. Itakura, K. Uchida, T. Osawa, A novel fluorescent malondialdehyde-lysine adduct, *Chemistry and Physics of Lipids* 84(1) (1996) 75-79.
- [170] J.A. Doorn, D.R. Petersen, Covalent modification of amino acid nucleophiles by the lipid peroxidation products 4-hydroxy-2-nonenal and 4-oxo-2-nonenal, *Chem Res Toxicol* 15(11) (2002) 1445-50.
- [171] X. Zhu, L.M. Sayre, Long-lived 4-oxo-2-enal-derived apparent lysine michael adducts are actually the isomeric 4-ketoamides, *Chem Res Toxicol* 20(2) (2007) 165-70.
- [172] T. Oe, S.H. Lee, M.V. Silva Elipse, B.H. Arison, I.A. Blair, A novel lipid hydroperoxide-derived modification to arginine, *Chem Res Toxicol* 16(12) (2003) 1598-605.
- [173] Y. Shimozu, T. Shibata, M. Ojika, K. Uchida, Identification of advanced reaction products originating from the initial 4-oxo-2-nonenal-cysteine Michael adducts, *Chem Res Toxicol* 22(5) (2009) 957-64.
- [174] A.K. Yocum, T. Oe, A.L. Yergey, I.A. Blair, Novel lipid hydroperoxide-derived hemoglobin histidine adducts as biomarkers of oxidative stress, *J Mass Spectrom* 40(6) (2005) 754-64.
- [175] G. Aldini, M. Carini, K.J. Yeum, G. Vistoli, Novel molecular approaches for improving enzymatic and nonenzymatic detoxification of 4-hydroxynonenal: toward the discovery of a novel class of bioactive compounds, *Free Radic Biol Med* 69 (2014) 145-56.
- [176] R.M. Lopachin, B.C. Geohagen, T. Gavin, Synaptosomal toxicity and nucleophilic targets of 4-hydroxy-2-nonenal, *Toxicol Sci* 107(1) (2009) 171-81.
- [177] C.M. Wong, L. Marcocci, D. Das, X. Wang, H. Luo, M. Zungu-Edmondson, Y.J. Suzuki, Mechanism of protein decarbonylation, *Free Radic Biol Med* 65 (2013) 1126-1133.
- [178] C.M. Wong, L. Marcocci, L. Liu, Y.J. Suzuki, Cell signaling by protein carbonylation and decarbonylation, *Antioxid Redox Signal* 12(3) (2010) 393-404.

- [179] M.J. Randall, M. Hristova, A. van der Vliet, Protein alkylation by the  $\alpha,\beta$ -unsaturated aldehyde acrolein. A reversible mechanism of electrophile signaling?, *FEBS Lett* 587(23) (2013) 3808-14.
- [180] G. Vistoli, C. Mantovani, S. Gervasoni, A. Pedretti, G. Aldini, Key factors regulating protein carbonylation by  $\alpha,\beta$  unsaturated carbonyls: A structural study based on a retrospective meta-analysis, *Biophys Chem* 230 (2017) 20-26.
- [181] G. Aldini, G. Vistoli, M. Stefek, N. Chondrogianni, T. Grune, J. Sereikaite, I. Sadowska-Bartosz, G. Bartosz, Molecular strategies to prevent, inhibit, and degrade advanced glycoxidation and advanced lipoxidation end products, *Free Radic Res* 47 Suppl 1 (2013) 93-137.
- [182] H. Esterbauer, H. Zollner, N. Scholz, Reaction of glutathione with conjugated carbonyls, *Z Naturforsch C Biosci* 30(4) (1975) 466-73.
- [183] Y. Nomi, H. Aizawa, T. Kurata, K. Shindo, C.V. Nguyen, Glutathione reacts with glyoxal at the N-terminal, *Biosci Biotechnol Biochem* 73(11) (2009) 2408-11.
- [184] E.J. Anderson, G. Vistoli, L.A. Katunga, K. Funai, L. Regazzoni, T.B. Monroe, E. Gilardoni, L. Cannizzaro, M. Colzani, D. De Maddis, G. Rossoni, R. Canevotti, S. Gagliardi, M. Carini, G. Aldini, A carnosine analog mitigates metabolic disorders of obesity by reducing carbonyl stress, *J Clin Invest* 128(12) (2018) 5280-5293.
- [185] H. Esterbauer, H. Zollner, Methods for determination of aldehydic lipid peroxidation products, *Free Radic Biol Med* 7(2) (1989) 197-203.
- [186] D. Tsikas, Assessment of lipid peroxidation by measuring malondialdehyde (MDA) and relatives in biological samples: Analytical and biological challenges, *Anal Biochem* 524 (2017) 13-30.
- [187] M. Giera, H. Lingeman, W.M. Niessen, Recent Advancements in the LC- and GC-Based Analysis of Malondialdehyde (MDA): A Brief Overview, *Chromatographia* 75(9-10) (2012) 433-440.
- [188] N. Breusing, T. Grune, L. Andrisic, M. Atalay, G. Bartosz, F. Biasi, S. Borovic, L. Bravo, I. Casals, R. Casillas, A. Dinischiotu, J. Drzewinska, H. Faber, N.M. Fauzi, A. Gajewska, J. Gambini, D. Gradinaru, T. Kokkola, A. Lojek, W. Łuczaj, D. Margina, C. Mascia, R. Mateos, A. Meinitzer, M.T. Mitjavila, L. Mrakovcic, M.C. Munteanu, M. Podborska, G. Poli, P. Sicinska, E. Skrzydlewska, J. Vina, I. Wiswedel, N. Zarkovic, S. Zelzer, C.M. Spickett, An inter-laboratory validation of methods of lipid peroxidation measurement in UVA-treated human plasma samples, *Free Radical Research* 44(10) (2010) 1203-1215.
- [189] L.J. Yan, M.J. Forster, Chemical probes for analysis of carbonylated proteins: a review, *J Chromatogr B Analyt Technol Biomed Life Sci* 879(17-18) (2011) 1308-15.
- [190] P. Li, G. Ding, Y. Deng, D. Punyapitak, D. Li, Y. Cao, Determination of malondialdehyde in biological fluids by high-performance liquid chromatography using rhodamine B hydrazide as the derivatization reagent, *Free Radical Biology and Medicine* 65 (2013) 224-231.
- [191] S. Zelzer, H. Mangge, R. Oberreither, C. Bernecker, H.J. Gruber, F. Prüller, G. Fauler, Oxidative stress: Determination of 4-hydroxy-2-nonenal by gas chromatography/mass spectrometry in human and rat plasma, *Free Radical Research* 49(10) (2015) 1233-1238.
- [192] W.-y. Wang, C.J. Albert, D.A. Ford, Approaches for the analysis of chlorinated lipids, *Analytical Biochemistry* 443(2) (2013) 148-152.
- [193] A.K. Thukkani, B.D. Martinson, C.J. Albert, G.A. Vogler, D.A. Ford, Neutrophil-mediated accumulation of 2-ClHDA during myocardial infarction: 2-ClHDA-mediated myocardial injury, *American Journal of Physiology-Heart and Circulatory Physiology* 288(6) (2005) H2955-H2964.
- [194] E.V. Berdyshev, Mass spectrometry of fatty aldehydes, *Biochimica et Biophysica Acta (BBA) - Molecular and Cell Biology of Lipids* 1811(11) (2011) 680-693.
- [195] C. Douny, P. Bayram, F. Brose, G. Degand, M.-L. Scippo, Development of an LC-MS/MS analytical method for the simultaneous measurement of aldehydes from polyunsaturated fatty acids degradation in animal feed, *Drug Testing and Analysis* 8(5-6) (2016) 458-464.

- [196] L.M. Balogh, W.M. Atkins, Interactions of glutathione transferases with 4-hydroxynonenal, *Drug Metabolism Reviews* 43(2) (2011) 165-178.
- [197] J. Alary, L. Debrauwer, Y. Fernandez, A. Paris, J.-P. Cravedi, L. Dolo, D. Rao, G. Bories, Identification of Novel Urinary Metabolites of the Lipid Peroxidation Product 4-Hydroxy-2-nonenal in Rats, *Chemical Research in Toxicology* 11(11) (1998) 1368-1376.
- [198] K.-L. Pan, W.-J. Huang, M.-H. Hsu, H.-L. Lee, H.-J. Liu, C.-W. Cheng, M.-H. Tsai, M.-Y. Shen, P. Lin, Identification of trans,trans-2,4-Decadienal Metabolites in Mouse and Human Cells Using Liquid Chromatography–Mass Spectrometry, *Chemical Research in Toxicology* 27(10) (2014) 1707-1719.
- [199] M.A. Duerr, R. Aurora, D.A. Ford, Identification of glutathione adducts of  $\alpha$ -chlorofatty aldehydes produced in activated neutrophils, *J Lipid Res* 56(5) (2015) 1014-24.
- [200] W. Palinski, M.E. Rosenfeld, S. Ylä-Herttuala, G.C. Gurtner, S.S. Socher, S.W. Butler, S. Parthasarathy, T.E. Carew, D. Steinberg, J.L. Witztum, Low density lipoprotein undergoes oxidative modification in vivo, *Proceedings of the National Academy of Sciences* 86(4) (1989) 1372.
- [201] K. Uchida, K. Sakai, K. Itakura, T. Osawa, S. Toyokuni, Protein Modification by Lipid Peroxidation Products: Formation of Malondialdehyde-Derived N $\epsilon$ -(2-Propenal)lysine in Proteins, *Archives of Biochemistry and Biophysics* 346(1) (1997) 45-52.
- [202] K. Uchida, M. Kanematsu, K. Sakai, T. Matsuda, N. Hattori, Y. Mizuno, D. Suzuki, T. Miyata, N. Noguchi, E. Niki, T. Osawa, Protein-bound acrolein: Potential markers for oxidative stress, *Proceedings of the National Academy of Sciences* 95(9) (1998) 4882.
- [203] N. Tanaka, S. Tajima, A. Ishibashi, K. Uchida, T. Shigematsu, Immunohistochemical detection of lipid peroxidation products, protein-bound acrolein and 4-hydroxynonenal protein adducts, in actinic elastosis of photodamaged skin, *Arch Dermatol Res* 293(7) (2001) 363-7.
- [204] H. Li, J. Wang, B.S. Kaphalia, G.A.S. Ansari, M.F. Khan, Quantitation of Acrolein–Protein Adducts: Potential Biomarker of Acrolein Exposure, *Journal of Toxicology and Environmental Health, Part A* 67(6) (2004) 513-524.
- [205] J. Pan, B. Awoyemi, Z. Xuan, P. Vohra, H.-T. Wang, M. Dyba, E. Greenspan, Y. Fu, K. Creswell, L. Zhang, D. Berry, M.-S. Tang, F.-L. Chung, Detection of Acrolein-Derived Cyclic DNA Adducts in Human Cells by Monoclonal Antibodies, *Chemical Research in Toxicology* 25(12) (2012) 2788-2795.
- [206] D.A. Butterfield, L. Gu, F.D. Domenico, R.A.S. Robinson, Mass spectrometry and redox proteomics: Applications in disease, *Mass Spectrometry Reviews* 33(4) (2014) 277-301.
- [207] E. Shacter, Quantification and significance of protein oxidation in biological samples, *Drug Metab Rev* 32(3-4) (2000) 307-26.
- [208] C.M. Spickett, A.R. Pitt, Protein oxidation: role in signalling and detection by mass spectrometry, *Amino Acids* 42(1) (2012) 5-21.
- [209] J.B. Fenn, M. Mann, C.K. Meng, S.F. Wong, C.M. Whitehouse, Electrospray ionization for mass spectrometry of large biomolecules, *Science* 246(4926) (1989) 64-71.
- [210] F. Hillenkamp, M. Karas, R.C. Beavis, B.T. Chait, Matrix-assisted laser desorption/ionization mass spectrometry of biopolymers, *Analytical Chemistry* 63(24) (1991) 1193A-1203A.
- [211] I. Verrastro, S. Pasha, K.T. Jensen, A.R. Pitt, C.M. Spickett, Mass spectrometry-based methods for identifying oxidized proteins in disease: advances and challenges, *Biomolecules* 5(2) (2015) 378-411.
- [212] M.A. Baraibar, R. Ladouce, B. Friguet, Proteomic quantification and identification of carbonylated proteins upon oxidative stress and during cellular aging, *J Proteomics* 92 (2013) 63-70.
- [213] T.T. Reed, W.M. Pierce, W.R. Markesbery, D.A. Butterfield, Proteomic identification of HNE-bound proteins in early Alzheimer disease: Insights into the role of lipid peroxidation in the progression of AD, *Brain Res* 1274 (2009) 66-76.

- [214] I. Perdivara, L.J. Deterding, M. Przybylski, K.B. Tomer, Mass spectrometric identification of oxidative modifications of tryptophan residues in proteins: chemical artifact or post-translational modification?, *J Am Soc Mass Spectrom* 21(7) (2010) 1114-7.
- [215] J.V. Olsen, S.-E. Ong, M. Mann, Trypsin Cleaves Exclusively C-terminal to Arginine and Lysine Residues, *Molecular & Cellular Proteomics* 3(6) (2004) 608.
- [216] A. Shevchenko, H. Tomas, J. Havlis, J.V. Olsen, M. Mann, In-gel digestion for mass spectrometric characterization of proteins and proteomes, *Nat Protoc* 1(6) (2006) 2856-60.
- [217] C.B. Afonso, B.C. Sousa, A.R. Pitt, C.M. Spickett, A mass spectrometry approach for the identification and localization of small aldehyde modifications of proteins, *Arch Biochem Biophys* 646 (2018) 38-45.
- [218] D.L. Swaney, C.D. Wenger, J.J. Coon, Value of using multiple proteases for large-scale mass spectrometry-based proteomics, *J Proteome Res* 9(3) (2010) 1323-9.
- [219] S.V. Saveliev, C.C. Woodroffe, G. Sabat, C.M. Adams, D. Klaubert, K. Wood, M. Uhr, Mass spectrometry compatible surfactant for optimized in-gel protein digestion, *Anal Chem* 85(2) (2013) 907-14.
- [220] Y.Q. Yu, M. Gilar, J. Kaska, J.C. Gebler, A rapid sample preparation method for mass spectrometric characterization of N-linked glycans, *Rapid Commun Mass Spectrom* 19(16) (2005) 2331-6.
- [221] D.C. Liebler, Protein Damage by Reactive Electrophiles: Targets and Consequences, *Chemical Research in Toxicology* 21(1) (2008) 117-128.
- [222] J. Chavez, J. Wu, B. Han, W.G. Chung, C.S. Maier, New role for an old probe: affinity labeling of oxylipid protein conjugates by N'-aminooxymethylcarbonylhydrazino d-biotin, *Anal Chem* 78(19) (2006) 6847-54.
- [223] J.D. Chavez, J. Wu, W. Bisson, C.S. Maier, Site-specific proteomic analysis of lipoxidation adducts in cardiac mitochondria reveals chemical diversity of 2-alkenal adduction, *J Proteomics* 74(11) (2011) 2417-29.
- [224] S.C. Tzeng, C.S. Maier, Label-Free Proteomics Assisted by Affinity Enrichment for Elucidating the Chemical Reactivity of the Liver Mitochondrial Proteome toward Adduction by the Lipid Electrophile 4-hydroxy-2-nonenal (HNE), *Front Chem* 4 (2016) 2.
- [225] B. Han, M. Hare, S. Wickramasekara, Y. Fang, C.S. Maier, A comparative 'bottom up' proteomics strategy for the site-specific identification and quantification of protein modifications by electrophilic lipids, *J Proteomics* 75(18) (2012) 5724-33.
- [226] R.C. Bollineni, M. Fedorova, R. Hoffmann, Qualitative and quantitative evaluation of derivatization reagents for different types of protein-bound carbonyl groups, *Analyst* 138(17) (2013) 5081-8.
- [227] S.G. Codreanu, D.C. Liebler, Novel approaches to identify protein adducts produced by lipid peroxidation, *Free Radical Research* 49(7) (2015) 881-887.
- [228] A. Vila, K.A. Tallman, A.T. Jacobs, D.C. Liebler, N.A. Porter, L.J. Marnett, Identification of protein targets of 4-hydroxynonenal using click chemistry for ex vivo biotinylation of azido and alkynyl derivatives, *Chem Res Toxicol* 21(2) (2008) 432-44.
- [229] O. Coskun, Separation techniques: Chromatography, *North Clin Istanb* 3(2) (2016) 156-160.
- [230] Y. Shi, R. Xiang, C. Horváth, J.A. Wilkins, The role of liquid chromatography in proteomics, *J Chromatogr A* 1053(1-2) (2004) 27-36.
- [231] M. Habberger, M. Leiss, A.K. Heidenreich, O. Pester, G. Hafenmair, M. Hook, L. Bonnington, H. Wegele, M. Haindl, D. Reusch, P. Bulau, Rapid characterization of biotherapeutic proteins by size-exclusion chromatography coupled to native mass spectrometry, *MAbs* 8(2) (2016) 331-9.
- [232] M. Schmidt, M. Hafner, C. Frech, Modeling of salt and pH gradient elution in ion-exchange chromatography, *J Sep Sci* 37(1-2) (2014) 5-13.
- [233] D.B. Wall, M.T. Kachman, S.S. Gong, S.J. Parus, M.W. Long, D.M. Lubman, Isoelectric focusing nonporous silica reversed-phase high-performance liquid chromatography/electrospray ionization time-of-flight mass spectrometry: a three-dimensional liquid-phase protein separation method as applied to the human erythroleukemia cell-line, *Rapid Commun Mass Spectrom* 15(18) (2001) 1649-61.

- [234] B.T. Chait, S.B. Kent, Weighing naked proteins: practical, high-accuracy mass measurement of peptides and proteins, *Science* 257(5078) (1992) 1885-94.
- [235] M. Zhou, S. Wu, D.L. Stenoien, Z. Zhang, L. Connolly, M. Freitag, L. Paša-Tolić, Profiling Changes in Histone Post-translational Modifications by Top-Down Mass Spectrometry, *Methods Mol Biol* 1507 (2017) 153-168.
- [236] D.C. Ehrmann, K. Rose, M.W. Calcutt, A.B. Beller, S. Hill, T.J. Rogers, S.D. Steele, D.L. Hachey, J.L. Aschner, Glutathionylated  $\gamma$ G and  $\gamma$ A subunits of hemoglobin F: a novel post-translational modification found in extremely premature infants by LC-MS and nanoLC-MS/MS, *J Mass Spectrom* 49(2) (2014) 178-83.
- [237] M. Carini, L. Regazzoni, G. Aldini, Mass spectrometric strategies and their applications for molecular mass determination of recombinant therapeutic proteins, *Curr Pharm Biotechnol* 12(10) (2011) 1548-57.
- [238] X. Zhu, X. Tang, J. Zhang, G.P. Tochtrop, V.E. Anderson, L.M. Sayre, Mass Spectrometric Evidence for the Existence of Distinct Modifications of Different Proteins by 2(E),4(E)-Decadienal, *Chemical Research in Toxicology* 23(3) (2010) 467-473.
- [239] L. Fornelli, K. Srzentić, R. Huguet, C. Mullen, S. Sharma, V. Zabrouskov, R.T. Fellers, K.R. Durbin, P.D. Compton, N.L. Kelleher, Accurate Sequence Analysis of a Monoclonal Antibody by Top-Down and Middle-Down Orbitrap Mass Spectrometry Applying Multiple Ion Activation Techniques, *Anal Chem* 90(14) (2018) 8421-8429.
- [240] H. Zhang, Y. Ge, Comprehensive analysis of protein modifications by top-down mass spectrometry, *Circ Cardiovasc Genet* 4(6) (2011) 711.
- [241] M. Colzani, A. Criscuolo, G. Casali, M. Carini, G. Aldini, A method to produce fully characterized ubiquitin covalently modified by 4-hydroxy-nonenal, glyoxal, methylglyoxal, and malondialdehyde, *Free Radical Research* 50(3) (2016) 328-336.
- [242] B. Domon, R. Aebersold, Options and considerations when selecting a quantitative proteomics strategy, *Nature Biotechnology* 28 (2010) 710.
- [243] S.M. Stevens, K. Prokai-Tatrai, L. Prokai, Factors that contribute to the misidentification of tyrosine nitration by shotgun proteomics, *Mol Cell Proteomics* 7(12) (2008) 2442-51.
- [244] B. Domon, R. Aebersold, Mass spectrometry and protein analysis, *Science* 312(5771) (2006) 212-7.
- [245] B. Thiede, W. Höhenwarter, A. Krah, J. Mattow, M. Schmid, F. Schmidt, P.R. Jungblut, Peptide mass fingerprinting, *Methods* 35(3) (2005) 237-247.
- [246] D.N. Perkins, D.J. Pappin, D.M. Creasy, J.S. Cottrell, Probability-based protein identification by searching sequence databases using mass spectrometry data, *Electrophoresis* 20(18) (1999) 3551-67.
- [247] H. Steen, M. Mann, The ABC's (and XYZ's) of peptide sequencing, *Nat Rev Mol Cell Biol* 5(9) (2004) 699-711.
- [248] R. Aebersold, M. Mann, Mass spectrometry-based proteomics, *Nature* 422(6928) (2003) 198-207.
- [249] P. Roepstorff, J. Fohlman, Proposal for a common nomenclature for sequence ions in mass spectra of peptides, *Biomed Mass Spectrom* 11(11) (1984) 601.
- [250] K. Biemann, Appendix 5. Nomenclature for peptide fragment ions (positive ions), *Methods Enzymol* 193 (1990) 886-7.
- [251] I.K. Chu, C.-K. Siu, J.K.-C. Lau, W.K. Tang, X. Mu, C.K. Lai, X. Guo, X. Wang, N. Li, Y. Xia, X. Kong, H.B. Oh, V. Ryzhov, F. Tureček, A.C. Hopkinson, K.W.M. Siu, Proposed nomenclature for peptide ion fragmentation, *International Journal of Mass Spectrometry* 390 (2015) 24-27.
- [252] F. Di Domenico, G. Pupo, A. Tramutola, A. Giorgi, M.E. Schininà, R. Coccia, E. Head, D.A. Butterfield, M. Perluigi, Redox proteomics analysis of HNE-modified proteins in Down syndrome brain: clues for understanding the development of Alzheimer disease, *Free Radical Biology and Medicine* 71 (2014) 270-280.
- [253] J. Wu, X. Luo, L.J. Yan, Two dimensional blue native/SDS-PAGE to identify mitochondrial complex I subunits modified by 4-hydroxynonenal (HNE), *Front Physiol* 6 (2015) 98.

- [254] T.N. Tran, M.G. Kosaraju, S. Tamamizu-Kato, O. Akintunde, Y. Zheng, J.K. Bielicki, K. Pinkerton, K. Uchida, Y.Y. Lee, V. Narayanaswami, Acrolein Modification Impairs Key Functional Features of Rat Apolipoprotein E: Identification of Modified Sites by Mass Spectrometry, *Biochemistry* 53(2) (2014) 361-375.
- [255] K. Tveen-Jensen, A. Reis, L. Mouls, A.R. Pitt, C.M. Spickett, Reporter ion-based mass spectrometry approaches for the detection of non-enzymatic protein modifications in biological samples, *J Proteomics* 92 (2013) 71-9.
- [256] L. Mouls, E. Silajdzic, N. Haroune, C.M. Spickett, A.R. Pitt, Development of novel mass spectrometric methods for identifying HOCl-induced modifications to proteins, *Proteomics* 9(6) (2009) 1617-31.
- [257] T.A. Couttas, M.J. Raftery, G. Bernardini, M.R. Wilkins, Immonium ion scanning for the discovery of post-translational modifications and its application to histones, *J Proteome Res* 7(7) (2008) 2632-41.
- [258] N. Rauniyar, L. Prokai, Isotope-coded dimethyl tagging for differential quantification of posttranslational protein carbonylation by 4-hydroxy-2-nonenal, an end-product of lipid peroxidation, *J Mass Spectrom* 46(10) (2011) 976-85.
- [259] N. Rauniyar, S.M. Stevens, K. Prokai-Tatrai, L. Prokai, Characterization of 4-hydroxy-2-nonenal-modified peptides by liquid chromatography-tandem mass spectrometry using data-dependent acquisition: neutral loss-driven MS3 versus neutral loss-driven electron capture dissociation, *Anal Chem* 81(2) (2009) 782-9.
- [260] D.M. Cox, F. Zhong, M. Du, E. Duchoslav, T. Sakuma, J.C. McDermott, Multiple reaction monitoring as a method for identifying protein posttranslational modifications, *J Biomol Tech* 16(2) (2005) 83-90.
- [261] M.K. Gupta, J.W. Jung, S.J. Uhm, H. Lee, H.T. Lee, K.P. Kim, Combining selected reaction monitoring with discovery proteomics in limited biological samples, *Proteomics* 9(21) (2009) 4834-6.
- [262] A.N. Hoofnagle, J.O. Becker, M.N. Oda, G. Cavigiolio, P. Mayer, T. Vaisar, Multiple-reaction monitoring-mass spectrometric assays can accurately measure the relative protein abundance in complex mixtures, *Clin Chem* 58(4) (2012) 777-81.
- [263] G. Aldini, M. Orioli, M. Carini, Alpha,beta-unsaturated aldehydes adducts to actin and albumin as potential biomarkers of carbonylation damage, *Redox Rep* 12(1) (2007) 20-5.
- [264] C. Charvet, W.L. Liao, G.Y. Heo, J. Laird, R.G. Salomon, I.V. Turko, I.A. Pikuleva, Isolevuglandins and mitochondrial enzymes in the retina: mass spectrometry detection of post-translational modification of sterol-metabolizing CYP27A1, *J Biol Chem* 286(23) (2011) 20413-22.
- [265] A. Kirabo, V. Fontana, A.P. de Faria, R. Loperena, C.L. Galindo, J. Wu, A.T. Bikineyeva, S. Dikalov, L. Xiao, W. Chen, M.A. Saleh, D.W. Trott, H.A. Itani, A. Vinh, V. Amarnath, K. Amarnath, T.J. Guzik, K.E. Bernstein, X.Z. Shen, Y. Shyr, S.C. Chen, R.L. Mernaugh, C.L. Laffer, F. Eljovich, S.S. Davies, H. Moreno, M.S. Madhur, J. Roberts, D.G. Harrison, DC isoketal-modified proteins activate T cells and promote hypertension, *J Clin Invest* 124(10) (2014) 4642-56.
- [266] S.S. Davies, V. Amarnath, L.J. Roberts, Isoketals: highly reactive gamma-ketoaldehydes formed from the H2-isoprostane pathway, *Chem Phys Lipids* 128(1-2) (2004) 85-99.
- [267] A.E. Holley, M.K. Walker, K.H. Cheeseman, T.F. Slater, Measurement of n-Alkanals and hydroxyalkenals in biological samples, *Free Radical Biology and Medicine* 15(3) (1993) 281-289.
- [268] D. Tsikas, S. Rothmann, J.Y. Schneider, M.T. Suchy, A. Trettin, D. Modun, N. Stuke, N. Maassen, J.C. Frölich, Development, validation and biomedical applications of stable-isotope dilution GC-MS and GC-MS/MS techniques for circulating malondialdehyde (MDA) after pentafluorobenzyl bromide derivatization: MDA as a biomarker of oxidative stress and its relation to 15(S)-8-iso-prostaglandin F2 $\alpha$  and nitric oxide (NO), *J Chromatogr B Analyt Technol Biomed Life Sci* 1019 (2016) 95-111.

- [269] M.H. El-Maghrabey, N. Kishikawa, K. Ohyama, N. Kuroda, Analytical method for lipoperoxidation relevant reactive aldehydes in human sera by high-performance liquid chromatography-fluorescence detection, *Anal Biochem* 464 (2014) 36-42.
- [270] O. WARBURG, On the origin of cancer cells, *Science* 123(3191) (1956) 309-14.
- [271] T. Ishii, E. Tatsuda, S. Kumazawa, T. Nakayama, K. Uchida, Molecular basis of enzyme inactivation by an endogenous electrophile 4-hydroxy-2-nonenal: identification of modification sites in glyceraldehyde-3-phosphate dehydrogenase, *Biochemistry* 42(12) (2003) 3474-80.
- [272] M. Nakamura, H. Tomitori, T. Suzuki, A. Sakamoto, Y. Terui, R. Saiki, N. Dohmae, K. Igarashi, K. Kashiwagi, Inactivation of GAPDH as one mechanism of acrolein toxicity, *Biochem Biophys Res Commun* 430(4) (2013) 1265-71.
- [273] J.M. Camarillo, J.C. Ullery, K.L. Rose, L.J. Marnett, Electrophilic Modification of PKM2 by 4-Hydroxynonenal and 4-Oxononenal Results in Protein Cross-Linking and Kinase Inhibition, *Chem Res Toxicol* 30(2) (2017) 635-641.
- [274] J.L. Markley, R. Brüschweiler, A.S. Edison, H.R. Eghbalnia, R. Powers, D. Raftery, D.S. Wishart, The future of NMR-based metabolomics, *Curr Opin Biotechnol* 43 (2017) 34-40.
- [275] R. Saborano, Z. Eraslan, J. Roberts, F.L. Khanim, P.F. Lalor, M.A.C. Reed, U.L. Günther, A framework for tracer-based metabolism in mammalian cells by NMR, *Scientific Reports* 9(1) (2019) 2520.
- [276] S. Ravanbakhsh, P. Liu, T.C. Bjorndahl, T.C. Bjordahl, R. Mandal, J.R. Grant, M. Wilson, R. Eisner, I. Sinelnikov, X. Hu, C. Luchinat, R. Greiner, D.S. Wishart, Accurate, fully-automated NMR spectral profiling for metabolomics, *PLoS One* 10(5) (2015) e0124219.
- [277] K. Bingol, R. Brüschweiler, Two elephants in the room: new hybrid nuclear magnetic resonance and mass spectrometry approaches for metabolomics, *Curr Opin Clin Nutr Metab Care* 18(5) (2015) 471-7.
- [278] K.V. Ramana, S. Srivastava, S.S. Singhal, Lipid peroxidation products in human health and disease, *Oxid Med Cell Longev* 2013 (2013) 583438.
- [279] U.C. Yadav, K.V. Ramana, Regulation of NF- $\kappa$ B-induced inflammatory signaling by lipid peroxidation-derived aldehydes, *Oxid Med Cell Longev* 2013 (2013) 690545.
- [280] S. Luo, L. Jiang, Q. Li, X. Sun, T. Liu, F. Pei, T. Zhang, L. Dong, X. Liu, Acrolein-induced autophagy-dependent apoptosis via activation of the lysosomal-mitochondrial pathway in EAhy926 cells, *Toxicol In Vitro* 52 (2018) 146-153.
- [281] R.M. Domingues, P. Domingues, T. Melo, D. Pérez-Sala, A. Reis, C.M. Spickett, Lipoxidation adducts with peptides and proteins: deleterious modifications or signaling mechanisms?, *J Proteomics* 92 (2013) 110-31.
- [282] E. Gianazza, M. Brioschi, A.M. Fernandez, C. Banfi, Lipoxidation in cardiovascular diseases, *Redox Biol* (2019) 101119.
- [283] D.A. Butterfield, T. Reed, R. Sultana, Roles of 3-nitrotyrosine- and 4-hydroxynonenal-modified brain proteins in the progression and pathogenesis of Alzheimer's disease, *Free Radic Res* 45(1) (2011) 59-72.
- [284] G. Aldini, L. Gamberoni, M. Orioli, G. Beretta, L. Regazzoni, R. Maffei Facino, M. Carini, Mass spectrometric characterization of covalent modification of human serum albumin by 4-hydroxy-trans-2-nonenal, *J Mass Spectrom* 41(9) (2006) 1149-61.
- [285] G. Aldini, M.R. Domingues, C.M. Spickett, P. Domingues, A. Altomare, F.J. Sánchez-Gómez, C.L. Oeste, D. Pérez-Sala, Protein lipoxidation: Detection strategies and challenges, *Redox Biol* 5 (2015) 253-266.
- [286] E. Witort, S. Capaccioli, M. Becatti, C. Fiorillo, G. Batignani, V. Pavoni, M. Piccini, M. Orioli, M. Carini, G. Aldini, M. Lulli, Albumin Cys34 adducted by acrolein as a marker of oxidative stress in ischemia-reperfusion injury during hepatectomy, *Free Radic Res* 50(8) (2016) 831-9.
- [287] M.E. Szapacs, J.N. Riggins, L.J. Zimmerman, D.C. Liebler, Covalent adduction of human serum albumin by 4-hydroxy-2-nonenal: kinetic analysis of competing alkylation reactions, *Biochemistry* 45(35) (2006) 10521-8.



- [288] G. Aldini, G. Vistoli, L. Regazzoni, L. Gamberoni, R.M. Facino, S. Yamaguchi, K. Uchida, M. Carini, Albumin is the main nucleophilic target of human plasma: a protective role against pro-atherogenic electrophilic reactive carbonyl species?, *Chem Res Toxicol* 21(4) (2008) 824-35.
- [289] J. Himmelfarb, E. McMonagle, Albumin is the major plasma protein target of oxidant stress in uremia, *Kidney Int* 60(1) (2001) 358-63.
- [290] S. Toyokuni, S. Yamada, M. Kashima, Y. Ihara, Y. Yamada, T. Tanaka, H. Hiai, Y. Seino, K. Uchida, Serum 4-hydroxy-2-nonenal-modified albumin is elevated in patients with type 2 diabetes mellitus, *Antioxid Redox Signal* 2(4) (2000) 681-5.
- [291] R. Saiki, K. Nishimura, I. Ishii, T. Omura, S. Okuyama, K. Kashiwagi, K. Igarashi, Intense correlation between brain infarction and protein-conjugated acrolein, *Stroke* 40(10) (2009) 3356-61.
- [292] T. Shibamoto, Analytical methods for trace levels of reactive carbonyl compounds formed in lipid peroxidation systems, *J Pharm Biomed Anal* 41(1) (2006) 12-25.
- [293] M. Carini, G. Aldini, R.M. Facino, Mass spectrometry for detection of 4-hydroxy-trans-2-nonenal (HNE) adducts with peptides and proteins, *Mass Spectrom Rev* 23(4) (2004) 281-305.
- [294] H.J. Cooper, K. Håkansson, A.G. Marshall, The role of electron capture dissociation in biomolecular analysis, *Mass Spectrom Rev* 24(2) (2005) 201-22.
- [295] Y.V. Vasil'ev, S.C. Tzeng, L. Huang, C.S. Maier, Protein modifications by electrophilic lipoxidation products: adduct formation, chemical strategies and tandem mass spectrometry for their detection and identification, *Mass Spectrom Rev* 33(3) (2014) 157-82.
- [296] X. Zhu, X. Tang, V.E. Anderson, L.M. Sayre, Mass spectrometric characterization of protein modification by the products of nonenzymatic oxidation of linoleic acid, *Chem Res Toxicol* 22(8) (2009) 1386-97.
- [297] N. Rauniyar, K. Prokai-Tatrai, L. Prokai, Identification of carbonylation sites in apomyoglobin after exposure to 4-hydroxy-2-nonenal by solid-phase enrichment and liquid chromatography-electrospray ionization tandem mass spectrometry, *J Mass Spectrom* 45(4) (2010) 398-410.
- [298] I. Verrastro, K. Tveen-Jensen, R. Woscholski, C.M. Spickett, A.R. Pitt, Reversible oxidation of phosphatase and tensin homolog (PTEN) alters its interactions with signaling and regulatory proteins, *Free Radic Biol Med* 90 (2016) 24-34.
- [299] B. Maclean, D.M. Tomazela, S.E. Abbatiello, S. Zhang, J.R. Whiteaker, A.G. Paulovich, S.A. Carr, M.J. Maccoss, Effect of collision energy optimization on the measurement of peptides by selected reaction monitoring (SRM) mass spectrometry, *Anal Chem* 82(24) (2010) 10116-24.
- [300] V. Lange, P. Picotti, B. Domon, R. Aebersold, Selected reaction monitoring for quantitative proteomics: a tutorial, *Mol Syst Biol* 4 (2008) 222.
- [301] D.J. Pappin, P. Hojrup, A.J. Bleasby, Rapid identification of proteins by peptide-mass fingerprinting, *Curr Biol* 3(6) (1993) 327-32.
- [302] G. Sabbioni, R.J. Turesky, Biomonitoring Human Albumin Adducts: The Past, the Present, and the Future, *Chem Res Toxicol* 30(1) (2017) 332-366.
- [303] K. Uchida, 4-Hydroxy-2-nonenal: a product and mediator of oxidative stress, *Prog Lipid Res* 42(4) (2003) 318-43.
- [304] C.M. Coffey, S. Gronert, A cleavable biotin tagging reagent that enables the enrichment and identification of carbonylation sites in proteins, *Anal Bioanal Chem* 408(3) (2016) 865-74.
- [305] C.A. Blindauer, I. Harvey, K.E. Bunyan, A.J. Stewart, D. Sleep, D.J. Harrison, S. Berezenko, P.J. Sadler, Structure, properties, and engineering of the major zinc binding site on human albumin, *J Biol Chem* 284(34) (2009) 23116-24.
- [306] A.J. Stewart, C.A. Blindauer, S. Berezenko, D. Sleep, P.J. Sadler, Interdomain zinc site on human albumin, *Proc Natl Acad Sci U S A* 100(7) (2003) 3701-6.
- [307] J.P. Barnett, C.A. Blindauer, O. Kassar, S. Khazaipoul, E.M. Martin, P.J. Sadler, A.J. Stewart, Allosteric modulation of zinc speciation by fatty acids, *Biochim Biophys Acta* 1830(12) (2013) 5456-64.

- [308] J. Cai, A. Bhatnagar, W.M. Pierce, Protein modification by acrolein: formation and stability of cysteine adducts, *Chem Res Toxicol* 22(4) (2009) 708-16.
- [309] R.M. LoPachin, T. Gavin, Molecular mechanism of acrylamide neurotoxicity: lessons learned from organic chemistry, *Environ Health Perspect* 120(12) (2012) 1650-7.
- [310] G. Aldini, M. Orioli, M. Carini, Protein modification by acrolein: relevance to pathological conditions and inhibition by aldehyde sequestering agents, *Mol Nutr Food Res* 55(9) (2011) 1301-19.
- [311] T. Maeshima, K. Honda, M. Chikazawa, T. Shibata, Y. Kawai, M. Akagawa, K. Uchida, Quantitative analysis of acrolein-specific adducts generated during lipid peroxidation-modification of proteins in vitro: identification of N( $\tau$ )-(3-propanal)histidine as the major adduct, *Chem Res Toxicol* 25(7) (2012) 1384-92.
- [312] Q. Fu, E. Grote, J. Zhu, C. Jelinek, A. Köttgen, J. Coresh, J.E. Van Eyk, An Empirical Approach to Signature Peptide Choice for Selected Reaction Monitoring: Quantification of Uromodulin in Urine, *Clin Chem* 62(1) (2016) 198-207.
- [313] L.A. Breci, D.L. Tabb, J.R. Yates, V.H. Wysocki, Cleavage N-Terminal to Proline: Analysis of a Database of Peptide Tandem Mass Spectra, *Analytical Chemistry* 75(9) (2003) 1963-1971.
- [314] G. Aldini, I. Dalle-Donne, R.M. Facino, A. Milzani, M. Carini, Intervention strategies to inhibit protein carbonylation by lipoxidation-derived reactive carbonyls, *Med Res Rev* 27(6) (2007) 817-68.
- [315] T. Ishii, T. Yamada, T. Mori, S. Kumazawa, K. Uchida, T. Nakayama, Characterization of acrolein-induced protein cross-links, *Free Radic Res* 41(11) (2007) 1253-60.
- [316] P.C. Burcham, S.M. Pyke, Hydralazine inhibits rapid acrolein-induced protein oligomerization: role of aldehyde scavenging and adduct trapping in cross-link blocking and cytoprotection, *Mol Pharmacol* 69(3) (2006) 1056-65.
- [317] P.C. Burcham, A. Raso, C. Thompson, D. Tan, Intermolecular protein cross-linking during acrolein toxicity: efficacy of carbonyl scavengers as inhibitors of heat shock protein-90 cross-linking in A549 cells, *Chem Res Toxicol* 20(11) (2007) 1629-37.
- [318] I.D. Kozekov, L.V. Nechev, A. Sanchez, C.M. Harris, R.S. Lloyd, T.M. Harris, Interchain cross-linking of DNA mediated by the principal adduct of acrolein, *Chem Res Toxicol* 14(11) (2001) 1482-5.
- [319] I.D. Kozekov, L.V. Nechev, M.S. Moseley, C.M. Harris, C.J. Rizzo, M.P. Stone, T.M. Harris, DNA interchain cross-links formed by acrolein and crotonaldehyde, *J Am Chem Soc* 125(1) (2003) 50-61.
- [320] K. Uchida, Role of reactive aldehyde in cardiovascular diseases, *Free Radic Biol Med* 28(12) (2000) 1685-96.
- [321] J.E. Harrison, J. Schultz, Studies on the chlorinating activity of myeloperoxidase, *J Biol Chem* 251(5) (1976) 1371-4.
- [322] M.J. Davies, C.L. Hawkins, D.I. Pattison, M.D. Rees, Mammalian heme peroxidases: from molecular mechanisms to health implications, *Antioxid Redox Signal* 10(7) (2008) 1199-234.
- [323] F.H. Chilton, T.R. Connell, 1-ether-linked phosphoglycerides. Major endogenous sources of arachidonate in the human neutrophil, *J Biol Chem* 263(11) (1988) 5260-5.
- [324] A.K. Thukkani, C.J. Albert, K.R. Wildsmith, M.C. Messner, B.D. Martinson, F.F. Hsu, D.A. Ford, Myeloperoxidase-derived reactive chlorinating species from human monocytes target plasmalogens in low density lipoprotein, *J Biol Chem* 278(38) (2003) 36365-72.
- [325] W.Y. Wang, C.J. Albert, D.A. Ford, Alpha-chlorofatty acid accumulates in activated monocytes and causes apoptosis through reactive oxygen species production and endoplasmic reticulum stress, *Arterioscler Thromb Vasc Biol* 34(3) (2014) 526-32.
- [326] K.R. Wildsmith, C.J. Albert, F.F. Hsu, J.L. Kao, D.A. Ford, Myeloperoxidase-derived 2-chlorohexadecanal forms Schiff bases with primary amines of ethanolamine glycerophospholipids and lysine, *Chem Phys Lipids* 139(2) (2006) 157-70.
- [327] A.K. Thukkani, B.D. Martinson, C.J. Albert, G.A. Vogler, D.A. Ford, Neutrophil-mediated accumulation of 2-ClHDA during myocardial infarction: 2-ClHDA-mediated myocardial injury, *Am J Physiol Heart Circ Physiol* 288(6) (2005) H2955-64.

- [328] R.A. Maki, V.A. Tyurin, R.C. Lyon, R.L. Hamilton, S.T. DeKosky, V.E. Kagan, W.F. Reynolds, Aberrant expression of myeloperoxidase in astrocytes promotes phospholipid oxidation and memory deficits in a mouse model of Alzheimer disease, *J Biol Chem* 284(5) (2009) 3158-69.
- [329] D.K. Choi, S. Pennathur, C. Perier, K. Tieu, P. Teismann, D.C. Wu, V. Jackson-Lewis, M. Vila, J.P. Vonsattel, J.W. Heinecke, S. Przedborski, Ablation of the inflammatory enzyme myeloperoxidase mitigates features of Parkinson's disease in mice, *J Neurosci* 25(28) (2005) 6594-600.
- [330] A. Üllen, E. Singewald, V. Konya, G. Fauler, H. Reicher, C. Nussold, A. Hammer, D. Kratky, A. Heinemann, P. Holzer, E. Malle, W. Sattler, Myeloperoxidase-derived oxidants induce blood-brain barrier dysfunction in vitro and in vivo, *PLoS One* 8(5) (2013) e64034.
- [331] C. Nussold, A. Üllen, N. Kogelnik, E. Bernhart, H. Reicher, I. Plastira, T. Glasnov, K. Zangger, G. Rechberger, M. Kollroser, G. Fauler, H. Wolinski, B.B. Weksler, I.A. Romero, S.D. Kohlwein, P.O. Couraud, E. Malle, W. Sattler, Assessment of electrophile damage in a human brain endothelial cell line utilizing a clickable alkyne analog of 2-chlorohexadecanal, *Free Radic Biol Med* 90 (2016) 59-74.
- [332] X. Lin, T.J. Cook, C.P. Zabetian, J.B. Leverenz, E.R. Peskind, S.C. Hu, K.C. Cain, C. Pan, J.S. Edgar, D.R. Goodlett, B.A. Racette, H. Checkoway, T.J. Montine, M. Shi, J. Zhang, DJ-1 isoforms in whole blood as potential biomarkers of Parkinson disease, *Sci Rep* 2 (2012) 954.
- [333] D.S. Anbukumar, L.P. Shornick, C.J. Albert, M.M. Steward, R.A. Zoeller, W.L. Neumann, D.A. Ford, Chlorinated lipid species in activated human neutrophils: lipid metabolites of 2-chlorohexadecanal, *J Lipid Res* 51(5) (2010) 1085-92.
- [334] I.A. Blair, Endogenous glutathione adducts, *Curr Drug Metab* 7(8) (2006) 853-72.
- [335] V.I. Lushchak, Glutathione homeostasis and functions: potential targets for medical interventions, *J Amino Acids* 2012 (2012) 736837.
- [336] B.K. Wacker, C.J. Albert, B.A. Ford, D.A. Ford, Strategies for the analysis of chlorinated lipids in biological systems, *Free Radic Biol Med* 59 (2013) 92-9.
- [337] A. Üllen, C. Nussold, T. Glasnov, R. Saf, D. Cantillo, G. Eibinger, H. Reicher, G. Fauler, E. Bernhart, S. Hallstrom, N. Kogelnik, K. Zangger, C. Oliver Kappe, E. Malle, W. Sattler, Covalent adduct formation between the plasmalogen-derived modification product 2-chlorohexadecanal and phloretin, *Biochem Pharmacol* 93(4) (2015) 470-81.
- [338] E.J. Corey, J.W. Suggs, Pyridinium chlorochromate. An efficient reagent for oxidation of primary and secondary alcohols to carbonyl compounds, *Tetrahedron Letters* 16(31) (1975) 2647-2650.
- [339] Y. Jing, C.G. Daniliuc, A. Studer, Direct conversion of alcohols to  $\alpha$ -chloro aldehydes and  $\alpha$ -chloro ketones, *Org Lett* 16(18) (2014) 4932-5.
- [340] M.P. Brochu, S.P. Brown, D.W.C. MacMillan, Direct and Enantioselective Organocatalytic  $\alpha$ -Chlorination of Aldehydes, *Journal of the American Chemical Society* 126(13) (2004) 4108-4109.
- [341] N. Halland, A. Braunton, S. Bachmann, M. Marigo, K.A. Jørgensen, Direct Organocatalytic Asymmetric  $\alpha$ -Chlorination of Aldehydes, *Journal of the American Chemical Society* 126(15) (2004) 4790-4791.
- [342] C. Nussold, M. Kollroser, H. Köfeler, G. Rechberger, H. Reicher, A. Ullen, E. Bernhart, S. Waltl, I. Kratzer, A. Hermetter, H. Hackl, Z. Trajanoski, A. Hrzenjak, E. Malle, W. Sattler, Hypochlorite modification of sphingomyelin generates chlorinated lipid species that induce apoptosis and proteome alterations in dopaminergic PC12 neurons in vitro, *Free Radic Biol Med* 48(12) (2010) 1588-600.
- [343] N. Halland, A. Braunton, S. Bachmann, M. Marigo, K.A. Jørgensen, Direct organocatalytic asymmetric alpha-chlorination of aldehydes, *J Am Chem Soc* 126(15) (2004) 4790-1.
- [344] B.G. Yasnitskii, E.B. Dol'berg, Mechanism of the formation of 2-aminothiazole in the reaction of chloroacetaldehyde with thiourea, *Chemistry of Heterocyclic Compounds* 7(7) (1971) 866-868.

- [345] R.A. Zubarev, The challenge of the proteome dynamic range and its implications for in-depth proteomics, *Proteomics* 13(5) (2013) 723-6.
- [346] K. Chandramouli, P.Y. Qian, Proteomics: challenges, techniques and possibilities to overcome biological sample complexity, *Hum Genomics Proteomics* 2009 (2009).
- [347] L.M. Smith, N.L. Kelleher, C.f.T.D. Proteomics, Proteoform: a single term describing protein complexity, *Nat Methods* 10(3) (2013) 186-7.
- [348] A.J. Matlin, F. Clark, C.W. Smith, Understanding alternative splicing: towards a cellular code, *Nat Rev Mol Cell Biol* 6(5) (2005) 386-98.
- [349] B.J. Perrin, J.M. Ervasti, The actin gene family: function follows isoform, *Cytoskeleton (Hoboken)* 67(10) (2010) 630-4.
- [350] W.J. Israelsen, M.G. Vander Heiden, Pyruvate kinase: Function, regulation and role in cancer, *Semin Cell Dev Biol* 43 (2015) 43-51.
- [351] M. Stastna, J.E. Van Eyk, Analysis of protein isoforms: can we do it better?, *Proteomics* 12(19-20) (2012) 2937-48.
- [352] A. Srebrow, A.R. Kornblihtt, The connection between splicing and cancer, *J Cell Sci* 119(Pt 13) (2006) 2635-41.
- [353] Y. Zhang, B.R. Fonslow, B. Shan, M.C. Baek, J.R. Yates, Protein analysis by shotgun/bottom-up proteomics, *Chem Rev* 113(4) (2013) 2343-94.
- [354] B.T. Chait, Chemistry. Mass spectrometry: bottom-up or top-down?, *Science* 314(5796) (2006) 65-6.
- [355] A.D. Catherman, O.S. Skinner, N.L. Kelleher, Top Down proteomics: facts and perspectives, *Biochem Biophys Res Commun* 445(4) (2014) 683-93.
- [356] N. Siuti, N.L. Kelleher, Decoding protein modifications using top-down mass spectrometry, *Nat Methods* 4(10) (2007) 817-21.
- [357] B.A. Garcia, J. Shabanowitz, D.F. Hunt, Characterization of histones and their post-translational modifications by mass spectrometry, *Curr Opin Chem Biol* 11(1) (2007) 66-73.
- [358] A. Beck, E. Wagner-Rousset, D. Ayoub, A. Van Dorsselaer, S. Sanglier-Cianférani, Characterization of therapeutic antibodies and related products, *Anal Chem* 85(2) (2013) 715-36.
- [359] B.A. Parks, L. Jiang, P.M. Thomas, C.D. Wenger, M.J. Roth, M.T. Boyne, P.V. Burke, K.E. Kwast, N.L. Kelleher, Top-down proteomics on a chromatographic time scale using linear ion trap fourier transform hybrid mass spectrometers, *Anal Chem* 79(21) (2007) 7984-91.
- [360] T.K. Toby, L. Fornelli, N.L. Kelleher, Progress in Top-Down Proteomics and the Analysis of Proteoforms, *Annu Rev Anal Chem (Palo Alto Calif)* 9(1) (2016) 499-519.
- [361] A.L. Capriotti, C. Cavaliere, P. Foglia, R. Samperi, A. Laganà, Intact protein separation by chromatographic and/or electrophoretic techniques for top-down proteomics, *J Chromatogr A* 1218(49) (2011) 8760-76.
- [362] D.P. Donnelly, C.M. Rawlins, C.J. DeHart, L. Fornelli, L.F. Schachner, Z. Lin, J.L. Lippens, K.C. Aluri, R. Sarin, B. Chen, C. Lantz, W. Jung, K.R. Johnson, A. Koller, J.J. Wolff, I.D.G. Campuzano, J.R. Auclair, A.R. Ivanov, J.P. Whitelegge, L. Paša-Tolić, J. Chamot-Rooke, P.O. Danis, L.M. Smith, Y.O. Tsybin, J.A. Loo, Y. Ge, N.L. Kelleher, J.N. Agar, Best practices and benchmarks for intact protein analysis for top-down mass spectrometry, *Nat Methods* 16(7) (2019) 587-594.
- [363] M.J. Roth, D.A. Plymire, A.N. Chang, J. Kim, E.M. Maresh, S.E. Larson, S.M. Patrie, Sensitive and reproducible intact mass analysis of complex protein mixtures with superficially porous capillary reversed-phase liquid chromatography mass spectrometry, *Anal Chem* 83(24) (2011) 9586-92.
- [364] B.E. Chong, F. Yan, D.M. Lubman, F.R. Miller, Chromatofocusing nonporous reversed-phase high-performance liquid chromatography/electrospray ionization time-of-flight mass spectrometry of proteins from human breast cancer whole cell lysates: a novel two-dimensional liquid chromatography/mass spectrometry method, *Rapid Commun Mass Spectrom* 15(4) (2001) 291-6.

- [365] A. Vaast, E. Tyteca, G. Desmet, P.J. Schoenmakers, S. Eeltink, Gradient-elution parameters in capillary liquid chromatography for high-speed separations of peptides and intact proteins, *J Chromatogr A* 1355 (2014) 149-57.
- [366] J.W. Eschelbach, J.W. Jorgenson, Improved protein recovery in reversed-phase liquid chromatography by the use of ultrahigh pressures, *Anal Chem* 78(5) (2006) 1697-706.
- [367] P. Szabelski, A. Cavazzini, K. Kaczmarek, X. Liu, J. Van Horn, G. Guiochon, Experimental studies of pressure/temperature dependence of protein adsorption equilibrium in reversed-phase high-performance liquid chromatography, *J Chromatogr A* 950(1-2) (2002) 41-53.
- [368] J. Ståhlberg, Retention models for ions in chromatography, *J Chromatogr A* 855(1) (1999) 3-55.
- [369] L. Shan, D.J. Anderson, Effect of buffer concentration on gradient chromatofocusing performance separating proteins on a high-performance DEAE column, *J Chromatogr A* 909(2) (2001) 191-205.
- [370] L. Shan, D.J. Anderson, Gradient chromatofocusing. versatile pH gradient separation of proteins in ion-exchange HPLC: characterization studies, *Anal Chem* 74(21) (2002) 5641-9.
- [371] M. Talebi, A. Nordborg, A. Gaspar, N.A. Lacher, Q. Wang, X.Z. He, P.R. Haddad, E.F. Hilder, Charge heterogeneity profiling of monoclonal antibodies using low ionic strength ion-exchange chromatography and well-controlled pH gradients on monolithic columns, *J Chromatogr A* 1317 (2013) 148-54.
- [372] L. Zhang, T. Patapoff, D. Farnan, B. Zhang, Improving pH gradient cation-exchange chromatography of monoclonal antibodies by controlling ionic strength, *J Chromatogr A* 1272 (2013) 56-64.
- [373] G.J. Opiteck, K.C. Lewis, J.W. Jorgenson, R.J. Andereg, Comprehensive on-line LC/LC/MS of proteins, *Anal Chem* 69(8) (1997) 1518-24.
- [374] K.M. Millea, I.S. Krull, S.A. Cohen, J.C. Gebler, S.J. Berger, Integration of multidimensional chromatographic protein separations with a combined "top-down" and "bottom-up" proteomic strategy, *J Proteome Res* 5(1) (2006) 135-46.
- [375] M.J. Roth, B.A. Parks, J.T. Ferguson, M.T. Boyne, N.L. Kelleher, "Proteotyping": population proteomics of human leukocytes using top down mass spectrometry, *Anal Chem* 80(8) (2008) 2857-66.
- [376] S. Era, K. Kuwata, H. Imai, K. Nakamura, T. Hayashi, M. Sogami, Age-related change in redox state of human serum albumin, *Biochim Biophys Acta* 1247(1) (1995) 12-6.
- [377] S. Era, T. Hamaguchi, M. Sogami, K. Kuwata, E. Suzuki, K. Miura, K. Kawai, Y. Kitazawa, H. Okabe, A. Noma, Further studies on the resolution of human mercapt- and nonmercaptalbumin and on human serum albumin in the elderly by high-performance liquid chromatography, *Int J Pept Protein Res* 31(5) (1988) 435-42.
- [378] L. Turell, H. Botti, L. Bonilla, M.J. Torres, F. Schopfer, B.A. Freeman, L. Armas, A. Ricciardi, B. Alvarez, R. Radi, HPLC separation of human serum albumin isoforms based on their isoelectric points, *J Chromatogr B Analyt Technol Biomed Life Sci* 944 (2014) 144-151.
- [379] Y. Leblanc, C. Ramon, N. Bihoreau, G. Chevreux, Charge variants characterization of a monoclonal antibody by ion exchange chromatography coupled on-line to native mass spectrometry: Case study after a long-term storage at +5°C, *J Chromatogr B Analyt Technol Biomed Life Sci* 1048 (2017) 130-139.
- [380] K. Muneeruddin, M. Nazzaro, I.A. Kaltashov, Characterization of intact protein conjugates and biopharmaceuticals using ion-exchange chromatography with online detection by native electrospray ionization mass spectrometry and top-down tandem mass spectrometry, *Anal Chem* 87(19) (2015) 10138-45.
- [381] Y. Leblanc, N. Bihoreau, G. Chevreux, Characterization of Human Serum Albumin isoforms by ion exchange chromatography coupled on-line to native mass spectrometry, *J Chromatogr B Analyt Technol Biomed Life Sci* 1095 (2018) 87-93.

- [382] A. Kumar, B. Gangadharan, J. Cobbold, M. Thursz, N. Zitzmann, Absolute quantitation of disease protein biomarkers in a single LC-MS acquisition using apolipoprotein F as an example, *Sci Rep* 7(1) (2017) 12072.
- [383] M. Costa, A. Mestre, R. Horrillo, A.M. Ortiz, A. Pérez, A. Ruiz, M. Boada, S. Grancha, Cross-Sectional Characterization of Albumin Glycation State in Cerebrospinal Fluid and Plasma from Alzheimer's Disease Patients, *J Prev Alzheimers Dis* 6(2) (2019) 139-143.
- [384] H. Cao, T. Chen, Y. Shi, Glycation of human serum albumin in diabetes: impacts on the structure and function, *Curr Med Chem* 22(1) (2015) 4-13.
- [385] B. Garcia, N. Siuti, C. Thomas, C. Mizzen, Characterization of neurohistone variants and post-translational modifications by electron capture dissociation mass spectrometry, *International Journal of Mass Spectrometry* 259(1) (2007) 184 - 196.
- [386] A. Petruczynik, K. Wróblewski, M. Deja, M. Waksmundzka-Hajnos, Ion-exchange vs reversed-phase chromatography for separation and determination of basic psychotropic drugs, *Biomed Chromatogr* 29(11) (2015) 1700-7.
- [387] B. Granvogl, M. Plösch, L.A. Eichacker, Sample preparation by in-gel digestion for mass spectrometry-based proteomics, *Anal Bioanal Chem* 389(4) (2007) 991-1002.
- [388] P. Feist, A.B. Hummon, Proteomic challenges: sample preparation techniques for microgram-quantity protein analysis from biological samples, *Int J Mol Sci* 16(2) (2015) 3537-63.
- [389] R.L. Gundry, M.Y. White, C.I. Murray, L.A. Kane, Q. Fu, B.A. Stanley, J.E. Van Eyk, Preparation of proteins and peptides for mass spectrometry analysis in a bottom-up proteomics workflow, *Curr Protoc Mol Biol Chapter 10* (2009) Unit10.25.
- [390] M.V. Gwangwa, A.M. Joubert, M.H. Visagie, Crosstalk between the Warburg effect, redox regulation and autophagy induction in tumourigenesis, *Cell Mol Biol Lett* 23 (2018) 20.
- [391] S.W. Kang, S. Lee, E.K. Lee, ROS and energy metabolism in cancer cells: alliance for fast growth, *Arch Pharm Res* 38(3) (2015) 338-45.
- [392] V. Sosa, T. Moline, R. Somoza, R. Paciucci, H. Kondoh, L.L. ME, Oxidative stress and cancer: an overview, *Ageing Res Rev* 12(1) (2013) 376-90.
- [393] E. Mullarky, L.C. Cantley, Diverting Glycolysis to Combat Oxidative Stress, in: K. Nakao, N. Minato, S. Uemoto (Eds.), *Innovative Medicine: Basic Research and Development*, Tokyo, 2015, pp. 3-23.
- [394] P. Eaton, N. Wright, D.J. Hearse, M.J. Shattock, Glyceraldehyde phosphate dehydrogenase oxidation during cardiac ischemia and reperfusion, *J Mol Cell Cardiol* 34(11) (2002) 1549-60.
- [395] T. Ishii, O. Sunami, H. Nakajima, H. Nishio, T. Takeuchi, F. Hata, Critical role of sulfenic acid formation of thiols in the inactivation of glyceraldehyde-3-phosphate dehydrogenase by nitric oxide, *Biochem Pharmacol* 58(1) (1999) 133-43.
- [396] J.M. Souza, R. Radi, Glyceraldehyde-3-phosphate dehydrogenase inactivation by peroxynitrite, *Archives of biochemistry and biophysics* 360(2) (1998) 187-94.
- [397] M. Yi, Y. Ban, Y. Tan, W. Xiong, G. Li, B. Xiang, 6-Phosphofructo-2-kinase/fructose-2,6-bisphosphatase 3 and 4: A pair of valves for fine-tuning of glucose metabolism in human cancer, *Mol Metab* 20 (2019) 1-13.
- [398] W. Luo, G.L. Semenza, Emerging roles of PKM2 in cell metabolism and cancer progression, *Trends Endocrinol Metab* 23(11) (2012) 560-6.
- [399] H.R. Christofk, M.G. Vander Heiden, M.H. Harris, A. Ramanathan, R.E. Gerszten, R. Wei, M.D. Fleming, S.L. Schreiber, L.C. Cantley, The M2 splice isoform of pyruvate kinase is important for cancer metabolism and tumour growth, *Nature* 452(7184) (2008) 230-3.
- [400] K. Ashizawa, P. McPhie, K.H. Lin, S.Y. Cheng, An in vitro novel mechanism of regulating the activity of pyruvate kinase M2 by thyroid hormone and fructose 1, 6-bisphosphate, *Biochemistry* 30(29) (1991) 7105-11.
- [401] J.D. Dombrauckas, B.D. Santarsiero, A.D. Mesecar, Structural basis for tumor pyruvate kinase M2 allosteric regulation and catalysis, *Biochemistry* 44(27) (2005) 9417-29.

- [402] M.S. Jurica, A. Mesecar, P.J. Heath, W. Shi, T. Nowak, B.L. Stoddard, The allosteric regulation of pyruvate kinase by fructose-1,6-bisphosphate, *Structure* 6(2) (1998) 195-210.
- [403] D. Anastasiou, G. Poulgiannis, J.M. Asara, M.B. Boxer, J.K. Jiang, M. Shen, G. Bellinger, A.T. Sasaki, J.W. Locasale, D.S. Auld, C.J. Thomas, M.G. Vander Heiden, L.C. Cantley, Inhibition of pyruvate kinase M2 by reactive oxygen species contributes to cellular antioxidant responses, *Science* 334(6060) (2011) 1278-83.
- [404] B. McDonagh, S. Ogueta, G. Lasarte, C.A. Padilla, J.A. Barcena, Shotgun redox proteomics identifies specifically modified cysteines in key metabolic enzymes under oxidative stress in *Saccharomyces cerevisiae*, *Journal of proteomics* 72(4) (2009) 677-89.
- [405] A.R. Mitchell, M. Yuan, H.P. Morgan, I.W. McNae, E.A. Blackburn, T. Le Bihan, R.A. Homem, M. Yu, G.J. Loake, P.A. Michels, M.A. Wear, M.D. Walkinshaw, Redox regulation of pyruvate kinase M2 by cysteine oxidation and S-nitrosation, *The Biochemical journal* 475(20) (2018) 3275-3291.
- [406] S.Y. Lunt, V. Muralidhar, A.M. Hosios, W.J. Israelsen, D.Y. Gui, L. Newhouse, M. Ogrodzinski, V. Hecht, K. Xu, P.N. Acevedo, D.P. Hollern, G. Bellinger, T.L. Dayton, S. Christen, I. Elia, A.T. Dinh, G. Stephanopoulos, S.R. Manalis, M.B. Yaffe, E.R. Andrechek, S.M. Fendt, M.G. Vander Heiden, Pyruvate kinase isoform expression alters nucleotide synthesis to impact cell proliferation, *Molecular cell* 57(1) (2015) 95-107.
- [407] N.M. Gruning, M. Rinnerthaler, K. Bluemlein, M. Mulleder, M.M. Wamelink, H. Lehrach, C. Jakobs, M. Breitenbach, M. Ralser, Pyruvate kinase triggers a metabolic feedback loop that controls redox metabolism in respiring cells, *Cell Metab* 14(3) (2011) 415-27.
- [408] E. Eigenbrodt, M. Reinacher, U. Scheefers-Borchel, H. Scheefers, R. Friis, Double role for pyruvate kinase type M2 in the expansion of phosphometabolite pools found in tumor cells, *Critical reviews in oncogenesis* 3(1-2) (1992) 91-115.
- [409] R.M. Domingues, P. Domingues, T. Melo, D. Perez-Sala, A. Reis, C.M. Spickett, Lipoxidation adducts with peptides and proteins: deleterious modifications or signaling mechanisms?, *Journal of proteomics* 92 (2013) 110-31.
- [410] S. Pizzimenti, E. Ciamporocero, M. Daga, P. Pettazzoni, A. Arcaro, G. Cetrangolo, R. Minelli, C. Dianzani, A. Lepore, F. Gentile, G. Barrera, Interaction of aldehydes derived from lipid peroxidation and membrane proteins, *Front Physiol* 4 (2013) 242.
- [411] A. Ayala, M.F. Munoz, S. Arguelles, Lipid peroxidation: production, metabolism, and signaling mechanisms of malondialdehyde and 4-hydroxy-2-nonenal, *Oxidative medicine and cellular longevity* 2014 (2014) 360438.
- [412] D. Aizenbud, I. Aizenbud, A.Z. Reznick, K. Avezov, Acrolein-an alpha,beta-Unsaturated Aldehyde: A Review of Oral Cavity Exposure and Oral Pathology Effects, *Rambam Maimonides medical journal* 7(3) (2016).
- [413] H. Zhong, H. Yin, Role of lipid peroxidation derived 4-hydroxynonenal (4-HNE) in cancer: focusing on mitochondria, *Redox Biol* 4 (2015) 193-9.
- [414] G. Barrera, Oxidative stress and lipid peroxidation products in cancer progression and therapy, *ISRN Oncol* 2012 (2012) 137289.
- [415] K. Igarashi, T. Uemura, K. Kashiwagi, Acrolein toxicity at advanced age: present and future, *Amino Acids* 50(2) (2018) 217-228.
- [416] J. Gerszon, A. Rodacka, Oxidatively modified glyceraldehyde-3-phosphate dehydrogenase in neurodegenerative processes and the role of low molecular weight compounds in counteracting its aggregation and nuclear translocation, *Ageing Res Rev* 48 (2018) 21-31.
- [417] C.J. Martyniuk, B. Fang, J.M. Koomen, T. Gavin, L. Zhang, D.S. Barber, R.M. Lopachin, Molecular mechanism of glyceraldehyde-3-phosphate dehydrogenase inactivation by alpha,beta-unsaturated carbonyl derivatives, *Chem Res Toxicol* 24(12) (2011) 2302-11.
- [418] L. Soulere, Y. Queneau, A. Doutheau, An expeditious synthesis of 4-hydroxy-2E-nonenal (4-HNE), its dimethyl acetal and of related compounds, *Chemistry and physics of lipids* 150(2) (2007) 239-43.

- [419] S. Bouzbouz, E. de Lemos, J. Cossy, J. Saez, X. Franck, B. Figadere, Natural (5'-oxoheptene-1'E,3'E-dienyl)-5,6-dihydro-2H- pyran-2-one: Total synthesis and revision of its absolute configuration, 2004.
- [420] D. Eisenberg, E. Schwarz, M. Komaromy, R. Wall, Analysis of membrane and surface protein sequences with the hydrophobic moment plot, *J Mol Biol* 179(1) (1984) 125-42.
- [421] C. Ludwig, U.L. Günther, MetaboLab - advanced NMR data processing and analysis for metabolomics, *BMC Bioinformatics* 12(1) (2011) 366.
- [422] D.S. Wishart, D. Tzur, C. Knox, R. Eisner, A.C. Guo, N. Young, D. Cheng, K. Jewell, D. Arndt, S. Sawhney, C. Fung, L. Nikolai, M. Lewis, M.A. Coutouly, I. Forsythe, P. Tang, S. Shrivastava, K. Jeroncic, P. Stothard, G. Amegbey, D. Block, D.D. Hau, J. Wagner, J. Miniaci, M. Clements, M. Gebremedhin, N. Guo, Y. Zhang, G.E. Duggan, G.D. Macinnis, A.M. Weljie, R. Dowlatabadi, F. Bamforth, D. Clive, R. Greiner, L. Li, T. Marrie, B.D. Sykes, H.J. Vogel, L. Querengesser, HMDB: the Human Metabolome Database, *Nucleic Acids Res* 35(Database issue) (2007) D521-6.
- [423] B.C. Sousa, T. Ahmed, W.L. Dann, J. Ashman, A. Guy, T. Durand, A.R. Pitt, C.M. Spickett, Short-chain lipid peroxidation products form covalent adducts with pyruvate kinase and inhibit its activity in vitro and in breast cancer cells, *Free Radic Biol Med* (2019).
- [424] K. Sakata, K. Kashiwagi, S. Sharmin, S. Ueda, Y. Irie, N. Murotani, K. Igarashi, Increase in putrescine, amine oxidase, and acrolein in plasma of renal failure patients, *Biochem Biophys Res Commun* 305(1) (2003) 143-9.
- [425] W.J. Israelsen, T.L. Dayton, S.M. Davidson, B.P. Fiske, A.M. Hosios, G. Bellinger, J. Li, Y. Yu, M. Sasaki, J.W. Horner, L.N. Burga, J. Xie, M.J. Jurczak, R.A. DePinho, C.B. Clish, T. Jacks, R.G. Kibbey, G.M. Wulf, D. Di Vizio, G.B. Mills, L.C. Cantley, M.G. Vander Heiden, PKM2 isoform-specific deletion reveals a differential requirement for pyruvate kinase in tumor cells, *Cell* 155(2) (2013) 397-409.
- [426] L. Lv, D. Li, D. Zhao, R. Lin, Y. Chu, H. Zhang, Z. Zha, Y. Liu, Z. Li, Y. Xu, G. Wang, Y. Huang, Y. Xiong, K.L. Guan, Q.Y. Lei, Acetylation targets the M2 isoform of pyruvate kinase for degradation through chaperone-mediated autophagy and promotes tumor growth, *Molecular cell* 42(6) (2011) 719-30.
- [427] H.R. Christofk, M.G. Vander Heiden, N. Wu, J.M. Asara, L.C. Cantley, Pyruvate kinase M2 is a phosphotyrosine-binding protein, *Nature* 452(7184) (2008) 181-6.
- [428] T. Hitosugi, S. Kang, M.G. Vander Heiden, T.W. Chung, S. Elf, K. Lythgoe, S. Dong, S. Lonial, X. Wang, G.Z. Chen, J. Xie, T.L. Gu, R.D. Polakiewicz, J.L. Roesel, T.J. Boggon, F.R. Khuri, D.G. Gilliland, L.C. Cantley, J. Kaufman, J. Chen, Tyrosine phosphorylation inhibits PKM2 to promote the Warburg effect and tumor growth, *Science signaling* 2(97) (2009) ra73.
- [429] B. Varghese, G. Swaminathan, A. Plotnikov, C. Tzimas, N. Yang, H. Rui, S.Y. Fuchs, Prolactin inhibits activity of pyruvate kinase M2 to stimulate cell proliferation, *Molecular endocrinology* 24(12) (2010) 2356-65.
- [430] K. Taniguchi, Y. Ito, N. Sugito, M. Kumazaki, H. Shinohara, N. Yamada, Y. Nakagawa, T. Sugiyama, M. Futamura, Y. Otsuki, K. Yoshida, K. Uchiyama, Y. Akao, Organ-specific PTB1-associated microRNAs determine expression of pyruvate kinase isoforms, *Sci Rep* 5 (2015) 8647.
- [431] S.G. Codreanu, J.C. Ullery, J. Zhu, K.A. Tallman, W.N. Beavers, N.A. Porter, L.J. Marnett, B. Zhang, D.C. Liebler, Alkylation damage by lipid electrophiles targets functional protein systems, *Mol Cell Proteomics* 13(3) (2014) 849-59.
- [432] D. Illg, D. Pette, Turnover rates of hexokinase I, phosphofructokinase, pyruvate kinase and creatine kinase in slow-twitch soleus muscle and heart of the rabbit, *Eur J Biochem* 97(1) (1979) 267-73.
- [433] J.P. Castro, T. Jung, T. Grune, W. Siems, 4-Hydroxynonenal (HNE) modified proteins in metabolic diseases, *Free radical biology & medicine* 111 (2017) 309-315.
- [434] B. Friguet, L.I. Szweda, Inhibition of the multicatalytic proteinase (proteasome) by 4-hydroxy-2-nonenal cross-linked protein, *FEBS letters* 405(1) (1997) 21-5.
- [435] A. Hohn, T. Jung, T. Grune, Pathophysiological importance of aggregated damaged proteins, *Free radical biology & medicine* 71 (2014) 70-89.



- [436] R.A. Harris, A.W. Fenton, A critical review of the role of M2PYK in the Warburg effect, *Biochim Biophys Acta Rev Cancer* 1871(2) (2019) 225-239.
- [437] A. Glasauer, N.S. Chandel, Targeting antioxidants for cancer therapy, *Biochem Pharmacol* 92(1) (2014) 90-101.
- [438] F. Hirschhaeuser, U.G. Sattler, W. Mueller-Klieser, Lactate: a metabolic key player in cancer, *Cancer Res* 71(22) (2011) 6921-5.
- [439] W.M. Pardridge, M.B. Davidson, Alanine metabolism in skeletal muscle in tissue culture, *Biochim Biophys Acta* 585(1) (1979) 34-42.
- [440] C.M. Sousa, D.E. Biancur, X. Wang, C.J. Halbrook, M.H. Sherman, L. Zhang, D. Kremer, R.F. Hwang, A.K. Witkiewicz, H. Ying, J.M. Asara, R.M. Evans, L.C. Cantley, C.A. Lyssiotis, A.C. Kimmelman, Pancreatic stellate cells support tumour metabolism through autophagic alanine secretion, *Nature* 536(7617) (2016) 479-83.
- [441] P.F. Fitzpatrick, Tetrahydropterin-dependent amino acid hydroxylases, *Annu Rev Biochem* 68 (1999) 355-81.
- [442] C.A. Schenck, H.A. Maeda, Tyrosine biosynthesis, metabolism, and catabolism in plants, *Phytochemistry* 149 (2018) 82-102.
- [443] N.M. Anderson, P. Mucka, J.G. Kern, H. Feng, The emerging role and targetability of the TCA cycle in cancer metabolism, *Protein Cell* 9(2) (2018) 216-237.
- [444] W. Wang, Z. Wu, Z. Dai, Y. Yang, J. Wang, G. Wu, Glycine metabolism in animals and humans: implications for nutrition and health, *Amino Acids* 45(3) (2013) 463-77.
- [445] A. Ruiz-Ramírez, E. Ortiz-Balderas, G. Cardozo-Saldaña, E. Diaz-Diaz, M. El-Hafidi, Glycine restores glutathione and protects against oxidative stress in vascular tissue from sucrose-fed rats, *Clin Sci (Lond)* 126(1) (2014) 19-29.
- [446] M.F. McCarty, J.H. O'Keefe, J.J. DiNicolantonio, Dietary Glycine Is Rate-Limiting for Glutathione Synthesis and May Have Broad Potential for Health Protection, *Ochsner J* 18(1) (2018) 81-87.
- [447] D.Y. Mitchell, D.R. Petersen, Metabolism of the glutathione-acrolein adduct, S-(2-aldehyde-ethyl)glutathione, by rat liver alcohol and aldehyde dehydrogenase, *J Pharmacol Exp Ther* 251(1) (1989) 193-8.
- [448] S. Horiyama, Y. Takahashi, M. Hatai, C. Honda, K. Suwa, A. Ichikawa, N. Yoshikawa, K. Nakamura, M. Kunitomo, S. Date, T. Masujima, M. Takayama, Methyl vinyl ketone, a toxic ingredient in cigarette smoke extract, modifies glutathione in mouse melanoma cells, *Chem Pharm Bull (Tokyo)* 62(8) (2014) 772-8.
- [449] S. Horiyama, M. Hatai, A. Ichikawa, N. Yoshikawa, K. Nakamura, M. Kunitomo, Detoxification Mechanism of  $\alpha,\beta$ -Unsaturated Carbonyl Compounds in Cigarette Smoke Observed in Sheep Erythrocytes, *Chem Pharm Bull (Tokyo)* 66(7) (2018) 721-726.
- [450] A. Kumar, A.K. Bachhawat, Pyroglutamic acid: throwing light on a lightly studied metabolite, *Current Science* 102(2) (2012) 288-297.
- [451] G. Ntatsi, K.A. Aliferis, Y. Rouphael, F. Napolitano, K. Makris, G. Kalala, G. Katopodis, D. Savvas, Salinity source alters mineral composition and metabolism of *Cichorium spinosum*, *Environmental and Experimental Botany* 141 (2017) 113-123.
- [452] O. Yoshinari, K. Igarashi, Anti-diabetic effect of pyroglutamic acid in type 2 diabetic Goto-Kakizaki rats and KK-Ay mice, *Br J Nutr* 106(7) (2011) 995-1004.
- [453] F. Huber, A. Boire, M.P. López, G.H. Koenderink, Cytoskeletal crosstalk: when three different personalities team up, *Curr Opin Cell Biol* 32 (2015) 39-47.
- [454] L. Chang, R.D. Goldman, Intermediate filaments mediate cytoskeletal crosstalk, *Nat Rev Mol Cell Biol* 5(8) (2004) 601-13.
- [455] A. Desai, T.J. Mitchison, Microtubule polymerization dynamics, *Annu Rev Cell Dev Biol* 13 (1997) 83-117.
- [456] R. Alfaro-Aco, S. Petry, Building the Microtubule Cytoskeleton Piece by Piece, *J Biol Chem* 290(28) (2015) 17154-62.
- [457] S. Gadadhar, S. Bodakuntla, K. Natarajan, C. Janke, The tubulin code at a glance, *J Cell Sci* 130(8) (2017) 1347-1353.
- [458] K.J. Verhey, J. Gaertig, The tubulin code, *Cell Cycle* 6(17) (2007) 2152-60.

- [459] T.D. Pollard, Actin and Actin-Binding Proteins, *Cold Spring Harb Perspect Biol* 8(8) (2016).
- [460] H.E. HUXLEY, ELECTRON MICROSCOPE STUDIES ON THE STRUCTURE OF NATURAL AND SYNTHETIC PROTEIN FILAMENTS FROM STRIATED MUSCLE, *J Mol Biol* 7 (1963) 281-308.
- [461] T. Fujii, A.H. Iwane, T. Yanagida, K. Namba, Direct visualization of secondary structures of F-actin by electron cryomicroscopy, *Nature* 467(7316) (2010) 724-8.
- [462] H.L. Sweeney, E.L.F. Holzbaur, Motor Proteins, *Cold Spring Harb Perspect Biol* 10(5) (2018).
- [463] M.A. Titus, Myosin-Driven Intracellular Transport, *Cold Spring Harb Perspect Biol* 10(3) (2018).
- [464] T. Svitkina, The Actin Cytoskeleton and Actin-Based Motility, *Cold Spring Harb Perspect Biol* 10(1) (2018).
- [465] H.L. Sweeney, D.W. Hammers, Muscle Contraction, *Cold Spring Harb Perspect Biol* 10(2) (2018).
- [466] M. Glotzer, Cytokinesis in Metazoa and Fungi, *Cold Spring Harb Perspect Biol* 9(10) (2017).
- [467] H. Herrmann, M. Hesse, M. Reichenzeller, U. Aebi, T.M. Magin, Functional complexity of intermediate filament cytoskeletons: from structure to assembly to gene ablation, *Int Rev Cytol* 223 (2003) 83-175.
- [468] S. Etienne-Manneville, Cytoplasmic Intermediate Filaments in Cell Biology, *Annu Rev Cell Dev Biol* 34 (2018) 1-28.
- [469] S.V. Strelkov, H. Herrmann, U. Aebi, Molecular architecture of intermediate filaments, *Bioessays* 25(3) (2003) 243-51.
- [470] A.V. Sokolova, L. Kreplak, T. Wedig, N. Mücke, D.I. Svergun, H. Herrmann, U. Aebi, S.V. Strelkov, Monitoring intermediate filament assembly by small-angle x-ray scattering reveals the molecular architecture of assembly intermediates, *Proc Natl Acad Sci U S A* 103(44) (2006) 16206-11.
- [471] O. Biskou, V. Casanova, K.M. Hooper, S. Kemp, G.P. Wright, J. Satsangi, P.G. Barlow, C. Stevens, The type III intermediate filament vimentin regulates organelle distribution and modulates autophagy, *PLoS One* 14(1) (2019) e0209665.
- [472] M.L. Styers, G. Salazar, R. Love, A.A. Peden, A.P. Kowalczyk, V. Faundez, The endo-lysosomal sorting machinery interacts with the intermediate filament cytoskeleton, *Mol Biol Cell* 15(12) (2004) 5369-82.
- [473] B. Eckes, D. Dogic, E. Colucci-Guyon, N. Wang, A. Maniotis, D. Ingber, A. Merckling, F. Langa, M. Aumailley, A. Delouvé, V. Koteliansky, C. Babinet, T. Krieg, Impaired mechanical stability, migration and contractile capacity in vimentin-deficient fibroblasts, *J Cell Sci* 111 ( Pt 13) (1998) 1897-907.
- [474] H. Kim, F. Nakamura, W. Lee, C. Hong, D. Pérez-Sala, C.A. McCulloch, Regulation of cell adhesion to collagen via beta1 integrins is dependent on interactions of filamin A with vimentin and protein kinase C epsilon, *Exp Cell Res* 316(11) (2010) 1829-44.
- [475] J.M. Paramio, J.L. Jorcano, Beyond structure: do intermediate filaments modulate cell signalling?, *Bioessays* 24(9) (2002) 836-44.
- [476] J. Ivaska, H.M. Pallari, J. Nevo, J.E. Eriksson, Novel functions of vimentin in cell adhesion, migration, and signaling, *Exp Cell Res* 313(10) (2007) 2050-62.
- [477] E. Perlson, I. Michaelevski, N. Kowalsman, K. Ben-Yaakov, M. Shaked, R. Seger, M. Eisenstein, M. Fainzilber, Vimentin binding to phosphorylated Erk sterically hinders enzymatic dephosphorylation of the kinase, *J Mol Biol* 364(5) (2006) 938-44.
- [478] M.I. Rodríguez, A. Peralta-Leal, F. O'Valle, J.M. Rodríguez-Vargas, A. Gonzalez-Flores, J. Majuelos-Melguizo, L. López, S. Serrano, A.G. de Herreros, J.C. Rodríguez-Manzanque, R. Fernández, R.G. Del Moral, J.M. de Almodóvar, F.J. Oliver, PARP-1 regulates metastatic melanoma through modulation of vimentin-induced malignant transformation, *PLoS Genet* 9(6) (2013) e1003531.

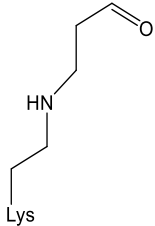
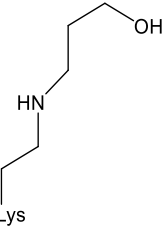
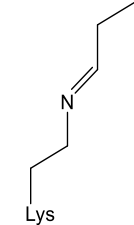
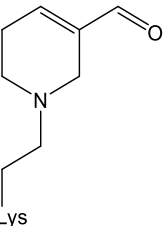
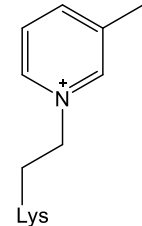
- [479] H. Bang, K. Egerer, A. Gauliard, K. Lühke, P.E. Rudolph, G. Fredenhagen, W. Berg, E. Feist, G.R. Burmester, Mutation and citrullination modifies vimentin to a novel autoantigen for rheumatoid arthritis, *Arthritis Rheum* 56(8) (2007) 2503-11.
- [480] L. Guilherme, J. Kalil, Rheumatic fever and rheumatic heart disease: cellular mechanisms leading autoimmune reactivity and disease, *J Clin Immunol* 30(1) (2010) 17-23.
- [481] F. Cheng, Y. Shen, P. Mohanasundaram, M. Lindström, J. Ivaska, T. Ny, J.E. Eriksson, Vimentin coordinates fibroblast proliferation and keratinocyte differentiation in wound healing via TGF- $\beta$ -Slug signaling, *Proc Natl Acad Sci U S A* 113(30) (2016) E4320-7.
- [482] B. Eckes, E. Colucci-Guyon, H. Smola, S. Nodder, C. Babinet, T. Krieg, P. Martin, Impaired wound healing in embryonic and adult mice lacking vimentin, *J Cell Sci* 113 ( Pt 13) (2000) 2455-62.
- [483] W. Wu, N. Panté, Vimentin plays a role in the release of the influenza A viral genome from endosomes, *Virology* 497 (2016) 41-52.
- [484] N. Fay, N. Panté, The intermediate filament network protein, vimentin, is required for parvoviral infection, *Virology* 444(1-2) (2013) 181-90.
- [485] B.T. Helfand, L. Chang, R.D. Goldman, Intermediate filaments are dynamic and motile elements of cellular architecture, *J Cell Sci* 117(Pt 2) (2004) 133-41.
- [486] N.T. Snider, M.B. Omary, Post-translational modifications of intermediate filament proteins: mechanisms and functions, *Nat Rev Mol Cell Biol* 15(3) (2014) 163-77.
- [487] M.B. West, B.G. Hill, Y.T. Xuan, A. Bhatnagar, Protein glutathiolation by nitric oxide: an intracellular mechanism regulating redox protein modification, *FASEB J* 20(10) (2006) 1715-7.
- [488] B. Huang, S.C. Chen, D.L. Wang, Shear flow increases S-nitrosylation of proteins in endothelial cells, *Cardiovasc Res* 83(3) (2009) 536-46.
- [489] J. Chavez, W.G. Chung, C.L. Miranda, M. Singhal, J.F. Stevens, C.S. Maier, Site-specific protein adducts of 4-hydroxy-2(E)-nonenal in human THP-1 monocytic cells: protein carbonylation is diminished by ascorbic acid, *Chem Res Toxicol* 23(1) (2010) 37-47.
- [490] G. Barrera, S. Pizzimenti, E.S. Ciamporcerro, M. Daga, C. Ullio, A. Arcaro, G.P. Cetrangolo, C. Ferretti, C. Dianzani, A. Lepore, F. Gentile, Role of 4-hydroxynonenal-protein adducts in human diseases, *Antioxid Redox Signal* 22(18) (2015) 1681-702.
- [491] V. Pekovic, I. Gibbs-Seymour, E. Markiewicz, F. Alzoghbi, A.M. Benham, R. Edwards, M. Wenhert, T. von Zglinicki, C.J. Hutchison, Conserved cysteine residues in the mammalian lamin A tail are essential for cellular responses to ROS generation, *Aging Cell* 10(6) (2011) 1067-79.
- [492] K. Stamatakis, F.J. Sánchez-Gómez, D. Pérez-Sala, Identification of novel protein targets for modification by 15-deoxy-Delta<sup>12,14</sup>-prostaglandin J<sub>2</sub> in mesangial cells reveals multiple interactions with the cytoskeleton, *J Am Soc Nephrol* 17(1) (2006) 89-98.
- [493] Á. Viedma-Poyatos, Y. de Pablo, M. Pekny, D. Pérez-Sala, The cysteine residue of glial fibrillary acidic protein is a critical target for lipoxidation and required for efficient network organization, *Free Radic Biol Med* 120 (2018) 380-394.
- [494] L. Rodríguez-Ribera, C. Slattery, T. Mc Morrow, R. Marcos, S. Pastor, Reactive carbonyl compounds impair wound healing by vimentin collapse and loss of the primary cilium, *Food Chem Toxicol* 108(Pt A) (2017) 128-138.
- [495] P.C. Burcham, A. Raso, C.A. Thompson, Intermediate filament carbonylation during acute acrolein toxicity in A549 lung cells: functional consequences, chaperone redistribution, and protection by bisulfite, *Antioxid Redox Signal* 12(3) (2010) 337-47.
- [496] P. Poggi, M.T. Rota, R. Boratto, Microtubules and vimentin associated filaments (VIFs) in cultured human gingival fibroblasts (HGFs) after exposure to acrolein and acetaldehyde, *Ann Anat* 183(2) (2001) 159-63.
- [497] A. Mónico, S. Duarte, M.A. Pajares, D. Pérez-Sala, Vimentin disruption by lipoxidation and electrophiles: Role of the cysteine residue and filament dynamics, *Redox Biol* (2019) 101098.

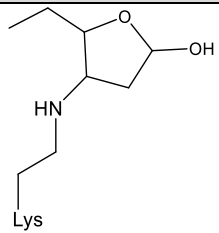
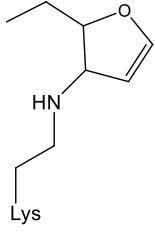
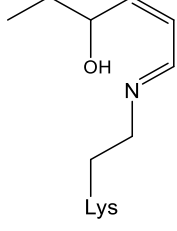
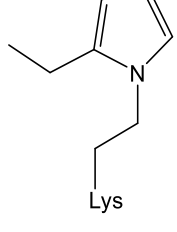
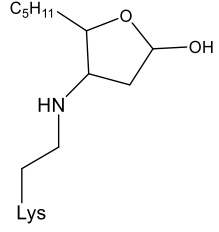
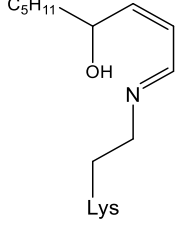
- [498] D. Pérez-Sala, C.L. Oeste, A.E. Martínez, M.J. Carrasco, B. Garzón, F.J. Cañada, Vimentin filament organization and stress sensing depend on its single cysteine residue and zinc binding, *Nat Commun* 6 (2015) 7287.
- [499] S. Gharbi, B. Garzón, J. Gayarre, J. Timms, D. Pérez-Sala, Study of protein targets for covalent modification by the antitumoral and anti-inflammatory prostaglandin PGA1: focus on vimentin, *J Mass Spectrom* 42(11) (2007) 1474-84.
- [500] A.J. Sarria, J.G. Lieber, S.K. Nordeen, R.M. Evans, The presence or absence of a vimentin-type intermediate filament network affects the shape of the nucleus in human SW-13 cells, *J Cell Sci* 107 ( Pt 6) (1994) 1593-607.
- [501] P. Eaton, M.E. Jones, E. McGregor, M.J. Dunn, N. Leeds, H.L. Byers, K.Y. Leung, M.A. Ward, J.R. Pratt, M.J. Shattock, Reversible cysteine-targeted oxidation of proteins during renal oxidative stress, *J Am Soc Nephrol* 14(8 Suppl 3) (2003) S290-6.
- [502] J. Jia, A. Arif, F. Terenzi, B. Willard, E.F. Plow, S.L. Hazen, P.L. Fox, Target-selective protein S-nitrosylation by sequence motif recognition, *Cell* 159(3) (2014) 623-34.
- [503] G. Vistoli, D. De Maddis, A. Cipak, N. Zarkovic, M. Carini, G. Aldini, Advanced glycoxidation and lipoxidation end products (AGEs and ALEs): an overview of their mechanisms of formation, *Free Radic Res* 47 Suppl 1 (2013) 3-27.
- [504] V. Magidson, A. Khodjakov, Circumventing photodamage in live-cell microscopy, *Methods Cell Biol* 114 (2013) 545-60.
- [505] A.G. Feroe, R. Attanasio, F. Scinicariello, Acrolein metabolites, diabetes and insulin resistance, *Environ Res* 148 (2016) 1-6.
- [506] C.J. Martyniuk, B. Fang, J.M. Koomen, T. Gavin, L. Zhang, D.S. Barber, R.M. Lopachin, Molecular mechanism of glyceraldehyde-3-phosphate dehydrogenase inactivation by  $\alpha,\beta$ -unsaturated carbonyl derivatives, *Chem Res Toxicol* 24(12) (2011) 2302-11.

## **Chapter 9. Appendix**

## 9.1 List of aldehyde modifications

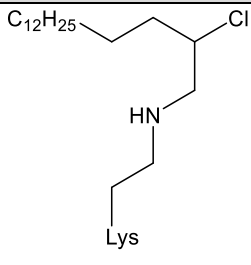
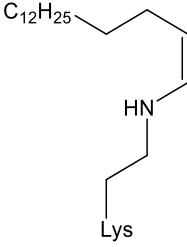
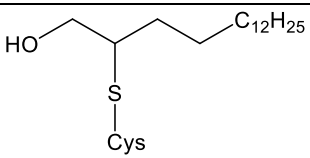
**Table 9.1. Aldehyde modifications searched on MASCOT.** Specificity site, monoisotopic and average mass, composition and proposed structure for ACR, HHE, HNE, MDA and 2-CIHDA adducts.

Type of adduct	Specificity site	Monoisotopic mass	Average mass	Composition	Proposed structure
<b>Acrolein</b>					
Propanal	C, H, K, W, R	56.026	56.063	C <sub>3</sub> H <sub>4</sub> O	
Propanal reduced	C, H, K, W, R	58.042	58.079	C <sub>3</sub> H <sub>6</sub> O	
Aldimine reduced	H, K	40.031	40.064	C <sub>3</sub> H <sub>4</sub>	
FDP-lysine	K	94.042	94.111	C <sub>6</sub> H <sub>6</sub> O	
MP-lysine	K	76.031	76.096	C <sub>6</sub> H <sub>4</sub>	

Type of adduct	Specificity site	Monoisotopic mass	Average mass	Composition	Proposed structure
<b>4-hydroxy-2-hexenal (HHE)</b>					
Michael	C, H, K, R	114.068	114.142	C <sub>6</sub> H <sub>10</sub> O <sub>2</sub>	
Michael Furane	C, H, K, R	96.058	96.127	C <sub>6</sub> H <sub>8</sub> O	
Imine	K, R	96.058	96.127	C <sub>6</sub> H <sub>8</sub> O	
Schiff Pyrrole	K, R	78.047	78.112	C <sub>6</sub> H <sub>6</sub>	
Type of adduct	Specificity site	Monoisotopic mass	Average mass	Composition	Proposed structure
<b>4-hydroxy-nonenal (HNE)</b>					
Michael	C, H, K, W	156.115	156.222	C <sub>9</sub> H <sub>16</sub> O <sub>2</sub>	
Imine	H, K, W	138.104	138.207	C <sub>9</sub> H <sub>14</sub> O	

Schiff Pyrrole	H, K, W	140.120	140.222	C <sub>9</sub> H <sub>16</sub> O	
<b>Type of adduct</b>	<b>Specificity site</b>	<b>Monoisotopic mass</b>	<b>Average mass</b>	<b>Composition</b>	<b>Proposed structure</b>
<b>Malondialdehyde (MDA)</b>					
Propenal	H, K	54.011	54.047	C <sub>3</sub> H <sub>2</sub> O	
Propenal reduced	K	56.026	56.063	C <sub>3</sub> H <sub>4</sub> O	
Pyrimidine	R	36.000	36.032	C <sub>3</sub>	
Dihydropyridine	K	134.037	134.132	C <sub>8</sub> H <sub>6</sub> O <sub>2</sub>	
Dihydropyridine reduced	K	138.068	138.164	C <sub>8</sub> H <sub>10</sub> O <sub>2</sub>	



Type of adduct	Specificity site	Monoisotopic mass	Average mass	Composition	Proposed structure
<b>2-chlorohexadecanal</b>					
Schiff reduced	H, K, R	258.211	258.870	C <sub>16</sub> H <sub>31</sub> Cl	
Schiff reduced minus Cl	H, K, R	222.235	222.409	C <sub>16</sub> H <sub>30</sub>	
Attack at CHCl	C	240.245	240.425	C <sub>16</sub> H <sub>32</sub> O	

## 9.2 List of publications

- Z. Ni, B.C. Sousa, S. Colombo, C.B. Afonso, T. Melo, A.R. Pitt, C.M. Spickett, P. Domingues, M.R. Domingues, M. Fedorova, A. Criscuolo, Evaluation of air oxidized PAPC: A multi laboratory study by LC-MS/MS, *Free Radic Biol Med* (2019).
- B.C. Sousa, T. Ahmed, W.L. Dann, J. Ashman, A. Guy, T. Durand, A.R. Pitt, C.M. Spickett, Short-chain lipid peroxidation products form covalent adducts with pyruvate kinase and inhibit its activity in vitro and in breast cancer cells, *Free Radic Biol Med* (2019).
- C.B. Afonso, B.C. Sousa, A.R. Pitt, C.M. Spickett, A mass spectrometry approach for the identification and localization of small aldehyde modifications of proteins, *Arch Biochem Biophys* 646 (2018) 38-45.
- B.C. Sousa, A.R. Pitt, C.M. Spickett, Chemistry and analysis of HNE and other prominent carbonyl-containing lipid oxidation compounds, *Free Radic Biol Med* 111 (2017) 294-308.
- J. Egea, et al. European contribution to the study of ROS: A summary of the findings and prospects for the future from the COST action BM1203 (EU-ROS), *Redox Biol* 13 (2017) 94-162. (one page contribution).

Pages removed for copyright restrictions.